TGT a Drug Target to Study p*K*a Shifts, Residual Solvation & Protein - Protein Interface Formation

Dissertation

zur

Erlangung des Doktorgrades

der Naturwissenschaften

(Dr. rer. nat.)

dem

Fachbereich Pharmazie

der PHILIPPS-UNIVERSITÄT MARBURG

vorgelegt von

Tina Ritschel

aus Wiesbaden

Marburg/Lahn 2009

Vom Fachbereich Pharmazie der Philipps-Universität Marburg
als Dissertation angenommen am:

Erstgutachter: Prof. Dr. Gerhard Klebe
Zweitgutachter: Prof. Dr. Klaus Reuter

Tag der mündlichen Prüfung: 20. August 2009

Die Untersuchungen zur vorliegenden Arbeit wurden auf Anregung von Herrn Prof. Dr. G. KLEBE am Institut für Pharmazeutische Chemie des Fachbereichs Pharmazie der Philipps-Universität Marburg in der Zeit von Januar 2006 bis Juni 2009 durchgeführt.

„Wege entstehen dadurch, dass man sie geht“

Franz Kafka

Abbreviations

Å	Ångström (1Å = 10^{-10} m)
A_{600}	absorption at 600 nm
CMC	critical micellar concentration
CSD	Cambridge Structural Database
DMSO	dimethylsulfoxide
dNTP	desoxynucleosidtriphosphate
DTT	dithiothreitol
E. coli	*Escherichia coli*
ECY2	unmodified *E. coli* $tRNA^{Tyr}$
EDTA	ethylenediamintetraacetate
ff	force field
h	hour
HEPES	2-[4-(2-hydroxyethyl)piperazino]ethansulfonic acid
IPTG	isopropylthio-β-galactosid
K	Klevin
kb	kilo bases
kDa	kilo Dalton
K_i	competitive inhibition constant
K_m	Michaelis Menten constant
Km	kanamycin
M	molarity ($mol \cdot l^{-1}$)
MD	Molecular dynamic
MES	2-morpholinoethansulfonic acid
min	minute
NMR	nuclear magnetic resonance
NPT	isobar-isothermes Ensemble; N, p, and T constant
NTP	nucleosidtriphosphate
PAGE	polyacrylamide gel electrophoresis
PAMPA	parallel artificial membrane permeability assays
PEG	polyethylenglycol
PCR	polymerase chain reaction

PDB	protein data bank
PMR	Particle Mesh Ewald
$preQ_0$	7-cyano-7-deazaguanine
$preQ_1$	7-aminomethyl-7-deazaguanine
Q	7-(((4,5-cis-dihydroxy-2-cyclopenten-1-yl)amino) methyl)-7-deazaguanosine
QueA	S-adenosylmethionine:tRNA-ribosyltransferase-isomerase
QueTGT	TGT involved in Q modification
SDS	sodiumdodecylsulfate
S. flexneri	*Shigella flexneri*
TCA	trichloroacetic acid
TGT	tRNA-guanine transglycosylase
TIM-barrel	triose-phosphate isomerase (TIM) / $(\beta\alpha)_8$ barrel
T. maritima	*Thermotoga maritima*
Tris	tris-(hydroxymethyl)-aminomethane
w/v	weight per volume
WT	wild type
YadB	glutamyl-queuosine $tRNA^{Asp}$ synthetase
Z. mobilis	*Zymomonas mobilis*

Table of contents

1 Introduction and Motivation

1.1 Drug design and TGT

The process of drug discovery and drug development has changed significantly in the history of humankind, especially in the last decades mainly due to the more detailed available information about cellular processes and the increase in computational power.

Earlier, medical plants were used after their potential was discovered by chance and the knowledge was passed on for generations. Later on, the extraction of drug molecules from medical plants, e.g. alkaloids, and microorganisms, e.g. penicillin, changed the understanding of drug activity. Small molecules were discovered as active compounds and consequently the relationship between structure of the small molecule and its activity was the main focus of interest. Today, not only the discovery of small molecules is supported by computational methods, additionally the optimization of e.g. bioavailability and selectivity are of utmost importance. The use of computational methods provides several new strategies, e.g. ligand or structure based approaches to create or improve drugs.

In March 2009, 56066 structures were deposited in the protein data bank (PDB; http://www.rcsb.org) derived from protein crystallography or NMR. The enormous amount of protein crystal structures in the last years facilitates the discovery and optimization of drugs. On the one hand, direct information can be gained from new complexes. In combination with affinity data the key interactions, important for the potency of the inhibitor, can be identified between ligand and protein.

On the other hand structural information about a protein which is not yet crystallized can be gained from homologous proteins. Today, the knowledge from the complex structures is the fundament for various strategies in the design of new drug candidates, e.g. pharmacophore or hotspot generation is based on the physico-chemical character of the protein surface.

A further possibility are ligand based approaches; here the information from large series of known drug candidates and their characteristics is used. Properties like binding affinity to a certain target or penetration through membranes can be capitalized for the invention or the optimization of candidates.

The enzyme TGT (tRNA-guanine transglycosylase) is a putative target to develop new selective antibiotics against *Shigella*, the causative agent of bacterial dysentery.

Supported by computational methods the discovery of structurally very different candidates, that are capable to inhibit TGT, was possible. [1-5] Many drug candidates were suited for crystallization in complex with TGT from *Zymomonas mobilis*. The interpretation of the successfully obtained complexes in combination with kinetic data is ideal for an ongoing optimization of the candidates in terms of high binding affinity and improved bioavailability. Finally, the improved drug candidate could become a potent antibiotic against *Shigella*, reducing the symptoms of bacterial dysentery.

1.2 Aim of the project

The aim of this PhD thesis was the development and/or optimization of TGT inhibitors and the investigation of the catalytic active complex of TGT and its substrate tRNA.

In the process of TGT inhibitor design and evaluation several different aims were tackled:

- *In silico* p*K*a calculations were used to explain charge assisted hydrogen bonds in protein-ligand complexes and their effect on binding affinity (section 2).
- The analysis of water molecules in the protein binding pocked delivered new ideas for the decoration of the lead structure and improved the docking solutions and binding affinities significantly (section 3).
- Based on molecular dynamic simulations, side chain flexibility of inhibitors was studied and an entropic contribution to the free binding energy was discovered (section 4).
- The membrane permeability of known inhibitors was calculated. Based on these data, functional groups were exchanged and the newly derived compounds showed improved membrane permeability (section 5).
- Details about ligand induced changes in the conformation of the protein´s homodimer interface were discovered and studied (section 3). The results deliver a new way to inhibit TGT (section 8).
- A fragment-based screening using DrugScoreFingerPrints discovered new lead structures showing an inhibition constant in the low micromolar range (section 6).

In addition the catalytic complex of TGT and tRNA was studied in detail. Site directed mutagenesis was used to alter the interaction in the dimer interface of TGT dimer and

tRNA binding site (section 8). Based on kinetic data and nanoESI-MS experiments the catalytic active complex of TGT was studied in detail.

1.3 Shigellosis

1.3.1 Disease and treatment

Shigellosis or bacillary dysentery, an acute inflammatory bowel disease, is caused by bacteria of the genus *Shigella*. After an oral uptake of the bacteria and the consecutive passage through the stomach and small intestine, the bacterium finally reaches the colon. In the colon, the bacterium invades the epithelium and the mucosa. This results in a destructive recto-colitis which is responsible for the dysenteric symptoms like watery and bloody diarrhea, fever, intestinal cramps, and rectal pain. [6]

The infection is transmitted by contaminated water, unsafe food, dirty hands, and vomit or stools of sick people. An uptake of only 10 bacteria is sufficient for an infection with *Shigella*. Lately published numbers estimates the *Shigella* disease burden at 165 million episodes and about 1 million deaths per year, predominantly in developing countries. [7] Additionally, about 500 000 infections with *Shigella* are reported each year among military personnel and travelers from industrialized countries. Humanitarian problems of the third world like natural disasters, civil wars, and refugee camps, in combination with poor water and food supply and a fragile constitution of the people facilitate the outbreak of the disease. The dehydration caused by water stools is especially dangerous for children under 4 years.

The World Health Organization (WHO) proposes an antibiotic treatment with ciprofloxacin and the replacement of water and electrolytes. An increasing problem is the multidrug resistance against, e.g., fluoroquinolones.

From epidemic areas, an immunity of patients after an overcome infection is reported, which comforts the development of a vaccine. In the group of Philippe Sansonetti at the Institute Pasteur the development of a vaccine is in process. [8] Lately, a successful clinical trial was performed with a *Shigella dysenteriae* 1 strain attenuated by deletion of photogenic genes (*icsA* (1.3.4), ion chelation (*ent*, *fep*), and shiga toxin (1.3.2)).

1.3.2 Shigella – Escherichia relationship

The genetic analysis of *Shigella* discovered, that the bacterium belongs to the family of Enterbacteriaceae and is strictly speaking not a separate genus. [7, 9] In 1898, the Japanese

bacteriologist Kiyoshi Shiga isolated the pathogen of bacteria dysentery. The bacterium is named after its discoverer and can be subdivided in 4 species:

Shigella dysenteriae (16 serotypes)

the most pathogen subtype of Shigella bacteria. It produces the potent cytotoxin (Shiga toxin) and is common in tropic regions

Shigella flexneri (6 serotypes)

an infection with this subtype is less fatal than an infection with *S. dysenteriae*. The bacterium appears worldwide

Shigella sonnei (1 serotype)

is the most common species in middle European countries and is responsible for most of the dysentery in summer times among children

Shigella boydii (8 serotypes)

only few infections in the Middle East are reported and usually the etiopathology is rather harmless compared to an infection with the three other subtypes

1.3.3 Cellular and molecular pathogenicity

After passing the stomach and small intestines *Shigella* infects the cells of the colon causing severe dysentery. *Shigella* is not able to enter the mucosa cells from the basolateral side, it invades indirectly via M cells (Figure 1.1). The M cells are specialized to transport antigens, e.g. bacteria, through the colon epithelium and present them to macrophages. Both are located in follicle-associated epithelia (FAE), which is responsible for intestinal immunity. It is remarkable that *Shigella* can enter the M cell associated macrophages without being damaged. After phagocytic uptake by the macrophage, they escape from the phagosome. Inside the macrophages they induce apoptosis and together with inflammatory interleukins (IL, e.g. IL-1β and IL-18) they are released into the mucosa. [6, 9] The liberation of IL attracts granulocyts to the scene, leading to a disruption in the integrity of the epithelial barrier and facilitates further *Shigella* invasion from the colon. From the basal side the bacteria can enter the mucosa cells and spread from cell to cell, without being detected by the immune system.

For the macropinocytotic uptake and transport to adjacent mucosa cells *Shigella* exhibits a set of virulence factors, which are controlled by VirF and VirB. These virulence factors are used to reprogram the cellular machinery of epithelial as well as immune cells by activating innate transport and signaling pathways. [10, 11] For the invasion into an epithelial

cell a tube like secretion apparatus is formed by *Shigella*. Upon contact to eukaryotic cells IpaB and IpaC are forming a pore through the membrane of the host cell. The flux of protein through the pore is controlled by IpaB and IpaD. The contact of IpaC with the host cell induces early events of actin polymerization via its C-terminal domain leading to an uptake of the bacterium into the eukaryotic cell.

After the uptake into the cytoplasm the intracellular mobility is controlled by the virulence factor VirG (IcsA). VirG is responsible for the actin-based mobility of *Shigella* and allows the passage from one cell to another.

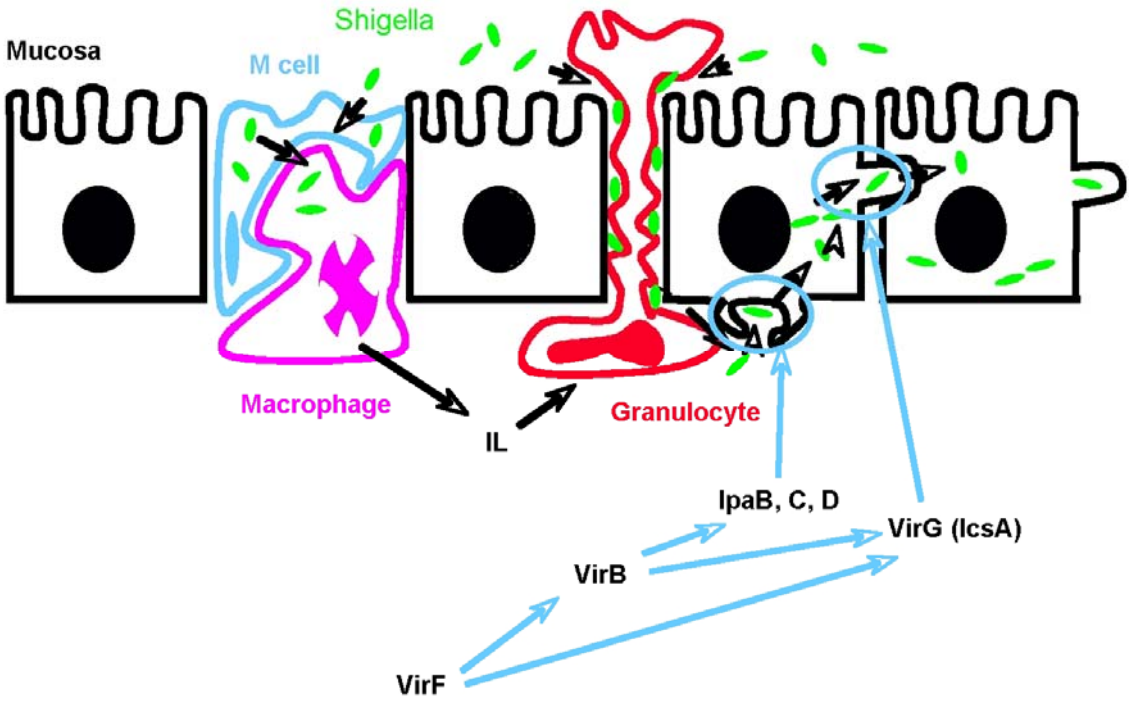

Figure 1.1 *Pathway of epithelial colonization and disintegration and macropinocytotic uptake of Shigella (figure from* http://sitemaker.umich.edu/garcia.lab/home)

1.3.4 The key role of VirF - regulation of pathogenicity

Pathogenic *Shigella* bacteria exhibits a virulence plasmid (214 kb) were the genetic information of the hierarchically organized sets of virulence factors is located. The sequence of the virulence plasmid is known for the subtype *S. flexneri*. [12] VirF and VirB are the key transcription activators for virulence gene expression (Figure 1.1). Expression of VirF directly activates the transcription of virulence factor genes *icsA* and *virB*. The

virB-gene product then activates the transcription of the *ipa*B-, C-, and D-genes. Based on this assembly VirF is in the controller of pathogenicity regulation.

The regulation of VirF depends on several factors like temperature, pH, osmolarity, and nutrition factors.[13] Additionally, the expression level is limited by the amount of modified tRNA which is mandatory for an efficient translation at the ribosome. In a gene knock-out experiment, where the modification of tRNA molecules was avoided, a significantly reduced virulence of *Shigella* was observed.

The tRNA molecules are modified in two positions. The first introduced mutation is performed by the *miaA* gene product in position A37 and the second modification is executed by the *tgt* / (*vacC*)-gene product. The *tgt* / (*vacC*)-gene product catalyzes the incorporation of a queuine precursor 34 into tRNA. Mutation of the *miaA* gene reduces the VirF level to 10%, and the haemolytic activity to 10 - 20% compared to the wild type and the mutation of the *tgt*-gene reduces both, VirF level and haemolytic activity, to 50 - 60% of the wild type. [14,13, 15] The gene product of *tgt* form E.coli – tRNA-guanine transglycosylase (TGT) – is characterized in detail. In addition the crystal structure of *Zymomonas mobilis* TGT, which is structurally nearly identical to *S. flexneri*, is available. This can be used for the design and optimization of putative drug candidates and the discovery of a new selective antibiotic against bacterial dysentery.

1.3.5 Procaryotic queuosin pathway

The post-transcriptional modification of proteins, DNA, and RNA is an essential step in cell processing. The modification of tRNA in position 34 with queuosine is one of the best described modifications. Nearly all prokaryotes are able to modify tRNA, only a few organisms are not suited for queuosin synthesis (*Saccharomyces cervisiae* and the eubacterial sterotypes of Actinobacteria: *Mycobacerium*, *Corynebacerium*, *Streptomyces*, *Bifidobacterium*).

In prokaryotic organisms the biosynthesis of queuosine starts with the modification of guanosine triphosphate (GTP) (Figure 1.2). In several consecutive steps, catalyzed by queC-, queD-, queE-, and queF-gene products, GTP is modified to $preQ_0$ and finally to $preQ_1$. [16, 17] The role of QueC is studied in detail, whereas the roles of queD- and queE-gene products are still unclear. [18] QueF is an NADPH-depending enzyme, which catalyzes the reduction of $preQ_0$ to $preQ_1$. [19] In the next step, TGT catalyzes the exchange of guanine by the modified base $preQ_1$ in the wobble position 34 of the anticodon loop of

tRNA. [20] [21] The anti codon recognized by TGT consist of $G_{34}U_{35}N_{36}$ (N = A, C, G, U) leading to a selective modification of four tRNA molecules.

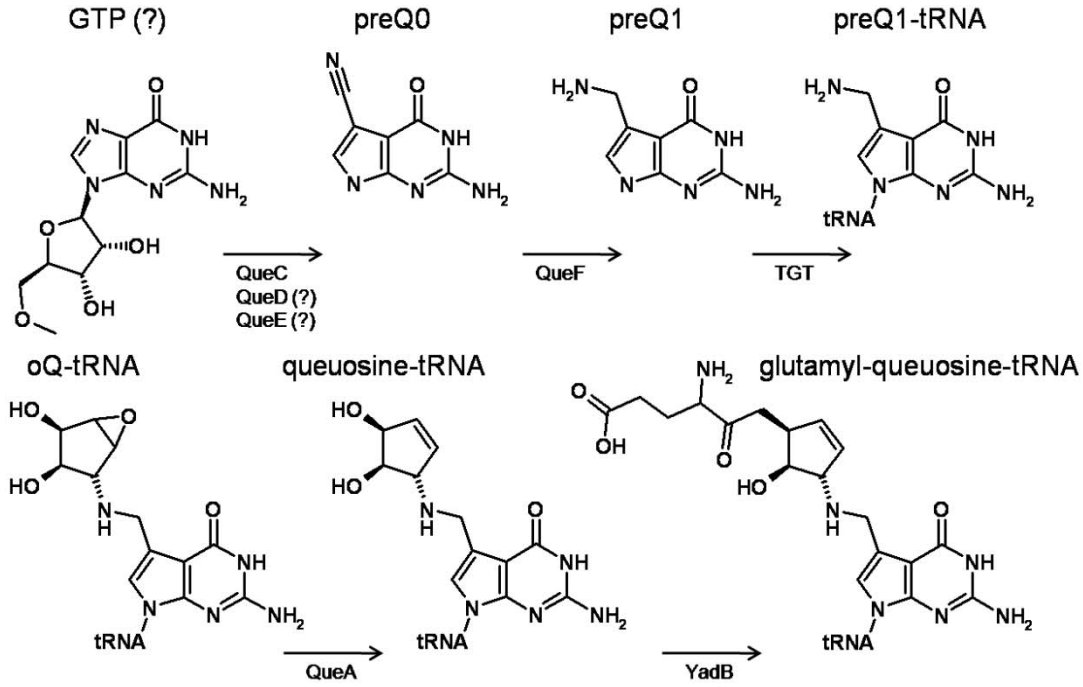

Figure 1.2 *queuine modification pathway in prokaryotic organisms (which OH-group is glutamylated is not known)*

These tRNAs are coding for the amino acids asparagines, aspartate, histidine, and tyrosine. Subsequently, the incorporated $preQ_1$ is further modified to epoxyqueuosine and finally to queuosine. [22, 23] The primary step is performed by QueA, which transfers a ribosyl moiety from S-adenosylmethionone to $preQ_1$, followed by a second step, where a cofactor B12-depending enzyme reduces epoxyqueuosine to queuosine. [20, 24] In some organisms a further modification of queuosine to the glutamyl-queuosine, which has a rather short half-life, was discovered.

In contrast to prokaryotic organisms, the assembly of queuosine from GTP in eukaryotes is not possible. The supply of queuosine comes from food or bacteria commensals. Modification of tRNA molecules are performed in a single step reaction, by eukaryotic TGT, which uses queuosine as substrate. Further modifications are glycosylations of the hydroxyl groups by unknown enzymes. [23, 25-28]

1.4 Mechanism of TGT

The assembly of the base exchange reaction follows a ping-pong mechanism. [29] Initiated by a nucleophilic attack of Asp280 towards the C_1 atom of ribose 34 in tRNA $^{Asn, Asp, His, Tyr}$ (Figure 1.3 a), a covalent intermediate is produced without breaking the phosphodiester backbone of tRNA (Figure 1.3 b). The formation of the covalent intermediate benefits from a 40° rotation of ribose 34 (induced by the bonds to phosphorous 34 and phosphorous 35), which weakens the bond between ribose and guanine. Guanine 34 is cleaved from the tRNA backbone and subsequently reprotonated before leaving the binding pocket. The vacant binding site now provides access for the modified base $preQ_1$.

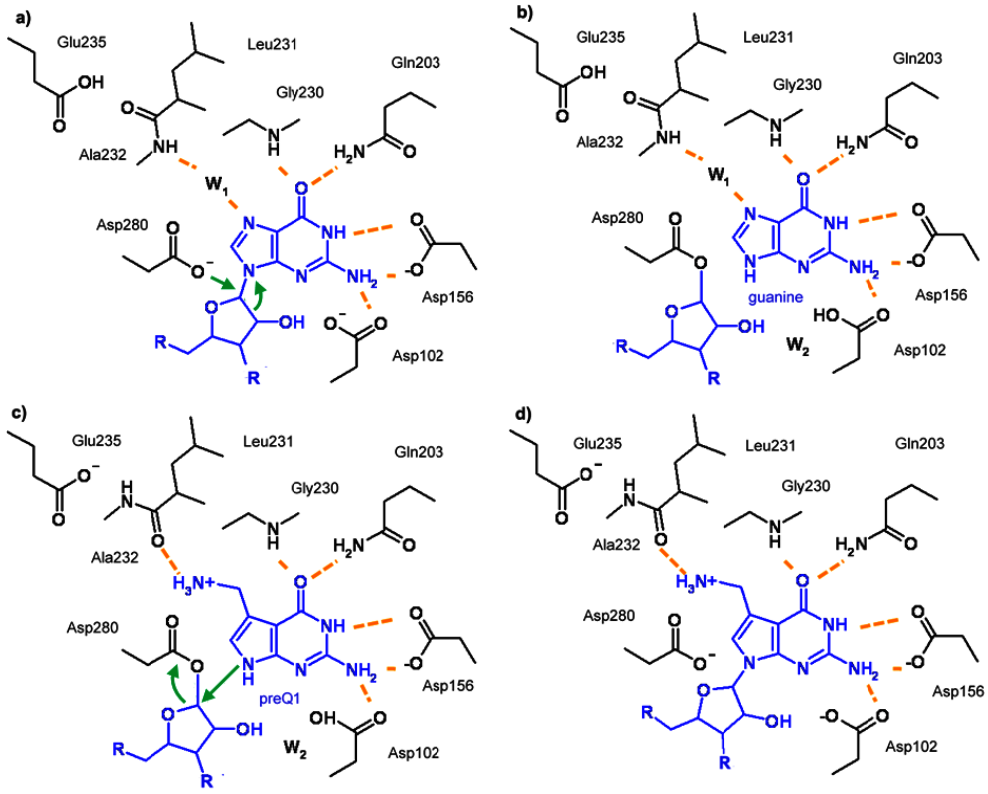

Figure1.3 *Base exchange mechanism in prokaryots*

This nucleobase exhibits an extracyclic amino function which replaces a water molecule previously mediating an interaction between protein and guanine (Figure 1.3 b/c). In due course of the mechanism, a flip of the peptide backbone is necessary to exchange the binding-site exposed hydrogen bonding facility from a donor to acceptor group to correctly recognize the new substrate. The peptide bond between Leu231 and Ala232 rearranges and performs an interaction via its carbonyl group to the extracyclic amino

function of $preQ_1$. As a controller of the peptide flip a carboxyl group of Glu235 was identified. [30] Depending on the orientation of the peptide backbone Glu235 acts as acid or base. A covalent bond between $preQ_1$ and tRNA is formed supported by a repulsive interaction between ribose 34 and Val45/Leu68, which moves the ribose towards $preQ_1$ and reduces the distance between ribose and modified base (Figure 1.3 d). The modified tRNA is released from the catalytic site. The described reaction path includes protonation and deprotonation steps of the guanine/$preQ_1$, a possible donor/acceptor of the proton is Asp102 and a close-by water molecule.

1.5 Structure of TGT

1.5.1 Folding and dimer formation

As the protein of the pathogenic organism *S. flexneri* is difficult to crystallize, the better crystallizing enzyme from *Zymomonas mobilis* is mainly used. It exhibits an active site of almost identical composition. Only Phe106 is exchanged by Tyr.[1, 31]

TGT adopts a folding comparable to the highly populated triose-phosphate isomerase (TIM)-type $(\beta\alpha)_8$-barrel fold (Figure 1.4). Two insertions (insertion beta7-alpha6 and the zinc binding site) are responsible for the recognition of the substrate. [32] The active site of TGT is located at the C-terminal end of the TIM-barrel scaffold and recognizes specifically the trinucleotide sequence $U_{33}G_{34}U_{35}$. [33, 34, 35]

A detailed analysis of TGT structures from different species in addition with a sequence alignment proposed that the catalytic form of TGT is a homodimer. [5, 29] The two monomers are associating with a 2-fold symmetry. Interactions between residues of the two monomers are conserved over most prokaryotic species. From the TIM-barrel side of the interface Lys52, Leu74, Pro78, Phe92 are forming interaction to Tyr330', His333', Leu334', Glu339', Leu345' from the zinc-binding domain. Additionally, residues with similar properties are located in position 49 (Gly/Ala), 50 (Thr/Ser/Cys), 326 (Phe/Tyr/Trp), 329 (Ala/Ser), and 341 (Leu/Phe).

A crystal structure with a tRNA stem loop is available and was used to superimpose a tRNA molecule. The received picture proposes that one tRNA molecule is binding to a TGT dimer, whereas one active site executes the base exchange reaction and the second monomer stabilizes the binding of the substrate. The key role in stabilizing the transient complex of TGT and tRNA would explain the location of several positively charged residues on the surface of TGT in the area of insertion beta7-alpha6. They can form

strong interactions to the negatively charged phosphate groups of the tRNA backbone (section 8).

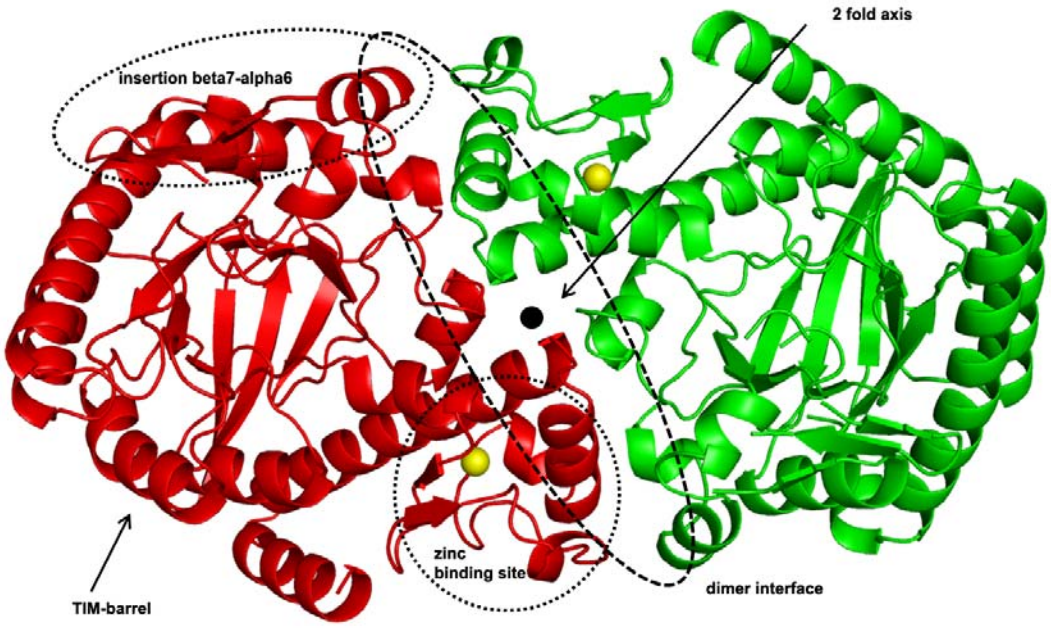

Figure 1.4 *Structural elements of TGT dimer*

1.5.2 Active site of TGT

To recognize and bind the phosphate-ribose backbone of the large substrate a channel is located on the surface of TGT. The nucleobases uracil 33, guanine 34, and uracil 35 are identified and fixed in cavities next to this channel. Uracil 33 and 35 are bound in a rather flat, solvent exposed binding pocket. In contrast, the guanine binding pocket is very deep. Several hydrogen bonds are formed to Leu231, Ala230, Gln203, Asp156, and Asp102 along with a pronounced parallel π-stacking to Tyr 106 flanking the binding site.

A variety of structural diverse inhibitors were crystallized in complex with TGT at different pH conditions. Two main differences were observed in the active site of TGT depending on the functionalities of the inhibitior or the applied pH conditions: A flip of the peptide backbone between Leu231 and Ala232 is known, leading to a bivalent characteristic in these areas of the binding site. Depending on the pH value the side chain of Asp102 can adopt two conformations. Additionally, the functionality of an inhibitor in the guanine binding site can lead to a rotation of Asp102 when no suitable interaction partners for the carbonyl group are available.

2 Crystal structure analysis and in-silico p*K*a calculations suggest strong p*K*a shifts of ligands as driving force for high affinity binding to TGT

All compounds presented in this section were developed in cooperation with Dr. Simone Hörtner (group of Prof. Dr. François Diederich, ETH Zurich, Switzerland).

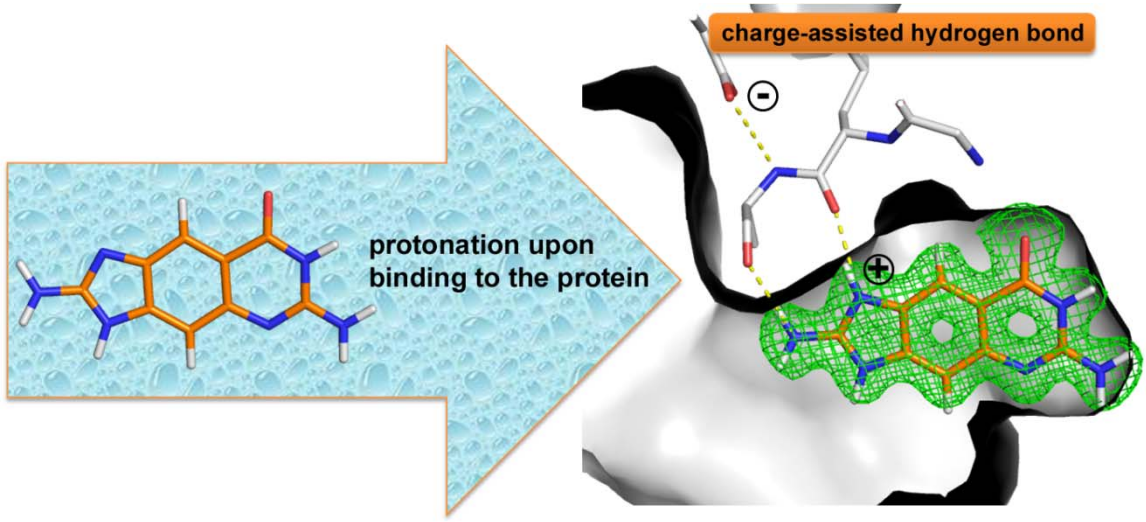

2.1 Abstract

A novel ligand series is presented to inhibit tRNA-guanine transglycosylase (TGT), a protein with a significant role in the pathogenicity mechanism of *Shigella flexneri*, the causative agent of Shigellosis. The enzyme exchanges guanine in the wobble position of tRNA $^{Asn,\ Asp,\ His,\ Tyr}$ against a modified base. To prevent the base exchange reaction, several series of inhibitors have already been designed, synthesized, and tested. One aim of previous studies was to address a hydrophobic pocket with different side chains attached to the parent skeletons. Disappointingly, no significant increase in binding affinity could be observed which could be explained by the disruption of a conserved water cluster. The ligand series examined in this study are based on the known scaffold *lin*-benzoguanine. Different side chains were introduced leading to 2-amino-*lin*-benzoguanines which address a different pocket of the protein and avoid disruption of the water cluster. With the introduction of an amino group in 2-position, a dramatic increase in binding affinity can be experienced. To explain this significant gain in binding affinity,

Poisson-Boltzmann calculations were performed to explore pK_a changes of ligand functional groups upon protein binding, they can differ significantly going from aqueous solution to protein environment. For all complexes, a permanent protonation of the newly designed ligands is suggested leading to a charge-assisted hydrogen bond in the protein-ligand complex. This increased strength in hydrogen bonding takes beneficial effect on binding affinity of the ligands resulting in low nanomolar binders. Crystal structures and docking emphasize the importance of the newly created charged-assisted hydrogen bond. A detailed analysis of the crystal structures in complex with substituted 2-amino-*lin*-benzoguanines indicate pronounced disorder of the attached side chains addressing the ribose 33 binding pocket. Docking suggests multiple orientations of these side chains. Obviously, an entropic advantage of the residual mobility experienced by these ligands in the bound state is beneficial and reveals an overall improved protein binding.

2.2 Introduction

During post-transcriptional modification, the prokaryotic enzyme tRNA-guanine transglycosylase (TGT, EC 2.4.2.29) catalyzes the exchange of guanine by the modified base preQ$_1$ (7-methylamino-7-deazaguanine) at the wobble position 34 of the anticodon loop of tRNA $^{Asn, Asp, His, Tyr}$ (Scheme 2.1).[36]

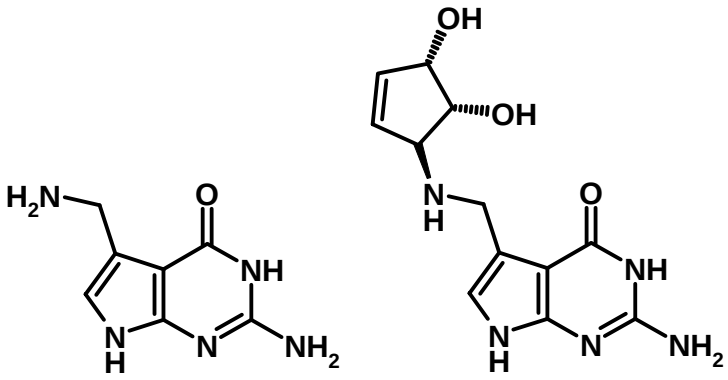

Scheme 2.1 *Structure of preQ$_1$ which replaces guanine 34 in the wobble position of the modified tRNA $^{Asn, Asp, His, Tyr}$ during the base exchange reaction of TGT. The precursor preQ$_1$ is further modified to queuine.*

Subsequently, the incorporated preQ$_1$ is further modified to queuine (7-(((4,5-*cis*-dihydroxy-2-cyclopenten-1-yl)amino)methyl)-7-diazaguanine) involving further enzymes in the biochemical pathway. The resulting tRNAs play a significant role in developing

pathogenicity of *Shigella flexneri***,** the causative agent of Shigellosis. Shigellosis is responsible for about 165 million infections and causes more than 1 million fatalities each year. A high rate of incidences is observed among children at the age of 1 to 4, predominantly in developing countries with poor hygienic conditions and unsafe water supplies. [7, 37] Increasing problems, with respect to an administered drug therapy, arise due to plasmid encoded resistances against most common antibiotics and due to the lack of effective vaccines. In previous studies, the TGT gene of *S. flexneri* was knocked out leading to a significantly decreased infection rate.[15] As an alternative prospective, we embarked upon the development of Shigella-specific antibiotics that prevent the evolvement of pathogenicity.

The bacterium carries a virulence plasmid as source of its pathogenity which encodes for a variety of virulence factor genes. Essential for the regulation of the pathogenicity-developing process of *Shigella* is the expression of the virulence factor VirF which activates directly the transcription of further virulence genes such as *icsA* and *virB*. [13] The modified tRNAs are required for an efficient translation of virF-mRNA at the ribosome. Reducing the amount of modified tRNA by preventing the base exchange reaction provides a novel strategy for an antibiotic therapy. The bacterium is blocked from access of the endothelial cells, prerequisite to create pathogenicity. This mode of action prevents irradication or any other influence in the function of the bacteria.

By means of structure-based drug design, we started the discovery of TGT specific inhibitors. As the protein of the pathogenic organism S. *flexneri* is difficult to crystallize, we performed all studies described in this contribution using the better crystallizing enzyme from *Zymomonas mobilis.* It exhibits an active site of almost identical composition. Only Phe 106 is exchanged by Tyr.[1]

TGT adopts a folding comparable to the highly populated triose-phosphate isomerase (TIM)-type $(\beta\alpha)_8$-barrel fold. Two insertions are responsible for the recognition of the substrate. [32] The active site of TGT is located at the C-terminal end of the TIM-barrel scaffold and recognizes specially the trinucleotide sequence $U_{33}G_{34}U_{35}$. [33 34 35] Uracil 33 and 35 are bound in a rather flat, solvent exposed binding pocket. In contrast, the guanine binding pocket is very deep. Several hydrogen bonds are formed to Leu231, Ala230, Gln203, Asp156, and Asp102 along with a pronounced parallel π-stacking to Tyr106 flanking the binding site (Figure 2.1 left).

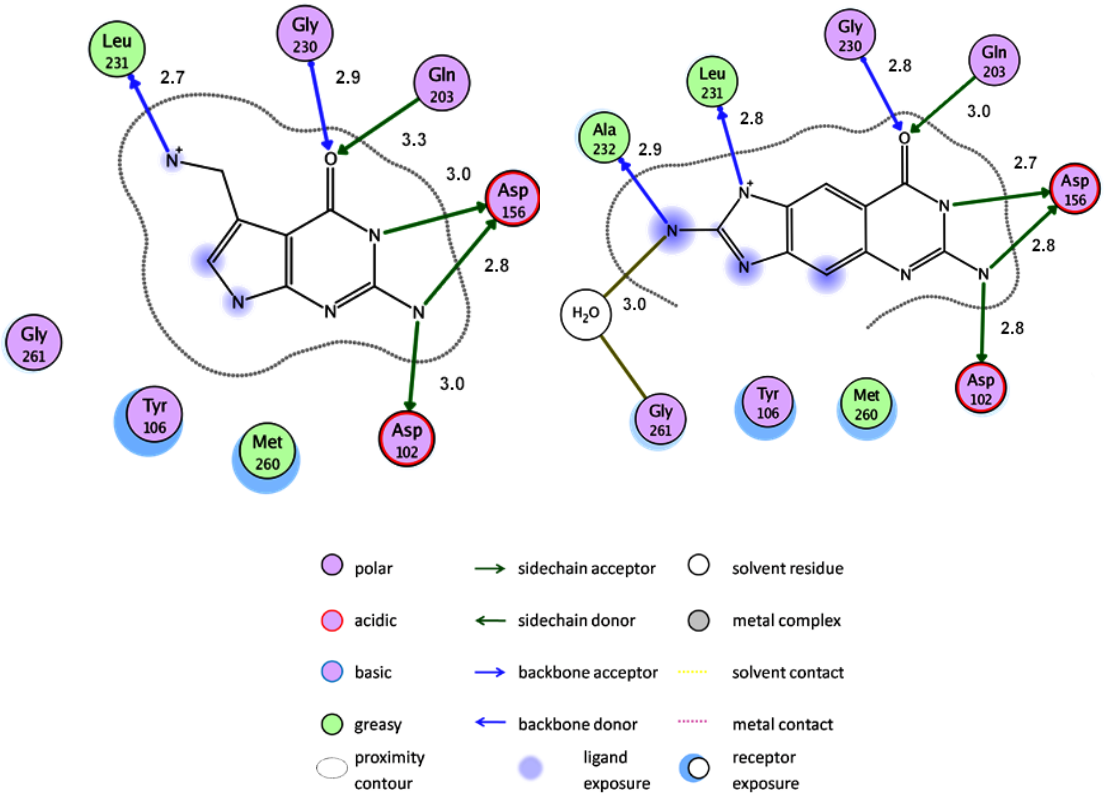

Figure 2. 1 *Schematic interaction pattern derived by MOE [38, 39]. For clarity the hydrogen atoms are not shown. Left: preQ$_1$ (pdb-code: 1P0E) in the guanine binding pocket. The protonated exocyclic amino function of the modified base forms a hydrogen bond to Leu231 (2.7 Å). A hydrogen bond network between the pyrimidine ring and Gly230, Gln203, Asp156 and Asp102 (bond length in Å) is responsible for the recognition of the modified base. Right:* **5** *in the guanine binding pocket with two hydrogen bonds between the newly introduced guanidinum group and Leu231 (2.8 Å) and Ala 232(2.9 Å) of TGT. The positive charge, which is delocalized through the conjugated system of the guanidinium moiety is presented on N1 forming a charged assisted hydrogen bond to Leu231. Furthermore, the ligand is fixed in the binding pocket by the above described hydrogen bonds to Gly230, Gln203, Asp156, and Asp102 (bond length in Å). Mediated by a water molecule, an additional interaction to Gly261 is observed.*

The pathway of the base exchange reaction follows a ping-pong mechanism. Initiated by a nucleophilic attack of Asp 280 towards C_1 of ribose 34, a covalent intermediate is produced without breaking the phosphodiester backbone of tRNA.[40, 41] Simultaneously, guanine 34 is cleaved from the tRNA backbone leaving the binding pocket, subsequently. The vacant binding site now provides access for the modified base preQ$_1$ (Scheme 2.1). This nucleobase exhibits an extracyclic amino function which replaces a water molecule previously mediating an interaction between protein and guanine. In due course of the mechanism, a flip of the peptide backbone is necessary to exchange the binding-site

exposed hydrogen bonding facility from a donor to acceptor group to correctly recognize the new substrate.

The peptide bond between Leu 31 and Ala232 rearranges and performs an interaction via its carbonyl group to the extracyclic amino function of $preQ_1$ (Figure 2.1 left). A covalent bond between $preQ_1$ and tRNA is formed and the modified tRNA is released from the catalytic site. The described reaction path requires Asp102 and a close-by water molecule as general base.

Taking into account the physico-chemical properties of the guanine-binding site, several lead structures have been designed and synthesized. Pyridazinones, pteridines, and quinazolinones emerged as promising scaffolds (Table 2.1). In addition, a "stretched" guanine with an inserted central six-membered ring, leading to *lin*-benzoguanine (**3**), was suggested (Table 2.2). [4, 5, 42]

Table 2.1 *Inhibitors based on a quinazolinone scaffold and their measured binding affinity*

compound	structure	enzyme K_i
1	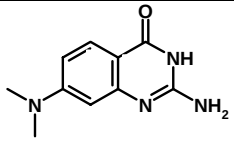	31 µM ± 10
2	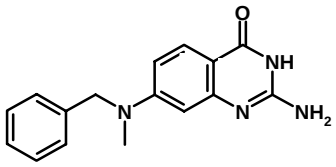	7.6 µM ± 3.7

All parent scaffolds are binding in the micromolar range. To improve their binding affinity, a hydrophobic subpocket composed by Val282, Leu68, and Val45 was addressed. Filling of unoccupied hydrophobic pockets with lipophilic side chains attached to the lead skeleton is an often used strategy in structure based drug design. Disappointingly, only an insignificant improvement in binding affinity towards TGT could be measured for inhibitors with a lipophilic side chain attached to the above-mentioned parent skeletons. A comprehensive study of crystal structures elucidated that the lipophilic vector disrupts a highly conserved water network between the catalytic aspartates (Figure 2.2). [5] This water network provides an essential contribution to the solvation of the two acidic residues.

Parallel to the synthesis of the inhibitors with the lipophilic vector, quinazolinones with a substitution in 7-position were prepared (Table 2.1). The introduction of a dimethylamino group produced **1** as two-digit micromolar inhibitor. Subsequent replacement of one methyl group by a benzyl moiety (**2**) resulted in a 4-fold increase in binding affinity. Obviously, introduction of the sterically more demanding lipophilic side chain did not result in a loss of affinity in this case. The crystal structure of **2** in complex with TGT that demonstrates the water network is not perturbed by the benzyl moiety. [43] Instead of addressing the small hydrophobic subpocket, the benzyl moiety binds most likely towards the region occupied by ribose 33 in the natural tRNA substrate as observed for the other ligands.

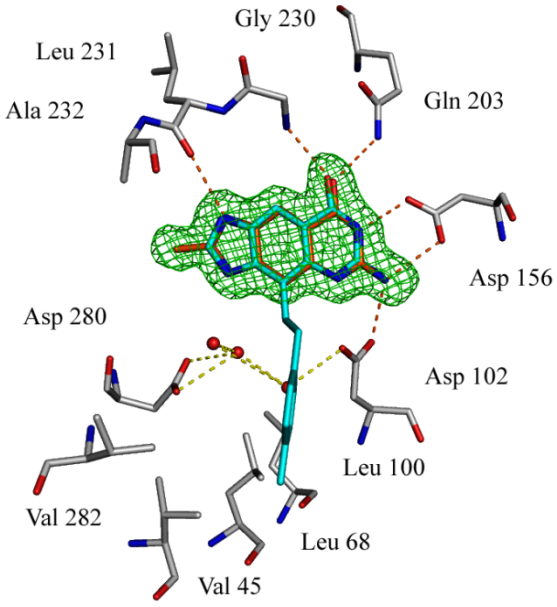

Figure 2.2 *TGT in complex with **4** (pdb-code: 3C2Y, carbon = gray, nitrogen = blue, oxygen = red). In the guanine binding pocket the 2-methyl-lin-benzoguanine skeleton of **4** (orange) fits perfect into the difference electron density (green). **4** is fixed in the binding pocket by several hydrogen bonds to the surrounding amino acids (orange dashes). Between the catalytically active aspartates three water molecules are bound (red; hydrogen pattern = yellow dashes). Superimposed is a ligand (pdb-code 1Y5W; carbon = cyan, nitrogen = blue, oxygen = red) with a hydrophobic side chain addressing a small hydrophobic subpocket created by Val282, Val45, Leu68, and Leu100. The hydrophobic side chain disturbs the water molecules between Asp102 and Asp280 upon binding.*

Stimulated by these promising results, we changed our design strategies now addressing the binding site of ribose 33 instead of the small hydrophobic pocket. This should avoid a disrupture of the water cluster network. *Lin*-benzoguanine was again chosen as parent scaffold, however now focussing on substitutents at 2-position.

The crystal structure of unsubstituted *lin*-benzoguanine in complex with TGT has been previously determined. [5] Its binding mode is similar to that of $preQ_1$ (Figure 2.1 left) and no interference with the water cluster network is observed. Additionally, substitution of *lin*-benzoguanine in 2-position provides the desired side chain orientation to address the ribose 33 subpocket. Several inhibitors with alkyl-, alkylamino- and arylalkylamino substituents were synthesized and tested. [42] The mixture of small and large side chains provided the possibility to experimentally investigate the influence of the side chain on the Gibbs free energy of binding.

Here, we present affinity data and crystallographic results of the newly designed inhibitors. In addition, we emphasize the introduction of a salt bridge between Leu231 and N1 of the inhibitor which finally bears nanomolar inhibitors.

2.3 Results and Discussion

2.3.1 Binding mechanism and affinity data

A series of 2-substituted *lin*-benzoguanines was synthesized and kinetically characterized (Table 2.2). Before the enzyme assay was performed, the binding mechanism was investigated by a trapping experiment. [29] For the newly synthesized inhibitors (**4**-**10**), a purely competitive binding mechanism was found. The inhibitors can only bind to TGT when no tRNA is bound. A simultaneous binding of inhibitor and tRNA, as detected for **3**, can be excluded. Obviously, substitution with a single methyl group in 2-position makes the skeleton already large enough to avoid any contemporaneous binding of tRNA and inhibitor.

The affinity is determined by the exchange rate of guanine against [8-^{3}H]-guanine in position 34 of $tRNA^{Tyr}$. The inhibitory constants are calculated based on the decrease of the initial velocity of the base exchange reaction in presence of the inhibitor. By introduction of a methyl group in 2-position (**4**) a 2.7 fold increase in binding affinity could be measured compared to the unsubstituted *lin*-benzoguanine (**3**). In an optimal situation, correct placement of a single methyl group can increase affinity up to 10 fold, particularly when the surface of the added methyl group is entirely buried. [44] Consulting

Table 2.2 *Structures of the inhibitors based on a lin-benzoguanine scaffold, and the corresponding inhibition constants determined by the enzyme assay, and pK_a values for the deprotonation of the imidazolium moiety in the parent scaffold*

name	structure	enzyme K_i	experimental pK_a [1)]	calculated pK_a [1)]	ΔpK_a shift [2)]
3	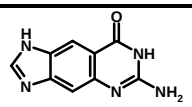	4.1 µM ± 1	5.2	7.2	2.0
4	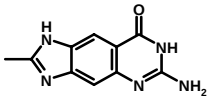	1.5 µM ± 0.4	5.4	7.5	2.1
5	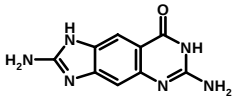	77 nM ± 12	6.3	8.3	2.0
6	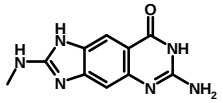	58 nM ± 36	6.2	8.6	2.4
7	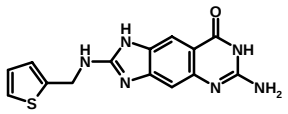	35 nM ± 9	5.8	7.4	1.6
8	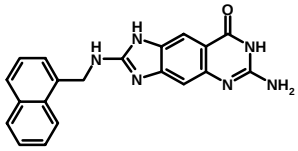	55 nM ± 11	5.9	7.0	1.1
9	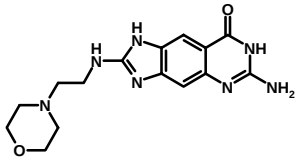	6 nM ± 6	5.2	6.5	1.3
10	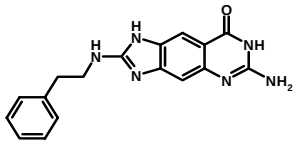	10 nM ± 3			

[1)] *For **3**-**9**, experimental pK_a values for imidazolium deprotonation were measured in aqueous solution and, additionally, the pK_a values of the inhibitors in complex with TGT were calculated.* [2)] *The shift of the pK_a values equals the difference between calculated and experimental ones.*

the crystal structure of **3**, the guanine binding pocked provides additional space for the methyl group.The addition of an amino group in 2-position creates a guanidinum-type moiety at our parent scaffold. From a synthesis point of view, it provides a convenient anchoring point to decorate the lead skeleton with a broad variety of side chains.

Surprisingly, a dramatic increase in binding affinity towards TGT was recorded upon replacement of the methyl by an amino group. A 20 fold higher affinity was measured for **5** compared to **4**. Subsequent addition of a further methyl group enhances affinity 1.3 fold. With larger substituents at the nitrogen, the affinity gradually improves towards one-digit nano-molar range, as achieved by **9** and **10** (Table 2.2). Referring to the previously determined crystal structure of **3** in complex with TGT the introduced guanidinum functionality offers the opportunity to form a hydrogen bond to the peptide backbone carbonyl group of Leu231. [42] Considering the basic character of a guanidinum group, a protonation of this functional group in the ligand appears most likely. In consequence there would be a positive charge created on this portion of ligands **5**-**10**. It will be delocalized through the conjugated system of the ligand and should provoke, due to charge assistance, an increasing strength of the hydrogen bond between the ligand and the carbonyl group of Leu231.

As a crude test of this hypothesis, the experimental pK_a-values of ligand **3**-**9** were determined in aqueous solution. [42] They actually point in the direction for increasing basicity. However, as not the situation in a water environment is of relevance of the present case and the protein environment can provoke pK_a shifts of several logarithmic units, Poisson-Boltzmann calculations within the binding pocket are performed based on our recently introduced *peoe_pb* (partial equalization of orbital electronegativities for Poisson-Boltzmann calculations) charges. [45]

2.3.2 In-silico pK_a calculation

The influences of specific charge distributions in protein binding sites are often ignored when protein-ligand interactions are analyzed. The aim of the pK_a calculation is to study the shift of the pK_a values of ligands upon protein binding.

For calculating the pK_a shifts, all residues within a radius of 12 Å around the guanine binding pocket were selected (Table 2.3). The protonation states of the considered amino acids are responsible for changes of the pK_a values of the ligands upon binding to the protein.

A first calculation of the unoccupied binding pocket at different *pH* values is necessary to study the protonation states of the participating residues (Table 2.3). The calculation only considers side chains where the protonation state might change under the applied *pH*

conditions (so-called titratable groups). The study was performed at three different *pH* conditions (5.5, 7.0, and 8.5). The results are listed in Table 2.3.

Table 2.3 *Calculation of pKa values of different titratable groups of TGT active site*

					pH 5.5			*pH* 7.0			*pH* 8.5
Residue[1)]	pK_a	prot[2)]	:	deprot[3)]	prot[2)]	:	deprot[3)]	prot[2)]	:	deprot[3)]	
Cys158	10.7	1.00	:	0	1.00	:	0	0.99	:	0.01	
Cys281	8.4	1.00	:	0	0.96	:	0.04	0.46	:	0.54	
Asp156	4.1	0.04	:	0.96	0	:	1.00	0	:	1.00	
Asp102	-0.4	0	:	1.00	0	:	1.00	0	:	1.00	
Asp280	1.7	0	:	1.00	0	:	1.00	0	:	1.00	
Lys125	10.3	1.00	:	0	1.00	:	0	0.98	:	0.02	
Lys264	12.2	1.00	:	0	1.00	:	0	1.00	:	0	
Glu157	4.9	0.18	:	0.82	0.01	:	0.99	0	:	1.00	
Glu235	2.7	0	:	1.00	0	:	1.00	0	:	1.00	
Tyr072	11.3	1.00	:	0	1.00	:	0	1.00	:	0	
Tyr106	11.6	1.00	:	0	1.00	:	0	1.00	:	0	
Tyr161	9.7	1.00	:	0	1.00	:	0	0.94	:	0.06	
Tyr258	14.4	1.00	:	0	1.00	:	0	1.00	:	0	

[1)] For the calculation of the pK_a values all titratable groups within a radius of 12 Å around the active site were determined (Cγ of Tyr106 was taken as origin of the selection). Each residue has an assigned pK_a value based on the modified peoe_pb charges. For each residue, the ratio of protonation vs. deprotonation at three different pH values (5.5, 7.0, and 8.5) is determined (a value of 1.00 corresponds to 100% protonation or deprotonation). [2)] Protonated form. [3)] Deprotonated form.

A value of 1.00 corresponds to 100% and a value of 0 to 0% protonation or deprotonation of a titratable group. The deprotonation of Asp102 and Asp280, as previously assumed for the catalytic reaction, was verified by the calculation for all three *pH* conditions. [32] The deprotonation of Asp280 allows the nucleophilic attack towards the ribose 34 C_1 atom during the base exchange reaction.

Recently, the importance of Glu235 as a trigger residue for the peptide flip of Leu231 was suggested.[5] Depending on the substrate bound in the guanine binding pocket, either the NH-group or the CO-group of Leu231 is facing the carboxyl functionality of Glu235 (Figure 2.3). Based on a pK_a value of 2.7 in the calculation, Glu235 would be considered as charged at all *pH* conditions while NH is facing Glu235 (Table 2.3). As mentioned, the pK_a values for the ligands were experimentally determined in aqueous solution. [42] A shift of approximately one logarithmic unit has been measured for the imidazolium or 2-

aminoimidazolium moiety comparing the *lin*-benzoguanines (5.2-5.4) and the 2-amino-*lin*-benzoguanines (5.8-6.3) (Table 2.2). The pK_a calculation for the complex structures is performed at *pH* 7. For the inhibitors, the experimentally determined pK_a values are taken as starting values. The calculation reveals, that upon complexation all pK_a values of the ligands are shifted towards basic range, overall by about 1.2 to 2.4 logarithmic units (Table 2.2). As described above, this shift suggests a permanent protonation of the ligands at the binding site under assay conditions (*pH* 7.3). The protonation of the guanidinum group creates a positive charge on this molecular portion. It increases the strength of the hydrogen bond between the imidazolium-type nitrogen of the ligand and the carbonyl group of Leu231. Towards the inner of the protein, the NH-group of the amide bond of Leu231 is stabilized by the deprotonated Glu235. The resulting arrangement suggests formation of a hydrogen bond with charge-assisted salt bridge character. The charged interaction enhances binding affinity of the 2-amino-*lin*-benzoguanines towards TGT.

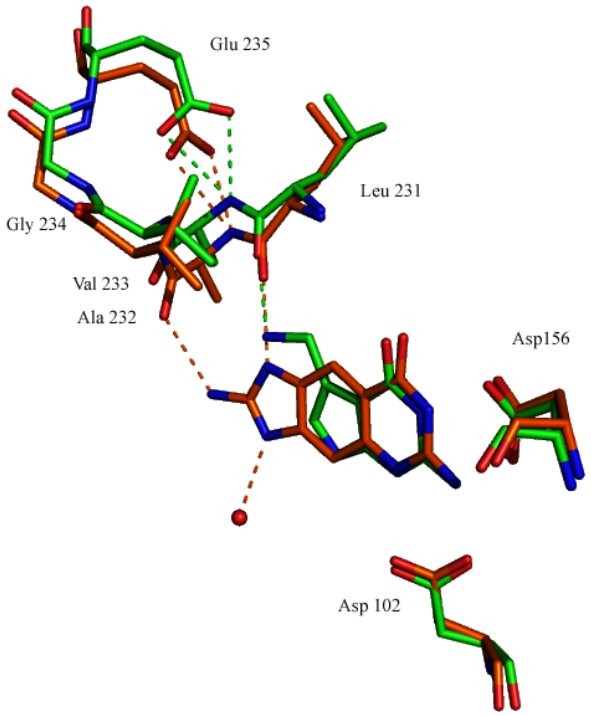

Figure 2.3 *Superposition of the TGT complexes with preQ$_1$ (pdb-code: 1P0E; carbon = green, nitrogen = blue, oxygen = red) and compound* ***5*** *(pdb-code: 2Z7K, carbon = orange, nitrogen = blue, oxygen = red). The shift in the backbone of the protein between the residues 230 and 235 is about 1 Å. The carbonyl group of Leu231 is orientated into the guanine binding pocket and a hydrogen bond between preQ$_1$ or* ***5*** *is formed (for* ***5****, additional hydrogen bonds to Ala232 and a close by water molecule W (red), which is part of the water cluster solvating the two catalytic aspatates side chains, are possible). The conformation of Leu231 is stabilized by the deprotonated Glu235. Hydrogen bonds in complex with preQ$_1$ are shown as dashed lines in green and for the complex with* ***5*** *in orange.*

2.3.3 Crystal structures

For the parent skeleton *lin*-benzoguanine and the modified 2-amino-*lin*-benzoguanines crystal structures in complex with TGT were determined (represented using **5** in Figure 2.1 right). The binding mode is similar to the one of $preQ_1$ (Figure 2.1 left). Accordingly, the peptide bond between Leu231 and Ala232 is found in its flipped orientation with the carbonyl group exposed towards the recognition site (Figure 2.3). For the newly synthesized compounds **4**, **5**, **7**, and **9**, binary complexes with Z. *mobilis* TGT could be obtained. The maximal resolution achieved by the structure determinations varies from 1.28 Å to 1.78 Å. Details about the refinement statistics are given in Crystal Data (Appendix 10.1) and information about the data collection can be found in Materials and Methods (section 9.2.7). The binding mode, previously discovered for **3,** is confirmed by **4**, **5**, **7**, and **9**. As expected, the water network between Asp102 and Asp280 is not disrupted. The peptide bond between Leu231 and Ala232 is flipped and the carbonyl oxygen forms a hydrogen bond to N1 of the ligand scaffold.For co-crystallization and soaking of TGT crystals two conditions have been discovered, one at *pH* 5.5 and another at *pH* 8.5. With respect to structures of TGT in complex with $preQ_1$ significant geometric differences, depending on *pH* conditions, have been observed. [30] At *pH* 5.5 (pdb-code 2Z1X), Asp102 is rotated to 75% into the guanine binding pocket whereas at *pH* 8.5 (pdb-code 2NQZ) the same residue is oriented to 100% out of the pocket. In order to evaluate whether the presence of a ligand can provoke the inwards orientation of Asp102, **7** was soaked into the apo crystal at a *pH* of 8.5. The observed electron density of **7** in complex with TGT discloses that Asp102 is actually rotated into the binding pocket. Obviously, a rotation of Asp102 is induced by the presence of the *lin*-benzoguanine scaffold. This is in contrast to previously studied protein-ligand complexes exhibiting different scaffolds. In all these examples, rotation of Asp102 towards the bound ligand was not observed at *pH* 8.5.For 2-methyl-*lin*-benzoguanine (**4),** a dataset with a maximum resolution of 1.78 Å could be collected. The above-described 2.7-fold increase in binding affinity compared to the unsubstituted *lin*-benzoguanine (**3**) can be ascribed to an additional efficient van der Waals contact to C_β of Ala232 (calculated with the program contacsym [46]) (Figure 2.4).By the introduction of the alkylamine substituent in 2-position, a dramatic increase of the binding affinity was observed. The analysis of the complexes with **5**, **9**, and **10** stresses an additional hydrogen bond to the carbonyl group of Ala232 exhibiting an average length of 2.8 Å (representatively shown for **5**, Figure 2.1 right, 2.5).

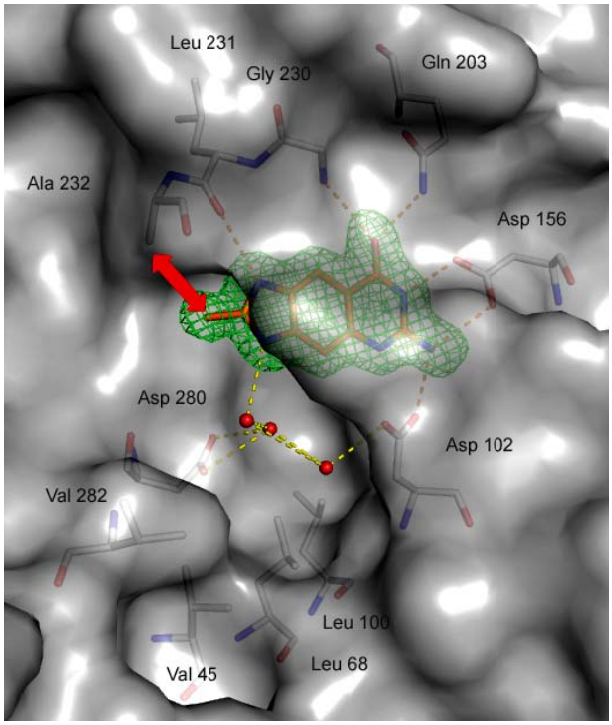

Figure 2.4 *Crystal structure of* ***4*** *in the binding pocket of TGT determined at 1.78 Å resolution. The solvent accessible surface of the protein is shown in gray. In addition some selected amino acids (carbon = gray, nitrogen = blue, oxygen = red) in the guanine binding pocket recognizing* ***4*** *are shown. The hydrogen bonds between TGT and 4 are highlighted by yellow dashed lines.* ***4*** *is contoured at 2.5 σ in the |Fo| - |Fc| density map (green) of the structural model refined without the ligand. The ligand (carbon = orange, nitrogen = blue, oxygen = red) is well depicted in the binding pocket. Several hydrogen bonds (orange dashes) are formed between the ligand and the protein. A short van der Waals interaction (3.3 Å, red arrow) between the methyl group in 2-position of the lin-benzoguanine scaffold and Cβ of Ala232 is present. In addition, three water molecules (red) are bound between Asp 102 and Asp280 (H-bonds: yellow dashes).*

Based on the performed *in-silico* pK_a studies, the protonation of **5**-**10** appears most likely. With the complexes of **5**, **7,** and **10**, this hypothesis has been further validated. A data set of TGT in complex with **5** could be collected to a maximum resolution of 1.28 Å. Based on the high resolution of this structure, a detailed picture of the protein could be obtained, indicating split conformations for several amino acids. The inhibitor in the guanine binding site is well defined and forms hydrogen bonds to Leu231, Ala232, Asp156, and Asp102 (Figure 2.5). The superposition of 2-amino-*lin*-benzoguanine (**5**) and preQ$_1$ in complex with TGT reflects a very similar hydrogen bond length towards the carbonyl group of Leu231 (2.7 Å preQ$_1$, pdb-code 1P0E; 2.8 Å **5**, pdb-code 2Z7K) (Figure 2.2, 2.3) although the inhibitor has no extracyclic amino function. In order to maintain the same distance, the backbone between residue 231 and 235 has been shifted towards the inhibitor and the hydrogen bond is formed to the nitrogen atom of the imidazole moiety

facing the CO-group of Leu231. In **7** (6-amino-2-[(thiophene-2-ylmethyl)-amino]-1,7-dihydro-imidazo[4,5-g]quinazolin-8-one), a thiophene-2-methylene moiety has been chosen as substituent to grow the inhibition skeleton towards the ribose 33 binding pocket (Figure 2.6a). Surprisingly, no properly defined electron density could be observed for the sulphur-containing ring system. At most, an ethyl group could be built into the electron density. The poorly-defined electron density indicates that the thiophene ring is probably scattered over multiple configurations. Taking the complex of TGT with bound tRNA as reference for the superposition with the present complex, it is possible to model the thiophene ring into the same region of the binding site as occupied by ribose 33 in the natural substrate (Figure 2.6a). This superposition suggests that the methylene spacer has the appropriate size to reach out into the ribose 33 binding pocket and to correctly place a terminally decorated thiophene moiety.Interestingly, the crystal structure shows a split conformation for Asp280 and Cys281 (Figure 2.6b). This observation is particularly surprising as Asp280 is involved a nucleophile in the catalytic mechanism. It might be possible that the thiophene ring perturbs to some degree the conformation of Asp280.

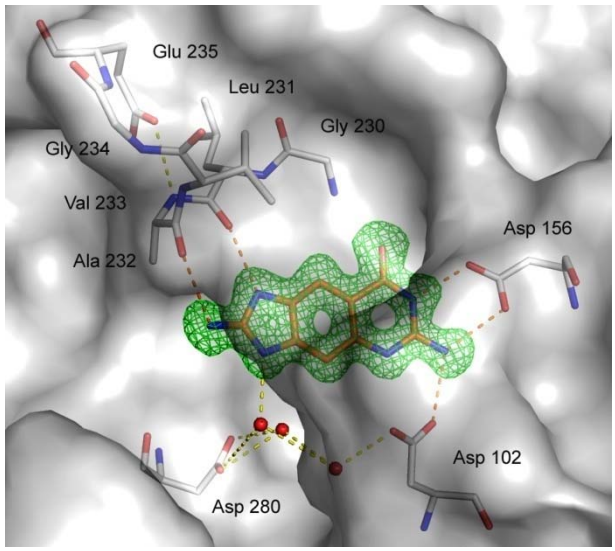

Figure 2.5 *Surface presentation (gray) of TGT in complex with* ***5*** *determined at 1.28 Å. In the guanine binding pocket* ***5*** *is shown in orange (carbon = orange, nitrogen = blue, oxygen = red) and the surrounding amino acids are shown in gray (carbon = gray, nitrogen = blue, oxygen = red). The* $|F_o|$ - $|F_c|$ *density map of* ***5*** *of the structural model refined without the ligand is shown at 2.5 σ (green). The inhibitor occupies completely the deep binding pocket of guanine. Several hydrogen bonds (orange dashes) are formed between* ***5*** *and the protein. Between the carboxyl groups of Asp102 and Asp280 three water molecules are placed (red, hydrogen bonds = yellow dashes).*

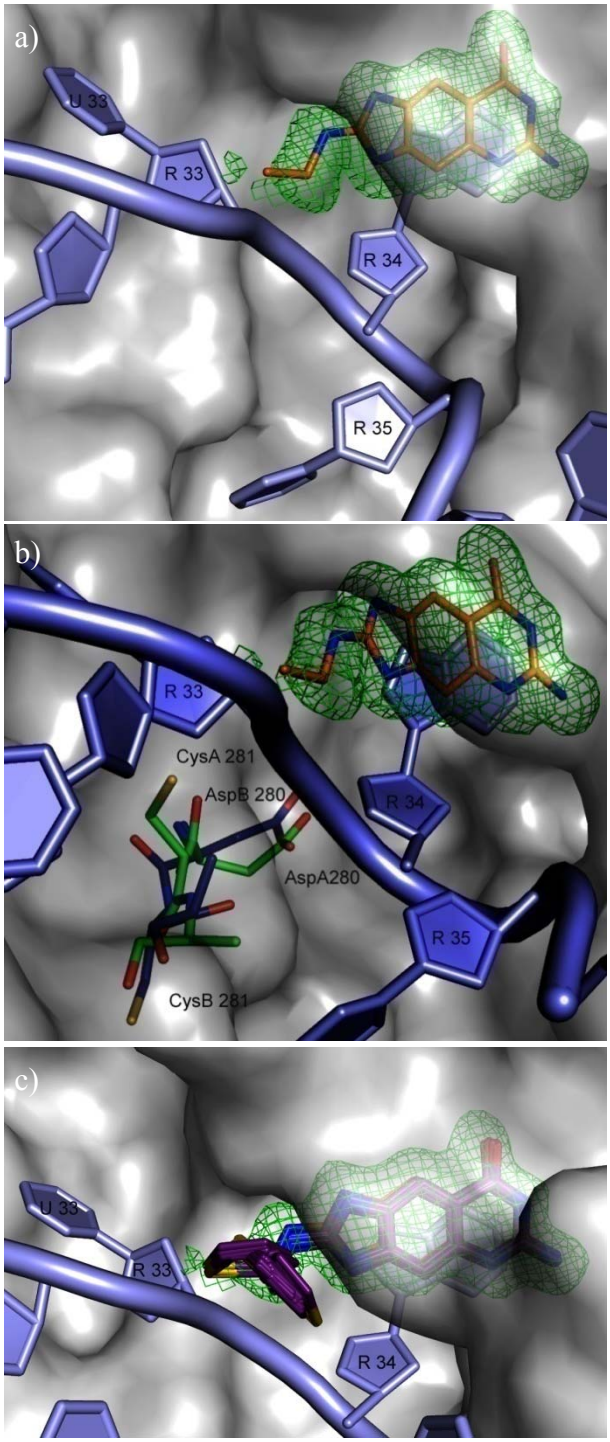

Legend on the following page

Figure 2.6 *Superimposition of TGT in complex with a preQ1 modified tRNA loop (pdb-code: 1Q2S; blue, only the ligand is shown) and compound 7 (pdb-code: 3C2Z; protein: surface presentation in gray; ligand: carbon = orange, nitrogen = blue, oxygen = red). For the 2-amino-lin-benzoguanine scaffold the difference electron density is well defined (|Fo| - |Fc| density map at 2.5 σ in green for the structural model refined without the ligand). a) The thiophene ring of 7 is dislocated but based on the position of the ethyl linker a localization of the thiophene ring similar to ribose 33 can be anticipated. b) For Asp280 and Cys281 two conformations are refined (conformation A: carbon = green, nitrogen = blue, oxygen = red, sulfur = yellow; conformation B: carbon = blue, nitrogen = blue, oxygen = red, sulfur = yellow). Conformation A orients the thiol group of Cys281 towards the surface of the protein whereas in conformation B the thiol group is rotated by 180 ° and faces to the interior of the protein. In addition, the position of Asp280 slightly shifted which is especially remarkable because Asp performs the nucleophilic attack towards C1 of the ribose during the base exchange reaction. c) Superposition of 20 docking solutions (carbon = purple, nitrogen = blue, oxygen = red; sulfur = yellow) generated with the program GOLD. The sulfur atom of the thiophene ring is fitted into the difference electron density, as it would contribute as strongest scatterer most to the density.*

Subsequently, the sterical displacement of the thiophene moiety translates into a 180 degree rotation of Cys281 from an orientation towards the surface of the protein into the cavity usually occupied by uracil 35 in the natural substrate.The best binding affinity is observed for 6-amino-2-(2-morpholin-4-yl-ethylamino)-1,7-dihydro-imidazo[4,5-g]quinazolin-8-one (**9**). This compound shows an affinity of 6 nM. The skeleton does not fit entirely into the difference electron density. The ethyl linker between the 2-amino-*lin*-benzoguanine and the morpholino moiety can be assigned to difference electron density ($|F_o|$-$|F_c|$ map at 2.5 σ) but for the highly scattered morpholino ring, no properly defined electron density could be observed (Figure 2.7a).

In a previous communication, the complete structure of a derivative with a naphthyl side chain added to 2-amino-*lin*-benzoguanine (**8**) skeleton has been presented. [42] In this complex, it was partly possible to assign the side chain of the ligand to the difference electron density (pdb- code: 2QZR). Interestingly, the lower part of the naphthyl moiety which is covalently attached to the *lin*-benzoguanine skeleton is visible in the difference electron density. The upper six-membered ring is ill-defined. Likely this corresponds to a kind of wiggling motion of the naphthyl moiety perpendicular to the protein surface. Compared to the complex of **9**, the hydrogen bonds between the guanidinum moiety of **8** and the carbonyl oxygen atom of Leu231 and Ala232 are expanded (hydrogen bond to Leu231: **5**: 2.8 Å; **8**: 3.0 Å; to Ala232: **9**: 2.7 Å; **8**: 3.6 Å (Figure 2.8). Obviously, the naphthyl side chain of **8** pushes the *lin*-benzoguanine scaffold away from Ala232. Accordingly, it induces a slight rotation of Tyr106 and Val233. Tyr106 closes up the binding pocket once no ligand or substrate is accommodated to TGT.

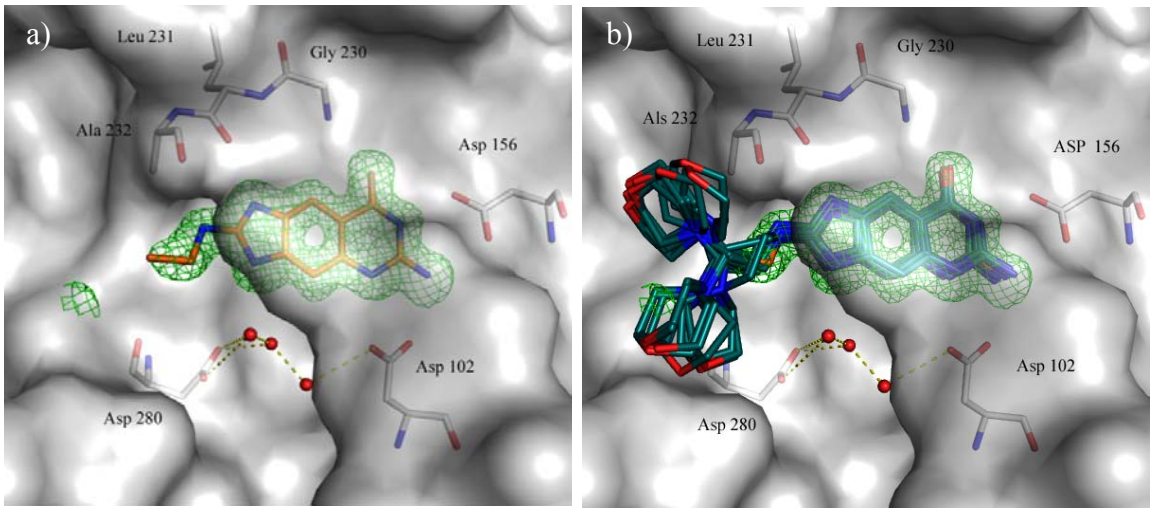

Figure 2.7 *Surface representation of TGT in gray; ligand: carbon = orange, nitrogen = blue, oxygen = red; $|F_o|$ - $|F_c|$ density map at 2.5 σ in green of the structural model refined without the ligand* ***9*** *in the guanine binding pocket. The morpholino ring system of* ***9*** *is not shown because no properly defined electron density could be observed during refinement. b) A total of 20 docking solutions derived with the program GOLD are superimposed on the complex with* ***9****. The docking solutions show that the morpholino side chain is solvent exposed and multiple conformations are possible.*

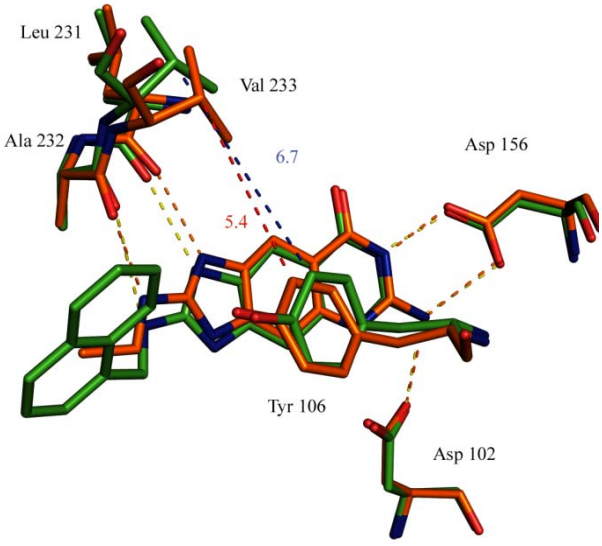

Figure 2.8 *Superposition of TGT in complex with* ***8*** *(pdb-code: 2QZR; carbon = green, nitrogen = blue, oxygen = red, hydrogen bonds = orange dashes) and* ***9*** *(pdb-code: 3C2N; carbon = orange, nitrogen = blue, oxygen = red, hydrogen bonds = yellow dashes). The side chain of Val233 is shifted in the complex of* ***8*** *which results in a larger distance between Tyr106 and Val233 (****8****: 6.7 Å, blue dashes;* ***9****: 5.4 Å, red dashes).*

In the apo structure, it forms a hydrogen bond to Asp156. When a ligand is entering the guanine binding pocket, Tyr106 performs a π-stacking with the aromatic ring system of

the bound ligand. In case of binding the naphthyl derivative, the position of Tyr106 is distorted. In addition, Val233 is rotated out of the binding pocket. The distance between Tyr106 C_ε and Val233 C_β increases in the complex of **8** (6.7 Å) compared to the complex of **9** (5.4 Å) leading to an opening of the guanine binding pocket (Figure 2.8). Surprisingly, the complex of **8** is up to now the only example where the side chain of the inhibitor could be fitted to a reasonably defined electron density. Probably, the binding mode with an ordered side chain orientation is based on a sterical interaction of the naphthyl moiety with Tyr106 leading to a shifted placement of the *lin*-benzoguanine scaffold in the guanine recognition pocket. Nevertheless, the affinity falls into the same range as for other ligands exhibiting a guanidinum-type moiety. Therefore, the opening of the guanine binding pocket has supposedly no impact on the affinity of ligand binding.

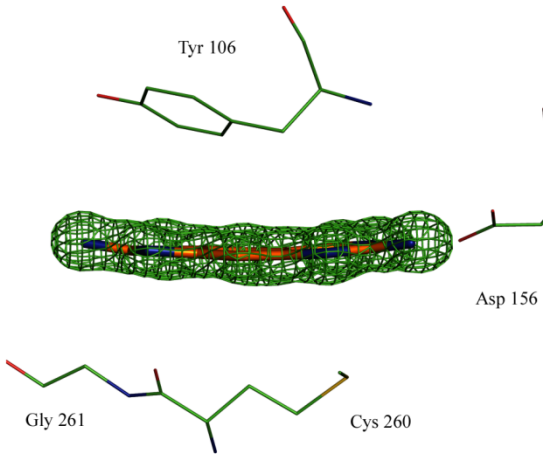

Figure 2.9 *Complex of* ***5*** *and TGT. The* $|F_o|$ - $|F_c|$ *density map of* ***5*** *of the structural model refined without the ligand is shown at 2.5 σ in green. The inhibitor is slightly bent in the guanine binding pocket (approximately 7.5°).*

All *lin*-benzoguanines are based on a tricyclic aromatic scaffold. It is remarkable that this ring system is not always planar (Figure 2.9). In complex with **5**, **7**, and **9**, the electron density for the scaffold is bent out of plane by approximately 7.5°. In a refinement cycle, where the ligand was artificially constrained to a planar geometry, residual negative and positive difference electron density has been received. The unexpected non-planarity can likely be explained by a protonation of the conjugated system of the guanidinum like moiety, providing further crystallographic evidence that the 2-amino-*lin*-benzoguanines are protonated upon binding to TGT.

2.3.4 Docking experiments

For the complexes of **7** and **9** with TGT, it was not possible to fit the side chain of the inhibitor into the electron density. Only some weak peaks of residual electron density are visible (Figure 2.6a, 2.7a). In order to estimate possible orientations of the side chain, docking experiments using the program GOLD were performed. [47] In Figure 2.6, the docking solutions for **7** are visualized. The docked geometries show a cluster for the side chain orientations close to the ribose 33 binding site as already indicated by the crystal structure. For **9,** the docking delivers two clusters (Figure 2.7b) for the morpholino side chain. The placement of the docking solutions supports the assumption that the side chain is rather solvent exposed and no particular arrangement with a set of preferred interactions appears possible.

2.4 Conclusion

The synthesis of new TGT inhibitors with the aim to address the ribose 33 binding pocket led to a dramatic increase in binding affinity. The modification of the scaffold *lin*-benzoguanine to synthetically easily accessible 2-amino-*lin*-benzoguanines changed the characteristics of our inhibitors. With this skeleton, it is now possible to form an additional hydrogen bond at the far end of the guanine binding pocket between the carbonyl group of Ala232 and the exocyclic amino function of the inhibitor (Figure 2.5). However, the most important contribution to the increased binding affinity results from a change of the physico-chemical properties of the scaffold. With the introduction of the guanidinum functionality, a permanent charge is most likely created on this portion of the inhibitor which results in the formation of a charge-assisted hydrogen bond to the carbonyl group of Leu231. This interaction is further stabilized by the negative charge of the deprotonated Glu235 facing the NH of Leu231 from the back. For the evaluation of the charge-assisted hydrogen bond between the ligands and TGT, we performed a novel application of *in-silico* pK_a calculation. So far the pK_a calculation with modified *peoe_pb* charges were only used to characterize the protonation state in active sites of HIV-protease and other proteases, such as trypsin and thrombin, but it was never consulted to explain trends in affinities. [48, 49] This evaluation shows that pK_a calculations can also be applied to study affinity relationships of protein-ligand complexes. The results of the pK_a calculation support the increasing basic character of our inhibitors, particularly once bound to the protein that strengthens the interaction to Leu231.

The crystal structures emphasize the conserved binding mode of the scaffold of the *lin*-benzoguanines in the guanine binding pocket. The introduced side chains in 2-position can bind to the ribose 33 binding pocket. The disruption of the water cluster network which had a detrimental effect on the binding energy in previous studies could not be observed for **4**-**10**. With our new design strategy we could bear the first nanomolar TGT inhibitors.

An additional interesting feature can be observed from the complexes of **7** and **9**, where it is not possible to fit the complete side chain of the ligand into the electron density. Nevertheless, the binding affinity is still increased compared to the complex of **6** (for **7** the increase is 1.7-fold, for **9** it is nearly 10-fold). The side chain is not fixed in one preferred orientation and in our docking experiments the thiophene and the morpholino moiety are scattered over multiple conformations. The residual mobility of the side chain in protein bound state obviously enhances binding affinity of a less intimate and shape-complementary complex between ligand and protein. Certainly, upon complex formation the overall residual conformational entropy is reduced, usually compensated by an enhanced enthalpy contribution experienced by the newly formed interactions with the ligand. In the present case, the residual amount of degrees of freedom resulting for the still activated conformational mobility of the side chain is beneficial for the entropic contribution to binding. A partial loss of degrees of freedom pays a smaller prize in entropy. Overall, an enhanced Gibbs free energy of binding is observed, particularly for **9**. As important message from this study, it can be concluded that enhancement of binding affinity not solely correlates with a unique and well-defined shape-complementary conformational of ligand portions. Recently, we could report a similar case where the complete disorder of a ligand side chain was not detrimental to binding affinity. [50] In this case, the binding constant, a typical free energy entity, is determined predominantly by either an enthalpic and entropic contribution. Possibly, our traditional thinking in terms of lead optimization in medical chemistry is too strongly biased towards an enthalpic view only accepting structural evidence once a properly defined ligand configuration can be discovered in the difference electron density of the complex. Also, a beneficial residual configuration entropy contribution can result in an improved protein-ligand bindining.

3 Replace active site water molecules to achieve nanomolar inhibition of tRNA-guanine transglycosylase

All compounds presented in this section were developed in cooperation with Philipp Kohler (group of Prof. Dr. François Diederich, ETH Zurich, Switzerland).

3.1 Abstract

The enzyme tRNA-guanine transglycosylase (TGT) plays a significant role in the complex pathogenic mechanism of *Shigella flexneri*, the causative agent of Shigellosis. TGT modifies $tRNA^{His, Asn, Asp, Tyr}$ molecules in the wobble position 34. Inhibition of TGT leads to a strong reduction of the bacterial virulence and presents therefore a novel approach towards the curation of this bacterial infection. A series of 2-amino-*lin*-benzoguanines was optimized to achieve highly potent inhibition in the nanomolar range. In this study we exploited the information about the presence of active site water molecules in the design process. These water molecules accomplish residual solvation of the carboxylate groups of the two facing and negatively charged, catalytic aspartic acid residues, therefore replacement by a positively charged hydrogen bond donor center in the ligand appeared appropriate to mimic the functional role of these water molecules. Hot spot analysis using DrugScore suggested secondary amines to optimally achieve this goal. In consequence several model compounds were docked with GOLD and consecutively rescored using $DrugScore^{CSD}$. Docking with GOLD appeared superior, as this tool features the consideration of either water-mediated interactions or displacement of distinct water molecules during docking. This strategy suggested the introduction of several functional groups and side chains. The proposed inhibitors could be synthesized and kinetically tested. Their subsequent crystallographic characterization discovered a common binding mode for the newly designed side chains. The novel inhibitors show affinities down to K_i-values of 2 nM and replace the water molecules without loss in binding affinity. Further enhancement could be achieved by decoration with hydrophobic cycloalkyl side chains optimally penetrating into a small hydrophobic subpocket. The present study underlines that the correct replacement of active site water molecules can achieve high potency in binding, however the design has to regard the properties of the replaced structural water molecules and their local physicochemical environment.

3.2 Introduction

3.2.1 The role of water molecules in structure-based drug design

For folding, flexibility, and stability of proteins, water molecules bound to the protein surface are essential. In addition, they often play a key role in the biological function of proteins or in protein-protein, protein-DNA/RNA, protein-small molecule interactions. In the field of structure-based drug design, the handling of water molecules is an ongoing challenge to crystallographers and computational chemists. Solvent water molecules are ubiquitously present in protein crystals, particularly next to charged functional groups to retain a partial solvent environment. The position of water molecules close to the protein surface forming hydrogen bonds or filling up hydrophilic subpockets of the protein can be characterized by diffraction experiments. Various studies in the past tried to classify water molecules based on kinetic studies, thermodynamic measurements, or computational methods. [51-53] In the context of the design of new inhibitors, the differentiation between displaceable water molecules and tightly bound water molecules is of utmost importance. Previous studies stressed the number of hydrogen bonds, B-factors, and the contact area between water and protein as features to classify water molecules on the surface of proteins. [51] Tightly bound water molecules experience three or more hydrogen bonds with the local protein/ligand environment. Usually, they are buried in highly polar cavities of the protein surface. Contrary, displaceable water molecules obtain higher temperature factors during refinement and often participate in a water network without making direct hydrogen bonds to the protein. Based on thermodynamic analyses, the average binding free energy of bound water molecules is estimated to about -6.2 kcal/mol and for displaceable water molecules a mean value of -3.7 kcal/mol has been assigned. [51]

The positions of water molecules in the active site of proteins can be interpreted as valuable indicators to be used in the design of putative ligands. The occupied position of a conserved, hardly displaceable water molecule can be regarded as integral portion in the active site that forms strong hydrogen bonds with the surrounding protein atoms. Such water molecules will be difficult to replace upon ligand binding. In contrast, the position of displaceable water molecules can be used to define a pharmacophore feature or other constraints in our ligand design, to construct an appropriate ligand skeleton capable to form the desired interactions with the protein. From a thermodynamic point of view, the

replacement of such water molecules from the active site will take most likely an affinity-enhancing impact due to entropic reasons.

3.2.2 Target protein

Using structure-based design, several inhibitor series of tRNA-guanine transglycosylase (TGT) have been developed and explored in the past. [1, 3, 5, 42, 54] The enzyme is an interesting target due to its significant role in the complex pathogenic mechanism of *Shigella flexneri*, the causative agent of Shigellosis. To invade human endothelial cells, the bacterium needs a set of genes which are located on a bacterial virulence plasmid. An efficient transcription of these genes is only possible when tRNA with modified bases in the anticodon loop is available. This modified tRNA is produced by TGT. The active form of the protein is most likely a homodimer which recognizes and binds one tRNA molecule. [5] The enzyme exchanges the nucleobase guanine against a modified base in the wobble position 34 of $tRNA^{His, Asn, Asp, Tyr}$. [36] During enzyme catalysis, Asp280 performs a nucleophilic attack on C1 atom of ribose 34 and a covalent bond is formed between protein and tRNA backbone. [29] Simultaneously, at this position the C–N bond between ribose and guanine is cleaved, which allows guanine to leave the binding pocket. Subsequently, the vacant binding site accommodates a modified base concurrently performing a conformational change of the protein backbone amide bond between Gly230 and Leu231. Once the modified base is successfully recognized, a novel C–N bond to ribose 34 is formed. The tRNA modification is completed and the altered tRNA dissolves from the protein. Our drug development strategy is therefore to inhibit the base exchange reaction of TGT to thus reduce the virulence of Shigella bacteria significantly. [13]

So far a variety of aromatic substituents have been introduced at different basic scaffolds for TGT inhibitors, among them pyridazinones, pteridines, quinazolinones, and a "stretched" guanine with an inserted central six-membered aromatic ring leading to *lin*-benzoguanine. [1, 3-5, 42, 54] All mentioned scaffolds bind into the deep binding pocket where guanine 34 is hosted during the catalytic reaction. The lead structures investigated up to now show affinity from the micromolar to nanomolar range (K_i-values). Next to the guanine-binding pocket, several other flat and solvent-exposed cavities are available that fix the backbone of the tRNA and the attached nucleobases. One of these cavities is occupied by ribose 34 during the base exchange reaction. To increase the binding affinity,

the lead structures were decorated in a way to address this rather hydrophobic ribose 34 binding pocket. First candidates of our design exhibited side chains interacting with the catalytic aspartates and filling the adjacent hydrophobic pocket. For the time, substituted 4-amino-phthalacidhydrazides[1], dihydropyridazinoquinolinetrione derivatives[3], and 6-amino-quinazolinones[4] were investigated. Their measured K_i-values did not show significant increase in binding affinity compared to the unsubstituted parent skeleton; some derivatives even decreased in binding affinity. Our side chain design was based on the hypothesis that Asp102 is the nucleophile of the base exchange reaction and Asp280 would function as general base. Later studies, however, suggested a reverse assignment to the mechanism. Accordingly, Asp280 was found to be the nucleophile, which is intermediately covalently attached to the tRNA backbone and Asp102 operates as general base. [29] A remarkable observation, possibly contributing to the moderate increase in binding affinity was the fact that in all the above-mentioned skeletons the attached hydrophobic side chain is scattered over multiple orientations in the ribose 34 subpocket. Parallel to the study of the 6-amino-quinazolinones, a new series of substituted *lin*-benzoguanines was synthesized. They also exhibited binding affinities in the low micromolar range, and apolar aromatic side chains attached to address the hydrophobic ribose 34 pocket flanked by Val45 and Leu68, did not increase affinity. [5] The crystal structure of the unsubstituted parent *lin*-benzoguanine (K_i = 4.1 µM, pdb-code: 2BBF) could be determined with a resolution of 1.7 Å. A detailed analysis of its crystal structure revealed that all introduced side chains in 3- and 4-position will disrupt a contiguous water network bridging between Asp102 and Asp280. As the replacement of several water molecules or perturbance of water networks between or next to polar residues might be crucial for affinity, our goal was to develop new side chains, which address the ribose 34 binding pocket without losing affinity. As parent skeleton, 2-methylamino-*lin*-benzguanine (**6**) (K_i = 58 nM) was selected. From another compound series stretching out into the uracil 33 binding pocket, the attached 2-amino group at the *lin*-benzoguanine scaffold orients towards this site and turns the hydrogen bond to the carbonyl backbone oxygen of Leu231 in a charge-assisted hydrogen bond. This interaction accounts for a major gain in binding affinity. [42, 54]

3.3 Results and Discussion

3.3.1 Computational studies

3.3.1.1 Water cluster analysis

Previous studies suggested the importance of water molecules accommodated between both catalytic aspartates. [5] To design new side chains for the ribose 35 subpocket of TGT, which can actively participate and simultaneously replace one or more water molecules, the actual positioning of the various water molecules in multiple crystal structures was investigated. A structural alignment of all considered crystal structures was performed with Relibase+.[55, 56] This superposition denoted five discrete water clusters in the catalytic site of TGT. All water molecules in the area of interest were extracted, and to increase data reliability, water molecules with a B-factor higher than 40 $Å^2$ were discarded.

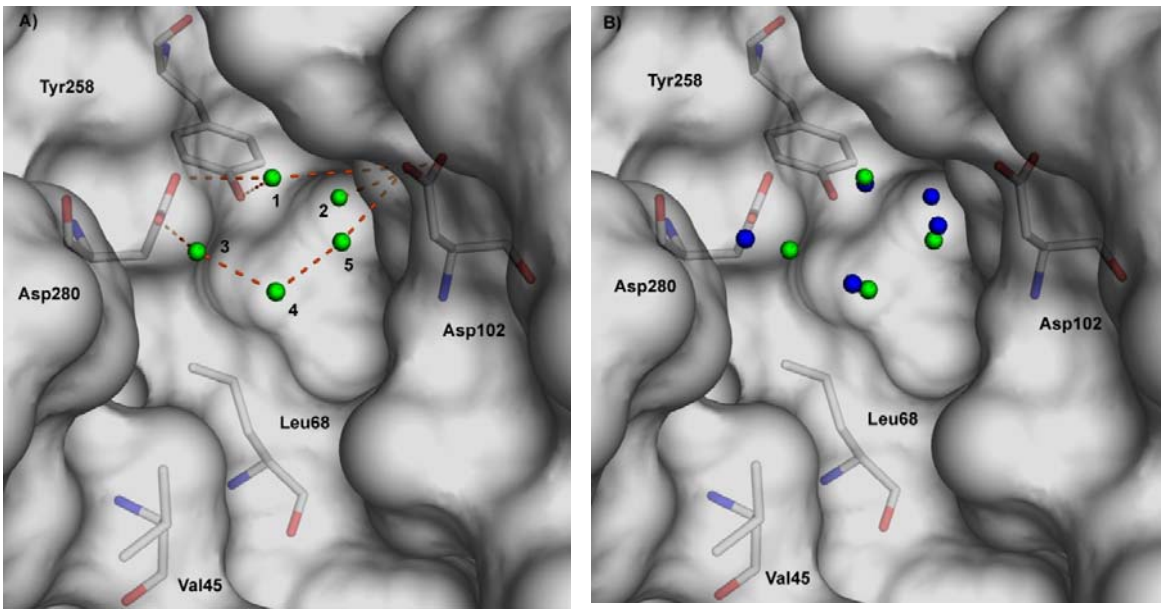

Figure 3.1 Surface representation of the active site of TGT. The solvent accessible surface of the protein is shown in gray. Furthermore, the amino acids involved in interactions to the water cluster network are indicated (carbon: gray, nitrogen: blue, oxygen: red). The different water molecules are located between the catalytic residues Asp102 and Asp280 next to the hydrophobic pocket floor formed by Val45 and Leu68. A) Consensus model with five water molecules (green spheres) derived as mean arrangement from seven superimposed complexes. An extended hydrogen bonding network is formed (orange dashes) buffering to some degree the negative charge on the carboxylate groups. B) The derived model is superimposed with the water molecules after a minimization in MOLOC (blue spheres) which show no significant changes in their position.

From the remaining water molecules for each visually apparent cluster, the center was determined. To each cluster, archetypical water molecules were assigned leading to an overall consensus water model. It consists of five representing water molecules (1-5) shown in Figure 3.1A. A tight hydrogen bonding network can be established between these water molecules and Asp102 and Asp280. The assigned consensus model of water molecules between the catalytic aspartates was validated with respect to the MAB-force field implemented into MOLOC (Figure 3.1B). [57] Here, only minor changes in the position of the water molecules are observed, which suggests that the consensus water cluster is a suitable model in agreement with local minima of a force field.

3.3.1.2 DrugScore ^{HotSpots}

Additionally to the consensus water analysis, hotspots were derived for the active site of TGT using DrugScore^{CSD} potentials. [58] The hotspots were calculated with respect to different atom types in order to suggest appropriate functionalities which can be used as guidelines to correctly decorate the side chain of our designed ligands (Figure 3.2). For the calculation TGT in complex with 2-amino-*lin*-benzoguanine was used (pdb-code: 2Z7K). The generated hotspot maps exhibit favorable regions for all selected atom types in the active site of TGT. A superposition of TGT with the tRNA-preQ$_1$ complex shows two phosphate groups of the tRNA backbone at a position located between both aspartates (Figure 3.2A). For the atom types present in tRNA (carbon sp^3, phosphorus sp^3, oxygen sp^2, and oxygen sp^3) hotspots were calculated (Figure 3.2B-E). Apart from sp^2 oxygen, significantly favorable regions were obtained between Asp102 and Asp280. For sp^2 hybridized oxygen, only two favorable regions are indicated at positions, where refinement suggests the location of two water molecules.

In addition, hotspots were calculated for nitrogen atoms adopting sp^3 hybridization. They exhibit a large favorable region next to Asp280. The DrugScore^{CSD} potentials used for this calculation consider uncharged and positively charged nitrogens. Accordingly, placement of functionality, with positively charged nitrogen next to the deprotonated aspartate appears as a good starting point for the design of a well-suited side chain. Simultaneously, this strategy will replace one or several water molecules. A phosphorus atom as, e.g. in a phosphate group, seems also suitable but was not considered in the first synthesis attempts. Therefore, only the amino group was further investigated.

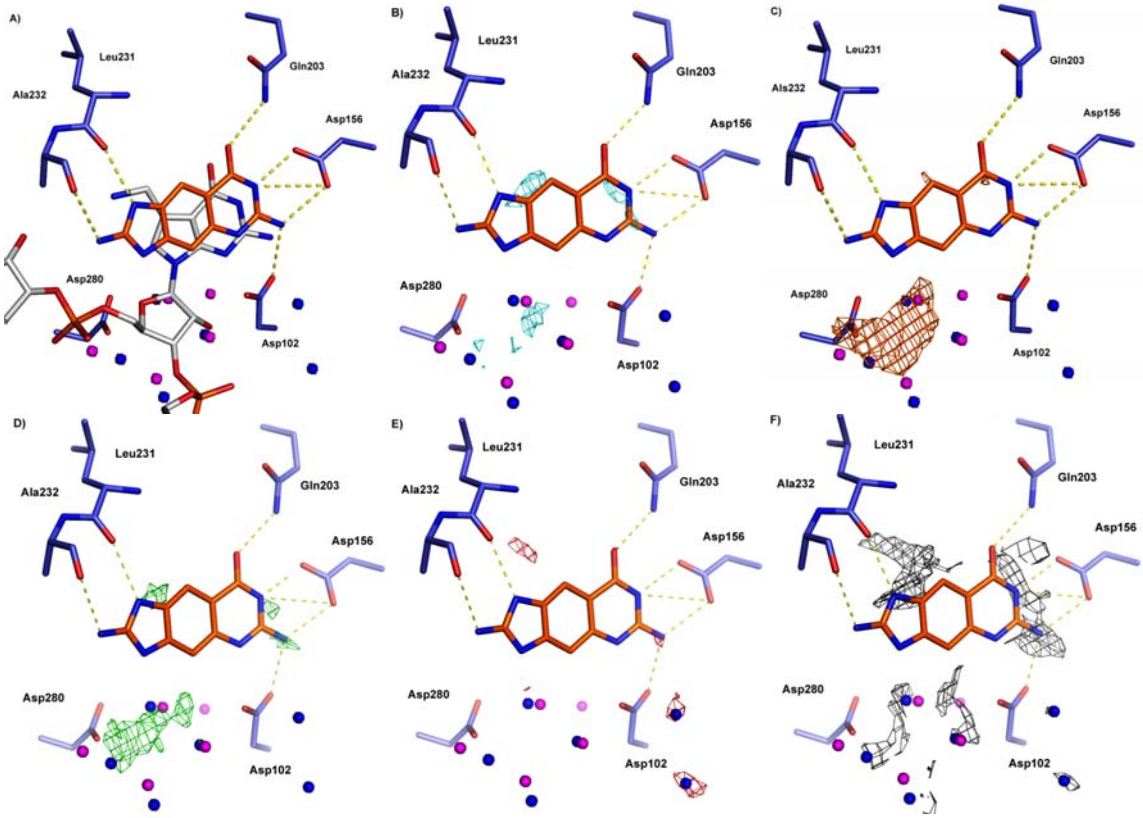

Figure 3.2 *DrugScore^{HotSpots} analysis: For the calculation of the hotspots, TGT (C, blue, O, red, N, dark blue, water blue spheres) in complex with 2-amino-lin-benzoguanine (C, orange, O, red, N, dark blue) (pdb-code: 2Z7K) was used, possible hydrogen bonds (yellow dashes) are plotted. The consensus water cluster is superimposed (magenta spheres). A) Superposition of TGT with bound lin-benzoguanine (pdb-code: 2Z7K) and tRNA-preQ$_1$ complex (pdb-code 1Q2S) (C, gray, O, red, N, dark blue). The ribose is located between Asp102 and Asp280. B) Hot spots for C (sp^3) in cyan (contour level: -17000). C) Hot spots for P (sp^3) in orange (contour level: -18000). D) Hot spots for N (sp^3, sp^3 positively charged) in green (contour level: -16000). E) Hot spots for O (sp^2) in red (contour level: -9000). F) Hot spots for O (sp^3) in black (contour level: -9000).*

3.3.1.3 Side chain design

As parent skeleton, 2-methylamino-*lin*-benzoguanine was chosen. Its high ligand efficiency, examined in earlier studies, makes this scaffold a promising starting point. In order to place the amino functionality into correct position, 3- or 4-substitutions at the parent skeleton were examined (Scheme 3.1). In addition to the correct positioning of nitrogen, an appropriate linker length had to be identified. For our docking attempts, we considered the structure of 1Y5X, as in this crystal structure the protein exhibits an expanded ribose 34 subpocket that is induced by an accommodated inhibitor.5 The consensus water model was added to the protein structure and the docking program GOLD applied in the “water toggle mode” to either regards or replaces water molecules

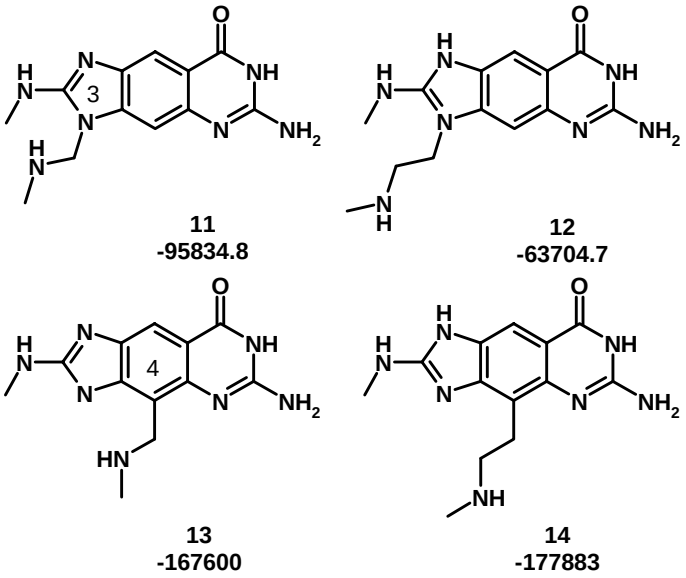

Scheme 3.1 *Possible substitutions at the parent skeleton in 3- or 4-position and variable linker lengths between the aromatic ring system and the secondary amino group. The obtained DrugScore is given.*

from docking solutions. [47] The knowledge-based scoring function DrugScore^{CSD} was applied to rescore all docking solutions and to evaluate generated interaction geometries between ligand, water, and surrounding protein. [58] As it incorporates a tailored potential for the consideration of water molecules which remained in the binding pocket during docking. The best scored solution for each candidate molecule is shown in Figure 3.3 displaying the per-atom DrugScore contribution: blue (favorable) or red (disfavorable) spheres placed at the atom position of the ligand and protein indicate the beneficial or detrimental contributions to the total score. Water molecules, not eliminated during docking, are shown in magenta. Substituents attached in 3-position reveal a significantly less favorable scoring compared to the substitutents in 4-position. The docking solutions for the attachment in 3- and 4-positions display deviating orientations of the 2-ethylamino group. In case of a 3-substituent (**11** and 1**2**, Scheme 3.1) the respective methyl group points towards Ala232 to avoid unfavorable intramolecular interactions with the attached 3-methylene- or ethylene-linker. As a consequence, the hydrogen bonds between the guanidinium moiety of the inhibitor and the carbonyl groups of Leu231 and Ala232 will be elongated. The docking solutions of the 4-substituted derivatives **13** and **14** suggest that the 2-methylamino group is rotated to the opposite site now allowing two strong hydrogen bonds to be formed between the guanidinum group and the backbone carbonyl groups. Previously determined crystal structures with this potent skeleton suggest

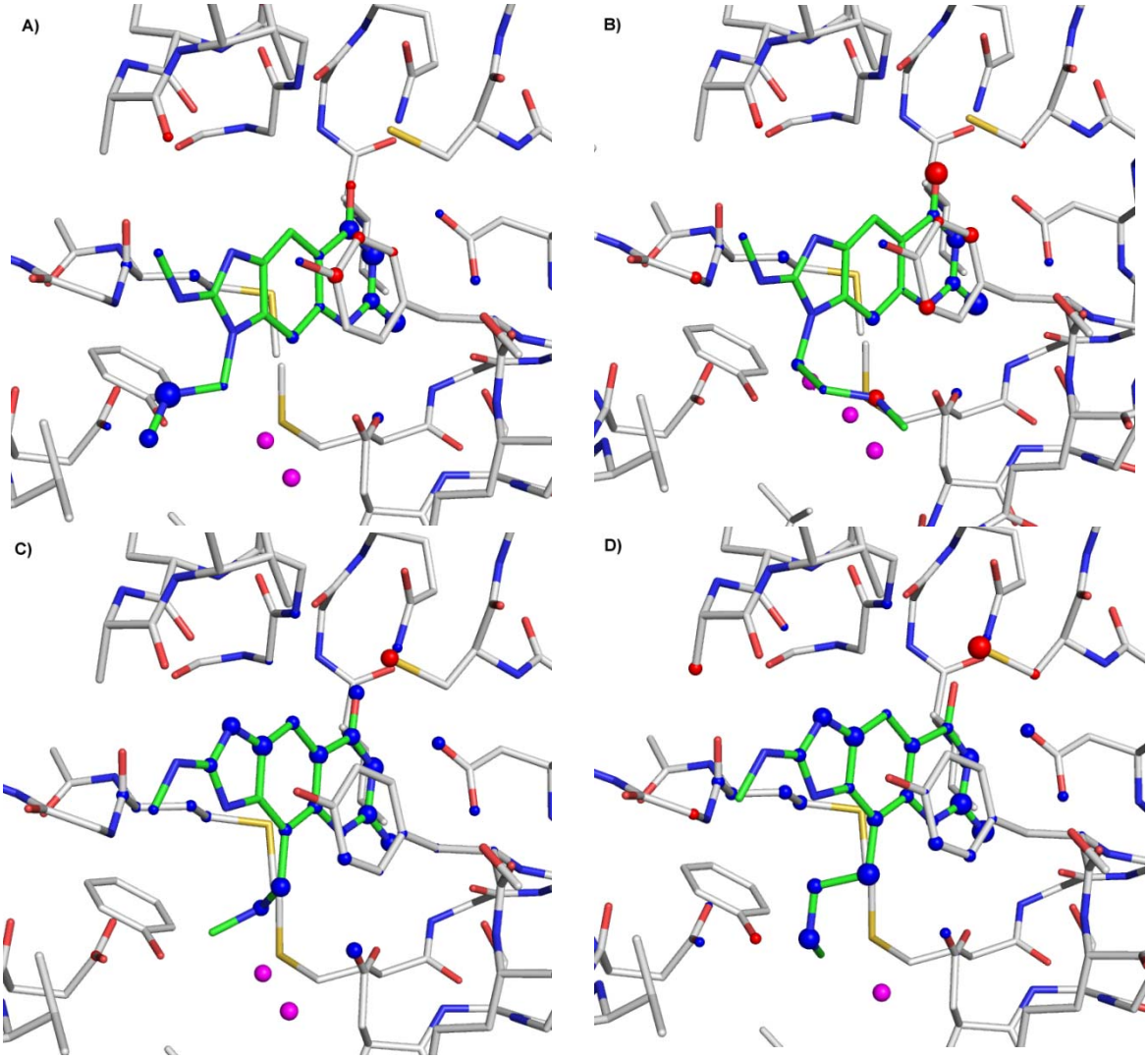

Figure 3.3 *Visualization of the best-scored GOLD docking solutions with DrugScoreCSD for the four test compounds (protein: carbon: gray, nitrogen: dark blue, oxygen: red; ligand: carbon: green, nitrogen: dark blue, oxygen: red; water: magenta spheres). With an methylaminomethylene or methylaminoethylene substituent attached to the 3- or 4-position. The solutions obtained the following relative energy scores on an arbitrary scale: a)* ***11*** *-95834.8, b)* ***12*** *-63704.7, c)* ***13*** *-167600, and d)* ***14*** *-177883. DrugScore is visualized in terms of per atom contributions using spheres of different radius at the individual atom positions: A favorable contribution to the score is shown in blue, whereas an unfavorable one is coloured in red. Substitution in 3-position of the parent skeleton (A and B) leads to a rotation of the side chain off from an optimal position which takes strong influences on the strength of the individual interactions formed between inhibitor and protein. In C and D the results considering substituents in 4-position are shown examining a methylene and ethylene linker. The secondary amino group can form a direct hydrogen bond to Asp 280 and mediated via an additional water molecule a hydrogen bond toAsp102 is possible.*

that the latter methyl orientation in **13** and **14** is a prerequisite for the potent binding of the 2-methylamino-*lin*-benzoguanine moiety. [42, 54] DrugScore ranks **14** slightly better than **13**. Furthermore, the derivative with the ethylene-linker experiences a more

convincing hydrogen bonding network between Asp102, Asp280, and the remaining water molecules. In addition, a further interaction to Asp102, mediated by a water molecule appears possible. According to this better ranking, substitution with an ethyl linker in 4-position of the parent skeleton was selected as most promising candidate to replace one or more water molecules for synthesis. In the next step, the terminal methyl group was systematically replaced by larger moieties. Accordingly, 602 primary, aliphatic amines were selected from the ZINC-database and computationally linked to the parent skeleton and docked with GOLD considering the consensus water model. [59]

Table 3.1 *Newly designed inhibitors based on the parent skeleton 2-amino-lin-benzoguanine. The corresponding DrugScore and rank are given.*

	compound	DrugScore	DrugScore rank
15	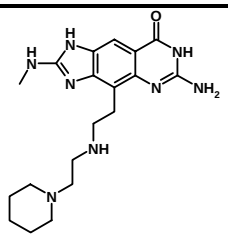	-253249	14
16	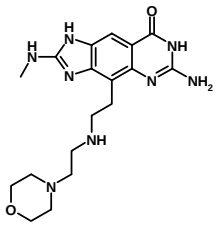	-249014	26
17	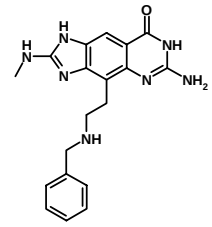	-250862	11
18	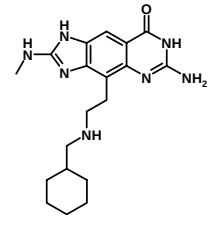	-251536	18

Again, the results were rescored with DrugScore^{CSD}. Compared to **14** which exhibits only a methyl group attached to the secondary amine, a 1.6-fold increase of the score could be achieved. The improved score suggests that attachment of lipophilic groups will achieve

higher potency compared to the parent skeleton. After visual inspection of the 100 top-scored docking solutions, four candidates with simple hydrophobic side chains were selected for synthesis (Table 3.1). Using the discovered side chain, the candidates should be able to form interactions with Val45 and Leu68. Ligand **17** features an aromatic ring system, whereas **15**, **16**, and **18** exhibit alicyclic substituents

3.3.2 Experimental characterization

3.3.2.1 Determination of the inhibition constant

The synthesis of the different inhibitors is described elsewhere. [60] To investigate their binding affinity, the K_i values were determined in a base exchange assay (Table 3.2). [32, 61] All inhibitors showed a pure competitive inhibition mode, implying that none of the inhibitors binds simultaneously with tRNA to TGT.

In addition to various amines, the inhibitor **20** derived from an intermediate of the synthesis with a 4-ethylhydroxy substitutent was tested. Based on the assumption that a positive functionality is required, capable to form H-bonds and replacing one or more water molecules without losing binding affinity, we did not expect an increase in binding affinity for this compound. Its measured K_i value of 97 nM is about 1.7 times less potent compared with the parent skeleton **6** (58 nM). This observation confirms our design hypothesis.

To introduce an additional potentially positively charged group between both aspatates a primary (**19**) and a secondary (**14**) amines were synthesized. The binding affinity of **19** (55 nM), falls into the same range as that of the parent compound **6** (58 nM) but the secondary amine (26 nM) shows an improvement by a factor of two, resulting from additional interactions picked up by the *N*-methyl group and the more favorable partitioning of the less polar secondary amine.

Obviously, the ethyleneamino linker provides an ideal handle to interfere favorably with the water network. Therefore in the subsequent design, we tried to decorate this handle with appropriate lipophilic groups to address the small hydrophobic subpocket formed by Val45 and Leu68. As substituents, a benzyl (**17**), a naphthyl (**21**), a cycloheptylmethylene (**22**), a cyclohexylmethylene (**18**), and cyclopentylmethylene (**23**) moiety were attached. Enzyme kinetics show that the aliphatic substituents feature the ligands with one digit

Table 3.2 *Structures of examined inhibitors. The K_i-values measured in the base exchange assay are listed.*

compound	structure	enzyme K_i
6	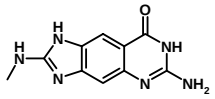	58 nM ± 36
19	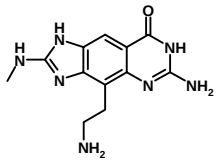	55 nM ± 3
20	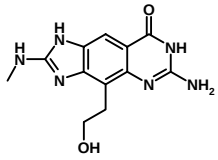	97 nM ± 5
14	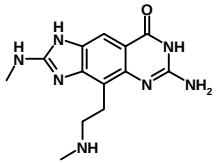	26 nM ± 6
17	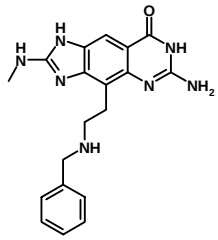	25 nM ± 2
21	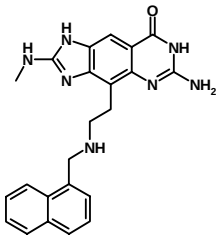	105 nM ± 10
18	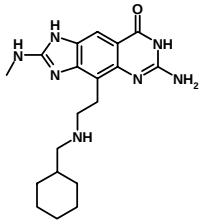	4 nM ± 2

compound	structure	enzyme K_i
22	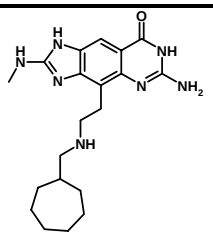	2.5 nM ± 1
23	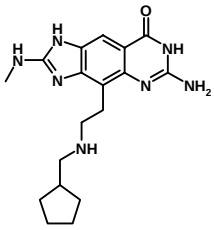	2 nM ± 1
24	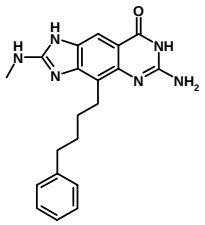	235 nM ± 50
25	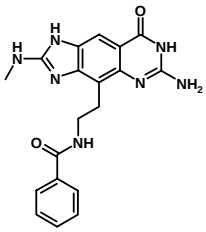	1.4 μM ± 0.1
26	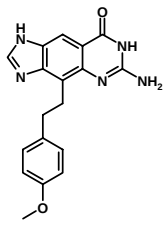	29 μM ± 7[61]

nanomolar affinity (**18**: 4 nM, **22**: 2.5 nM, **23**: 2 nM) whereas the benzyl substituent (**17**: 25 nM) remains surprisingly in the same range as the small methyl substituent. For the naphthyl moiety (**21**) and the reference coumpound, which have no amino group in the side chain (**24**, **25**), a significant decrease in the binding affinity (**21**: 105 nM, **24**: 235 nM, **25**: 1.4 μM) was measured. The obtained binding affinies support our design

strategy to choose an amino group as an appropriate interaction partner to Asp280 and decorate the side chain with a small hydrophobic moiety.

3.3.2.2 Crystal structures

The kinetic data suggest successful design. To validate our design hypothesis, crystal structures of TGT in complex with **17-20**, **23** were determined. The compounds were successfully soaked into crystals of apo TGT, and data sets with resolutions between 1.40 Å and 1.93 Å were collected. Detailed information about the experimental conditions are given in Materials and Methods section.

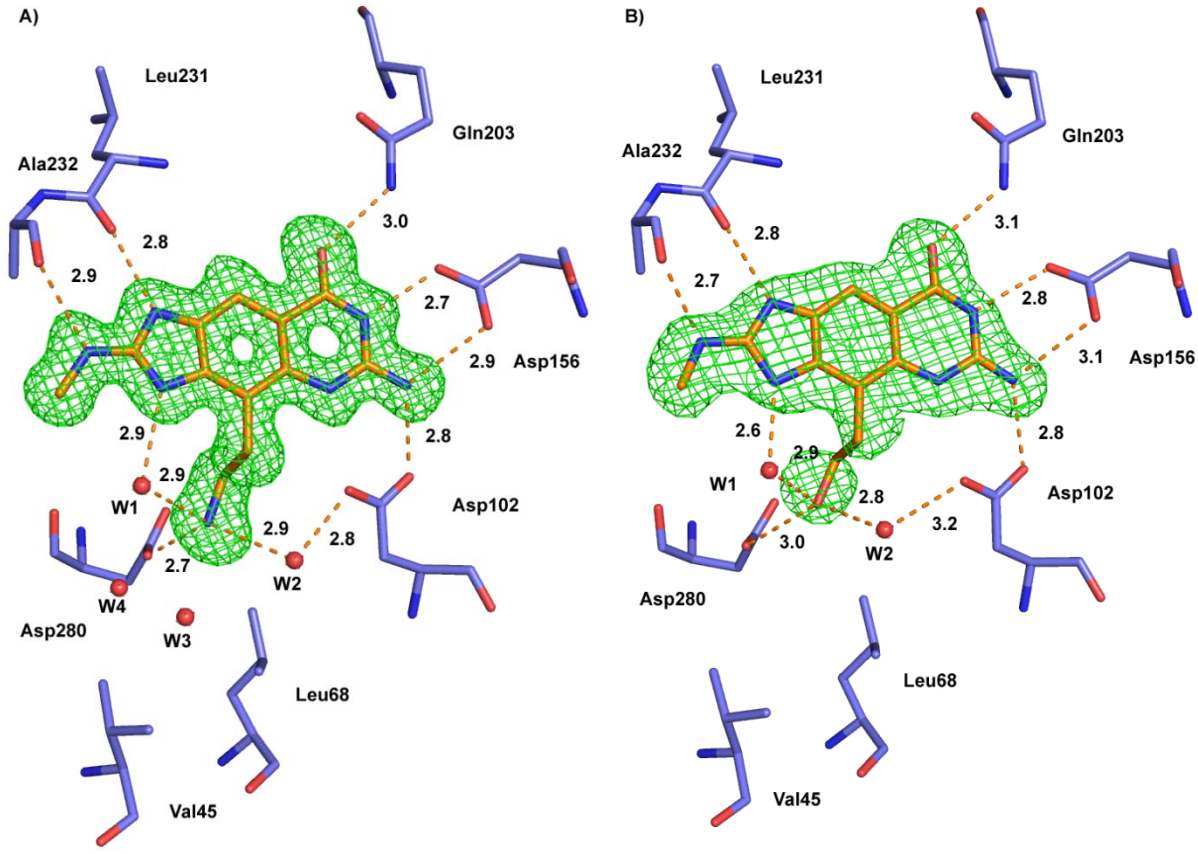

Figure 3.4 *Crystal structure of TGT in complex with* ***19*** *(A) and* ***20*** *(B) (protein: carbon: blue, nitrogen: dark blue, oxygen: red; ligand: carbon: orange, nitrogen: dark blue, oxygen: red; water: red spheres). For the inhibitor, the Fo-Fc difference electron density is shown (green) at a sigma level of 2.5 after refinement excluding the inhibitor. The parent skeleton 2-methylamino-lin-benzoguanine forms multiple strong hydrogen bonds (orange dashes; distances are given in Å). Two water molecules are found in the active site of TGT. Water W2 mediate hydrogen bonds to the carboxyl group of Asp102, whereas water molecule W1 forms hydrogen bonds to N3 of the inhibitior. In complex* ***19****, two additional water molecules (W3, W4) are solvating the amino group.*

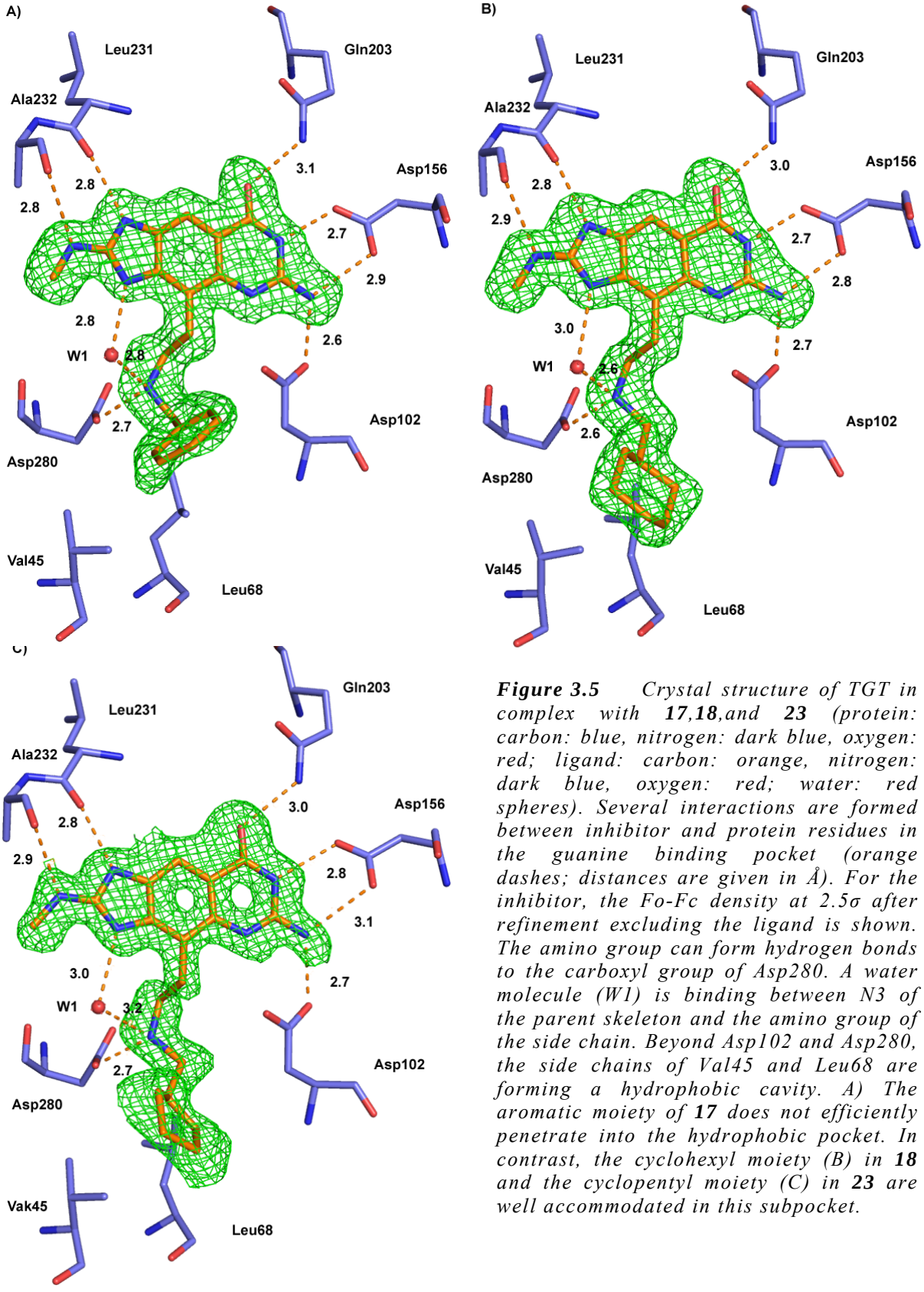

Figure 3.5 *Crystal structure of TGT in complex with* ***17***,***18***,*and* ***23*** *(protein: carbon: blue, nitrogen: dark blue, oxygen: red; ligand: carbon: orange, nitrogen: dark blue, oxygen: red; water: red spheres). Several interactions are formed between inhibitor and protein residues in the guanine binding pocket (orange dashes; distances are given in Å). For the inhibitor, the Fo-Fc density at 2.5σ after refinement excluding the ligand is shown. The amino group can form hydrogen bonds to the carboxyl group of Asp280. A water molecule (W1) is binding between N3 of the parent skeleton and the amino group of the side chain. Beyond Asp102 and Asp280, the side chains of Val45 and Leu68 are forming a hydrophobic cavity. A) The aromatic moiety of* ***17*** *does not efficiently penetrate into the hydrophobic pocket. In contrast, the cyclohexyl moiety (B) in* ***18*** *and the cyclopentyl moiety (C) in* ***23*** *are well accommodated in this subpocket.*

All inhibitors are well visible in the *Fo-Fc* difference electron density after refinement of the protein (Figure 3.4, 3.5). The *lin*-benzoguanine skeleton forms hydrogen bonds to the side chains of Asp102, Asp156, and Gln203 and to backbone atoms of Leu231 and Ala232. In addition π–stacking with Tyr106 the Met260 is observed, holding the *lin*-benzoguanine skeleton in place (for clarity not shown in the Figures). Interestingly, in all structures a surprising backbone conformation is found close to the active site. The peptide bond between Val262 and Gly263 adopts the *cis*-conformation (Figure 3.7). In proteins, non-proline *cis*-oriented peptide bonds occur very rarely in only about 0.05% of all cases. [62] Most likely, the *cis*-conformation is less stable compared to the *trans*-orientation, due to mutual steric repulsion of the two neighboring C_α atoms. [63]Notably, most of the observed examples with *cis* orientations are of functional importance and occur close to the active site of the proteins. The present 4-substituted 2-methylamino-*lin*-benzoguanines are the first examples obviously capable to induce this surprising backbone flip. In TGT·**19**, the primary amino group of the side chain forms a hydrogen bond to Asp280 (2.8 Å), and a second interaction to Asp102 is mediated *via* a water molecule (W1) (Figure 3.4A). The interaction pattern corresponds to the initially suggested docking geometry of **14** and confirms the design hypothesis. Furthermore, a second water molecule (W2) is found next to N3 of the parent skeleton (2.9 Å).

As this ligand is equipotent to the parent structure, placement of the ethyleneamino linker is fully balanced out in interacting inventory. The kinetic data suggest that the 4-ethylenehydroxyl substituent of **20** is not efficiently interfering with the water network between the aspartates. Analysis of the crystal structure of the TGT·**20** complex shows a very similar binding mode to the isostructural amino derivative **19**. The terminal OH-group interacts presumably *via* its hydrogen directly with the neighboring carboxylate group of Asp280 (3.0 Å) (Figure 3.4B). One water molecule (W2) remains in the complex and binds to N3 of the inhibitor (2.6 Å). A second water molecule (W1) is found between Asp102 (3.2 Å) and the hydroxyl group of the inhibitor (2.8 Å); obviously the missing charge on the terminal hydroxyl group is responsible for the reduced affinity of this derivative compared with **19**.

Decoration with hydrophobic groups to address the small hydrophobic ribose 34 pocket is realized in **17**, **18**, and **23** (Figure 3.5). A detailed analysis of the complexes with these ligands reveals that the water molecules of the consensus water cluster are replaced by the secondary amino group. In all complexes, one water molecule (W1, Figure 3.5) remains

and mediates an interaction between N3 of the tricyclic ring system (2.8-3.0 Å) and the secondary amino group (2.6-3.2 Å). Furthermore, this nitrogen experiences a strong hydrogen bond ($d_{N...O}$ ~ 2.6 Å) to the catalytic Asp280. Considering the basicity of a secondary aliphatic amine, the nitrogen is most likely protonated. Its positive charge would enhance the hydrogen bond to Asp280. [64] An explanation for the significant affinity difference between aromatic (**17**) and aliphatic (**18** and **23**) side chains becomes obvious upon consulting the binding mode in the crystal structures. The aliphatic ring systems penetrate deeply into the hydrophilic subpocket whereas the phenyl ring is not comparably accommodated. It remains as a kind of lid on the top of the pocket. Better burial would require a 90° rotation of the phenyl moiety thus requiring an in-plane conformation of the attached methylene linker. However, the attachment of a terminal phenyl group *via* a -CH_2-group reinforces as energetically most favorable geometry an orientation of the aromatic moiety perpendicular to the side chain. Possibly, the energy to be spent to drive the phenyl substituent in coplanar geometry with the side chain is too high and cannot be compensated by the gained hydrophobic contacts to be experienced in an edge-on binding orientation in the small hydrophobic crevice.

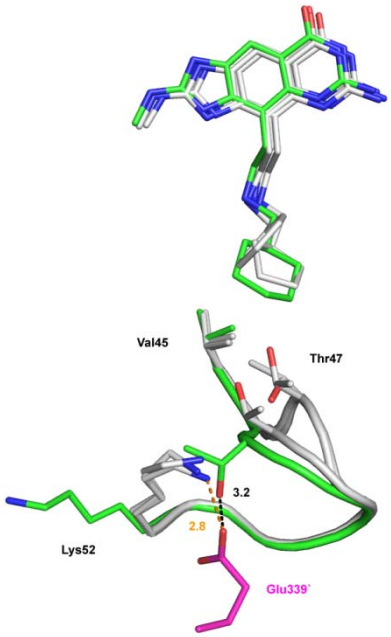

Figure 3.6 *A section through the TGT dimer interface is shown. The interaction (orange dash) is formed between Thr47 and Glu339' (pink) for the complexes of* ***19***, ***17***, *and* ***23*** *(carbon: gray, nitrogen: blue, oxygen: red). For TGT·****18*** *(carbon: green, nitrogen: blue, oxygen: red) a surprising rotation of Thr47 displaces the side chain of Lys52 and forms a direct interaction (black dash) to Glu339` of the neighboring monomer.*

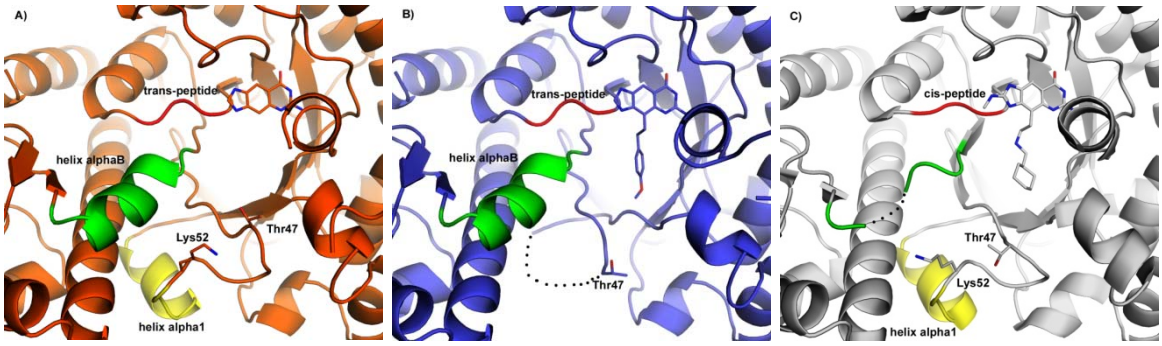

Figure 3.7 *Comparison of different TGT complexes highlights the ligand induced changes in the active site of TGT. Introducing a side chain in 4-position leads to a conformational change of a loop containing Thr47 (B,C) compared to the TGT in complex with lin-benzoguanine (A). In the case of TGT·**26** (B), the methoxyphenyl substituent prompt a disorder of helix α1 (yellow in A, C). In TGT·**18** (C) the ligand causes a rotation of Thr47 and Lys52 leading to a dislocation of helix αB (green). In C a cis-peptide conformation (red) is observed.*

The cyclohexyl ring of **18** is found in a chair and the cyclopentyl ring of **22** is found in a twist envelop conformation with average B-value of ~26 Å^2. The well-defined electron density emphasizes that both rings occur in one single conformation and orientation. Here, the attachment *via* the methylene groups allows an ideal orientation of the hydrophobic face of the ring substituents towards the hydrophobic wall of the small crevice.

Surprisingly, the complex of TGT·**18** shows a deviating orientation of Thr47, skipped by about 90°, compared to the other complexes (Figure 3.6). The new position of Thr47 leads to a different location of Lys52, as observed in other complexes. Our previous studies suggest that TGT forms a homodimer. One interaction in the dimer interface is established between Leu52 and Glu339` of the dimer mate. The observed rotation of Thr47 in TGT·**18** displaces the basic functionality of Lys52 and instead the interface contact is now formed between Thr47 and Glu339`. As the interaction between Lys52 and Glu339` has most likely salt-bridge character weakening of the dimer interface due to the less charge-assisted hydrogen bond between Thr47 and Glu339` in TGT·**18** seems likely. Influences on the formation of the dimer interface are already known from TGT·**21**, here the ligand provokes to a dislocation of helix α1 (yellow, Figure 7.3). In the present case helix α1 is not disordered but the side chain of Lys52 refines to a position where in the previously determined complexes the residues 284-290 form an αB helix (green, Figure 3.7). Possibly in consequence, this helix becomes disordered in TGT·**18**. [5]

3.4 Conclusion

In the present study computational tools were applied to suggest possible optimization strategies for a parent *lin*-benzoguanine skeleton. A detailed analysis of the residual solvation structure of two polar Asp residues in the TGT active site indicated the location of several crucial water molecules which were considered in the ligand design processes. A protein-based hot spot analysis supported selection of favorable ligand functionalities to be incorporated into possible side chains. As promising candidate, a secondary amino group linked *via* an ethylene spacer was chosen. Once synthesized, the candidates were characterized by enzyme kinetics and crystallography. As suggested by docking, the protonated secondary amino group forms an ionic hydrogen bond with the carboxyl group of Asp280. Further, decoration with hydrophobic moieties increases the basic character of the amino group and allows occupation of a small hydrophobic crevice formed by Val45 and Leu68. The presence of a protonated primary, and preferentially secondary ammonium center, allowing formation of a hydrogen-bonded ion pair with the catalytic Asp280 side chain makes an essential contribution to the measured binding free energy. This finding is supported by the reduced binding affinity of the isostructural binding hydroxyl derivative that lacks the terminal charge. The subsequent attachment of hydrophobic groups increases the binding affinity. Significant improvement is achieved by a cyclohexyl- (**17**), cyclopentyl- (**23**) and cyclohepylmethylene (**22**) substituent. Surprisingly, a benzyl attachment shows no advantage compared to a single methyl group. A naphthyl moiety even exhibits a significant loss in binding affinity. This observation is likely due to detrimental conformational properties of the benzyl and naphthyl group thwarting favorable accommodation in the small hydrophobic pocket. In contrast, the aliphatic cycloalkyl moieties penetrate deeply into this pocket. This results in an enhanced contact area of the aliphatic ring systems compared to the aromatic one, most likely explaining the improved binding affinity.

The binding site of TGT·**18** shows interesting structural adaptations, which modifies the interaction pattern in the dimer interface. We hypothesized that dimer formation is required for TGT activity. Interestingly, in the present complex a salt-bridge is replaced by a hydrogen-bond contact assisted by a less charged group. Destabilization of the interface can be assumed.

The present series of complexes, along with ligands studied in previous investigations, highlights the importance of understanding the determining influences of water on ligand binding. Simple classifications in terms of “tightly bond” and “replaceable” water molecules need more sophisticated consideration. In the present case, up to five water molecules can principly be replaced. Based on classifications suggested in literature, all five water molecules found in the complex with the unsubstituted *lin*-benzoguanine parent skeleton would have to be considered “replaceable” suggesting a significant increase in binding affinity due to entropic effects. However, in the present case, the residual solvation of two close-by and most likely negatively charged aspartates is of utmost importance. Possibly, the water molecules buffer to some degree the otherwise highly repulsive interactions of the facing carboxylate groups. Even protonation of one of the interstitial water molecules to be present as H_3O^+ cannot be excluded. In consequence, all our attempts to replace the water cluster by appropriate space-filling substituents of hydrophobic nature failed and no affinity gain could be experienced. However, placing a most likely positively charged amino group inbetween the two aspartates and using this functionality to link to remote putative occupants for the small hydrophobic crevice actually reveals the desired significant affinity gain. In conclusion, classification of water molecules to be replaced in a ligand design hypothesis has to take the local residual environment, particular with respect to charge distribution, into consideration.

4 Side chain variations

In section 2 the introduction of an amino group in 2-position of the *lin*-benzoguanine skeleton was discovered as the driving force for an increased binding affinity due to the formation of a charge-assisted hydrogen bond. The substitution of the amino group in 2-position with an thiophene (**7**), morpholino (**9**), or benzyl moiety (**10**) showed further increase in binding affinity but for the side chain no electron density could be detected in the X-ray experiments. More inhibitors with new side chains were synthesized by Philipp Kohler at the ETH in Zurich (Group of Prof. Dr. Diederich).

The constitution of subpocket occupied by uracil 33 of the natural substrate during the base exchange reaction is rather flat and solvent exposed. Involved in the recognition and binding of uracil 33 are Gly236, Gln237, Lys264, and Arg267 (Figure 4.1).

The strongest inhibitor discovered in section 2 is substituted by morpholine (**9** K_i 6 nM). It was reasoned that the morpholino nitrogen might be protonated, thus undergoing an additional ionic hydrogen bond with the Gly261 carbonyl. This bond should be strengthened in order to improve the binding and rigidify the side chain. As N3 of the *lin*-benzoguanine skeleton is assumed to occur in protonated form as well, the two positive charges should be further separated by elongating the two-carbon to a three-carbon linker (**27**), with the intention of decreasing the σ-inductive effect between the two basic centers, simultaneously increasing the basicity of the morpholino moiety. Alternatively, the morpholine should be replaced by a more basic piperidine (**28**), or the two modifications combined (**29**). It was predicted that a hydroxy group in 4-position of the piperidine moiety possibly be involved in several hydrogen bonds either to the backbone NH of Gly263 (not shown in Figure 4.1), the backbone NH of Lys264 or to the carboxylate of Asp267, which should arrest the side chain more firmly (**30**, **31**). Fluorine was meant to pick up weak interactions to the backbone of Gly263–Lys264 stretch without increasing polarity too much (**32**).

Stimulated by the strong inhibition of thiophene-substituted inhibitor **7** (K_i of 35 nM) we decided, to further substitute this moiety (Table 4.1). Thiophene is similar in size to a phenyl ring, but offers side chain attachment in position 5 (ca. 150°). This exit angle falls inbetween a 1,3- and a 1,4-disubstituted benzene portion (120° and 180°). From a crystallography point of view, we anticipated to better spot the stronger diffracting sulfur

atom in the X-ray crystal structure. To improve water solubility and to mimic uracil 33, morpholine, either linked via a carbonyl (**38**) or a methylene bridge (**39**) were prepared. Alternatively, a pyridone (**40**) was chosen as terminal substituents. To increase lipophilicity the thiophene was decorated by an additional methyl group in 4- or 5-position (**36**, **37**), or a fused benzothiophene ring (**41**) was attached.

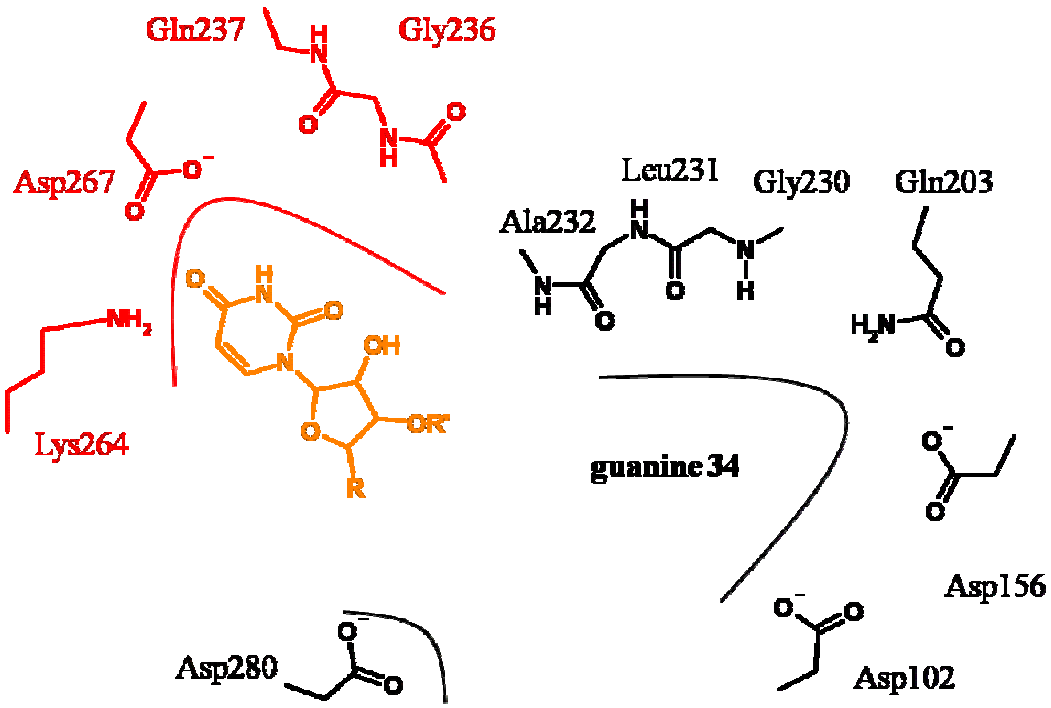

Figure 4.1 *Schematic presentation of the guanine 34 (black) and uracil 33 (red) subpockets. The portion of the tRNA substrate binding into the uracil 33 site is highlighted in orange.*

4.1 Binding affinity

For all synthesized compounds the binding affinity was measured in the enzyme assay (Table 4.1). Each compound did exhibit a pure competitive inhibition, as already described in section 2 for the 2-amino-*lin*-benzoguanines. Unfortunately, no straightforward relationship between attached side chain decoration and observed binding affinities is apparent. Comparing different spacer length and deviating terminal ring systems no superior combination could be selected.

Table 4.1 *Structure of 2-amino-lin-benzoguanine side chains and the corresponding binding affinity, along with the pH value used in the crystallization experiments.*

name	side chain	Ki [nM]	complex	Figure
	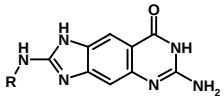			
9	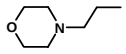	6	pH 5.5	2.7 b)
27	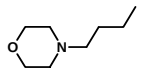	35	pH 5.5	4.1 a)
28	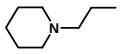	45	pH 5.5	4.1 b)
29	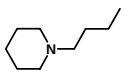	15	pH 5.5 & pH 8.5	4.1 c)
30	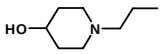	55	pH 5.5	4.1 d)
31	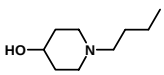	40	pH 5.5	4.1 e)
32	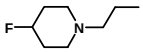	25	-	4.1 f)
33	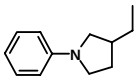	7.5	pH 5.5	4.1 g, h)
34	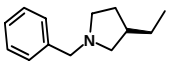	10		4.1 i)
35	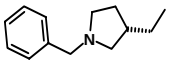	5		4.1 j)
7		33	pH 8.5	2.6 c)
36	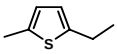	77	-	4.1 k)
37		99	-	4.1 l)
38	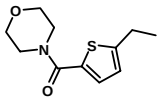	40	-	4.1 m)
39	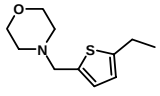	65	pH 5.5	4.1 n)
40	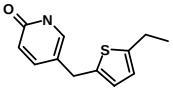	85	pH 5.5	4.1 o)
41	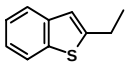	23	pH 5.5	4.1 p)

4.2 Crystal structure

For various examples soaking experiments were performed using different pH conditions (Table 4.1). In total twelve protein inhibitor complexes were obtained. As already described in section 2 the diffraction experiments revealed well-defined electron density for the parent *lin*-benzoguanine skeleton but for the different side chains no reasonable electron density was obtained. A continuously defined electron density can only be observed in the diffraction experiments, when the diffracting atoms are periodically repeated across the individual protein molecules in crystallographically identical positions. In the present case the parent skeleton satisfies these conditions leading to well-defined electron density, whereas the atoms of the side chains must be scattered quite diversely without exhibiting periodity from unit cell to unit cell.

4.3 Docking solutions

In order to estimate putative binding position of the side chains, docking poses were generated with the program GOLD. In Figure 4.2 30 top-scored docking solutions of each inhibitor in Table 4.1 are shown. Apart from a few poses where the parent skeleton is rotated about 180° (Figure 4.2 i-l) the position of the *lin*-benzoguanine skeleton is well reproduced with respect to the crystal structures. For compounds **27-32** the aliphatic linker shows high flexibility leading to multiple orientations of the attached 6-membered ring (Figure 4.2 a-f) (docking of **7** and **9** are in section 2, Figure 2.6 c and 2.7 b). Considering the docking solution a propyl linker seems not superior to a ethyl linker to enhance penetration of the attached morpholino-, piperidine- or phenyl moiety into the uracil 33 binding side. The basic nitrogen in the side chains of **9**, **27-32** is not able to fix the side chain in one position. In some docking poses a hydrogen bond to the carbonyl backbone of Gly261 seems likely, but is obviously not strong enough to fix the position of the side chain in the uracil 33 subpocket.

Using a pyrrolidine ring (**33-35**) as linker in order to decrease the flexibility introduces a stereo center. For docking, both enantiomers were used (**33**, Figure 4.2 g, h; **34**, **35** Figure 4.2. i, j). The R-enantiomer exhibits in both cases a better placement towards the uracil 33 subpocket, which may explain the better binding affinity measured in the assay for **35** compared to **34**. Similar to the docking poses of the aliphatic linkers a hydrogen bond between the pyrrolidine-nitrogen of **35** and the carbonyl group of Gly261 is formed in some docking poses.

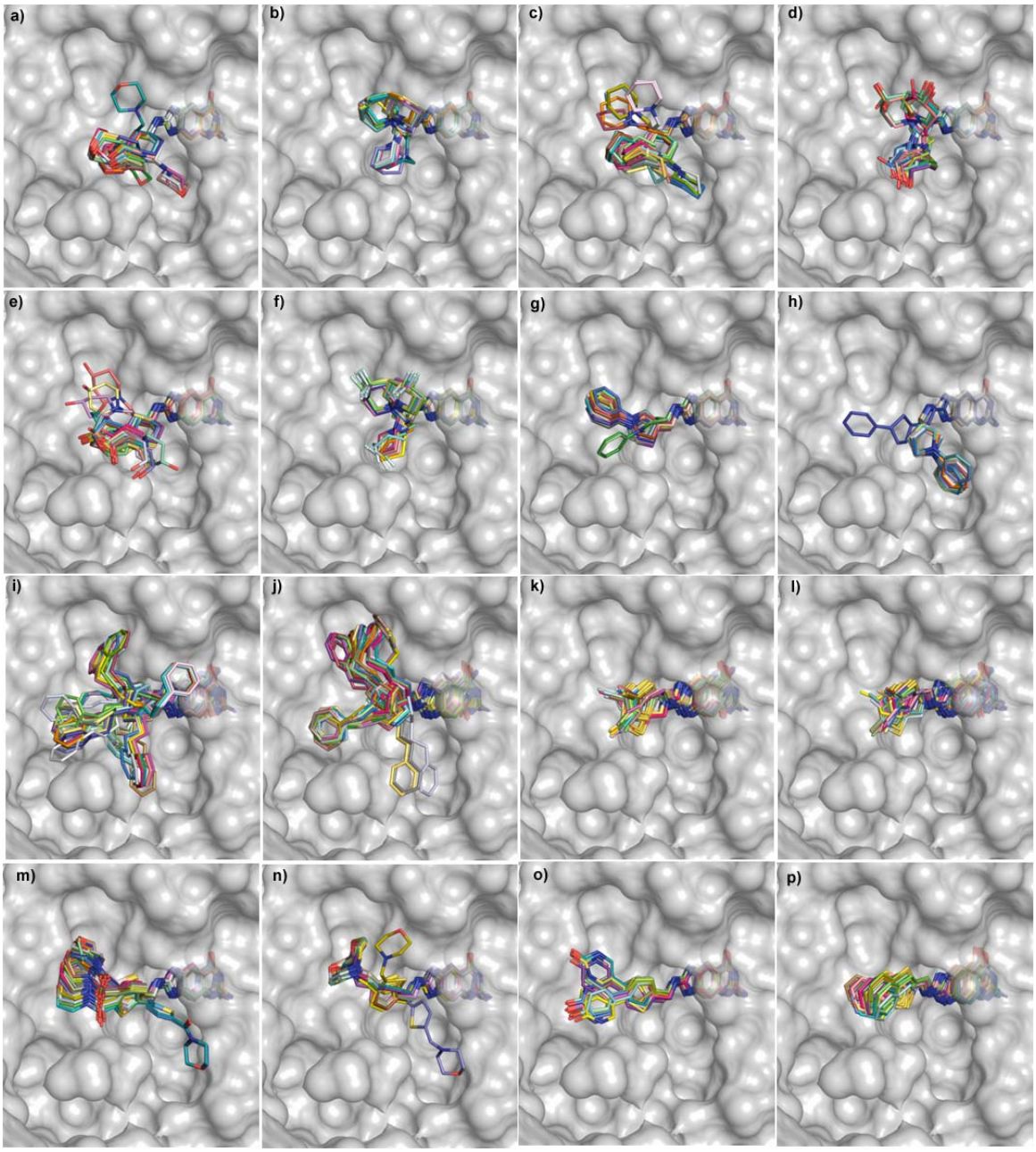

Figure 4.2 *Docking poses of the new tested compounds. The surface of the protein is shown in gray. The inhibitors are shown in stick presentation (oxygen: red, nitrogen: blue, sulfur: yellow).*

Furthermore, derivatives of the thiophene substituted compound **7** were docked to TGT. For **36** and **37** with a methyl group in 4- or 5- position of the thiophene ring and for **41** with a fused benzyl ring the docking poses suggested that the apolar side chains are pointing towards the solvent. The area where the diverse thiophene rings are placed is usually occupied by the phosphate ribose backbone of the tRNA substrate and therefore the surface of TGT in this region has polar character.

4.4 MD simulation

The results of the crystal structures and the docking solutions do not provide satisfactory information about the actual placement of inhibitors side chains. Therefore, molecular dynamic (MD) simulations were performed with **28** in order to obtain some data about the putative orientations and flexibility of the side chains and possible interactions with the protein. As protein model for the simulation the coordinates of the pdb-entry 2Z7K were used and a reasonable ligand conformation in the binding site was derived from one of the GOLD docking solutions. Based on the basicity of the piperidine nitrogen in the side chain, it is most likely protonated, therefore two simulations were prepared. In one the piperidine ring is uncharged and in the other the piperidine nitrogen is protonated.

For the interpretation of the MD simulation, distances between ligand and protein and the internal torsion angles of the ligand were recorded along the simulation. The distances between the parent skeleton and the protein demonstrate, that there are no significant movements observed of the fused aromatic system in the guanine binding pocket (Figure 4.3 a, b, d, e).

With respect to the distance between Asp102 and the inhibitor (Figure 4.3 c, f) the side chain of this residue is not fixed stationarily in one position during the simulation time, as indicated in the crystal structure. Using standard protonation states for all residues, Asp102 is assumed to be deprotonated. This probably leads to a repulsive interaction between the carboxyl group of the amino acid and the inhibitor. The observed flexibility is quite remarkable because Asp102 and a close by water molecule are most likely responsible for the proton transfer during the base exchange reaction of TGT (see section 1). Accordingly, even a temporary change in protonation state due to the mechanistic considerations could be given for the carboxyl function of this residue, possibly even dependant on the actual spatial location of this group with respect to a bound ligand.

To further explore the side chain proparties of the **28**, intended to occupy the uracil 33 subpocket, the MD simulations show an initial movement of the substituent into solvent environment, once the simulation has been performed with the piperidine nitrogen positivly charged. We assume that the protonated side chain is quite easily solvated and therefore its rotation into the solvent is observed already at the beginning of the simulation.

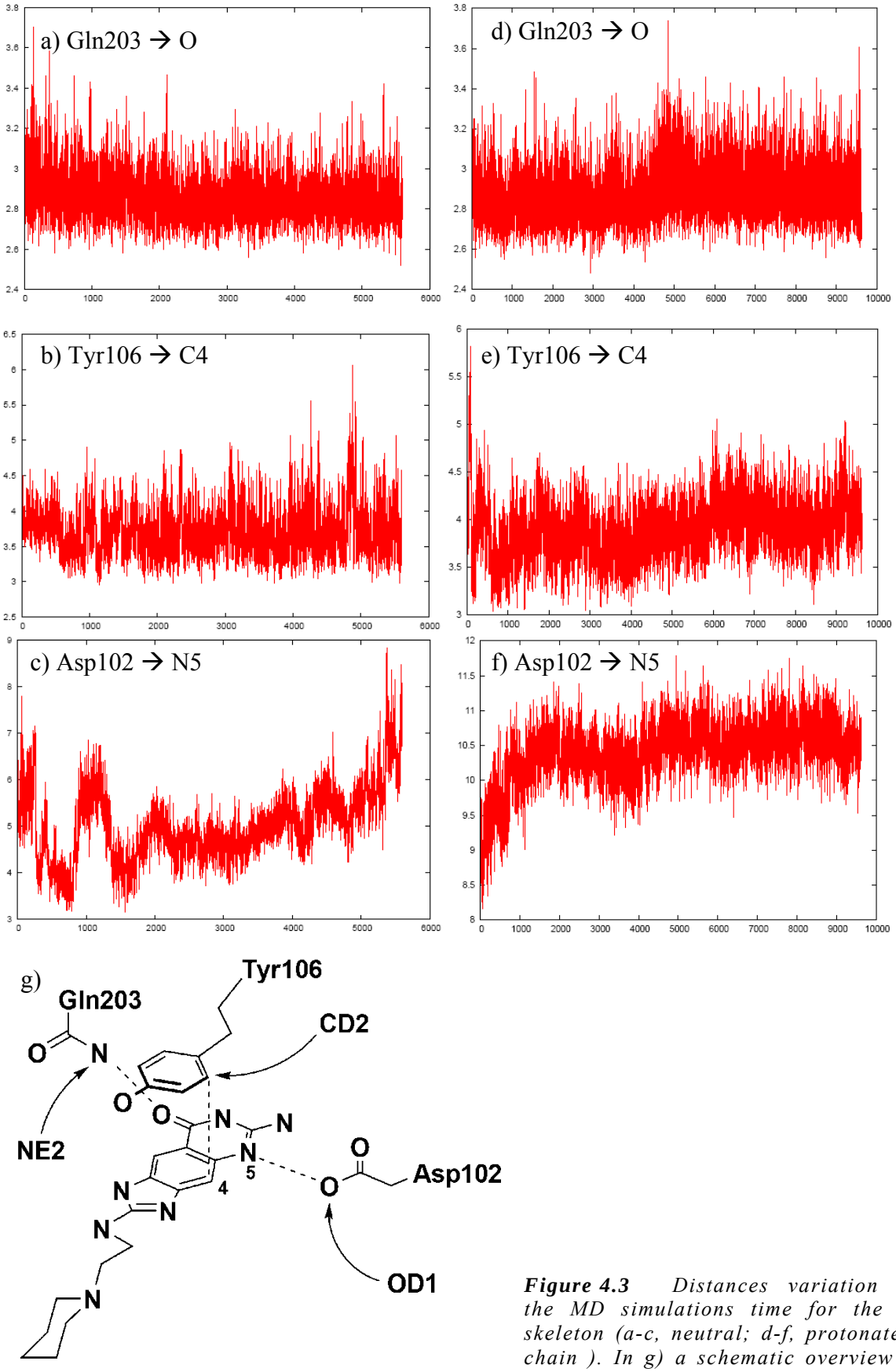

Figure 4.3 *Distances variation during the MD simulations time for the parent skeleton (a-c, neutral; d-f, protonated side chain). In g) a schematic overview of the measured distances is shown.*

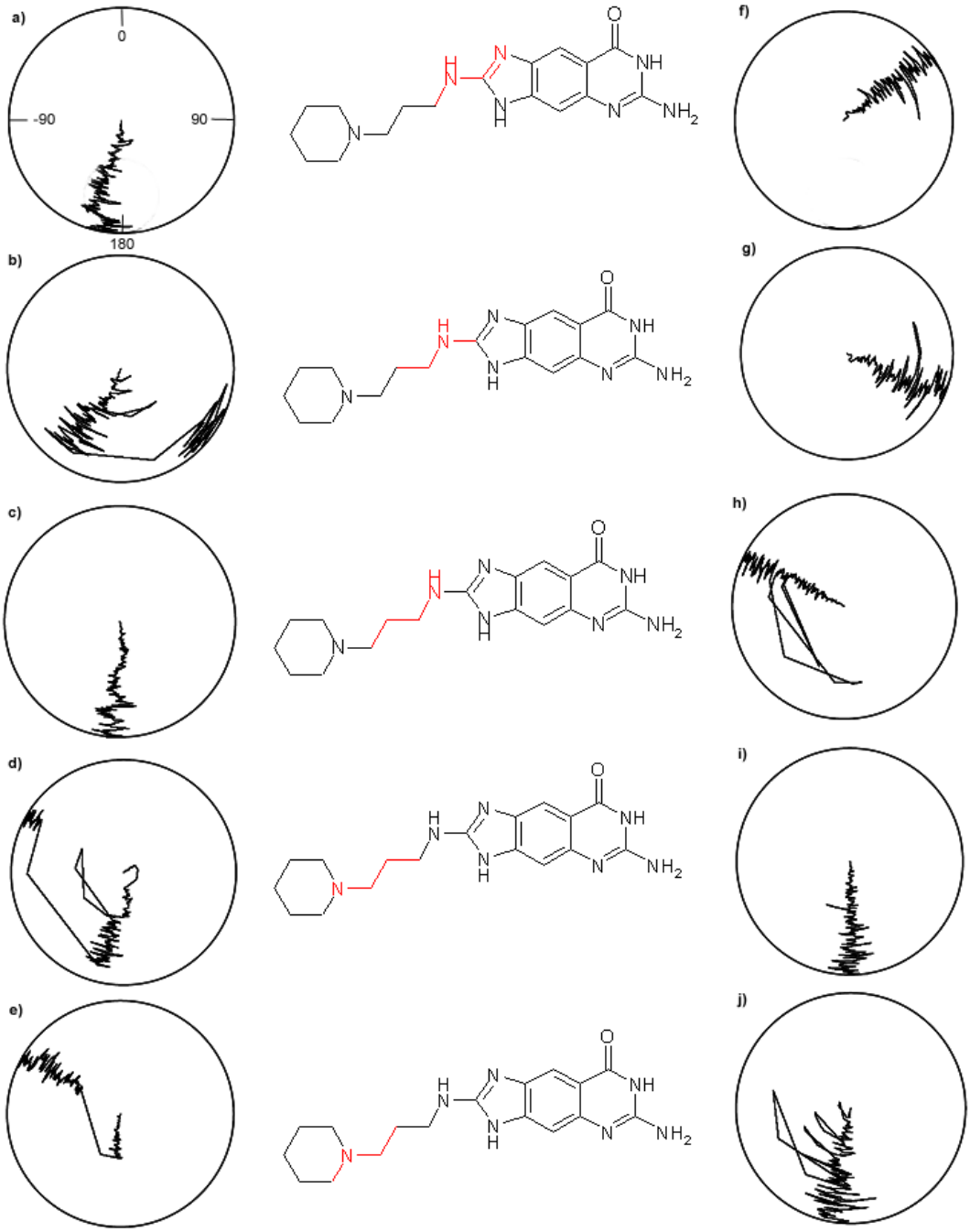

Figure 4.4 *Dialsplots of all possible torsion angles of the linker found in* ***28*** *(neutral form a)- e) and protonated form f)-j). In dialsplots the radius of the circle represents the time axis and the position on the circumference the value for the torsional angle itself.*

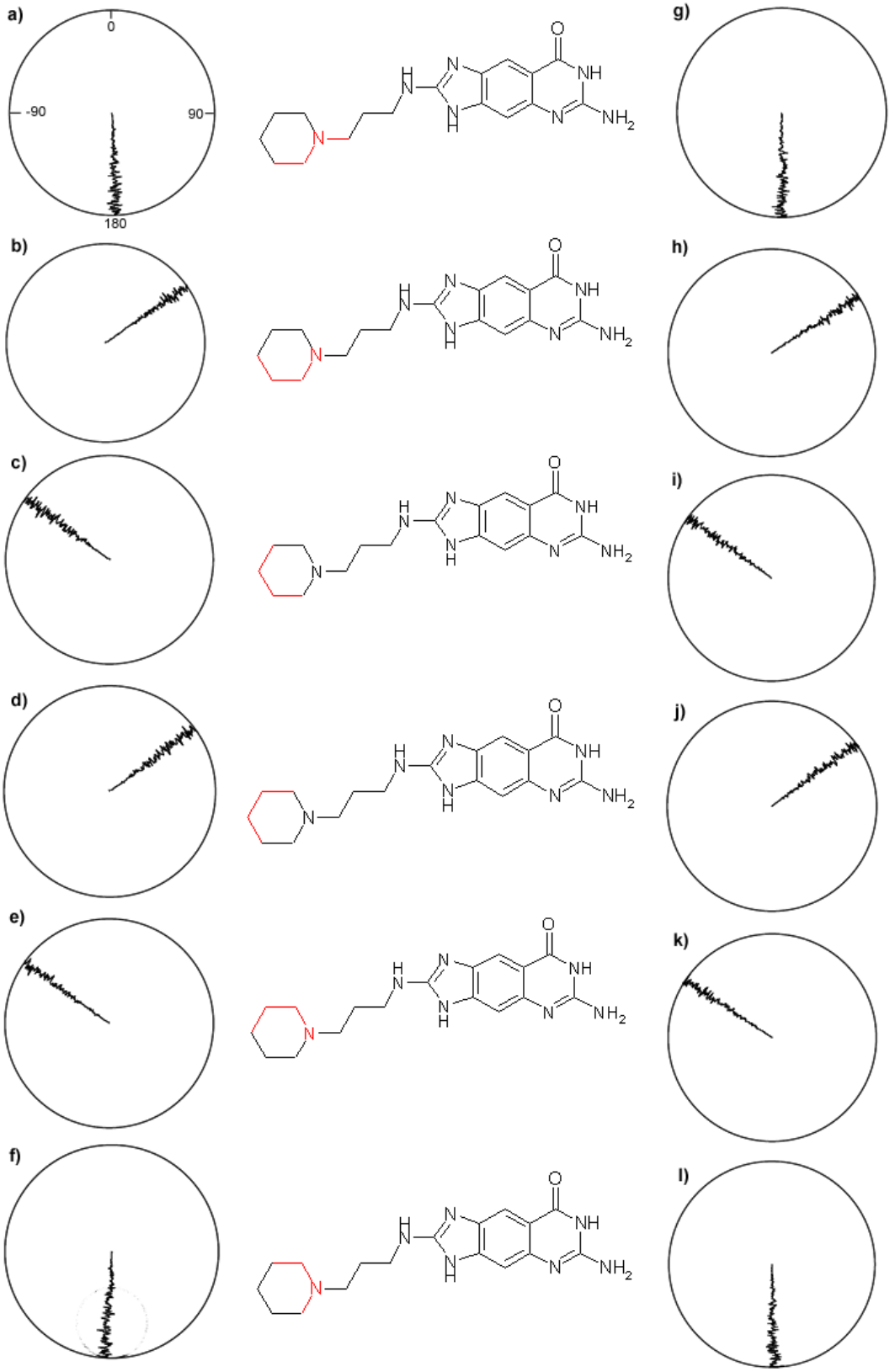

Figure 4.5 *Dialsplots of all possible torsion angles of the piperidine ring in* ***28*** *(neutral form a)- e) and protonated form f)-j). In dialsplots the radius of the circle represents the time axis and the position on the circumference the value for the torsional angle itself.*

Considering the simulation with the uncharged side chain, it remains closer to the surface of the protein, even so no polar interaction interms of a short hydrogen bond are formed.
Additionally, the torsion angles of the ligand provide information about the flexibility of the side chain in complex with the protein. As long as no specific interactions between the ligand and the protein are formed, we can assume that the aliphatic linker prefers a *trans*-conformations while the piperidine ring is in a chair-conformation. With respect to the dialsplots in Figure 4.4 and 4.5 in both simulations the energetically more favored *trans*-conformation for the linker and the chair-conformation for the piperidine ring are conserved over the simulation time.
The distance plots showed that in the simulation with the uncharged side chain this portion remains in closer contact to the protein surface. It also takes some impact on the torsion angles. The change of the angle shown in Figure 4.4 b) is between ± 120°, in accordance with the low rotational barrier between a sp^3 and sp^2 center. In Figure 4.4 d), e), h), and j)) deviations of the side chain conformations from pure *trans*-conformation is indicated alog the trajectory.

4.5 Conclusion

Pure increase in size of the side chains addressing the uracil binding site did not lead to a fixed binding mode of the inhibitor´s side chain. For all inhibitors used in the crystallization experiments the placement of the side chain into a reasonably defined electron density was not possible, which leads to the assumption that no defined interactions between the side chain and the protein are formed. With respect to the docking solutions the basic nitrogen in the side chains are not able to form a strong interaction to e.g. the carbonyl group of Gly261 in the uracil 33 binding site. In addition, the MD simulations of **28** support this observation; as no preferred and over several time steps structurally stable orientations were formed during the simulations.
With regard to the kinetic measurements, this orientational scatter of the side chain is not detrimental to binding affinity, which is in agreement with the following thermodynamic interpretation: Retaining some residual conformational flexibility in the bound state of the ligand is beneficial to its binding entropy. Simultaneously, the occupation of several positions would require desolation of a larger portion of the ribose 33 pocket. This example shows that a large, solvent exposed binding pocket, such as the TGT ribose-33 pocket, is generally best addressed with somewhat flexible substituents.

The relative factorization of entropy and enthalpy to the overall Gibbs free energy of binding can be further investigated by ITC measurements. As a result, an increased entropic contribution of the inhibitors with high binding affinity can be expected. The ITC study possibly provides an alternative view on the relationship between structural elements of the inhibitors and their binding affinity.

5 *lin*-Benzohypoxanthine-based inhibitors

5.1 Introduction

The penetration of inhibitors through human membranes and membranes of the Shigella bacteria is a prerequisite before any enzyme inhibition can take place. The character of membranes requires a balance of lipophilic and hydrophilic characteristics in the inhibitor molecule to facilitate the passage through membranes. For known TGT inhibitors based on quinazolinone- and *lin*-benzoguanine-scaffolds (structure of the molecules are listed in appendix) the membrane permeability was calculated based on statistic data derived from parallel artificial membrane permeability assays (PAMPA) in cooperation with Dr. Manfred Kansy and Dr. Stefanie Bendels at F.Hoffmann-LaRoche.

5.2 Prediction of membrane permeability & modification of the parent skeleton

The calculated PAMPA score is a first estimate to predict the membrane permeability of an inhibitor under investigation. A classification was conducted into low (score < 0.6), borderline (0.6 < score > 0.65), and medium (score > 0.7) membrane permeability. In Figure 5.1 the binding affinity is plotted against the PAMPA score. For inhibitors with high affinity a low PAMPA score is predicted, whereas binders with a moderate affinity receive a medium probability to penetrate membranes. The inhibitor with the highest predicted score is **23**, a molecule based on a modified *lin*-benzoguanine scaffold. In this example the exocyclic amino functionality at C6 is missing. To achive nano molar binding affinity, the inhibitor **7** based on a 2-amino-*lin*-benzogunaine skeleton is compared with **23** (Figure 5.1). The introduction of the amino function at 2-position introduces a positive charge on the parent skeleton and increases the binding affinity significantly. To maintain the higher binding affinities of the 2-amino-*lin*-benzoguanines this amino function in 2-position is mandatory (see section 2). The second difference in the parent skeleton is the presence or lack of an amino group at position C6. Based on this observation the amino function at C6 was removed for all 2-amino-*lin*-benzoguanines leading to the new skeleton of *lin*-benzohypoxanthines. The PAMPA score was calculated for *lin*-benzohypoxanthines (Figure 5.2) and compared to the score of the previous compounds. For all *lin*-benzohypoxanthinen a significant increase in the PAMPA score is obtained compared to the *lin*-benzoguanine analogues.

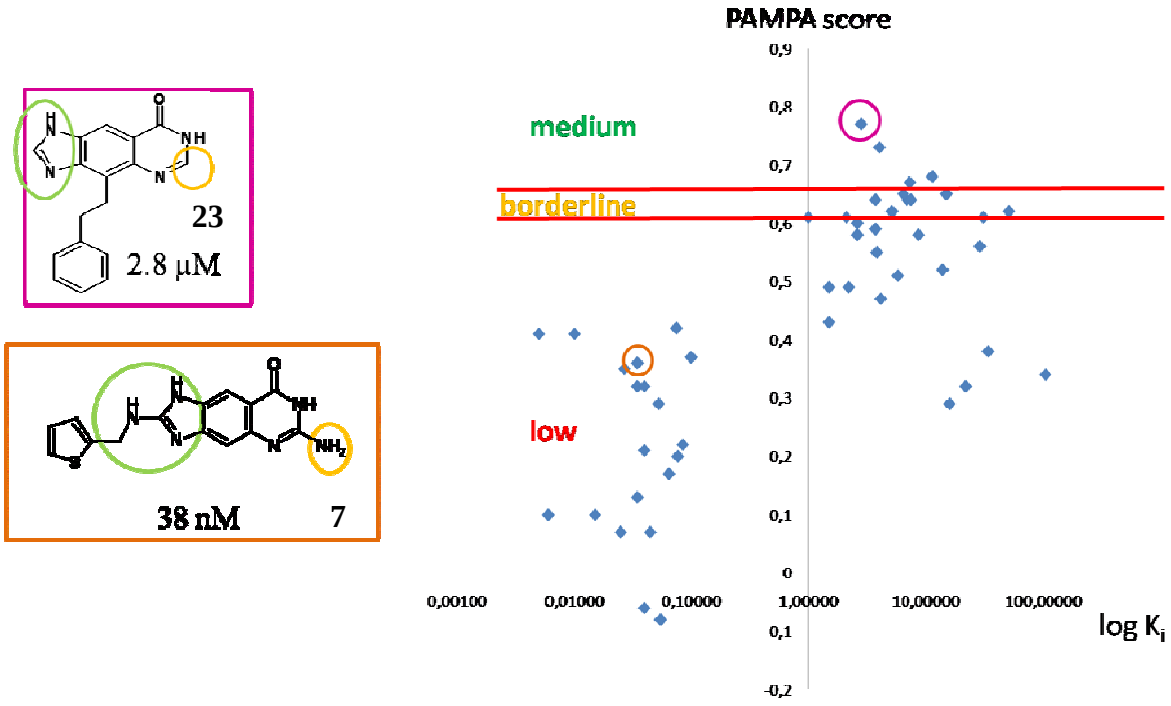

Figure 5.1 *The chart shows the binding affinity of each inhibitor on the x-axis (log scale) and the corresponding predicted PAMP score on the y-axis. The best scored compound is highlighted in magenta (**23**). The structural differences between the best scored compound and the 2-amino-lin-benzoguanine based inhibitors (**7**) (orange) are indicated (green and yellow circles).*

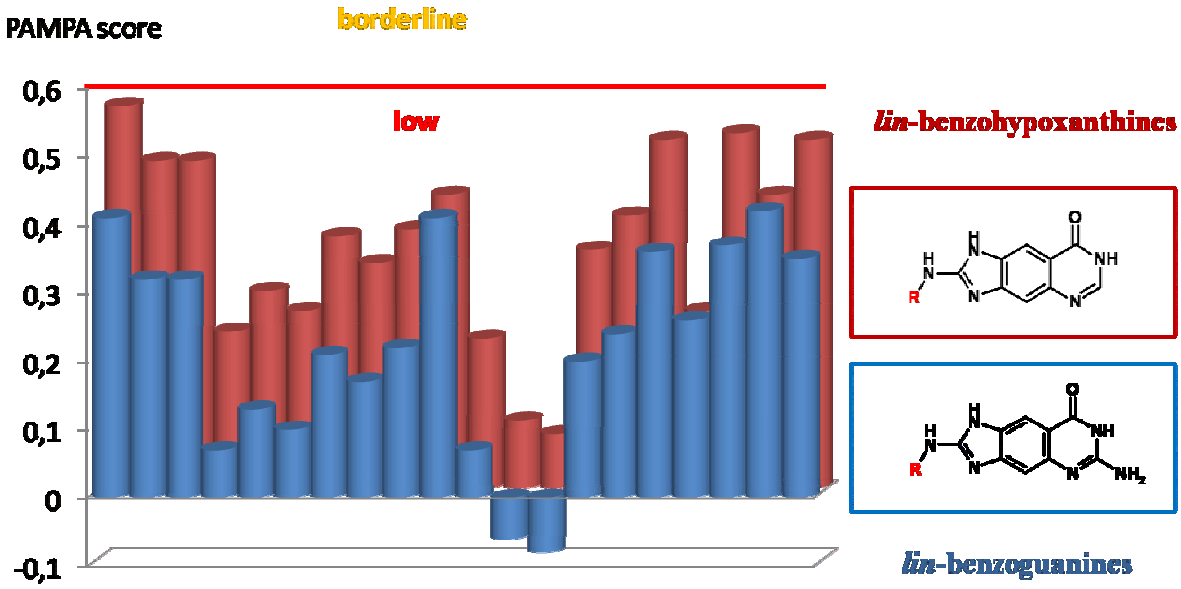

Figure 5.2 *Calculated PAMPA score for lin-benzoguanines (blue) and the corresponding lin-benzohypoxanthines (red).*

5.3 Kinetic characterization

Three inhibitors based on the *lin*-benzohypoxanthine skeleton were synthesized (Table 5.1) in order to evaluate the influence of the lacking amino group. Compounds **42-44** exhibit pure competitive inhibition in the enzyme assay. Disappointingly, the binding affinity of the tested compounds shows a huge decrease (Table 5.1) compared to the corresponding *lin*-benzoguanines. All *lin*-benzohypoxanthines exhibit a binding affinity in the micro molar range. The best affinity is achieved for **42** with 2.9 µM followed by **43** with 3.7 µM and **44** with 4.1 µM.

Table 5.1 *Structure and K_i values of compared lin-benzoguanines and lin-benzohypoxanthines*

compound	structure	K_i [nM]	compound	structure	K_i [µM]
7	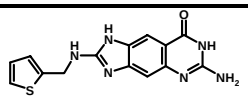	58	**42**	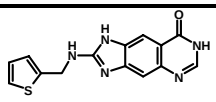	2.9
9	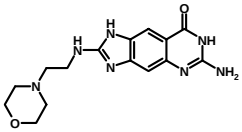	6	**43**	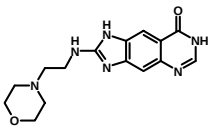	3.7
10	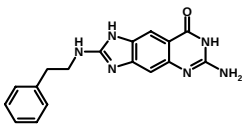	10	**44**	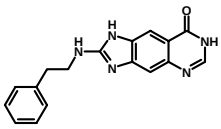	4.1

5.5 Crystal structure

A complex of TGT with **42** and **43** was obtained in this study and compared to the complexes for **7** and **9** (Figure 5.3). In all complexes the aromatic ring system is binding into the guanine binding site and the position is fixed with hydrogen bonds to Asp156, Gln203, Leu231, and Ala232. In contrast to the complexes of **42** and **43,** the side chain of Asp102 is rotated out of the guanine binding pocket and no interactions between inhibitor and side chain of Asp102 are formed. The emerging space is filled with water molecules W3-W5, which can mediate interactions between the inhibitors and Ser103 and Ala154. The movement of Asp102 induced the rotation of Asn70. The position of Asp102 is already known from complexes of other TGT inhibitors and occurs when no hydrogen bond donor facility of the inhibitor is in an appropriate position to form an interaction to the carboxylate group of Asp102.

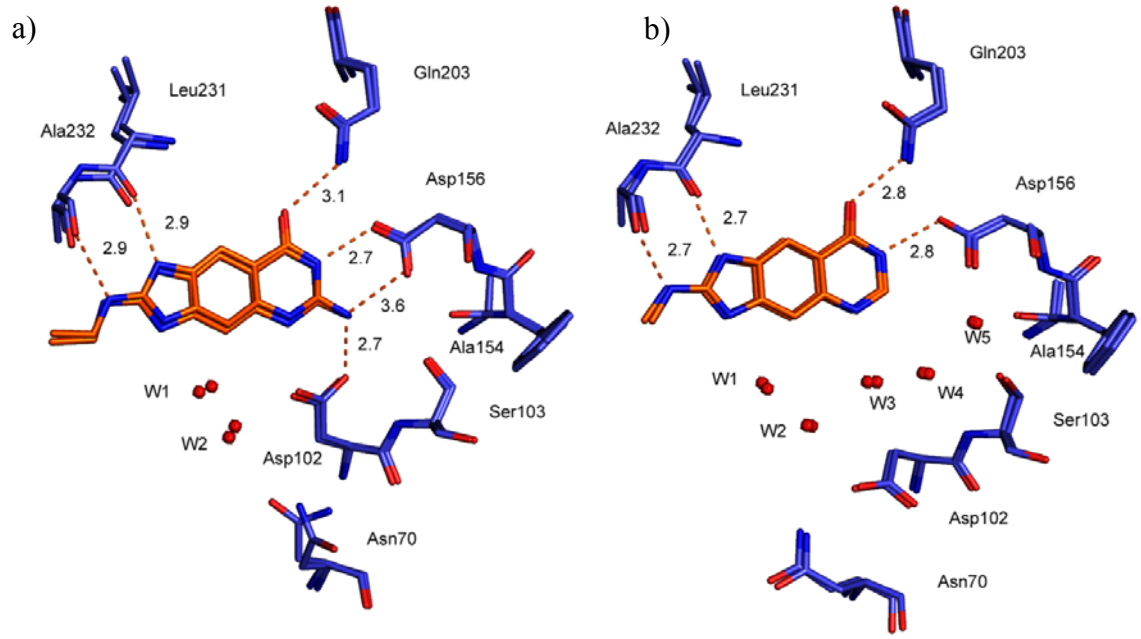

Figure 5.3 *a) Structural superposition of lin-benzoguanines (**7** and **9**) (pdb-code: 3C2N, 3C2Z) and b) lin-benzohypoxanthines (**42** and **43**) (pdb-code: 3GEV, 3GFN). In the complexes of the new skeleton the interaction between the aromatic ring system and Asp102 is missing, because the side chain of Asp102 is rotated out of the binding pocket. The emerging space is filled with water molecule W3-W5. The water molecules are mediating interactions to Ser103 and Ala154.*

5.6 Can new combinations of functional groups improve the PAMPA score?

A next step to improve the binding affinity could be a substitution of the *lin*-benzohypoxanthines in 4-position as shown for the *lin*-benzoguanines in section 3 (Table 5.2). The introduced amino group (e.g. in **46**) could then form interaction to Asp280 and Asp102 simultaneously, which may improve the binding affinities of the compounds. However, most likely these derivatives will be doubly charged again, which can be detrimental for their possibility crossing of membranes. The prediction of the 4-substitutied compounds **46** and **48** does not show an improved prediction, which supports our assumption that the additional charge is detrimental for a good penetration.

With respect to the PAMAP score of the fragment-like inhibitors, presented in Section 6, the introduction of a thiole group in 6-position seemed favorable. Compound **FP3** exhibits a medium probability (0.75) to cross membranes. Introducing a thiol group at the parent skeleton (**47**) reveals a similar PAMPA score (0.39) as for the corresponding *lin*-benzohypoxanthine (**45**: 0.35). Both are significant higher than those calculated for *lin*-benzoguanine (**5**: 0.2). Therefore the thiol in 6-position may be an appropriate interaction

Table 5.2 *Comparison between lin-benzoguanine and lin-benzohypoxanthine based parent skeletons and the newly designed thiole substituted compound. The predicted PAMPA score is given.*

compound	structure	PAMPA score
5	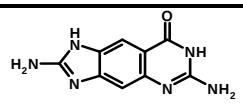	0.20
45	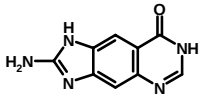	0.35
18	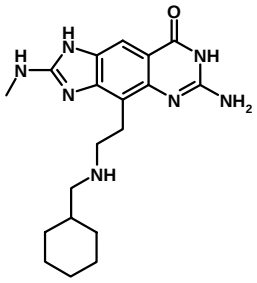	0.26
46	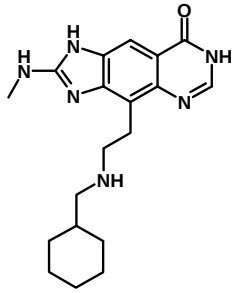	0.23
FP3	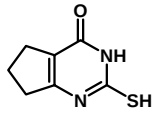	0.75
47	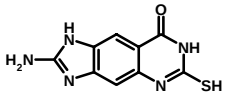	0.39
48	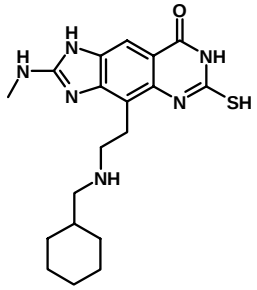	0.27

partner for the carboxylate group of Asp102, which should increase the binding affinity significantly. In combination with the side chain in 4-position the thiol group does not improve the core (**48**: 0.23).

5.7 Conclusion

Disappointingly, the *lin*-benzohypoxanthines showed only reduced potency in the enzyme inhibition assay. No direct interaction between Asp102 and the parent skeleton is observed for the modified scaffold, therefore at least one strong hydrogen bond between Asp102 and the inhibitor is lost.

Consulting the crystal structures, presented in section 2 and 4, the exocyclic amino group at C6 of the *lin*-benzoguanine skeleton is essential of an interaction to Asp102 and has a significant contribution to binding affinity.

The modification of the parent skeleton was successfully performed with respect to an increased probability to penetrate membranes (considering the increased PAMPA score). With the elimination of the exocyclic amino group we remove a positive charge from the molecule, which is favorable for membrane permeability. First measurements in a cell-based assay confirm a higher biological response of the *lin*-benzohypoxanthinen compared to the *lin*-benzoguanines on preventing the Shigella cell invasion process (Adam et al. personal communication).

6 Suche nach neuartigen Fragmenten zur Inhibition von TGT mit Hilfe von DrugScoreFP

DrugScore Fingerprint (DrugScoreFP) ist ein neuartiger Ansatz zur Bewertung von computergenerierten Bindemodi potentieller Liganden für eine bestimmte Zielstruktur. Die Entwicklung des Programms wurde von Gerd Neudert und Patrick Pfeffer in der Arbeitsgruppe Klebe durchgeführt. Für die Validierung wurde eine Suche nach neuartigen Fragmenten, die TGT inhibieren könnten, durchgeführt. Die vorgeschlagenen Fragmente wurden kinetisch und kristallographisch untersucht.

6.1 DrugScoreFP

Das Programm basiert auf der etablierten Bewertungsfunktion DrugScore^{CSD}, die mit aus Kristallstrukturen abgeleiteten, wissensbasierten Potentialen arbeitet. Der Unterschied zu DrugScore^{CSD} und anderen etablierten Bewertungsfunktionen besteht darin, dass nicht alle Einzelbeiträge der verschiedenen Protein-Ligand-Wechselwirkungen zu einem Wert aufaddiert werden. Stattdessen wird anhand bereits bekannter Kristallstrukturen für die zu untersuchende Zielstruktur ein Vektor generiert, der zu jedem einzelnen Bindetaschenatom für jede mögliche Ligand-Wechselwirkung mit diesem Atom einen Wert enthält, welcher aus den wissensbasierten Potentialen stammt. Dieser Referenzvektor ist der so generierte Fingerprint der Bindetasche, welcher ein Bindungsprofil auf Basis der bereits bekannten, aktiven Liganden darstellt. Für jeden neuen, computergenerierten Bindungsmodus eines Liganden lässt sich ein entsprechender Vektor generieren. Dessen euklidische Distanz zum Referenzvektor ist ein Maß dafür, wie stark generierte Bindungsmodi zu bereits bekannten Ähnlichkeit aufweisen. Ein Vorteil dieser Methode ist, dass bereits bekanntes Wissen über die Zielstruktur in die Bewertung neuer Liganden explizit mit einfließt. Während herkömmliche Bewertungsfunktionen auch Bindungsmodi gut bewerten können, die erheblich von der nativen Lage abweichen, wird jede „unnatürliche“ Geometrie von DrugScore^{FP} bestraft. Von besonderem Interesse ist dies zur Bewertung von fragmentartigen Liganden, da es für diese besonders kleinen Moleküle oft eine Vielzahl theoretisch günstiger Bindungsgeometrien in einer Proteintasche gibt. DrugScoreFP ist in der Lage, darunter diejenigen Geometrien herauszufiltern, welche den bereits bekannten Bindungsmodi ähneln, bzw. die gleichen essentiellen Wechselwirkungen aufweisen.

6.2 Suche nach Fragmenten für TGT

Ein erstes Anwendungsbeispiel ist am Beispiel der TGT durchgeführt worden. Hierfür wurde zunächst eine Auswahl an Molekülen mit Fragmentcharakter aus der ZINC-Datenbank und dem NCI-Datensatz zusammengestellt und mit Hilfe von GOLD in die jeweilige Bindetasche eingepasst. Für die Bewertung der entstandenen Bindungsgeometrien wurde der erhaltene Vektor mit dem zuvor generierten Referenzvektor verglichen.

Für TGT sind mehrere Konformationen der Guaninbindetasche bekannt. Je nach pH Wert der Kristallisationsbedingungen oder der physikochemischen Beschaffenheit des Inhibitors kommt es zu einer Rotation von Asp102 in oder aus der Bindetasche und zu einem Peptidflip im Bereich von Leu231/Ala232 (Kapitel 1). Somit wurden für TGT zwei Referenzvektoren erstellt, um der Donor- (NH) und Akzeptor- (C=O) Eigenschaften in Bereich der Bindetasche gerecht zu werden.

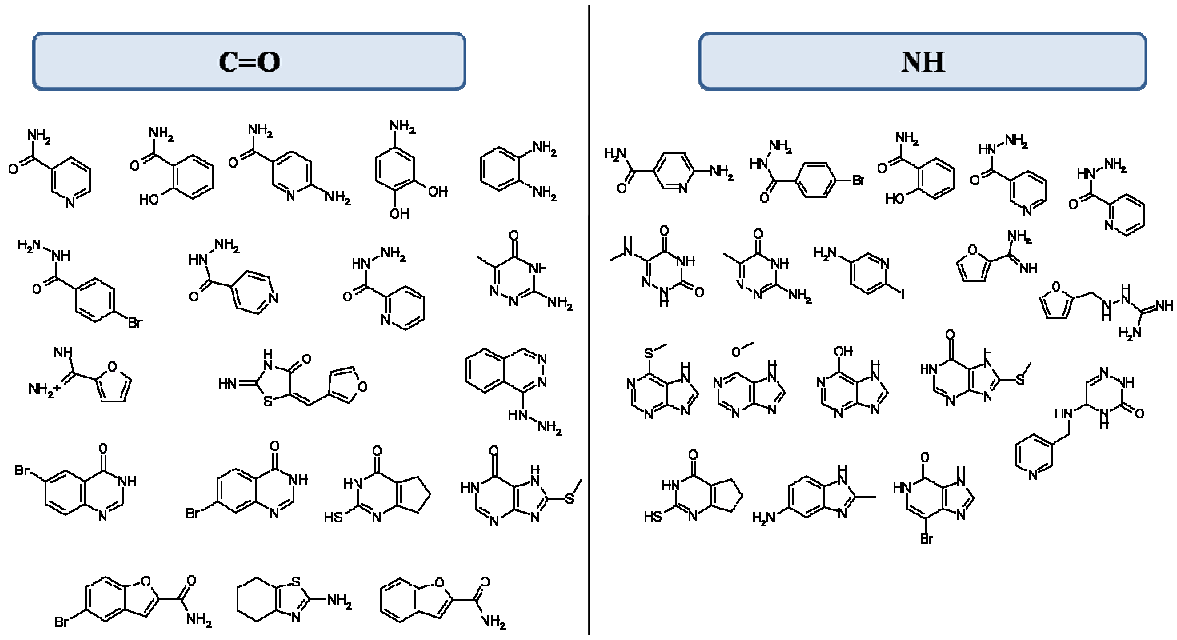

Abbildung 6.1 *Von DrugScore FP gefundene Fragmente für TGT. Die Suche wurde mit zwei Refernzvektoren durchgeführt die im Bereich des Proteinrückgrats von Leu231 und Ala232 entweder die Carbonylgruppe (C=O) oder die NH-Funktion in der Guaninbindetasche aufweisen.*

Die Konformation von Asp102 ist in beiden Fällen so gewählt worden, dass die Seitenkette in die Guaninbindetasche zeigt. Auf diese Weise wird die Bindetasche in ihrer Größe begrenzt und die Platzierung der Fragmente im Docking erleichtert. Zudem zeigen

die Ergebnisse aus Kapitel 5, dass eine Wechselwirkung zur Carboxylfunktion von Asp102 einen entscheidenden Beitrag zur Bindungsaffinität hat.
Die von DrugScoreFP am besten bewerteten Verbindungen sind in Abbildung 6.1 zusammengestellt. Es fällt auf, dass einige Verbindungen von beiden Referenzvektoren erfasst werden. Dies kann auftreten, wenn die gefundenen Fragmente keine Wechselwirkung zum Proteinrückgrat von Leu231 und Ala 232 eingehen.

6.3 Experimentelle Untersuchung

Von den in Figure 6.1 gezeigten Verbindungen wurden 4 Fragmente ausgewählt, gekauft und ihre Affinität bestimmt (Abbildung 6.2). Drei der vier Fragmente zeigen eine Bindungsaffinität im mikomolaren Bereich (K_i-Wert 25 µM (**FP1**), 23 µM (**FP2**) und 6 µM (**FP3**)). Bei **FP4** handelt es sich um das bekannte Tuberkulostatikum Isoniazid, für das keine Bindungsaktivität gemessen werden konnte.
Berechnet man auf der Grundlage der erhaltenen Ki-Werte die für **FP1**-**FP3** die „Ligand Efficiency“ (**FP1**=2.22 kJ/mol (0.53 kcal/mol), **FP2**=2.94 kJ/mol (0.7 kcal/mol) und **FP3**=2.73 kJ/mol (0.65 kcal/mol) ergeben sich Werte die den Fragmenten ein großes Potenzial im Hinblick auf ihre weitere Dekoration mit funktionellen Gruppen bescheinigen, um die Bindungsaffinität zu steigern. Zudem sind für die Fragmente die in Kapitel 5 vorgestellten PAMPA-Werte berechnet worden (**FP1** 0,81, **FP2** 0,51 und **FP3** 0,75) die den Molekülen eine gute Membrangängigkeit bescheinigt. Die gute Passage der humanen oder bakteriellen Zellmembran ist notwendig für eine gute Bioverfügbarkeit des möglichen Arzneistoffes. Bei der weiteren Dekoration sind die „Ligand Efficienca“ und PAMPA-Klassifizierung wertvolle Anhaltspunkte im Optimierungsprozess. Um die weitere Dekoration der erhaltenen Fragmente nicht dem Zufall zu überlassen, sind für alle drei Fragmente Kristallisationsversuche unternommen worden, um ihre Bindungsgeometrie in der Bindetasche zu bestimmen. Die Vermessung der Proteinkristalle in Marburg und am Synchrotron in Berlin (BESSY) ergab trotz einer Auflösung von 1,6-1,7 Å keine signifikante Differenzelektronendichte in der Bindetasche von TGT.

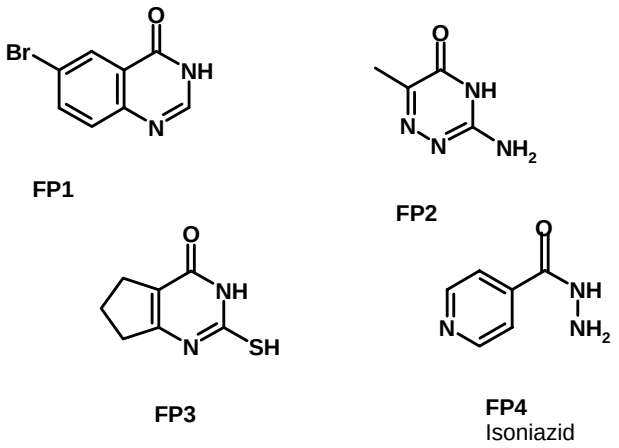

Figure 6.2 *Struktur der vier ausgewählten Fragmente*

Es ist anzunehmen, dass die Moleküle möglicherweise auf Grund ihrer geringen Größe keinen geordneten Zustand in der Bindetasche einnehmen. Die Problematik der völligen Unordnung wird näher in Kapitel 7 am Beispiel der Benzimidazolin-2-on/-thiol basierten Inhibitoren besprochen und soll daher hier nicht weiter behandelt werden.

6.4 Ausblick

Vergleicht man die entdeckten Fragmente mit den natürlichen Substraten Guanin oder $preQ_1$ und den bekannten Inhibitoren der TGT lassen sich strukturelle Ähnlichkeiten erkennen. Das zeigt zum Einen, dass mit DrugScore FP Fragmente gefunden werden können, die mit hoher Wahrscheinlichkeit in die Proteinbindetasche binden. Und zum Anderen lassen sich die gefundenen Fragmente dazu nutzen, bestimmte Strukturen im Grundkörper bekannter Inhibitoren auszutauschen, um z.B. die Löslichkeit, Membrangängigkeit oder metabolische Eigenschaften zu verbessern.

7 Benzimidazolin-2-on/-thiol basierte Inhibitoren

7.1 Virtuelles Screening liefert eine neue Leitstruktur

Ein virtuelles Screening für die Guaninbindetasche der TGT lieferte verschiedene neue Leitstrukturen (Tabelle 7.1). [2] Die gefundenen Verbindungen besitzen Bindungsaffinitäten im mikromolaren Bereich. Für das Screening wurde eine Konformation der Bindetasche verwendet, die zwei Wassermoleküle in Nachbarschaft von Ser103 und Gly104 aufweist. Diese Wassermoleküle nehmen den Raum ein der entsteht, wenn die Seitenkette von Asp 102 aus der Bindetasche gedreht ist.

Tabelle 7.1 *Screeninghits und die dazugehörigen Inhibitionskonstanten in µM (°unmodifizierter Assay; fett: modifizierter Assay nach Stengl et al. [61]).*

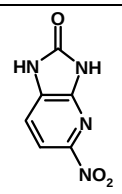	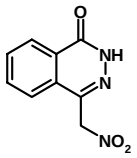	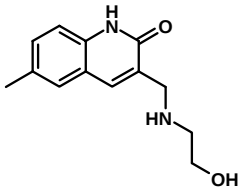
B3 36 ± 24 27 ± 3°	31 ± 5°	58 ± 15°
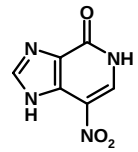	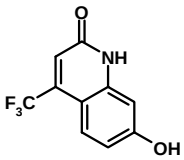	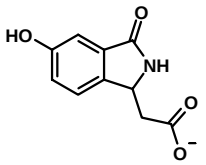
15,1 ± 5°	158 ± 17°	403 ± 33°

Im verwendeten Pharmakophormodell (Abbildung 7.1) sind die Positionen der beiden Wassermoleküle als Akzeptorgruppe (Acc2a/b) berücksichtigt worden. Zusätzlich wurden weitere Akzeptor-/Donorgruppen (Acc1, D1a/b)) in das Modell aufgenommen. Abschließend wurde ein hydrophober Bereich (hydrophobic) eingebaut, der eine π-π-Wechselwirkung mit dem aromatischen Rest von Tyr106 ermöglichen soll. Als erfolgsversprechende Leitstruktur wurde ein Benzimidazolin-2-on-Grundgerüst **B3** identifiziert, das eine Bindungsaffinität von 36 µM aufweist (Tabelle 7.1). Die Dockinglösung des Bizyklus zeigt einen veränderten Bindungsmodus gegenüber bekannten TGT Inhibitoren (Abbildung 7.2) [4, 42, 54]. Danach nimmt das Ringsystem eine um 90° gedrehte Position im Vergleich zu den bisher untersuchten Inhibitoren ein und

liefert somit einen neuartigen Bindungsmodus in der Guaninbindetasche. Es bilden sich Wasserstoffbrücken zu Gly230, Gln203 und Asp156 aus, die die Position der neuen

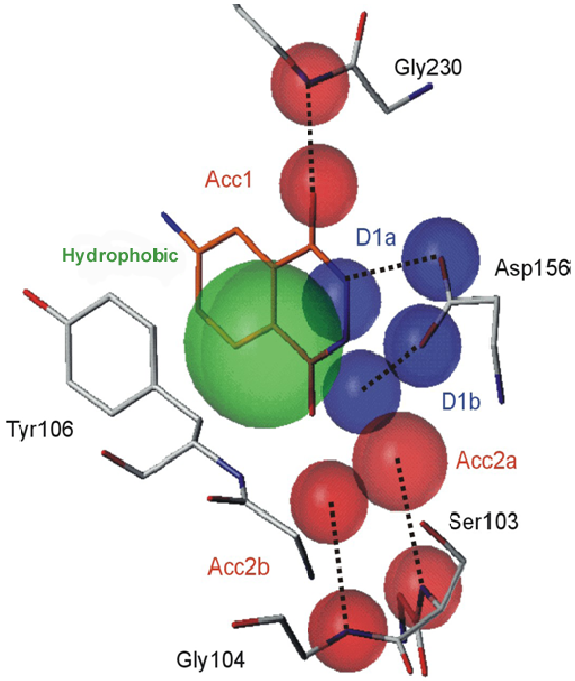

Abbildung 7.1 *Pharmakophormodell, das für das virtuelle Screening verwendet wurde. Zur Übersicht ist ein Ausschnitt der Bindetasche (C, grau, O, rot, N, blau) und ein darin gebundener Inhibitor (C, orange, O, rot, N, blau) gezeigt. Die im Modell verwendeten Akzeptorgruppen und die korrespondierenden Donorgruppen auf Seiten des Proteins sind in rot dargestellt. Die Donorgruppen und die korrespondierenden Akzeptorgruppen auf Proteinseite sind in blau dargestellt. Zusätzlich ist im Modell ein Bereich mit hydrophoben Eigenschaften aufgenommen worden (grün).*

Leitstruktur fixieren. Die Nitrogruppe von **B3** kann gemäß der Dockinglösung die Akzeptorgruppen Acc2a/b des Pharmakophormodells besetzen und die in der Bindetasche vorhandenen Wasser verdrängen. Die Sauerstoffatome der Nitrofunktion können dabei Wasserstoffbrücken zu Ser103 und Gly104 ausbilden.

7.2 Modifikation und Erweiterung der Leitstruktur

Die gefundene Leitstruktur bietet verschiedene Ansatzpunkte zur Modifizierung und Erweiterung des Grundgerüstes (Tabelle 7.2). Alle im Folgenden vorgestellten Verbindungen sind von Dr. Tim Larsen, Marcus Freitag und Khattab El Gaghlab (Arbeitsgruppe von Prof. Dr. Andreas Link, Universität Greifswald) synthetisiert worden.

Tabelle 7.2 *Darstellung der neuen Leitstruktur, die mit Hilfe des virtuellen Screening gefunden wurde (links) und die möglichen Positionen an denen zur Optimierung der Verbindung Veränderungen vorgenommen wurden (rechts).*

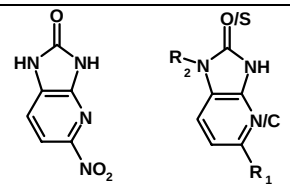

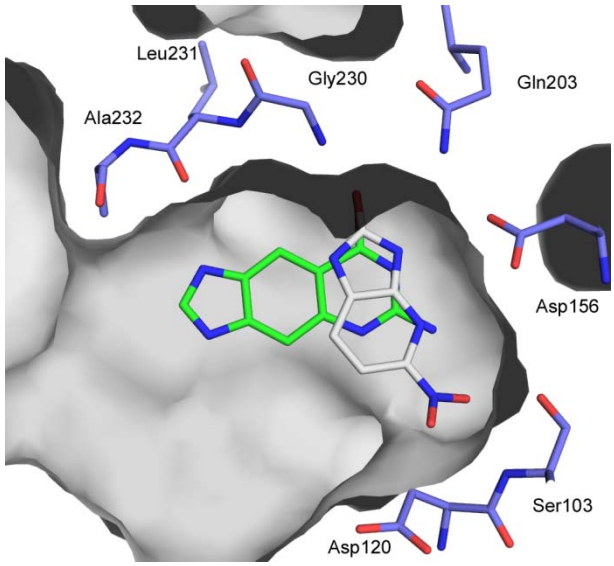

Abbildung 7.2 *Dockinglösung des Screeninghits B3 (C, grau, N, blau, O, rot) in der TGT Bindetasche (Oberfläche grau, C, hellblau, N, blau, O, rot). Überlagert ist ein bekannter Inhibitor (C, grün, N, blau, O, rot) der um 90° gedreht in der Guaninbindetasche bindet, ähnlich den natürlichen Substraten des Enzymes.*

7.2.1 Veränderungen im Grundgerüst

Verbindungen, die eine Modifikation am Grundgerüst tragen, sind in Tabelle 7.3 aufgeführt. Ein Austausch von Sauerstoff gegen Schwefel in 2-Position ermöglicht die Synthese von Benzimidazolin-2-thiolen. Der Austausch des Pyridinrings gegen einen Phenylring, um die Synthese der Verbindungen zu erleichtern, hat keinen signifikanten Unterschied in den Bindungsaffinitäten für das Inhibitorpaar **B2**/**B3** gezeigt, jedoch für das Inhibitorpaar **T11**/**T12** konnte eine Abnahme der Bindungsaffinität beobachtet werden. Die Analyse der Dockinglösungen zeigt, dass eine zusätzliche Wasserstoffbrücke zwischen dem Pyridinstickstoff und Asp156 (Abbildung 7.2) gebildet werden könnte. Der Einfluss des Pyridinstickstoffs auf die Bindungsaffinität ist jedoch von der weiteren Substitution am Grundgerüst abhängig. Für beide Grundgerüste Benzimidazolin-2-on und

Tabelle 7.3 *Benzimidazolin-2-on/-thiol-basierte Inhibitoren mit Bindungsaffinitäten in µM. Zusätzlich ist der Score der besten Dockingpose angegeben.*

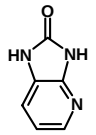	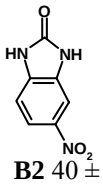	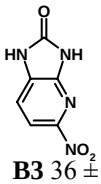	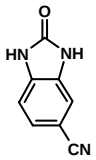	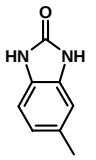
B1 143 ± 49	**B2** 40 ± 17	**B3** 36 ± 24	**B4** 91 ± 29	**B5** 33 ± 9
35,13	40,36	40,78	39,93	39,01
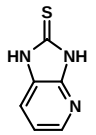	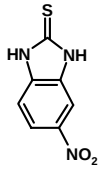		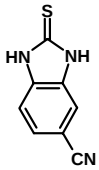	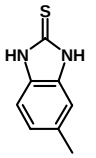
T1 5 ± 1	**T2** 12 ± 4		**T4** 8 ± 4	**T5** 25 ± 10
38,66	41,58		43,84	42,83
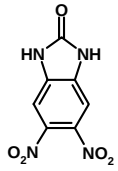	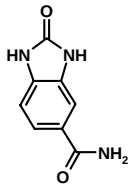	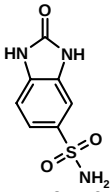	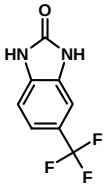	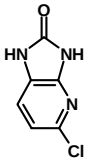
B6 13 ± 3	**B7** 63 ± 12	**B8** 8 ± 3	**B9** 30 ± 4	**B10** 64 ± 14
	41,26	45,92	37,26	37,20
		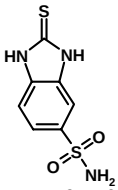	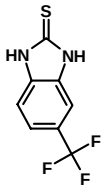	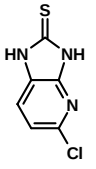
		T8 52 ± 38	**T9** 15 ± 9	**T10** 0,6 ± 0,1
		50,73	41,27	41,01
		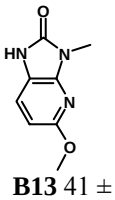		
		B13 41 ± 38		
		37,41		
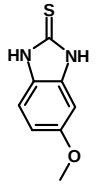	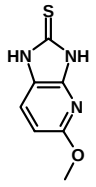	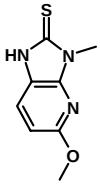		
T11 26 ± 15 *	**T12** 0,85 ± 0,6	**T13** 6,4 ± 5		
42,01	41,96	41,97		

-thiol ist der Einfluss des Substituenten in 5-Position untersucht worden. Ohne die Nitrogruppe in 5-Position kommt es im Falle der Benzimidazolin-2-one zu einem Verlust an Bindungsaffinität (**B1**/**B3**), wohingegen die Bindungsaffinität für die Benzimidazolin-2-thiole offensichtlich keine Verschlechterung erfährt (Vergleich von **T1**/**T2**, da die Verbindung **T3** nicht vorliegt). Der Austausch der Nitrogruppe gegen Trifluormethyl-, Nitril-, Methyl-, Sufonamid-, Amid-, Oxomethyl- und Chlorsubstituenten hat einen unterschiedlichen Einfluss auf die Bindungsaffinität.

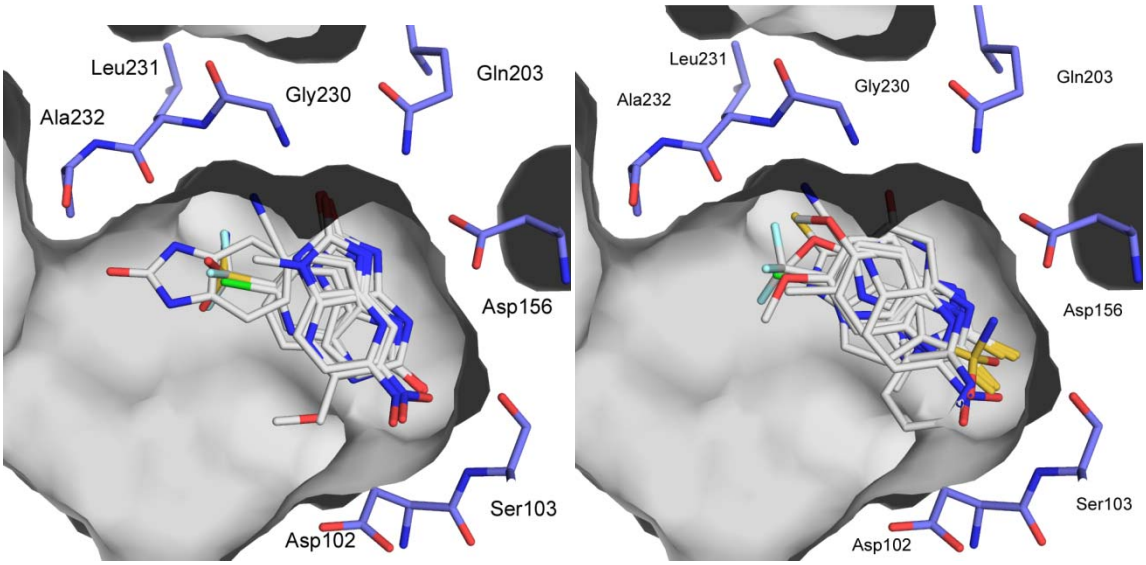

Abbildung 7.3 *Ausschnitt der TGT Bindetasche (Oberfläche grau) mit einer Auswahl von Aminosäuren der Bindetasche, die für die Inhibitorbindung essentiell erscheinen (C, hellblau, N, blau, N, rot). Beste Dockinglösung der Benzimidazolin-2-one B1 – B13 (links) und der Benzimidazolin-2-thiole T1 – T13 (rechts)(C, grau, N, blau, O, rot)*

Im Falle der Benzimidazolin-2-one zeigt die Substitution mit Methyl (**B5**), Sulfonamid (**B8**) und Trifluormethyl (**B9**) eine Verbesserung der Affinität wohingegen die Substitution zur Nitril- (**B4**), Amid- (**B7**), Chlor- (**B10**) und Oxomethylverbindung (**B13**) eine Verschlechterung im Vergleich zu **B2** erbringt. Wird eine zweite Nitrogruppe am aromatischen Ringsystem eingefügt (**B6**), wird eine um das Dreifache gesteigerte Bindungsaffinität im Enzymassay gemessen. Dies lässt vermuten, dass die eingefügte Nitrogruppe zusätzliche Wechselwirkungen zum Protein ausbildet. Innerhalb der Serie der Benzimidazolin-2-thiole, ergibt die Betrachtung der Struktur-Wirkungsbeziehung ein anderes Bild und führt zu folgender Einteilung: eine Erhöhung der Bindungsaffinität ist bei Substitution zur Nitril-(**T4**), Chlor-(**T10**) und Oxomethylverbindung (**T13**) zu

beobachten und im Vergleich zu **T2** eine Erniedrigung nach einfügen eines Methyl- (**T5**), Sulfonamid- (**T8**) und Trifluormethylrestes (**T9**). Hervorzuheben sind **T10** und **T12**, da diese Verbindungen die ersten Vertreter sind, die eine Affinität im submikromolaren Bereich aufweisen. Basierend auf den gemessenen Ergebnissen lassen sich nur schwer vergleichbare Trends im Bindungsverhalten von Benzimidazolin-2-one und Benzimidazolin-2-thiole feststellen. Betrachtet man die Dockinglösungen (Abbildung 7.3) der einzelnen Verbindungen fällt auf, dass bei einem Teil der Verbindungen der Bindungsmodus des Screeninghits **B3** vom Dockingprogramm nicht in vergleichbarer Weise reproduziert wird, sondern offensichtlich eine abweichende Pose als energetisch beste Lösung in der Bindetasche vorgeschlagen wird. Im Docking wurden zusätzlich zu den abgebildeten Molekülen auch die tautomeren Formen getestet (Abbildung 7.4), ohne das ein signifikant anderes Bild für die vorgeschlagene Bindepose erhalten wurde.

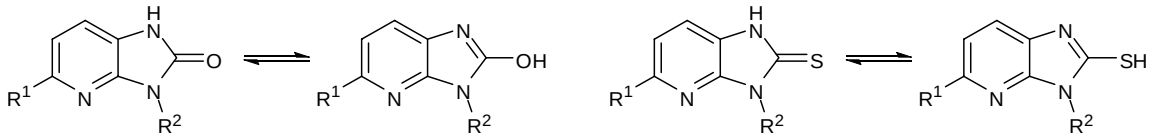

Abbildung 7.4 *Tautomere Formen der Benzimidazol-2-one und Benzimidazol-2-thione.*

Für die Benzimidazolin-2-one haben **B4**, **B8**, **B9** und **B10** einen abweichenden Bindungsmodus, wobei die Carbonylfunktion eine Interaktion zu Ser103 ausbilden kann. Die Substituenten in 5-Position können gemäß der Dockinglösung mit dem Proteinrückgrat von Gly230 und Leu231 wechselwirken. Für Verbindungen der Benzimidazolin-2-thiolserie werden für **T4**, **T5** und **T9-13** abweichende Bindungsmoden im Vergleich zu **B3** erhalten. Wie schon bei den Dockinglösungen der Benzimidazolin-2-one beobachtet, zeigt die Thioharnstofffunktion des Inhibitors zu Ser103 und der Stickstoff in N1 Position des Inhibitorgrundgerüsts bildet eine Wasserstoffbrücke zur Seitenkette von Asp156. Die verschiedenen Substituenten in 5-Position gehen Wechselwirkungen mit dem Proteinrückgrat im Bereich von Gly230 und Leu231 ein. Für Verbindung **T8**, die eine Sulfonamidgruppe in 5-Position trägt, zeigt die Dockinglösung einen Bindungsmodus ähnlich zur ursprünglichen Screeninglösung **B3**. Hier zeigt der Schwefel zum Proteinrückgrat von Gly230 und Leu231, wobei beide NH Gruppen des Proteins in einem Abstand zueinander liegen, der eine Wasserstoffbrückenbindung ermöglicht (jeweils 3.2 Å). Die Sulfonamidgruppe ist in der Dockinglösung durch Wechselwirkungen zu Asp156, Ser203 und Gly204 fixiert.

Die Scoringwerte der einzelnen Verbindungen liegen im Bereich von 35,13 bis 50,73 (Tabelle 7.3). Vergleicht man diese Werte mit den Bindungsaffinitäten, so ist leider zu vermerken, dass keine signifikante Korrelation zwischen den beiden Werten besteht. Die Verbindungen aus der untersuchten Serie besitzen alle eine niedrige Molmasse, sowie eine limitierte Anzahl an Donor/Akzeptorfunktionen und frei drehbare Bindungen. Daher erfüllen sie Kriterien, die man heute im Rahmen einer fragmentbasierten Leitstruktursuche an denkbaren Testkandidaten anlegt.[65-67] Die weltweite Erfahrung zeigt aber auch, dass gerade das Docking von Fragmenten offensichtlich einige Schwierigkeiten mit sich bringt: Aufgrund der begrenzten Anzahl mögliche Wechselwirkungen aufzubauen und der geringen Größe im Vergleich zu der Weite der als Zielstruktur betrachteten Bindetasche erlaubt es, dass mehrere Bindungsmoden in der Proteinbindetasche gefunden werden. Umso mehr ist es essenziell, dass eine zuverlässige Diskriminierung zwischen den möglichen Dockingposen und derjenigen Geometrie, die der so genannten nativen (sprich experimentell analogen) Geometrie nahe kommt, gelingt. Allerdings stellt derzeit diese Aufgabe eine große und bislang keinesfalls befriedigend gelöste Aufgabe an die Entwickler von Dockingprogrammen und Scoringfunktionen. Es bleibt abzuwarten, ob es gelingt, eine verlässlichere Bewertung von Fragmenten, die in eine Bindetasche platziert wurden, zu erhalten.

Zusätzlich zu den Ergebnissen des Dockings unterstreichen die Affinitätsdaten von Verbindungen **B13** und **T13** einen abweichenden Bindungsmodus im Vergleich zum ursprünglichen Screeninghit, da die in 3-Position angefügte Methylgruppe nur eine geringfügige Verschlechterung der Affinität herbeiführt. Würden die Verbindungen, wie postuliert, in der Bindetasche liegen, sollte es zu einer repulsiven Interaktion zwischen dieser Methylgruppe und den geladenen Seitenketten von Asp156 und Gln203 kommen, was sich in einem Verlust an Bindungsaffinität ausdrücken müsste.

7.2.2 Variationen in 1-Position

Für eine weitere Dekoration des Screeninghits bietet sich das Anfügen von verschiedenen aliphatischen Resten in 1-Position an (Tabelle 7.4).

Bindet die modifizierte Base $preQ_1$ in der Bindetasche, entsteht eine Wechselwirkung zu Leu231. Zusammen mit den Erkenntnissen aus anderen Inhibitorserien, die wir in anderen Projekten bestimmen konnten (Kapitel 2), stellt die Erweiterung des Grundgerüstes in 1-Position, mit dem Ziel eine Interaktion zu Leu231 aufzubauen, eine erfolgsversprechende Modifikation des Grundgerüsts dar. [4, 5, 30, 32, 42, 54]

Als bevorzugte Substitution wurde eine Amidgruppe mit einem zweigliedrigen Linker einer Ethylenbrücke in 1-Position eingefügt (beste Dockinglösung jeder Verbindung Abbildung 7.5). Die Dockingscores erhöhen sich im Vergleich zu den Verbindungen aus Abschnitt 7.2 signifikant, was in den zusätzlich gebildeten Interaktionen der Seitenkette zu dem Protein seine Erklärung findet.

Tabelle 7.4 *Benzimidazolin-2-on/-thiol basierte Inhibitoren mit Substituenten in 1-Position. Die Bindungsaffinitäten der Verbindungen sind in µM aufgeführt. Für jede Verbindung ist zusätzlich der Dockingscore angegeben.*

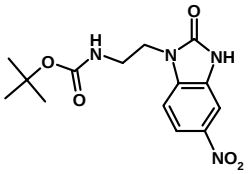			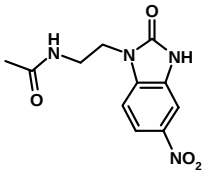
B14 159 ± 40			**B17** 15 ± 2
58,61			57,92
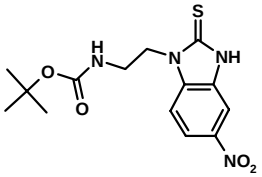	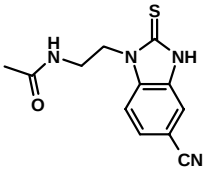	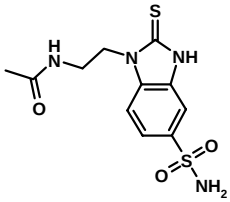	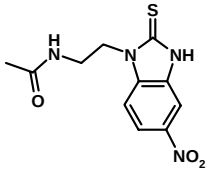
T14 44 ± 5	**T15** 1, 4 ± 0,7	**T16** 5 ± 4	**T17** 2 ± 0,3
56,71	58,17	63,24	56,48
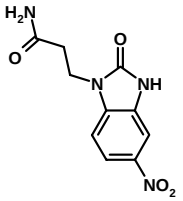		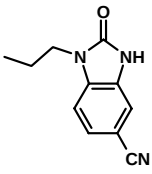	
B18 5 ± 1		**B20** 0,5 ± 0,1	
50,14		47,48	
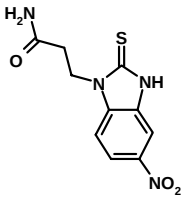	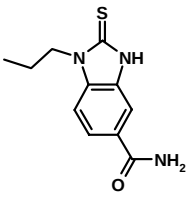	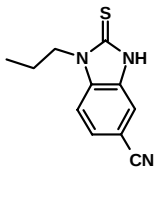	
T18 2 ± 1	**T19** 25 ± 3	**T20** 6 ± 2	
50,50	51,48	47,56	

Die Synthesezwischenstufen **B14** und **T14** tragen eine Boc-Schutzgruppe. Für beide Verbindungen ist eine Abnahme der Affinität im Vergleich zu den unsubstituierten Verbindungen **B2** und **T2** zu erkennen. Der voluminöse *tertiär*-Bultylrest scheint bei **T14** durch seinen Volumenanspruch die Einpassung in die Bindetasche zu erschweren. Die Verbindungen **B17** und **T15-17** zeigen unabhängig vom Substituenten in 5-Position gesteigerte Bindungsaffinitäten. Unter Berücksichtigung der Dockinglösung ist für **B14**, **B17**, **T15** und **T17** die erwünschte Interaktion zu Leu231 möglich, wohin gegen das Dockingprogramm für die räumlich größeren Benzimidazolin-2-thiolverbindungen **T16** und **T14** diesen Bindemodus als eine energetisch günstige Lösung vorschlägt. In Verbindung **B18** und **T18** ist die Amidgruppe zu den vorher beschriebenen Verbindungen in der Seitenkette mit reverser Laufrichtung eingebaut worden. Für das Benzimidazolin-2-on-Derivat **B18** wird eine dreimal höhere Affinität im Vergleich zu **B17** vermessen. Die Dockinglösung von **B18** (Abbildung 7.5) ermöglicht zwei Wasserstoffbrücken zwischen der Amidfunktion und dem Proteinrückgrat im Bereich von Gly230 und Leu231. Für die Verbindungen **T15** bis **T18** ist kein signifikanter Unterschied zu erkennen, die Veränderung in der Seitenkette scheint keinen Einfluss auf die Stärke der Bindung zu haben.

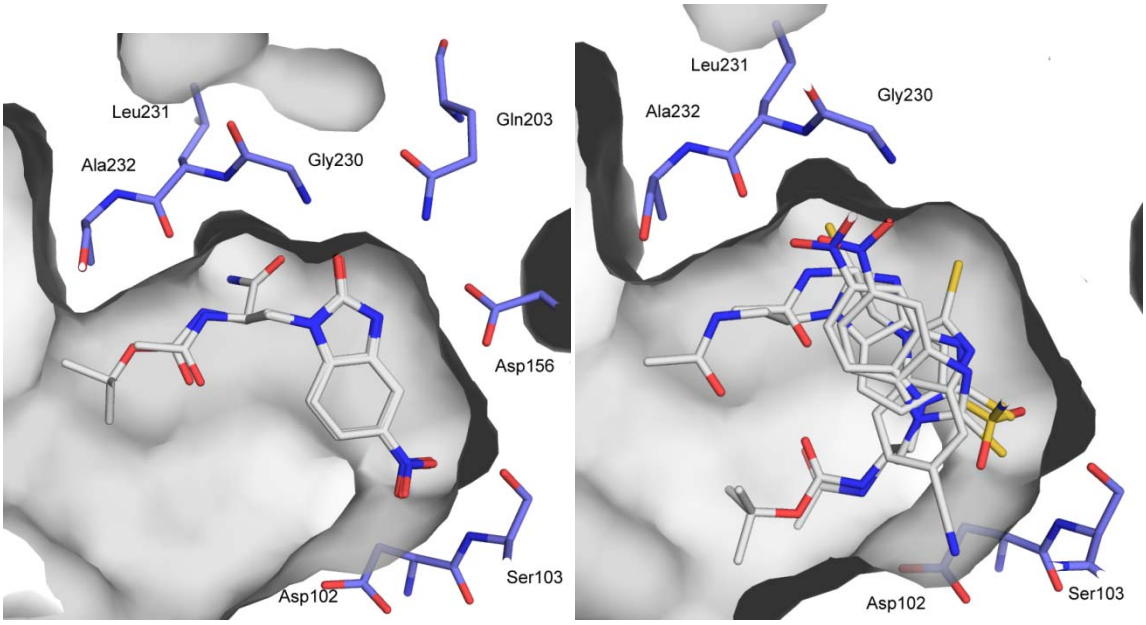

Abbildung 7.5 *Die jeweils beste Dockinglösung (links: Benzimidazolin-2-one* ***B14*** *–* ***B18****, rechts: Benzimidazolin-2-thiole* ***T14*** *–* ***T18****; C, grau, N, blau, O, rot) der Verbindungen mit Variationen in 1-Position sind in der TGT Bindetasche dargestellt (Oberfläche grau, C, hellblau, N, blau, O, rot).*

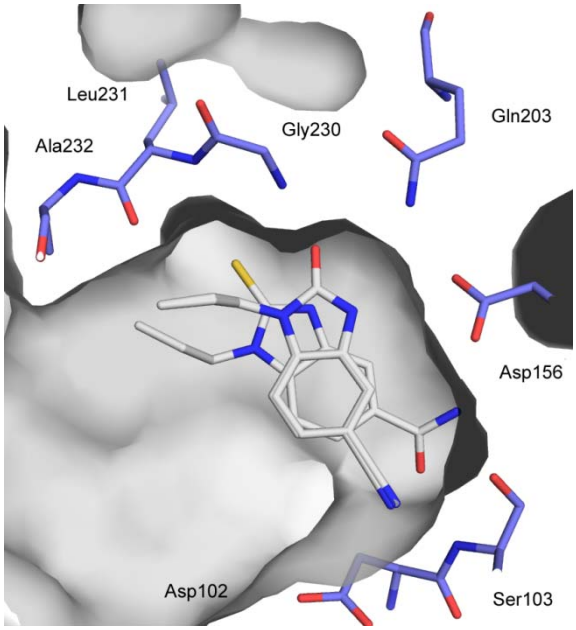

Abbildung 7.6 *Beste Dockingpose der alkylsubstituierten Verbindungen* ***B20***, ***T19*** *und* ***T20*** *(C, grau, N, blau, O, rot) in der Guaninbindetasche (Oberfläche, grau, C, hellblau, N, blau, O, rot)*

Dieses Faktum unterstützt die auf den ersten Blick ungewöhnliche Hypothese eines abweichenden Bindungsmodus der Benzimidazolin-2-on-Serie im Vergleich zu den Schwefelanalogen.Um einen Referenzpunkt für die Wichtigkeit des Vorliegens einer terminalen Amidfunktion in der Seitenkette zu erhalten, sind **B20**, **T19** und **T20** mit einer reinen aliphatischen Kette synthetisiert worden. Diese Verbindungen tragen eine Alkylkette in 1-Position (Abbildung 7.6). Im direkten Vergleich mit **T19** und **T20** fällt erneut die erhöhte Bindungsaffinität für die nitrilsubstituierte Verbindung **B20** auf. Die Substitution mit einer Nitrilfunktion in 5-Position nimmt offensichtlich einen positiven Einfluss auf die Bindungsaffinität. Hervorzuheben ist auch, dass **B20** mit einer Bindungskonstante von 500 nM das Enzym blockiert. Damit ist **B20** die einzige Verbindung der Benzimidazolin-2-one-Serie, die eine Inhibitionskonstante im nanomolaren Bereich aufweist. Aus diesem Grund weisen wir ihr, wie von dem Dockingprogramm vorgeschlagen, einen analogen Bindungsmodus wie den ähnlich potenten Schwefelanalogen zu.

7.2 Kristallstrukturanalyse

Trotz intensivster Bemühungen einer einheitlichen Auswertung und Interpretation der umfangreichen kinetischen Untersuchungen in Kombination mit den erhaltenen

Dockingmoden lässt sich keine einheitliche und in sich widerspruchsfreie Struktur-Wirkungsbeziehung der synthetisierten Verbindungen aufstellen. Leicht liegt es auf der Hand, die beiden Serien mit den Sauerstoff – bzw. Schwefelanalogen Derivaten anhand abweichender Bindungsmoden zu diskutieren. Die Dockingprogramme legen eine solche Diskussion nahe. Auf der anderen Seite ist bekannt, dass kleine strukturelle Adaptionen der Proteinbindetasche leicht bestimmte Dockinglösungen ausschließen bzw. die relative energetische Bewertung der Lösungsvorschläge umkehren. In einer solchen Situation kann nur die experimentelle Bestimmung des Bindungsmodus durch eine Kristallstrukturanalyse eine Klärung herbeiführen. Daher wurden mit den Verbindungen aus Abschnitt 7.1 und den Verbindungen, die in Tabelle 7.5 aufgeführten sind, Kristallisationsversuche durchgeführt.

Tabelle 7.5 *Verbindungen der Benzimidazolin-2-one/thiolserie die kristallographisch untersucht worden sind.*

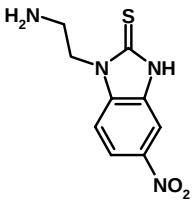	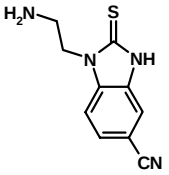	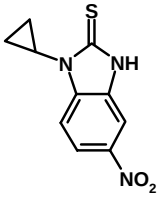	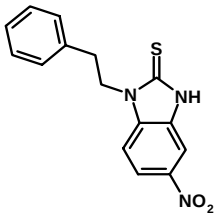	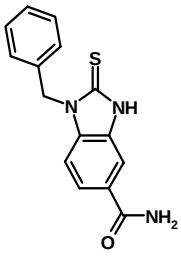	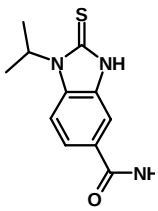
T21	**T22**	**T23**	**T24**	**T25**	**T26**

In Tabelle 7.6 und 7.7 sind die Verbindungen zusammengefasst, für die Protein-Ligand-Komplexe mit *Z. mobilis* TGT gezüchtet und kristallographisch mit Beugungsexperimenten Strukturen bestimmt wurden. Für die Kristallisation wurde die entsprechende Inhibitorlösung zu unkomplexierten Kristallen des Apoenzyms gegeben, wobei der Inhibitor in die Kristalle ein diffundieren sollte. Analoge Soakingprotokolle haben in anderen Studien dieser Arbeit und früheren Dissertationen an mehr als 50 Inhibitoren zum Erfolg geführt, wobei sich die Affinitätsspanne der untersuchten Inhibitoren vom zweistellig mikromolar bis einstellig nanomolar dehnte. [1-5, 42, 54, 61] Trotz intensiver Abwandlung der einzelnen Züchtungs- und Messprotokolle konnte leider für keine der hier beschriebenen Verbindungen eine ausreichende und interpretierbare Elektronendichte in der Bindetasche erhalten werden, die das Einpassen der entsprechenden Verbindung gesichert ermöglicht hätte. Jedoch sind Veränderungen in der

Bindetasche und kristallographischen Packungssymmetrie beobachtet worden, die möglicherweise durch das Binden eines Inhibitors ausgelöst wurden.

7.2.1 Konformationsänderungen in der Bindetasche

Die in Abschnitt 7.1 beschriebene Konformation der Proteinbindetasche, die für die Ableitung des Pharmakophormodells verwendet wurde, basiert auf TGT Kristallen, die bei pH 8,5 gewachsen sind (Tabelle 7.6). In der unkomplexierten Struktur ist die Seitenkette von Asp102 von der Bindeposition eines möglichen Liganden weggedreht und die Ausrichtung des Proteinrückgrats zwischen Gly230 und Leu231 lässt die Carbonylfunktion von Leu231 in die Bindetasche zeigen. Zusätzlich wurden für die Kristallisationsversuche mit den hier beschriebenen. Liganden auch Kristalle verwendet, die bei pH 5,5 (Tabelle 7.7) gezüchtet wurden. Bei diesem pH-Wert ist Asp102 zu 75% in die Proteinbindetasche hinein rotiert und das Proteinrückgrat zwischen Gly230 und Leu231 nimmt eine umgeklappte Orientierung an, wobei nun die NH-Gruppe von Leu231 in die Bindetasche zeigt. [30] Durch die Variation der Kristallisationsbedingungen sollte sich die Wahrscheinlichkeit erhöhen, Konditionen zu finden, die einen Inhibitor in der Bindetasche fixieren. Leider konnte auch unter den veränderten Kristallisationsbedingungen keine Komplexstruktur mit einer brauchbar zu interpretierenden Differenzelektronendichte eines Inhibitors mit der TGT erhalten werden. Vereinzelt lassen sich jedoch in der Proteinbindetasche Veränderungen beobachten, die, wie in erfolgreich populierten Protein-Ligandkomplexen mit der TGT nachgewiesen, nur durch das Binden eines Liganden in der Bindetasche hervorgerufen werden können (Tabelle 7.6 und 7.7). In beiden Apoformen ist der Benzylrest von Tyr106 in die Bindetasche rotiert und geht eine Wasserstoffbrücke zur Säuregruppe von Asp156 ein. [36] In dieser Orientierung nimmt er praktisch den Platz des natürlichen Substrats des Guanins oder $preQ_1$ im katalytischen Zentrum ein. Um substratkompetitiven Inhibitoren Einlass zu gewähren, muss dieser Rest aus der Bindeposition in der Apostruktur verdrängt werden. Folglich ist für alle erfolgreich bestimmten Inhibitorkomplexe der TGT zu beobachten, dass der Benzylrest eine Orientierung einnimmt, die eine Bindung des Inhibitors in der Bindetasche freigibt.

Tabelle 7.6 *Konformationsanalyse der Bindetasche (BT) von TGT bei pH 8,5*

Komplex	Tyr 106	Asp 102	Leu 231 NH in der BT	Leu 231 C=O in der BT
apo	verschließt die BT	100% raus		x
B8	BT offen	raus		x
T10	BT offen	raus		x
T17	BT offen	raus	x	
B17	BT offen	raus		x

Tabelle 7.7 *Konformationsanalyse der Bindetasche (BT) von TGT bei pH 5,5*

Komplex	Tyr 106	Asp 102	Leu 231 NH in der BT	Leu 321 C=O in der BT
apo	Verschließt die BT	25% raus	x	
B20	BT offen	raus		x
T21	BT offen	raus	x	
T22	BT offen	-	x	
T23	BT offen	raus	x	
T24	BT offen	raus	x	
T25	BT offen	raus	x	
T1+T17+T26	BT offen	raus	x	

Durch die veränderte Position können die aromatischen Grundkörper der komplexierten Inhibitoren eine π-π Interaktion mit dem verdrängtenTyr106 und Met260 eingehen. Für die erfolgreich kristallisierten Leitstrukturen führt diese Interaktion zu deren Fixierung in der Bindetasche. Die Verdrängung des Benzylrests aus der Bindetasche konnte auch in allen Datensätzen beobachtet werden, die an Kristallen vermessen wurden, die sich unter Zusatz der Benzimidazolin-2-one/-thiole gewinnen ließen. Jedoch ist in diesen Datensätzen kein Hinweis auf eine Elektronendichte zwischen Tyr106 und Met260 zu finden, die auf eine Inhibitorfixierung in der Bindetasche hindeuten würde.

Die Lage der Seitenkette von Asp102 ist für alle vermessenen Datensätze aus den Kristallisationsversuchen mit den Benzimidazolin-2-onen und –thiolen gleich, d.h. die Carboxylfunktion zeigt in Übereinstimmung mit dem für die Docking- und Screeningversuche verwendeten Pharmakophormodell aus der Bindetasche. Im Vergleich zur Apostruktur bei pH 5,5 wird deutlich, dass Inhibitoren aus der Serie möglicherweise in die Tasche ein diffundieren und die Konformation der Seitenkette beeinflussen, wodurch es zu einer Rotation der Seitenkette aus der Bindetasche kommt. Dies könnte ein

indirekter Hinweis sein, dass trotz des Fehlens eines durch eine brauchbare Differenzelektronendichte angezeigten Inhibitors, die Bindetasche von einem Liganden besetzt wird.

Hervorzuheben sind auch die im Proteinrückgrat beobachteten Veränderungen zwischen Gly230 und Leu231. Für Verbindung **T17** und **B20** sind die Kristallstrukturen jeweils mit einer gedrehten Konformation der Amidbindung erhalten worden im Vergleich zur korrespondierenden Apostruktur. [30, 36] Auch diese Veränderung verweist auf eine Bindung eines Inhibitors. Dass dennoch keine auswertbare Differenzdichte auf die Anwesenheit eines Inhibitors schließen lässt, könnte möglicherweise in einem total ungeordneten Bindungsverhalten seine Erklärung finden. Ein Diffraktionsmuster belegt nur dann die Anwesenheit eines gebundenen Liganden, wenn dieser periodisch von einer Elementarzelle zur nächsten im zeitlichen Mittel und gleicher Ausrichtung in der Bindetasche auftritt. Das Phänomen einer totalen Unordnung des gesamten, über polare Wechselwirkungsgruppen verfügenden Liganden erscheint unwahrscheinlich und ist selbst für Liganden der hier vorliegenden „Fragmentgröße“ bisher kaum beschrieben – vielleicht aber auch, weil es so schwierig nachzuweisen ist! Denkbar ist ein solches Verhalten, allerdings ist der Nachweis solcher Eigenschaften äußerst komplex und nur durch indirekte Beobachtungen abzusichern.

7.2.2 Raumgruppenänderung

Die Verbindungen, die in diesem Abschnitt vorgestellt wurden, haben alle ein relativ geringes Molekulargewicht mit einer begrenzten Anzahl rotierbarer Bindungen und Donor-/ Akzeptorfunktionen. Somit fallen sie, wie beschrieben, in die typische Kategorie von Fragmenten. [65-67] Auf der Suche nach neuartigen Molekülbausteinen, die in eine Proteinbindetasche binden können, wurde in den letzten Jahren vermehrt diese Art des Fragmentscreenings durchgeführt (Kapitel 6). Eine häufig angewendete Strategie ist dabei die Verwendung von Fragmentcocktails. [68] Dazu werden Inhibitoren mit unterschiedlichen strukturellen Bausteinen gleichzeitig den Apokristallen des Proteins unter geeigneten Soaking-Bedingungen ausgesetzt. Für das TGT-Enzym wurden bereits verschiedene Fragmentcocktails für ein Screening eingesetzt. Leider konnten auch im Rahmen dieser Versuche keine Datensätzen und ausreichenden Differenzelektronendichten erhalten werden, die die Präsenz eines gebundenen Fragments andeuten.

Bei der Verwendung einer Mischung aus den Verbindungen **T1**, **T17** und **T26** wurde allerdings eine Raumgruppensymmetrieerniedrigung von *C2*, in der das Apoenzym kristallisiert, zu *P2* beobachtet. Dieses Phänomen bei der Bindung eines Liganden konnten wir bereits früher an einem anderen Komplex beobachten. [5] Dort bestand der strukturelle Unterschied darin, dass in der Raumgruppe *C2* die Dimere, mit denen die TGT aus funktionellen Gründen vorliegt (Kapitel 8), durch symmetrieäquivalente Monomere erzeugt werden. Daher sind in dieser Raumgruppe die beiden Monomere des Dimers aus Symmetriegründen strukturell identisch. In der Raumgruppe *P2* sind die beiden Monomere der TGT-Dimere nicht mehr zwingend symmetrieäquivalent, da die kristallographische Symmetriebedingung nicht mehr gegeben ist. Auch in den hier mit dem „Cocktail“ aus **T1**, **T17** und **T26** erhaltenen Datensatz deutet sich das gleiche Strukturphänomen an. In einem der ursprünglich symmetrieäquivalenten Homodimere kommt es zu einer Fehlordnung der Helix α1. Diese Veränderung konnte auch in dem Komplex der TGT mit einem in 4-Position substituierten *lin*-Benzoguanininhibitor beobachtet werden. [5] Hierbei führte die Seitenkette des Inhibitors zu einer Verdrängung der Helix α1. Allerdings lässt sich bei genauer Auswertung der Differenzelektronendichte kein Hinweis auf eine geordnete Anwesenheit eines der drei in dem Verbindungscocktail eingesetzten Verbindungen erkennen.

7.3 ESI-MS Experimente

Für alle im Rahmen dieser Arbeit kristallographisch untersuchten Verbindungen der Benzimidazolin-2-on/-thiol Serie war es nicht möglich, ausreichend Differenzelektronendichte in der Proteinbindetasche zu entdecken, die die geordnete Anwesenheit eines Inhibitors gesichert anzeigt. Daher wurde mit Hilfe von nicht-defragmentierenden MS-Experimenten versucht anhand einer Erhöhung der Masse festzustellen, ob ein Inhibitor an das aktive Protein bindet (Abschnitt 8). [69] Stellvertretend wurde an dieser Stelle **T20** untersucht (Daten werden für **T20** nicht explizit gezeigt). In diesen Experimenten war festzustellen, dass kein Hinweis durch veränderte Massenpeaks auf die erfolgreiche Bildung eines Protein-Inhibitor-Komplexes gefunden werden konnte. Es ist auch kein Einfluss auf die Stabilität bzw. Ausbildung des TGT Homodimers zu beobachten, was man erwarten würde, wenn der Inhibitor in der Schnittstelle zwischen den Dimerkontaktflächen binden und diese signifikant schwächen würde. Das Binden im „Dimerinterface“ scheint bei der TGT im Prinzip möglich, da das Protein in Lösung im Gleichgewicht zum Teil als Monomer vorliegt.

7.4 Ausblick

Basierend auf dem Screeninghit **B3** ist eine Serie von Benzimidazol-2-on/-thioninhibitoren entstanden, die durch Modifikation an verschiedenen Positionen des Grundgerüsts weiterentwickelt wurden. Es ist gelungen, die ursprüngliche Affinität von 36 µM auf 500 nM zu verbessern. Die kinetischen Untersuchungen in Kombination mit den Dockinglösungen suggeriert jedoch, dass für die Inhibitorserie keine Diskussion der beobachteten Struktur-Wirkungsbeziehung anhand eines einheitlichen Bindungsmodus möglich ist. Folglich deutet das Docking mehrere Bindungsmodi an. Allerdings erschwert das Docking der Verbindungen ihr Fragment-Charakter, so dass aufgrund ihrer geringen Größe das Einnehmen multiple Bindungsmodi in der Bindetasche denkbar wäre. Das Fehlen der gesicherten Geometrie eines Protein-Inhibitor-Komplexes aus der Serie beeinträchtigt die Deutung der kinetischen Ergebnisse, obwohl verschiedene Veränderungen in der Proteinbindetasche auf ein Binden der Inhibitoren an das Protein hindeuten. Wie schon durch die Dockinglösungen angedeutet, könnte es für eine Verbindung mehrere Möglichkeiten, geben in die TGT Bindetasche zu binden. Falls ein solches Verhalten tatsächlich vorliegen sollte, kann in der Kristallstruktur aufgrund der ausgeprägten Unordnung keine ausreichend definierte Differenzelektronendichte für einen ausgezeichneten Bindemodus erhalten werden.

Zusätzlich zeigen auch die MS-Experimente, dass es nicht zur Ausbildung eines eindeutigen Protein-Ligand-Komplexes kommt. Es lässt sich vermuten, dass die Inhibitoren an TGT binden, aber keinen Komplex mit einer eindeutigen rigiden Bindungsgeometrie bilden. Ein solcher „transienter“, vermutlich rein entropisch begünstigter Komplex, ist weder mit der Röntgenkristallographie noch mit den MS-Experimenten nachzuweisen.

Ein Ziel für das Design nachfolgender Verbindungen wäre eine weitere Vergrößerung des Grundgerüstes, um einen einheitlichen Bindungsmodus in der Proteinbindetasche zu erhalten. Ein Ansatz, der in Folge versucht werden soll, konzentriert sich auf eine kovalente Fixierung der Verbindungen über einen flexiblen Linker und dem Protein. Gegebenenfalls lässt sich so eine gerichtete Bindungsgeometrie ermitteln. Das angesprochene Verfahren wird in der Literatur als *Tethering* bezeichnet. [70] Über den Weg der Umsetzung mit Disulfiden mit einem nahe der Bindetasche befindlichen Cysteinrest lässt sich eine solche kovalente Verankerung erzielen. Im vorliegenden Fall soll der Cystein 281 zu diesem Zweck verwendet werden, entsprechende Disulfide

müssen mit den untersuchten Benzimidazol-2-on/-thionen gebildet werden. Weiterhin planen wir, thermodynamische Untersuchungen der Bindung dieser Liganden an die TGT vorzunehmen. Es ist zu erwarten, dass die Bindung dieser Inhibitoren stark entropiegetrieben erfolgen sollte.

8 An integrative approach combining noncovalent mass spectrometry, enzyme kinetics and X-ray crystallography to decipher TGT protein-protein and protein-RNA interaction

The nanoESI-MS measurents in ths section are prepared by *Cédric Atmanene* in the group of Dr. *Sarah Sanglier-Cianferani* at the Laboratoire de Spectrométrie de Masse Bio-Organique in Strasbourg.

8.1 Abstract

The tRNA modifying enzyme, tRNA-guanine transglycosylase (TGT), constitutes a putative target for new selective antibiotics against *Shigella* bacteria. Based on several crystal structures of TGT in complex with RNA the formation of a TGT homodimer was suggested. In the present study, noncovalent mass spectrometry was used i) to confirm the dimeric oligomerisation state of TGT in solution and ii) to evidence the binding stoichiometry of the complex formed between TGT and its full-length substrate tRNA. To further investigate the importance of TGT protein-protein interaction, point mutations were introduced into the dimer interface and the tRNA binding site in order to study their influence on the formation of the catalytically active complex. Enzyme kinetics revealed a reduced catalytic activity of these mutated variants which could be related to a destabilization of the dimer formation as evidenced by both noncovalent mass spectrometry and X-ray crystallography. Finally, effect of inhibitor binding was investigated by noncovalent mass spectrometry, providing thus the binding stoichiometries of TGT : inhibitor complexes and showing competitive interactions in the presence of tRNA. Inhibitors, which display an influence on the formation of the dimer interface in the crystal structure, are promising candidates to alter the protein-protein interaction, which could bear a new way to inhibit TGT.

8.2 Introduction

Shigella ssp constitute the causative agent of bacillary dysentery, an acute inflammatory disease of the colon characterized by bloody, mucopurulent stools. [9] Although Shigellosis is spread all over the world, the vast majority of cases occur in developing countries, where this disease causes the death of more than one million humans (mainly infants) per

year.[7] A null-mutation in the *tgt* gene encoding the tRNA modifying enzyme tRNA-guanine transglycosylase (TGT, E.C. 2.4.2.29) was found to drastically decrease pathogenicity of *Shigella* ssp. [13] Bacterial TGT is involved in the biosynthesis of the hypermodified tRNA nucleoside queuosine (Q) by catalyzing the replacement of the genetically encoded guanine at position 34 (the wobble position) of tRNAs$^{Asp, Asn, His, Tyr}$ by $preQ_1$ (Figure 1.2 page 17). This premodified base is produced from guanosine triphosphate by means of the *queC, queD, queE* and *queF* gene products. [19, 17, 16, 18] After insertion into tRNA it is further converted to Q base by the enzyme *S*-adenosylmethionine:tRNA ribosyltransferase-isomerase (QueA) [24] [20] and a putative coenzyme B_{12} dependent enzyme which still remains to be identified. [23] In many bacteria, Q experiences a further modification catalyzed by the *yadB* gene product which attaches a glutamyl residue to one of the hydroxyl groups of the cyclopentenediol moiety of Q. [25, 26, 27, 28]

The base exchange catalyzed by bacterial TGT follows a ping pong reaction mechanism (Figure 1.3 page 18). [41] After binding of substrate tRNA the glycosidic bond of guanine 34 is cleaved *via* a nucleophilic attack by the Asp280 side chain carboxylate producing a covalent TGT:tRNA complex intermediate (Figure 1.3a, b page 18). Subsequently, $preQ_1$ replaces guanine within the binding pocket and is incorporated into tRNA in a reverse reaction step (Figure 1.3c, d page 18). Remarkably, the replacement of guanine by $preQ_1$ induces a flip of the Leu231 / Ala232 peptide bond within the substrate binding pocket. While *N*7 of the bound guanine contacts the main chain amide of Ala232 *via* a water molecule (W1 in Figure 1.3a, b page 18), the main chain carbonyl of Leu231 is required to *H*-bond the exocyclic amino methyl group of $preQ_1$. Both peptide back bone conformations are stabilized by the side chain carboxyl of the strictly conserved Glu235. [30] Depending on its protonation state, it either donates an *H*-bond to the backward oriented carbonyl oxygen of Leu231 or accepts an *H*-bond from the Ala232 main chain amide.

It was shown that a functional TGT is prerequisite for efficient translation of *virF*-mRNA encoding the most-upstream positive transcriptional regulator of *Shigella* pathogenicity genes. Probably, the presence of Q at the wobble position of tRNAs$^{Asp, Asn, His, Tyr}$ is critical for smooth decoding of this particular mRNA. In a recent publication, however, Hurt *et al*. provided a hint, that the loss of *Shigella* pathogenicity due to inactivation of the *tgt* gene may be differently explained. [71] This group showed that *in vitro* TGT is able

to recognize *virF*-mRNA as a substrate and to replace the guanine at position 421 of this mRNA by $preQ_1$. Similar to guanine 34 in tRNAs constituting TGT substrates, guanine 421 of *virF*-mRNA is present in the loop region of a stem loop structure and is flanked by a U nucleotide on either side. Nevertheless, whether the modification of *virF*-mRNA with $preQ_1$ takes place *in vivo* and plays a regulatory role reminiscent of mRNA riboswitches, still remains to be elucidated. In any case, the fact that full pathogenicity of *Shigella* ssp depends on TGT activity renders this enzyme a promising target for the development of drugs against Shigellosis.

Accordingly, using computer aided techniques, several small molecules where designed and identified as inhibitors of TGT with the most potent ones having affinities in the low nanomolar range. [1, 2, 3, 4, 42, 5, 54] The design of these inhibitors was based on the crystal structure of TGT from *Zymomonas mobilis* whose active centre is virtually identical to the one of the *Shigella* enzyme. The binding pockets of both orthologs solely differ by a conservative Phe to Tyr exchange proven to be irrelevant for ligand binding. [31]

Since various experiments which were aimed to seek for a quarternary structure of bacterial TGT yielded contradictory results, the subunit composition of this enzyme has long been a matter of debate. Okada and Nishimura, who were the first to isolate TGT from *Escherichia coli* to homogeneity, deduced from a size exclusion chromatography experiment an apparent molecular mass of 58 kDa for this enzyme. [33, 34] In view of the calculated molecular mass of 42.5 kDa, this is most consistent with a monomeric state in solution. In contrast, the migration behavior of recombinantly produced *E. coli* TGT in native PAGE suggests a pentameric or even hexameric state, although the results of SDS-PAGE of this enzyme crosslinked with bisimidoesters render the formation of a trimer likely. [72] In a subsequent work it was shown that size exclusion chromatography performed with recombinant *E. coli* TGT does not yield unitary results. [73] Instead, the apparent molecular weight deduced from each run depends on the concentration of the enzyme loaded to the gel filtration column and, at high concentrations, asymptotically reaches a value of ca. 140 kDa (corresponding to a trimer). In contrast, the apparent molecular mass of the recombinant orthologous enzyme from *Z. mobilis* deduced from size exclusion chromatography constantly amounts to ca. 55 kDa independently of the concentration applied.

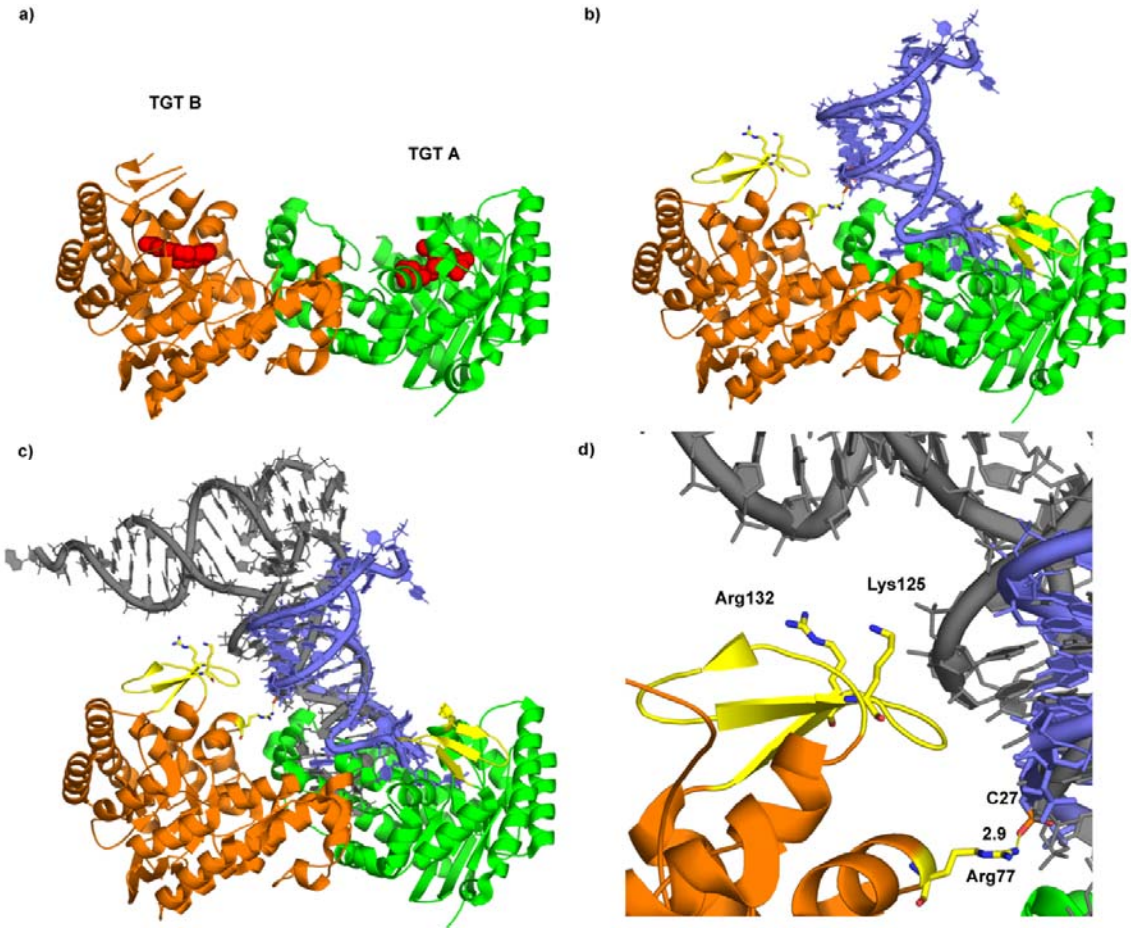

Figure 8.1. Ribbon representation of homodimeric Z. mobilis TGT (monomer A, green; monomer B, orange). a) The active sites of the monomers, both occupied by an inhibitor (red, spheres), are located on the same face of the complex (pdb-code: 2Z7K). b) Complex of TGT with a tRNA anticodon stem-loop (blue) (pdb-code: 1Q2R). The portions of TGT most likely being involved in tRNA recognition and binding are highlighted in yellow. Due to sterical hindering only one tRNA molecule can bind to the TGT dimer. c) Superposition of the anticodon stem-loop bound to Z. mobilis TGT with the complete tRNAPhe molecule of yeast (gray) (pdb-code: 1EHZ). d) Detailed view of tRNA binding. Protonatable residues, potentially able to interact with the phosphate groups of the tRNA backbone, are shown in stick representation.

Ultimately, the crystal structures of *Z. mobilis* TGT in its apo-form and with bound $preQ_1$, displayed a homodimer with an interface producing a buried surface area of 1667 $Å^2$. [31, 5] The identical dimer interface was observed in the crystal structure of *Z. mobilis* TGT bound to a substrate tRNA anticodon stem loop, even though the corresponding crystal belonged to a completely different space group than crystals of apo- or $preQ_1$ containing TGT. [29] As the active sites of both subunits are in close vicinity and present on the same face of the dimer (Figure 8.1a), binding of two anticodon stem loops is sterically hindered. Accordingly, only one RNA molecule is bound per TGT dimer (Figure 8.1b) occupying the binding site of one TGT subunit (henceforth referred to as A) while leaving

empty the active site of the second subunit (referred to as B). Nevertheless, subunit B interacts with the anticodon stem loop of the bound
substrate RNA *via* Arg77 which *H*-bonds the phosphate group of the cytosine 27 nucleotide (Figure 8.1d). In addition, superimposing full length tRNA onto the TGT bound anticodon stem loop (Figure 8.1c) shows that the positively charged residues Lys125 and Arg132 of subunit B are well positioned to salt bridge the phosphate groups of nucleotides 11 and 12 within the dihydrouridine stem (Figure 8.1c). These observations suggest that the functional unity of TGT is indeed a homodimer, which is, however, able to bind and convert only one substrate RNA molecule at a time. This assumption was corroborated by an alignment of 18 bacterial TGT sequences showing that residues forming the dimer interface are highly conserved. [5] In addition, the crystal structure of TGT from *Thermotoga maritima* (PDB-code: 2ASH) determined by the Joint Center for Structural Genomics also exhibits a homodimer whose assembly is virtually identical to the one found for *Z. mobilis* TGT.

Recently, a *lin*-benzoguanine based TGT inhibitor (**26** in Table 8.1) designed to competitively inhibit binding of substrate tRNAs was unexpectedly found to influence the properties of the dimer interface. [5] This became obvious by a space group symmetry reduction upon soaking of apo-TGT crystals with **26**. Usually, in the absence of RNA, Z. mobilis TGT crystallizes in space group *C2* with two identical TGT dimers being present in one unit cell. In crystals containing TGT complexed to **26** this space group is reduced to *P2* with the unit cell containing two non-identical dimers. This is due to the fact, that **26** is bound in a slightly different way by both dimers of the unit cell. One of the dimers binds **26** in a fashion which leaves the dimer interface unchanged compared to virtually all other known TGT crystal structures, whereas the way the second dimer binds **26** clearly influences the dimer interface. Here, helix α1 as well as the preceding loop which both are normally involved in dimer interface formation and perfectly defined in all TGT crystal structures determined previously become disordered upon binding of **26**. [5] Meanwhile, the crystal structure of TGT with a further inhibitor (**18** in Table 8.1) revealed that also this inhibitor impairs the proper formation of the TGT dimer interface. [74] The serendipitous discovery that small molecule inhibitors originally intended to address the guanine / $preQ_1$ binding site and small surrounding subpockets, interferred with TGT dimer formation, prompted us to launch a project aimed to systematically

Table 8.1 *Structures and binding affinities of the used inhibitors in the MS experiments*

name	structure	MW	K_i
26	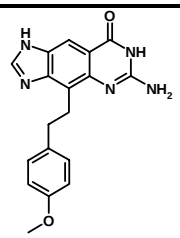	335.4 Da	3.7 μM [5]
29	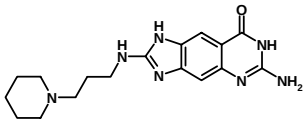	341.4 Da	15 nM [44]
18	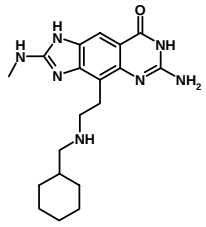	369.5 Da	4 nM [31]
23	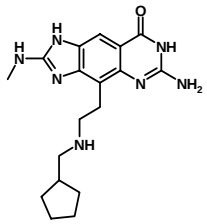	355.4 Da	2 nM [31]
17	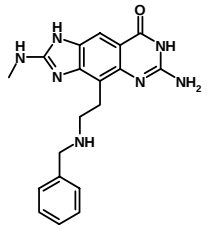	363.4 Da	25 nM [31]

perturb TGT dimierization with the idea to provide some novel strategies to possibly interfere and inhibit enzyme function. In the present study, as a first step in this direction, a combination of automated chip-based nanoelectrospray mass spectrometry (nanoESI-MS), enzyme kinetics and X-ray crystallography techniques was used to get deeper insights into the biological relevance of TGT quarternary structure for catalysis. Particularly, noncovalent spectrometry was first used to unambiguously confirm TGToligomerisation state as well as the binding stoichiometry of its complex with full-length tRNA. Mutations intended to impede dimer formation and the tRNA binding were

then introduced into TGT and their influence on the enzyme catalytic efficiency as well as on dimer stability was examined. Indeed, one of the produced mutated TGT variants was characterized crystallographically revealing thus important structural changes in the interface region coinciding with that perturbed by the small molecule inhibitors **26** and **18**. Finally, these inhibitors were investigated to determine their protein binding stoichiometries as well as their effect on the TGT : tRNA complex stability.

8.3 Results and discussion

8.3.1 Dimeric TGT binds a single tRNA molecule

Previously published works on bacterial TGT have reported contradictory oligomerisation states ranging from monomer to hexamer. [33, 72] As a first step in this study, noncovalent mass spectrometry experiments were carried out with *Z. mobilis* TGT to unambiguously confirm its oligomerisation state. This technique enables accurate mass measurements of intact noncovalent assemblies in the gas phase providing thus reliable information on protein oligomerisation state as well as on protein : RNA binding stoichiometries.[75-78] TGT was first analyzed alone under non-denaturing conditions (Figure 8.2a) revealing the presence of a single species which can be assigned to dimeric TGT according to the good agreement between the measured molecular weight (85613 ± 4 Da) and the mass expected for TGT dimer containing one structural Zn^{2+} per subunit (85604 Da). NanoESI-MS experiments were then performed with TGT in the presence of increasing concentrations of tRNA. When the protein (10 µM in monomer) is incubated with tRNA (5 µM), two main ion distributions are detected (Figure 8.2b), namely in the mass ranges m/z 4200-5000 and m/z 5200 to 6500. While the former one corresponds to a TGT dimer, the second one, with a molecular mass of 113147 ± 9 Da, corresponds to the 2:1 TGT : tRNA complex. Upon increase of tRNA concentration to 10 µM, nanoESI-MS analysis reveals that the equilibrium completely shifts towards the protein : tRNA complex (Figure 8.2c). Notably, no higher order complex is detected even in presence of a three-fold molar excess of tRNA over TGT dimer (Figure 8.2d) which evidences that TGT dimer specifically binds one single tRNA molecule. These results obtained with a full-length

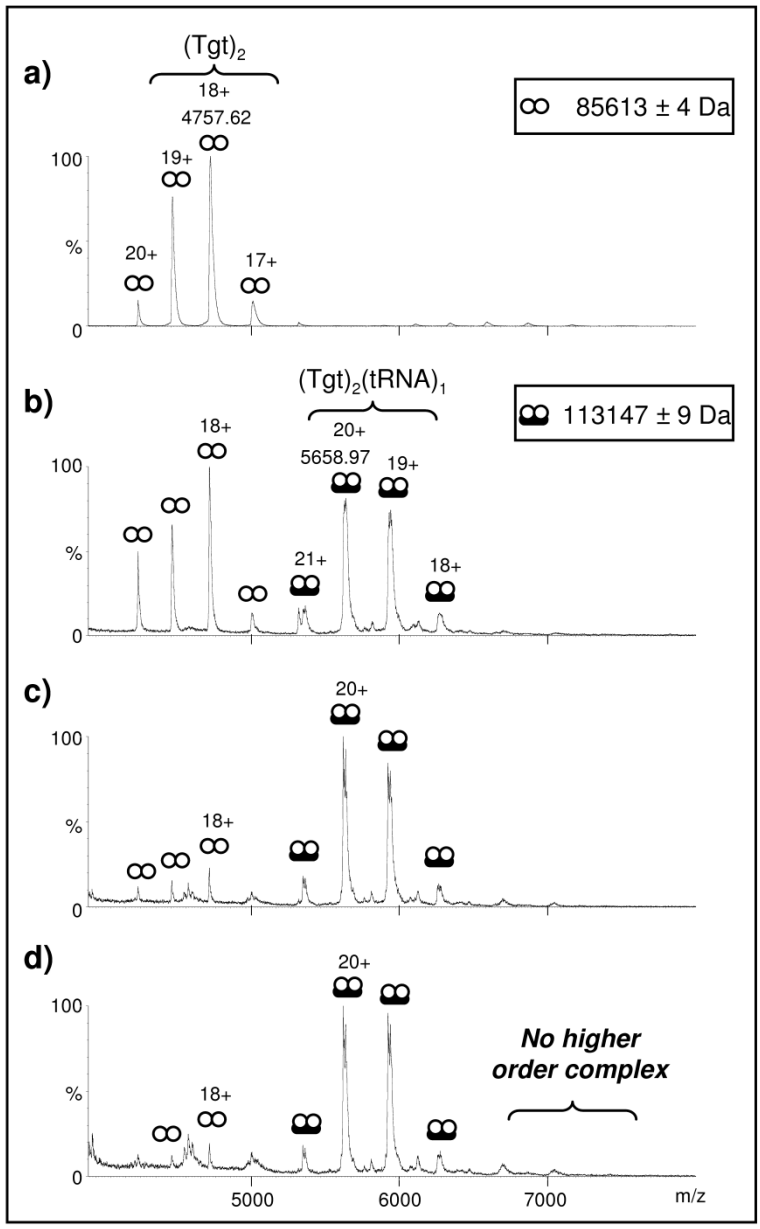

Figure 8.2 *Noncovalent mass spectrometry analysis of TGT and TGT : tRNA assemblies. nanoESI mass spectra were obtained with TGT diluted to 10 µM (monomer concentration) either (a) alone or in presence of (b) 5 µM, (c) 10 µM and d) 15 µM tRNA. (∞) and (∞) are respectively related to dimeric TGT and the 2:1 TGT : tRNA complex. Vc = 150 V, Pi = 6.0 mbar.*

tRNA corroborate the results from a recent crystallographic study showing bacterial TGT homodimer interacting with a single substrate tRNA anticodon stem loop. [29]

Together with recent crystallographic data, the present results definitely confirm the dimeric oligomerisation state of TGT as well as the 2:1 binding stoichiometry of the TGT : tRNA complex.

8.3.2 Point mutations aimed to destabilize the homodimer interface alter TGT catalytic efficiency

To get deeper insights into the importance of homodimer formation for catalytic activity, we created two mutated variants of *Z. mobilis* TGT, each containing an amino acid exchange, aimed at disturbing a protein / protein interaction thought to be important for dimer interface stability. With this respect it should be noted that, based on a 2-fold symmetry of the dimer interface, each amino acid exchange will disrupt two (identical) protein / protein interactions per dimer. In the first variant, Tyr330 was changed to Phe in order to disrupt an *H*-bond formed between the main chain carbonyl of Ala49 and the Tyr330´ side chain hydroxyl. In the second variant, a salt bridge formed between the side chain ammonium of Lys52 and the side chain carboxylate of Glu339´ was eliminated by changing Lys52 to a sterically similar but uncharged Met (Figure 8.3).

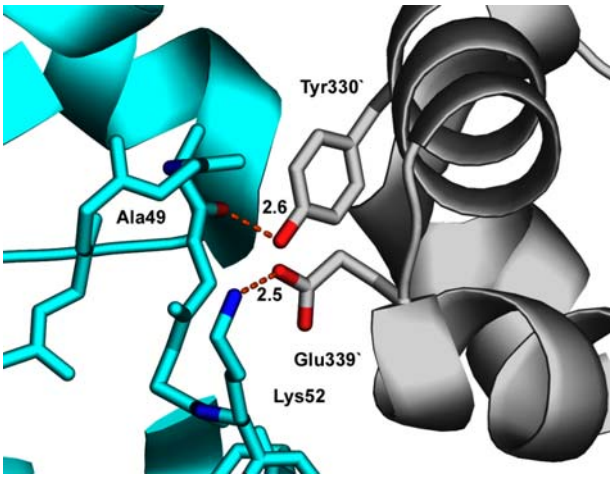

Figure 8.3 *Interactions within the homodimer interface of TGT selected for mutagenesis. The hydrogen bond formed between Ala49 (cyan) and the Tyr330` (gray) as well as the salt bridge formed between Lys52 (cyan) and Glu339` (gray) are shown as dashed lines (distances are given in Å).*

To analyze the influence of the introduced mutations on tRNA binding and catalytic efficiency, we determined K_M(tRNA) and k_{cat} of both mutated variants using radiolabelled guanine as second substrate. The kinetic parameters measured for TGT(Tyr330Phe) and TGT(Lys52Met) as well as those determined for wild-type enzyme are summarized in Table 8.2. While K_M(tRNA) was, with respect to the error range of the

used assay, virtually unchanged for both mutated TGT variants, k_{cat} was reduced by a factor of about 10 for TGT(Tyr330Phe) and by a factor of ca. 50 for TGT(Lys52Met).

Table 8.2 k_{cat} and K_M(tRNA) for TGT and mutated variants of TGT

	TGT (wild type)	TGT(Tyr330Phe)	TGT(Lys52Met)
k_{cat} [$10^{-2}\cdot s^{-1}$]*	1.10	0.095	0.023
K_M(tRNA) [µM]	2.17	1.580	0.980

** taking into account the presence of TGT as a homodimer able to bind and convert only one substrate tRNA molecule at a time.*

These results may be interpreted most plausibly such that dimer formation is a precondition for catalytic activity of TGT. The more efficient is the mutation-induced dimer destabilization, the smaller is the fraction of catalytically active dimeric TGT, resulting thus in the observed reductions of k_{cat}. Alternatively or in addition, the mutations may result in modified dimer interfaces, which may, in turn, affect the exact orientation and geometry of nearby active site residues, thus negatively influencing catalysis. In any case, from unchanged K_M(tRNA) values of both mutated variants compared to wild type TGT, it may be deduced that, once a dimer has formed, it will bind the tRNA substrate with virtually the same affinity as wild type TGT.

8.3.3 Point mutations aimed to alter the recognition and binding of tRNA to TGT

The superposition of TGT:tRNA-stem look with a full length of tRNA (Figure 8.1 c, d) proposed that β7-σ6-insertion (Figure 8.1 yellow) is responsible for the recognition and binding of tRNA. Especially, Lys125 and Arg132 can form interaction to the ribose phosphate backbone. The exchange of Arg to Gly in position 132 of TGT was successfully performed. For TGT(Arg132Gly) the K_m (3.87) and k_{cat} (0.45 $10^{-2}{*}s^{-1}$) was measured as described for the mutants in 8.3.2. The effect on K_m and k_{cat} is less than observed for the mutants with alternation in the dimer interface but still significant reduces compared to the WT. Therefore we can assume that Arg132 is indeed involved in the recognition and binding of tRNA.

Unfortunately, the protein started to denature under the conditions used in the nanoESI-MS experiments and no measurements of the TGT variant with tRNA in complex was possible.

8.3.4 NanoESI-MS experiments reveal mutation-induced destabilization of TGT dimer

In order to check whether the reduced turnover values measured for TGT(Lys52Met) and TGT(Tyr330Phe) are due to a destabilized protein / protein interface, nanoESI-MS experiments were performed under non-denaturing conditions with these mutated variants as well.

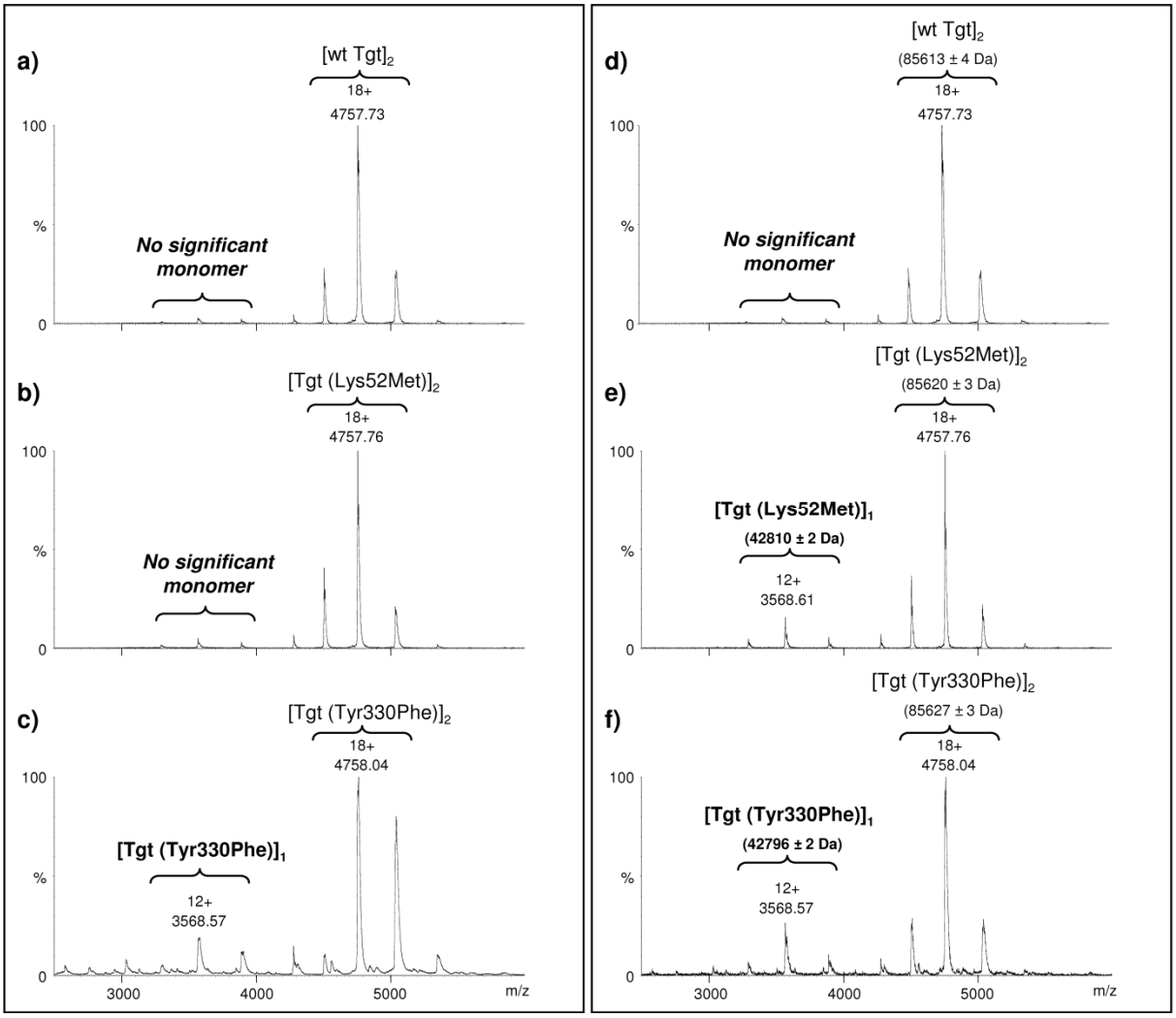

Figure 8.4 *Effect of mutation points on TGT dimer stability. (a, d) wild type TGT, (b, e) TGT (Lys52Met) and (c, f) TGT (Tyr330Phe) were diluted either to (a-c) 10 µM or (d-f) 1 µM (monomer concentration) in 500 mM ammonium acetate at pH 8.0. Vc = 100 V, Pi = 6 mbar.*

Using a concentration of 10 µM in monomer, TGT(Lys52Met) appears, like wild type TGT, almost exclusively as a homodimer, while the mass spectrum obtained for 10 µM TGT(Tyr330Phe) also reveals a significant amount of monomer (Figure 8.4a-c). When protein concentration is lowered to a minimal value of 1 µM, a substantial proportion of

monomer becomes evident for both variants (Figure 8.4d-f). In contrast, wild type TGT remains totally dimeric at this concentration. The finding that the monomer to dimer ratios of TGT(Lys52Met) and TGT(Tyr330Phe) obviously depend on the protein concentrations confirmed that the introduced mutations did not completely disrupt but solely destabilize the dimer interface. Since in the assay applied to determine k_{cat} and K_M(tRNA) an enzyme concentration as low as 150 nM was used, the strongly reduced turnover numbers observed for TGT(Lys52Met) and TGT(Tyr330Phe) are well consistent with the results obtained from the nanoESI-MS experiments.

8.3.5 Crystal structure of TGT(Lys52Met)

In order to interpret at a structural level the reduced turnover values as well as the data obtained from nanoESI-MS experiments for TGT(Lys52Met) and TGT(Tyr330Phe), we tried to crystallize these mutated variants. Yet, solely TGT(Lys52Met) formed crystals under the same conditions as wild type TGT, while all attempts to obtain diffracting crystals from TGT(Tyr330Phe) were unsuccessful. Moreover, compared to crystals of wild type TGT, crystals of TGT(Lys52Met) turned out to be highly fragile and only showed a limited diffraction quality. Nevertheless, using a dataset collected at the BESSY Synchrotron (Berlin) we finally determined the crystal structure of TGT(Lys52Met) at a resolution of 2.0 Å. The structure indeed reveals a significant modification of the dimer interface which is clearly caused by the introduced mutation (Figure 8.5). The loss of the salt bridge normally formed between the Lys52 ammonium and the Glu339′ carboxylate group results in a complete collapse of helix α1. While this helix is perfectly defined in the crystal structure of wild type TGT, no density could be assigned to this structural element in the electron density map of TGT(Lys52Met). In addition, the *C*-terminal half of the loop preceding helix α1 (and containing Met52) is disordered as well, while the *N*-terminal half of this loop takes a significantly different course compared to the corresponding section in wild type TGT. The loss of a defined conformation of helix α1 and of a part of the preceding loop, in turn, results in a slight dislocation of helices αE′ and αF′. It should be noted here that the crystal structure of RNA bound to TGT shows that the loop connecting β-strand 1 and helix α1 interacts with the uridine 35 nucleotide of the tRNA anticodon. A destabilisation of its conformation might ultimately lead to a slightly distorted orientation of active site residues and substrate and thus supposedly contribute to the reduced turnover values observed for TGT(Lys52Met).

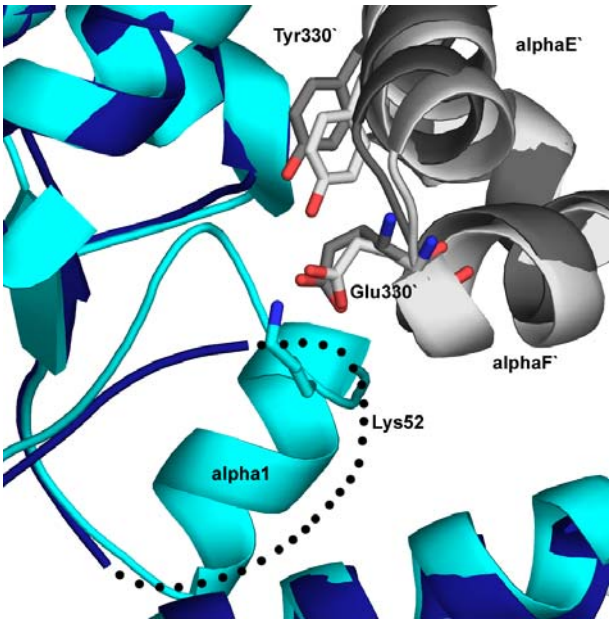

Figure 8.5 *Superposition of TGT (pdb-code:2Z7K; monomer A gray, monomer B cyan) and TGT(Lys52Met) (monomer A dark gray, monomer B blue). In TGT(Lys52Met) helix α1 as well as the loop connecting β-strand 1 and helix α1 are disordered thus reducing the contact area in the interface and leading to the dislocation of helices αE` and αF`.*

8.3.6 NanoESI-MS monitoring of inhibitor binding effect on TGT homodimer and TGT:tRNA complex

According to the above-described results, altering dimer interface appears as a promising strategy to inhibit TGT activity. In this context, nanoESI-MS experiments were performed with wild type TGT in the presence of a number of small molecule inhibitors (Table 8.1) in order to determine inhibitor binding stoichiometries and to reveal potential influence of inhibitor binding on TGT homodimer stability. For inhibitors **26** and **18** it was shown by X-ray crystallography that these compounds are able to modify the structure of the dimer interface.[5, 74] Furthermore, inhibitors **23** and **17** address a hydrophobic subpocket close to the dimer interface which might affect quarternary structure formation.[74] In contrast, compound **29** addresses a different subpocket and no impact on dimer formation can be expected. [79] As shown in Figure 8.6, mass spectra obtained after incubation of TGT (10 µM) in presence of five molar equivalents of inhibitor (50 µM) exclusively reveal a homodimer population with one inhibitor molecule

bound to each subunit. Accordingly, at this concentration, inhibitors fully saturate TGT binding sites, which is in agreement with previously reported K_i values (Table 8.1). However, none of these ligands is able to disrupt TGT homodimer.

In order to investigate their influence on TGT:tRNA complex stability, nanoESI-MS indirect competition experiments were carried out between tRNA and the different inhibitors. Importantly, desolvation and transmission of TGT:tRNA assembly require harsh instrumental conditions which induce the disruption of TGT:inhibitor complex in the gas phase. As a consequence, these competition experiments aimed only at monitoring inhibitor effect on TGT:tRNA complex stability in solution; no inhibitor binding stoichiometry could be obtained using these instrumental conditions. In a first series of experiments, TGT (10 µM) was first incubated with a five-fold molar excess of inhibitor (50 µM) followed by the addition of tRNA (10 µM). Note that above-described results showed that, at these concentrations, TGT is almost exclusively detected as a 2:1 tRNA complex and a 2:2 TGT:inhibitor complex, respectively. In the present competition experiments, deconvoluted mass spectra show, without exception, a main peak corresponding to TGT homodimer beside a considerably smaller peak corresponding to the TGT dimer in complex with one tRNA molecule (Figure 8.7). In contrast, in the deconvoluted mass spectrum of the control experiment, where TGT was incubated with an equimolar concentration of tRNA but in absence of any small molecule inhibitor, the most intense peak corresponds to the 2:1 TGT:tRNA complex (Figure 8.7a).These results clearly illustrate inhibitor ability to prevent the formation of the TGT:tRNA complex.Interestingly, in a second series of experiments, TGT (10 µM) was incubated with tRNA (10 µM) to first allow the formation of the TGT:tRNA complex. Subsequent addition of inhibitor (50 µM) led to identical nanoESI mass spectra as those exposed in Figure 8.8. As a conclusion for these competition experiments, inhibitors **17**, **18**, **26**, **23**, and **29** are not only able to prevent the formation of the catalytically active TGT:tRNA complex, but are also able to disrupt the preformed complex. This kind of information is of crucial importance for the understanding of inhibitor mechanism of action.

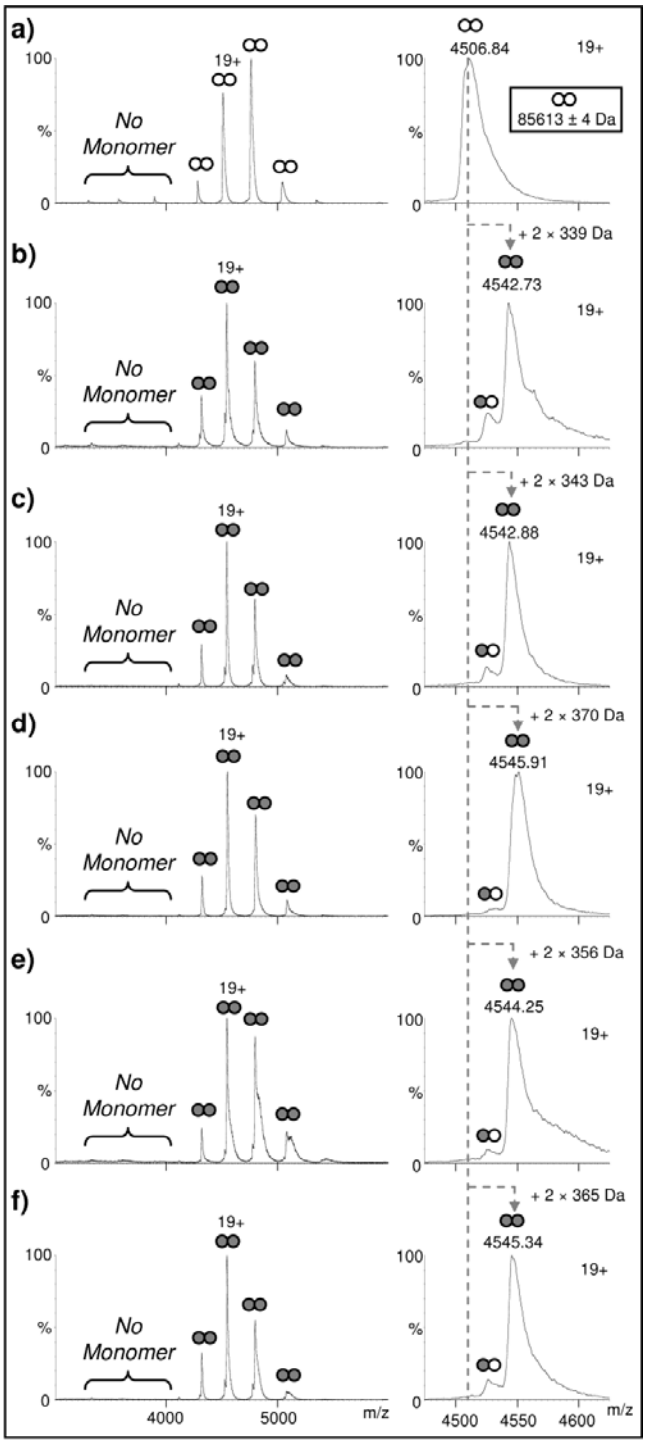

Figure 8.6 *Investigation of inhibitor binding effect on TGT oligomerisation state. TGT (10 µM in monomer) was incubated either (a) alone or in presence of 50 µM of inhibitor (b)* ***26****, (c)* ***29****, (d)* ***18****, (e)* ***23*** *and (f)* ***17****. Mass spectra in the right-hand column correspond to an enlargement of the +19 charge state of free and bound TGT. (∞), (∞) and (∞) correspond to free TGT dimer, 2:1 and 2:2 TGT : inhibitor complexes, respectively. Vc = 60 V, Pi = 6 mbar.*

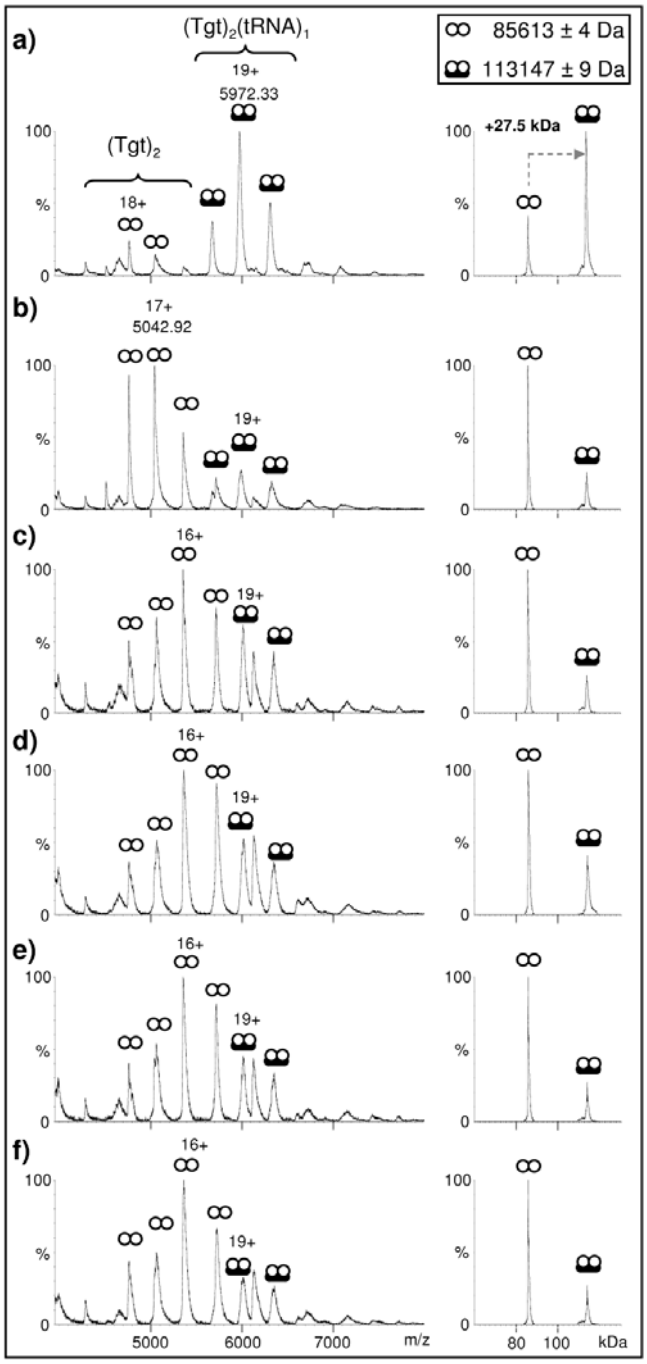

Figure 8.7 *Investigation of inhibitor binding effect on the formation of TGT : tRNA complex. (a) TGT (10 µM in monomer) was incubated in presence of tRNA (10 µM). (b-f) TGT (10 µM) was first incubated with 50 µM inhibitor (b)* ***26****, (c)* ***29****, (d)* ***18****, (e)* ***23*** *and (f)* ***17****, followed by the addition of tRNA (10 µM). Mass spectra in the right-hand column were deconvoluted with the Transform algorithm from MassLynx 4.0. (∞) and (∞) are respectively related to dimeric TGT and the 2:1 TGT : tRNA complex. Vc = 150 V, Pi = 6 mbar.*

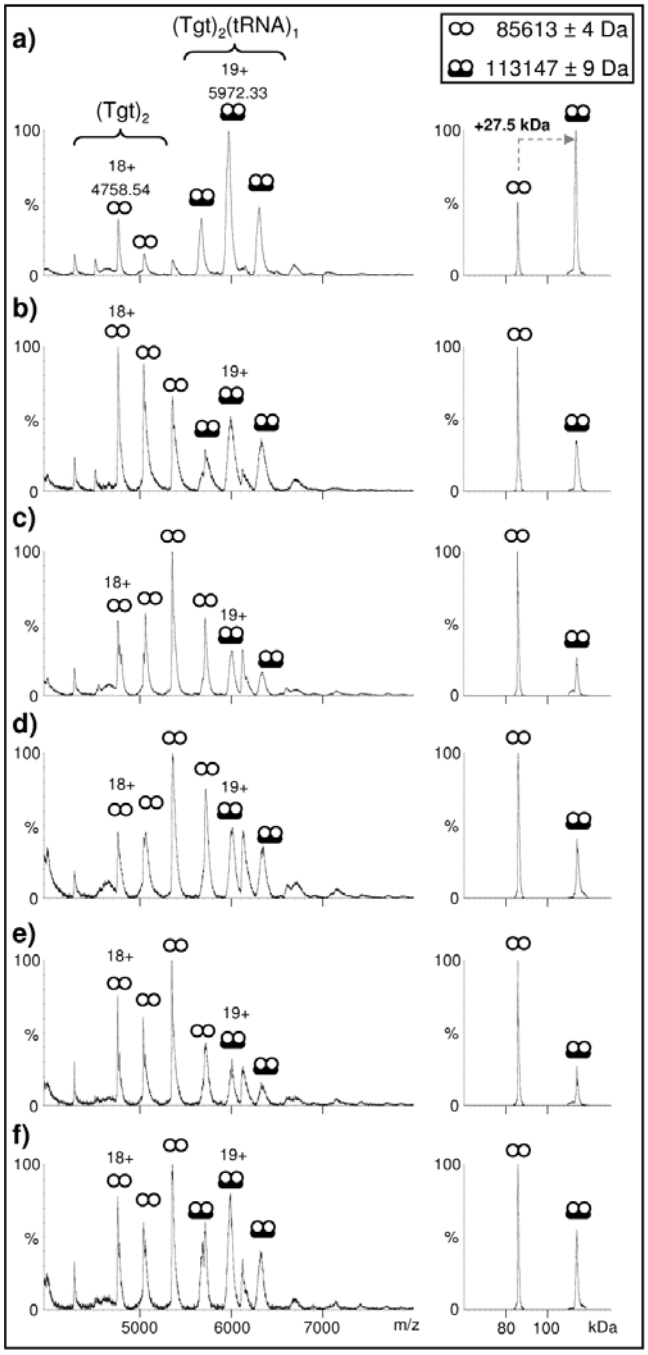

Figure 8.8 *Investigation of inhibitor ability to disrupt pre-formed TGT : tRNA complex. TGT (10 µM) was pre-incubated with tRNA (10 µM) and was subsequently analyzed either (a)without inhibitor or (b-f) after addition of 50 µM of inhibitor (b)* ***26****, (c)* ***29****, (d)* ***18****, (e)* ***23*** *and (f)* ***17****. Mass spectra in the right-hand column were deconvoluted with the Transform algorithm from MassLynx 4.0. (∞) and (🝙) are respectively related to dimeric TGT and the 2:1 TGT : tRNA complex. Vc = 150 V, Pi = 6 mbar.*

8.4 Conclusion and outlook

In the present chapter, an integrative approach combining the benefits of noncovalent nanoESI-MS, site-directed mutagenesis, enzyme kinetics, and protein X-ray crystallography has been presented to investigate the quarternary structure of TGT and the binding stoichiometry of the TGT:substrate tRNA complex. The results of nanoESI-MS analyses reported in this section provide clear evidence that bacterial TGT is present in solution as a homodimer able to bind specifically only one substrate tRNA molecule at a time. This corroborates the conclusions drawn from the crystal structure of *Z. mobilis* TGT in complex with a substrate tRNA anticodon stem loop suggesting a 2:1 stoichiometry for the catalytically active TGT:tRNA complex. The fact, that the active sites of both subunits are located on the same face of the dimer renders, for sterical reasons, simultaneous binding of two tRNA molecules virtually impossible. Yet, the TGT:tRNA complex structure suggests that the subunit with its active site unoccupied supports binding and correct orientation of the substrate tRNA through a number of salt bridges.

In order to ascertain the significance of homodimer formation for the catalytic activity of bacterial TGT we created a TGT(Tyr330Phe) as well as a TGT(Lys52Met) variant using site directed mutagenesis. While the Tyr330Phe mutation abolishes two inter-subunit hydrogen bonds, the Lys52Met mutation disables the formation of two inter-subunit salt bridges. Indeed, nanoESI-MS experiments performed with these variants evidenced that the introduced mutations lead to the destabilization of the dimer interface which, in both cases, is accompanied by a significant loss of catalytic activity. With this respect it should be noted that for a TGT(Tyr330Phe, Lys52Met) double mutated variant which was also created in the course of this study, no catalytic activity was detectable any more. Unfortunately, we were not able to purify this variant to homogeneity, possibly because it showed, compared to wild type TGT, a completely different behavior during all purification steps. This rendered a detailed analysis of TGT(Tyr330Phe, Lys52Met) impossible, yet it provided further evidence for the importance of homodimer formation for integrity and functionality of the bacterial TGT enzyme.

The alteration of an Arg residue on the surface of the protein, which is most likely involved in the recognition and binding of the tRNA substrate was successfully exchanged to Gly using site directed mutagenesis. A significant influence on kinetic

parameters was measured which supports the assumption that the 7β-6σ-insertion is involved in the recognition of the substrate.

Altogether, these results highlight a crucial structure-activity relationship controlling TGT catalytic efficiency, which justifies the initiation of a new project with the objective to create TGT inhibitors aiming at impeding homodimer formation. The serendipitous discovery of competitive TGT inhibitors able to alter TGT dimer interface organization constitutes a promising starting point for this intention. In the present study, we investigated, by means of nanoESI-MS, the influence of several inhibitors on both TGT dimer and TGT:tRNA complex formation. While, all of them were able to bind TGT dimer with a 2:2 protein : ligand binding stoichiometry, no dimer dissociation could be observed, even for those inhibitors which are known to influence the architecture of the TGT dimer interface (**26** and **18** in Table 8.1). However, competition experiments revealed that each tested inhibitor is able to at least partially prevent the formation of the TGT:tRNA complex, but can also disrupt the preformed protein : RNA complex. Inhibitors **26** and **18** constitute derivatives of a *lin*-benzoguanine skeletal structure substituted with an extended side chain at position 4. From crystallographic analyses it is known that the *lin*-benzoguanine moieties of both inhibitors occupy the guanine / $preQ_1$ binding pocket of TGT, while their extended side chains reach the dimer interface region and take influence on its architecture. In a forthcoming work we plan to further enlarge the side chains of inhibitors **26** and **18** with intent to more effectively disrupt protein-protein interactions between the TGT subunits. As soon as we have identified moieties which tightly bind to the dimer interface area and thus inhibit dimerization, we will try to omit the *lin*-benzoguanine skeleton. Following this strategy, we hope to reduce the problem of designing small molecule inhibitors aiming at disturbing a protein-protein interface and lacking a defined cavity which is normally defined by substrate binding pockets of enzymes.

9 Conclusion and outlook

9.1 Conclusion

In this thesis multiple computer aided methods of structure based drug design along with X-ray crystallography and kinetic measurements were used to investigate inhibitors of tRNA-guanine transglycosylase (TGT) a putative target for a new specific antibiotic against Shigella bacteria. Within a year about 160 million infections are reported leading to approximately 1 million deaths, predominantly in developing countries where poor hygienic conditions and malnutrition are in common. In addition, the constitution of the catalytic active complex of TGT and its substrate-tRNA was studied, applying site directed mutagenesis, kinetic measurements and nanoESI-MS experiments.

The crystallization of *Z. mobilis* TGT, which offers a nearly identical active site as TGT from *S. flexneri,* was successfully performed in previous studies. Several scaffolds based on pyridazinones, pteridines, and quinazolinones were discovered with binding affinities in the micro molar range. In addition, a "stretched" guanine with an inserted central six-membered ring, leading to *lin*-benzoguanine, was discovered and further evaluated in this thesis.

During the optimization process of the *lin*-benzoguanine skeleton two often neglected aspects of ligand binding to a protein are highlighted. In section 2 p*K*a shifts are studied once the inhibitor is transferred from aqueous solution to a protein environment and in section 3 a successful example is described for a design step correctly considering water molecules.

The importance of the protonation states and induced p*K*a shifts emerged when in 2-position of the *lin*-benzoguanine skeleton an amino group was introduced to facilitate the attachment of side chains addressing an additional subpocket of TGT. The introduction of an amino group in 2-position modified the imidazol ring of the parent skeleton resulting in a guanidino group. With respect to the physico-chemical properties the guanidino group increases the basicity of the parent skeleton. The p*K*a values of the ligands were experimentally determined in aqueous solution and used for the calculation of the p*K*a shifts in complex with the protein. A Poisson-Boltzmann calculation was performed and revealed that the p*K*a values of all compounds are shifted toward basic range, when the ligands are in complex with the protein. In consequence the guanidinium-like portion of the ligand bears a permanent charge and the hydrogen bond formed to Leu321 is

transformed into a charge-assisted contract. In addition, a significantly higher pKa value was obtained for all 2-amino-*lin*-benzoguanines. The ligand series showed that the often neglected induced p*K*a shifts can take significant influence on the binding strength.

Another superficially regarded issue are water molecules bound or associated to the proteins surface. A successful example how to include water molecules in a drug design process is presented in section 3. A cluster of five water molecules conserved over multiple complexes was found in crystal structures of TGT. They are located between the two catalytic aspartates. The role of these water molecules is most likely the residual solvation of the closely neighboring negative charges of the two catalytic aspartates. In a previous study, the water molecules were displaced with hydrophobic substituent attached at the 3- or 4-position of the *lin*-benzoguanine skeleton, but disappointingly no significant improvement of the binding affinity was achieved. Taking the obtained results into account, a new decoration of the side chain was planed. With respect to a DrugScore Hot Spot analysis, which highlights favorable locations for certain atom types in the binding site of TGT, an amino group was selected for the replacement of one or more water molecules between the catalytic aspartates. The kinetic and crystallographic characterization of the newly synthesized compounds with an amino group in the side chain confirmed our design strategy. A further decoration of the amino group with an aliphatic and aromatic ring system to fill up a hydrophobic cleft remote of aspartates delivered highest binding affinities of the inhibitors (up to 2 nM).

The results in section 3 underline that water molecules bonded to the protein surface can provide valuable information for the design of new inhibitors or the decoration of a lead structure. The terms which are common in literature to describe water molecules are not yet satisfactory and have to be adapted. This work should encourage appropriate consideration of water molecules in *in silico* methods used in structure based drug design in order to use the information provided by water molecules bound to the uncomplexed protein.

A frequently used approach in structure based drug design is the correlation of the binding affinity data with obtained binding modes in complex structures. Within a series of ligands the features responsible for an increased binding affinity can be selected and combined to improve the next generation of ligands. But what strategy should be followed when diverse side chains attached to the parent *lin*-benzoguanine skeleton are not visible in any crystal structure? In section 2 and 4 about 20 compounds with different

side chains are introduced. For 13 compounds a crystal structure was successfully obtain but in all cases no electron density was visible for the side chains. Nevertheless, the binding affinity was improved for some of the compounds. In addition to the crystal structure, a MD simulation was preformed to sample possible binding modes of these side chains. The analysis of the MD simulation showed that the side chain can adopt multiple conformations and is only partially accommodated in the binding pocket.

On first glance, the missing electron density for the side chains appears disappointing, but on second glance an alternative phenomenon, less frequently reported in literature, is observed and can be seen as the point of inflection for this project. The contributions to Gibbs free energy of binding can be split into entropy and enthalpy. Usually the binding of a small molecule to an active site is assumed to be enthalpically driven and the simultaneous displacement of water molecules in the active side contributes to the entropic part of the Gibbs free energy of binding. In the present case the partitioning into enthalpy or entropy governed by different aspects. The residual mobility of the side chains is highly activated and contributes most likely to the entropic part to the Gibbs free energy.

In conclusion the distribution of some inhibitor parts in the crystal structures over multiple states is not unfavorable for the design of potent inhibitors, rather it describes an additional way to increase the binding affinity.

The inhibitors based on the *lin*-benzoguanine skeleton in section 2, 3, and 4 have at least two basic nitrogen. In order to inhibit TGT the molecules have to penetrate first the membrane of human endothelial cells and second the membranes of Shigella bacteria. Based on the charged character of the molecules a hindered passage through the membranes can be expected.

A possibility to predict *in silico* the membrane permeability of the compounds is based on statistical data derived from PAMPA measurements. For all known TGT inhibitors the PAMPA score was predicted and correlated with the potency of the inhibitors. Disappointingly, the best binders are predicted to exhibit the lowest membrane permeability. Removing an exto-cyclic amino group from the *lin*-benzoguanine delivered a new parent skeleton the *lin*-benzohypoxanthines. The *in silico* prediction suggested significantly better penetration for the *lin*-benzohyopxanthin but in inhibition assay showed only affinity in the micro molar range.

In the last years the search for small molecules, so called fragments, binding to a protein became fashionable. Finding a fragment which binds to the active site of a protein is a starting point for the systematic decoration to increase interaction with the protein. In section 6 a new approach to use information about known complexes to search a database for new compounds was tested. A reference fingerprint of the interaction between known inhibitors and a protein is derived using DrugScore potentials. A library of candidate fragments is docked into the binding site of TGT and for each docking solution a fingerprint is calculated. The fingerprints of the generated docking solutions are then compared to the reference fingerprint of the known complexes to score the docking pose of the fragment. Using this approach three new fragments were discovered with a binding affinity in the low micro molar range. The found fragments are very similar compared to the natural substrates and the known inhibitors of TGT, which points toward the selective pattern the active site of TGT.

For the fragments in section 6 and the benzimidazole based inhibitors in section 7 no complex structure could be obtained. The tested compounds are all rather small and exhibit a binding affinity in the low micro molar range. A possible explanation for missing electron density is that the rather small ligands are scattered over multiple configurations in the active site of TGT. Similar to the results in section 4, where disordered side chains were not detrimental to the binding affinity, a full disorder of a fragment may also be a way to inhibit the catalytic reaction of TGT.

In the last section of this thesis the catalytic complex of TGT and tRNA is studied in detail. Based on a crystal structure of TGT with a tRNA-stem loop we suggested that TGT is active as a homo dimer and can bind one tRNA molecule for catalysis.

NanoESI-MS experiments confirmed that TGT is a homo dimer and binds one tRNA molecule. In order to study the formation of the dimer complex, mutations were introduced in the dimer interface with the aim to decrease the interactions between the two monomers. Kinetic data showed less activity for the mutated enzymes and furthermore the monomeric form of the protein was observed in nanoESI-MS experiments. Attachment of large side chains in 4-position (e.g. section 3) of the *lin*-benzoguanine skeleton did lead to significant changes in the dimer interface as observed in the crystal structures but they exhibited no influence on the dimer formation and stability in the nanoESI-MS experiments.

Using the crystal structure of TGT in complex with the tRNA-stem loop, a superposition with a complete tRNA molecule showed that the insertion β7-α6 bearing several positively charged residues on the protein surface could be involved in the recognition and binding of tRNA. The exchange of Arg to Gly in this insertion was successfully performed by site directed mutagenesis. The kinetic measurements showed a lower activity of the mutant compared to the WT, which supports the assumption that the residues in insertion β7-α6 are involved in the recognition and binding of TGT.

9.2 Outlook

The great increase in binding affinity of the 2-amino-*lin*-benzoguanines offered the possibility to test inhibitors preventing Shigella invasion assay under *in vivo* conditions at the Charité in Berlin. The establishment of the assay is still under construction but the first results are promising. Especially the *lin*-benzohypoxanthines (section 5) are showing significant influence on the invasion rate of the bacteria.

Furthermore, the idea that rather low membrane permeability is not unfavorable in the case of an antibiotic treatment in this particular case did arise. A local distribution of the antibiotic could be sufficient to reduce the invasion rate and could lower possible side effect upon drug treatment.

In order to complete the idea, that an entropic contribution is the force behind the increase in binding affinity of the compounds in section 2 and 4 ITC measurements could be an appropriate method. So far no correlation between the affinity data and the obtained structures was possible but the results of ITC measurements provide some clarification.

The proof that TGT is active as a homo dimer offers a new way to inhibit the enzyme. It seems possible to develop inhibitors which prevent the formation of the dimer. In the last years several attempts were performed to hinder protein-protein interactions. A major problem is the fact that the interface usually does not exhibits defined cavities which could be occupied by small molecules. In addition conformational changes are often involved to adjust the interface for dimerization. For example in the case of TGT no monomer structure is yet available and can be used to screen for small molecules binding to the interface.

To obtain a monomer structure of TGT two strategies are planed: First the inhibitors which already induce changes in the interface are enlarged with the aim to prevent the dimerization of TGT and second further mutations are introduced in the interface, e.g. a large residue like tryptophan which could hinder the formation of the complex. The first computer generated poses of inhibitors with enlarged side chains in 4-position of the *lin*-benzoguanine skeleton favored a biphenyl or an alkyne substituents.

Once the monomer of TGT is successfully crystallized the structure can be used in a virtual screening to select possible interface binders. The found moieties can then be attached to the existing *lin*-benzoguanine skeleton which would guarantee potent binding to TGT. In section 6 and 7 the problem to localize small molecules were explained in details, therefore it seems very promising to use the *lin*-benzoguanines as an anchor in the

first design cycle. After a structure is found which binds to a defined position of the interface the *lin*-benzoguanine anchor can be removed subsequently, bearing inhibitors which are only binding to the interface.

9 Zusammenfassung und Ausblick

9.1 Zusammenfassung

Im Rahmen dieser Dissertation sind diverse Methoden des computergestützten, strukturbasierten Wirkstoffdesigns in Kombination mit röntgenkristallographischen Methoden und kinetische Messungen angewendet worden, um Inhibitoren für das Enzym tRNA-Guanin Transglykosylase (TGT) zu finden. Durch die gezielte Hemmung, der von TGT katalysierten Basenaustauschreaktion (Kapitel 1), könnten erste, spezifisch gegen den Erreger der bakteriellen Ruhr (*Shigellosis*) wirksame Antibiotika entwickelt werden. Jährlich kommt es zu ca. 160 Millionen Infektionen. Vor allen in Entwicklungsländern sterben auf Grund von Mangelernährung und schlechten hygienischen Bedingungen über eine Million der Infizierten. Darüber hinaus wurde in dieser Arbeit der katalytisch aktive Komplex von TGT und dem Substrat tRNA mit Hilfe von Mutationen, kinetischen Messungen und nanoESI-MS Experimenten untersucht.

Die Kristallisation von TGT ist in vorangegangenen Arbeiten erfolgreich mit dem TGT Enzym von *Z. mobilis* durchgeführt worden, das nahezu identisch ist zu dem von *S. flexneri*. Verschiedene Grundgerüste wurden bereits in vorangegangenen Arbeiten entdeckt, darunter Pyridazinone, Pteridine und Quinazolinone, die alle eine Bindungsaffinität im mikromolaren Bereich aufweisen. Zusätzlich wurde das *lin*-Benzoguaningrundgerüst, das ein Guanin mit einem zusätzlichen Benzolring in seiner Mitte darstellt, gefunden und im Rahmen dieser Arbeit weiter verfolgt.

Während des Optimierungsprozesses des *lin*-Benzoguanins sind zwei Aspekte in den Vordergrund getreten, die in vielen Designansätzen vernachlässigt werden. In Kapitel 2 wird deutlich, wie entscheidend die Veränderung von Protonierungszuständen durch Verschiebungen des p*K*a Wertes sein können, wenn der Ligand vom wässrigen Milieu in die Poteinbindetasche überführt wird. In Kapitel 3 wird ein erfolgreiches Beispiel gezeigt, wie Wassermoleküle in den Wirkstoffdesignzyklus integriert werden können.

Der Einfluss von p*K*a Verschiebungen ist deutlich geworden, nachdem eine Aminogruppe in 2-Position des *lin*-Benzoguaningrundgerüstes eingefügt wurde, um die Synthese von Verbindungen zu erleichtern, die eine zusätzliche Bindetasche der TGT adressieren. Durch das Anfügen der Aminogruppe ist aus dem Imidazolgrundgerüst eine Guanidiniumgruppe entstanden. In Bezug auf die physiko-chemischen Eigenschaften erhöht die Guanidiniumgruppe den basischen Charakter der Moleküle. Die p*K*a-Werte der

einzelnen Verbindungen wurden im wässrigen Milieu bestimmt und dienten als Grundlage für die Berechnung der p*K*a-Verschiebungen in den Protein-Ligand-Komplexen. Mit Hilfe einer Poisson-Boltzmann Rechnung wurde gezeigt, dass die p*K*a Werte der Liganden durch die Proteinumgebung in den basischen Bereich verschoben werden. Dadurch trägt der guanidinium-ähnliche Teil des Liganden eine permanente Ladung und eine Wasserstoffbrücke zur Carbonylgruppe von Leu231 wird in einen ladungsunterstützten Kontakt überführt. Zusätzlich konnte auch gezeigt werden, dass die 2-Amino-*lin*-benzoguanine einen basischeren Charakter besitzen als die *lin*-Benzoguanine.

Die Ergebnisse in Kapitel 2 zeigen, dass der Einfluss der oft vernachlässigten induzierten p*K*a Verschiebungen einen entscheidenden Beitrag zur Bindungsaffinität haben kann.

Eine weitere Vereinfachung resultiert aus der sträflichen Vernachlässigung von Wassermolekülen, die an die Proteinoberfläche gebunden oder assoziiert sind. Ein erfolgreiches Beispiel für die Berücksichtigung von Wassermolekülen in den Wirkstoffdesignprozess ist in Kapitel 3 gezeigt. Ein Cluster aus fünf konservierten Wassermolekülen konnte zwischen den katalytischen Aspartaten in zahlreichen TGT Strukturen gefunden werden. Als mögliche Funktion des Wasserclusters wird die verbleibende Restsolvatisierung der zueinander benachbarten negativen Ladungen der beiden katalytischen Aspatarten angeführt. Bei Verdrängung der Wassermoleküle mit *lin*-Benzoguaninen, die in 3- bzw. 4-Position mit rein hydrophoben Resten substituiert waren, konnte leider kein Anstieg in der Bindungsaffinität beobachtet werden. Unter Berücksichtigung dieser Ergebnisse wurde eine neue Strategie für die Substitution des Grundgerüstes geplant. Basierend auf einer „Hot-Spot“ Analyse der Bindetasche mit Drug Score, die bevorzugte Positionen für bestimmte Atomtypen hervorhebt, ist eine Aminogruppe ausgewählt worden, um ein oder mehrere Wassermoleküle zwischen den Aspartaten zu verdrängen. Die kinetischen und röntgenkristallographischen Untersuchungen der neu synthetisierten Verbindungen bestätigten die gewählte Designstrategie. Die weitere Dekoration der Aminogruppe mit aliphatischen und aromatischen Ringsystemen, um eine kleine hydrophobe Tasche im Protein auszufüllen, resultierte in Verbindungen mit sehr guten Affinitätsdaten (bis zu 2 nM).

Die Ergebnisse aus Kapitel 3 zeigen, dass Wassermoleküle, die an der Oberfläche von Proteinen gebunden sind, wertvolle Informationen für die Entwicklung neuer Inhibitoren oder die für die Optimierung bestehender Leitstrukturen bereithalten. Die

Charakterisierung von Wassermolekülen, die an die Proteinoberfläche gebunden sind, ist in der Literatur noch unzulänglich beschreiben. Zudem soll das gezeigte Beispiel als Anregung dienen, die Wassermoleküle vermehrt in *in silico* Methoden zu implementieren, um die Information, die sie bereitstellen, zu nutzen.

Ein gängiges Vorgehen im strukturbasierten Wirkstoffdesign ist der Vergleich von Bindungsaffinitäten der Inhibitoren und der korrespondierenden Kristallstruktur. Innerhalb einer Ligandserie können so die Wechselwirkungen erkannt werden, die am Wichtigsten für eine gute Bindungsaffinität sind und gemeinsam die nächste Generation des Liganden verbessern. Jedoch stellt sich die Frage, was zu tun ist, wenn die verschiedenen Seitenketten der Liganden wie im Fall der *lin*-Benzoguanine nicht in der Kristallstruktur zu sehen sind? In Kapitel 2 und 4 sind 20 Verbindungen mit unterschiedlicher Seitenkette vorgestellt worden. Von 13 Verbindungen sind Kristallstrukturen im Komplex mit TGT gelöst worden, aber in allen Beispielen konnte keine Elektronendichte für die diversen Seitenketten erhalten werden. Trotzdem verbesserte sich für einige der Verbindung die Bindungsaffinität. Zusätzlich zu den Kristallstrukturen wurde eine MD Simulation durchgeführt. Diese bestätigte, dass die Seitenkette verschiedene Konformationen einnehmen kann.

Auf den ersten Blick suggeriert das Fehlen einer eindeutig definierte Elektronendichte für die Seitenkette keine befriedigende Proteinbindung, jedoch lässt sich auf den zweiten Blick ein bis heute kaum beschriebenes Phänomen erkennen, dass dem Projekt eine völlig neue Bedeutung gegeben hat. Die freie Bindungsenergie lässt sich in einen entropischen und enthalpischen Beitrag aufteilen. Es wird angenommen, dass die Bindung eines kleinen Moleküls an das aktive Zentrum zum enthalpischen und die Verdrängung von Wassermolekülen aus dem aktiven Zentrum zum entropischen Beitrag beitragen. Im vorliegenden Beispiel bestimmt sich die freie Bindungsenergie durch andere Beiträge. Da die Mobilität der Seitenkette auch nach der Bindung an das Protein erhalten bleibt erhöht sie zusätzlich den entropischen Bindungsbeitrag. Zusammenfassend lässt sich sagen, dass eine Fehlordnung einer Seitenkette kein Nachteil beim Design von Wirkstoffen sein muss. Vielmehr bietet sich hier eine kaum genutzte Möglichkeit die Bindungsaffinität zu erhöhen.

Die in Kapitel 2, 3 und 4 beschriebenen Verbindungen tragen mindestens zwei basische Stickstoffe. Damit es zu einer Hemmung der TGT kommen kann, müssen die Verbindungen zunächst die Zellemembranen der Shigellenbakterien und die der humanen

Endothelzellen überwinden. Die Ladung auf dem Molekül könnte jedoch das Passieren der Membranen erschweren.

Eine Möglichkeit die Membranpermeabilität der Verbindungen am Computer vorherzusagen, basiert auf einer statistischen Auswertung von PAMPA Messungen. Für alle bekannten Inhibitoren der TGT wurde dieser PAMPA-Wert berechnet und mit der Bindungsaffinität verglichen. Leider stellte sich dabei heraus, dass die affinsten Inhibitoren in dieser Arbeit eine schlechte Bewertung erhielten.

Durch das Entfernen einer der extozyklischen Aminogruppen entstanden aus den *lin*-Benzoguaninen die *lin*-Benzohypoxanthine. Bei der Vorhersage der Membrangängigkeit konnten die *lin*-Benzohypoxanthine eine deutliche Verbesserung erzielen, jedoch ergaben die Messungen der Bindungsaffinität im Enzymassay nur eine Inhibition im mikromolaren Bereich.

In den letzten Jahren ist die Untersuchung kleiner Moleküle, so genannten Fragmenten, die an Proteine binden in den Focus des Interesses gerückt. Fragmente, die in das aktive Zentrum eines Proteins binden, können anschließend systematisch erweitert werden, um ihre Bindungsaffinität zu steigern.

In Kapitel 6 wurde eine neue Methode getestet, die bei der Suche nach neuen Verbindungen, die Informationen von bereits bekannten Komplexen berücksichtigt. Ein Referenzfingerprint, der die Interaktionen zwischen Inhibitor und Protein beschreibt, ist mit Hilfe von DrugScore Potenzialen errechnet worden. Eine Fragmentbibliotek ist in die Bindetasche der TGT gedockt worden und zu jeder Dockingpose ist ein Fingerprint erstellt worden. Für die Bewertung der Dockinglösungen ist dann der Fingerprint der Dockingpose mit dem Referenzfingerprint verglichen worden. Durch diese neue Methode konnten drei Fragmente identifiziert werden, die Bindungsaffinitäten im mikromolaren Bereich aufweisen. Die gefundenen Fragmente ähneln sehr den natürlichen Substraten und bekannten TGT Inhibitoren, was die hohe Selektivität des Enzyms für ausschließlich Substrat-ähnliche Verbindungen widerspiegelt.

Für die Fragmente in Kapitel 6 und die Verbindungen der Benzimidazole in Kapitel 7 konnte keine Komplexstruktur mit TGT erhalten werden. Alle diese Verbindungen besitzen ein geringes Molekulargewicht und eine Bindungsaffinität im niedrig mikromolaren Bereich. Eine mögliche Erklärung für das Fehlen einer interpretierbaren Elektronendichte ist, dass die Verbindungen mehrere Konfigurationen in der Bindetasche einnehmen. Ähnlich den Ergebnissen aus Kapitel 4, in denen die Unordnung der

Inhibitorseitenkette keinen Nachteil für die Bindungsaffinität darstellen, wäre es auch hier denkbar, dass die Bindung völlig ungeordneter Verbindungen an das aktive Zentrum des Proteins eine Möglichkeit darstellt, seine katalytischen Eigenschaften zu hemmen.

Im letzen Kapitel dieser Dissertation wurde der aktive Komplex von TGT und tRNA untersucht. Als Grundlage diente eine Kristallstruktur der TGT mit einem tRNA-Fragment. Die TGT bildet ein Homodimer an das nur ein tRNA Molekül binden kann.

NanoESI-MS Untersuchungen konnte bestätigen, dass TGT als Homodimer vorliegt und ein tRNA Molekül bindet. Um die Eigenschaften des Homodimeres näher zu untersuchen, wurden Mutationen in die Grenzfläche zwischen den beiden Monomeren eingefügt, um die Anzahl der Wechselwirkungen zu vermindern. Die kinetische Charakterisierung der TGT Mutanten zeigte eine verminderte Aktivität und zudem konnte in nanoESI-MS Untersuchungen die monomere Form des Proteins beobachtet werden. Das Anhängen von großen Substituenten in 4-Position des *lin*-Benzoguanins (bzw. in Kapitel 3) hat eine strukturelle Veränderung im Bereich der Proteingrenzfläche hervorgerufen die in den Kristallstrukturen sichtbar wurde, jedoch zeigte sich in den nanoESI-MS Messungen kein nacheisbar destabilisierender Einfluss auf das Dimer.

Eine Überlagerung der TGT:tRNA Kristallstruktur mit einem kompletten tRNA Molekül hat gezeigt, dass Aminosäuren im Bereich von β7-α6 mit ihren positiv geladenen Seitenketten an der Erkennung und Bindung der tRNA beteiligt sein könnten. Der Austausch von Arg gegen Gly in diesem Bereich konnte erfolgreich durchgeführt werden. Bei der kinetischen Untersuchung dieser TGT Variante konnte eine geringere Aktivität als beim WT festgestellt werden, was die Annahme bestätigt, dass der Bereich von 7β-6α in die Erkennung und Fixierung der tRNA involviert ist.

9.2 Ausblick

Der große Anstieg in der Bindungsaffinität für die 2-Amino-*lin*-benzoguanine bietet die Möglichkeit die Verbindungen in einem *in vivo* Shigellen-Invasionsassay an der Charité Berlin zu testen. Die Etablierung des Testsystems ist noch nicht abgeschlossen, jedoch zeigen erste Versuche vielversprechende Ergebnisse. Besonders die *lin*-Benzohypoxanthine (Kapitel 5) scheinen einen deutlichen Einfluss auf die Invastionsrate zu nehmen.

Zudem ist es auch möglich, dass eine geringe Membrangängigkeit bei dieser speziellen Anwendung nicht nachteilig sein könnte. Eine lokale Verteilung des Wirkstoffs sollte ausreichend für eine Hemmung der TGT sein und zudem sollten die systemischen Nebenwirkungen verringert werden.

Die Überlegungen aus Kapitel 4, dass ein erhöhter entropischer Beitrag günstig für die Bindungsaffinität ist, könnte durch ITC Messungen abgerundet werden. Bis jetzt ist kein eindeutiger Zusammenhang zwischen Bindungsaffinität und Struktur der Seitenkette aufzufinden, jedoch könnten ITC Messungen hier für mehr Klarheit sorgen.

Der Nachweis, dass TGT als Homodimer aktiv ist, ermöglicht einen neuen Weg das Enzym zu hemmen. Es erscheint möglich Inhibitoren zu entwickeln, die die Ausbildung des Dimers verhindern. In den letzten Jahren sind mehrere Versuche unternommen worden Protein-Protein-Wechselwirkungen zu verhindern. Das größte Problem dabei ist, dass die Grenzfläche normalerweise keine Vertiefungen aufweist, die mit kleinen Molekülen besetzt werden könnten. Zudem kommt es im Protein häufig zu Konformationsänderungen, wenn die Zusammenlagerung der einzelnen Domänen stattfindet. Für TGT fehlt derzeit eine Kristallstruktur, die das Monomer allein zeigt. Somit fehlt die Grundlage für ein virtuelles Screening nach kleinen Molekülen, die in die Grenzfläche binden können.

Um die Struktur des Monomers zu erhalten sind zwei Möglichkeiten denkbar: Zum einen können die in Kapitel 3 vorgestellten Verbindungen, die bereits einen Einfluss auf Bereiche der Grenzfläche haben vergrößert werden, um die Zusammenlagerung zu verhindern oder es könnte durch eine gezielte Mutation eine Aminosäure mit großer Seitenkette, z.B. Tryptophan, in den Bereich der Grenzfläche eingebracht werden, die die Zusammenlagerung stört. Erste Untersuchungen mit Computermethoden zeigen, dass Inhibitoren mit vergrößerter Seitenkette, wie ein Biphenyl- oder Alkinsubstituent geeignet sind.

Steht die Struktur des TGT-Monomers zur Verfügung, könnte durch ein virtuelles Screening eine Vorauswahl an kleinen Molekülen getroffen werden, die in den Grenzbereich binden. Verknüpft man diese Moleküle zunächst mit dem *lin*-Benzoguaningrundgerüst erhöht sich die Wahrscheinlichkeit, dass eine Komplexstruktur erhalten werden kann. In Kapitel 6 und 7 konnte bereits gezeigt werden, dass das Binden von fragmentartigen Molekülen problematisch ist. Benutzt man jedoch im ersten Designzyklus das *lin*-Benzoguanin als Anker erhöhen sich die Erfolgschancen. Nachdem eine Struktur gelöst wurde in dem ein kleines Molekül eine definierte Position in der Grenzfläche einnimmt, kann der Anker im katalytischen Zentrum schrittweise abgebaut werden und man erhält Inhibitoren, die ausschließlich in die Grenzfläche binden.

10 Materials and Methods

10.1 in silico Methods

10.1.1 in silico p*K*a calculations

A consistent charge model is produced by a modified version of the charge distribution algorithm suggested by Gasteiger and Marsili, named 'partial equalization of orbital electronegativities' (PEOE). [80]

The *in silico* calculation is based on the charge distribution in the active site of TGT derived from the modified *peoe_pb* charges. Another value important for the calculation is the assigned dielectric constant ε. For the binding site an approximate estimation of this value is crucial. To adjust a reasonable value that closely resembles the properties of the binding site, we tested two different values: ε = 10 and ε = 20. A shift of about one logarithmic unit to a more basic range for all inhibitor complexes is obtained using a dielectric constant of ε = 20. At a value of ε = 10, the pK_a shift was larger (2.4-4.4 logarithmic units) and resulted in values which appear exaggerated to correctly represent the observed effects of the formed protein-ligand complex.

For the calculation of the pK_a values all titratable groups in a radius of 12 Å around the active site are determined (Cγ of Tyr 106 was taken as centre of the selection) (Table 2.3). Using the program REDUSE hydrogens are added to the protein where all acidic amino acids are deprotonated and basic amino acids are protonated. [81]

SYBYL ligand atom types were assigned to the ligands to generate its unprotonated and its protonated form. Based on the modified peoe_pb charges a total net charge is assigned for both ligand states. After this preparation, the Poisson-Boltzmann calculation is started. The resulting pK_a shifts are listed in Table 2.2 (section 2, page 28) at a pH of 7.0.

10.1.2 Docking experiments

The docking is performed with GOLD 4.0 using default settings for the genetic algorithm (population size: 100, selection pressure: 1.1, maximal number of operations: 100000, number of island: 5, niche size: 2, crossover frequency: 95, mutation frequency: 95, and migration frequency: 10). [47] For the selection of the binding site a radius of 10 Å around the ligand of complex 1K4G is used. The protein utilized for docking is 1BBF in section 2.1, 1Y5X in section 2.2 and 1K4G in section 7. The number of generated solution is 20 for docking in section 2 and section 7 and 30 in section 3 and section 4.

10.1.2.1 Docking and rescoring including a consensus water model (section 3)

For the docking in section 3 five water molecules of the consensus water cluster are included. The orientation of the hydrogens of water molecules are allowed to be rearranged for an optimal hydrogen bond network. Additionally, the program evaluated for each docking solution whether one or more water molecules should be replaced by the side chain of the inhibitor.

All derived docking solutions are rescored using DrugScore^{CSD}. [58] The settings during the docking delivered results with different numbers of water molecules in the active site for each docking solution. Therefore, a new extension for DrugScore^{CSD} is developed to include the water molecule which remained in the docking solution for scoring. The remaining water molecules are considered separately from the ligand and protein which allowed the water molecules to form interaction to protein and ligand. The used atom type for the water molecules is a sp3 hybridized oxygen.

10.1.3 Relibase^{+} search

As query structure 1P0B is used and all TGT crystal structures with a sequence identity of 98% are superimposed, resulting in 34 structures. The obtained structures are analyzed in detail. Only entries where the side chain of Asp102 is rotated into the guanine binding pocket are used. Additionally, structures where the water molecules between Asp102 and Asp280 are replaced by a ligand or tRNA and Asp102 is mutated are neglected. Finally, seven structures (pdb-code: 1P0B, 1P4W, 1R5Y, 1S38, 1S39, 1WKE, 1WKF) are remaining which exhibit information about water molecules between Asp102 and Asp280. All water molecules in the active site are selected and together with the corresponding B-values extracted. Water molecules with a B-factor lower than 40 Å are used to retrieve the water clusters. Based on the numbering in Figure 3.1 for position 1-3 four molecules, position 4 six molecules, and position 5 seven molecules are used to calculate the center of each cluster. The received model was used in the GOLD docking runs and rescoring with DrugScore^{CSD}.

10.1.4 MOLOC minimization

The extracted consensus waters are minimized in complex with 1Y5X. The entire protein is kept rigid during the minimization using the MAB-force field. [57]

10.1.5 DrugScore HotSpots

For the calculation of the hotspots the complex of TGT with 2-amino-*lin*-benzoguanine (pdb-code: 2Z7K) is used. The ligand and the water molecules are not considered during the generation of the hotspots in order to derive interaction points in the active site of TGT. The used atom types are based on the atom classification in DrugScore^{CSD}. [58]

10.1.6 ZINC-database search

Primary, aliphatic amines are selected from the ZINC-database using the web interface. The molecular weight is limited to 300 Da. [59] About 600 molecules are downloaded as smiles and converted to mol2 files with CORINA. [82] In this step hydrogens are added and possible stereoisomers are produced. Subsequently, the molecules are attached to the 2-methylamino-4-ethyl-*lin*-benzoguanine using FlexX^{C}. [83] With the program SYBYL Gasteiger-Marsili charges are calculated on each derived molecule and afterwards the molecule is minimized using default parameters. [84]

10.1.7 MD simulation

The MD simulation and all setup steps are performed with the Amber 9.0 suite of programs using the Amber 1999 force field. [85] The protein structure of TGT (pdb-code: 2Z7K) is used as starting coordinates. The ligand and all crystallographic water molecules are removed. Missing residues and side chains of the protein are added and minimized with the Amber 1999 force field. After estimating protonation states of all histidines by visual inspection of interactions, histidines are set to the appropriate form (double protonated: 'HIP'/ protonated at N_δ: 'HID' (HIS#: 73, 257, 319, 332, 333)/ protonated at N_ε: 'HIE' (HIS#: 90, 127, 133, 145, 349)). Cysteins coordinating the Zn^{2+} ion are set to 'CYM' (CYS#: 319, 320, 323). Hydrogen atoms are added with PROTONATE.

Compound **28** (with neutral and protonated piperidine nitrogen) is docked into the structure using GOLD. [47] For the assignment of the ligand charges the program package Gaussian 03 is used. In a Single-Point-Hartree-Fock-calculation RESP charges are assigned to the ligand.

After merging protein and ligand an initial minimization using 200 steps of minimization with a generalized Born solvation model are performed. Subsequently, the systems are solvated in a box of TIP3P water molecules, and two sodium ions are added to ensure neutrality. [86] After 200 steps of minimization of the solvated systems, the MD simulations are started by heating the solvent to 300 K over a period of 20 ps and cooling to 100 K

over 5 ps, keeping the protein fixed. Then the entire system is brought to 300 K over a period of 25 ps and the simulation is carried on for 5 ns (protonated piperidine) or 3 ns (neutral piperidine) under NPT conditions, using a time step of 2 fs and PME for evaluating the electrostatic interactions. Energy data are saved every 20 fs, protein coordinates every 0.5 ps. CARNAL is used for further analysis of the trajectory and VMD 1.8.2 for visualization.

10.2 Materialen und Methoden für experimentelle Arbeiten

10.2.1 Chemikalien

Die verwendeten Chemikalien sind in Tabelle 10.1 aufgeführt.

Tabelle 10.1 Chemikalienliste in alphabetischer Reihenfolge

Name	Hersteller
[8-^{3}H]-Guanin	Hartmann Analytik oder Sigma Aldrich
1,4-Dithiothreitol (DTT)	ROTH
Acrylamind/Bisacrylamid (30%/0,8%)	ROTH
Agar-Agar	ROTH
Agarose	Fluka
Ammoniumpersulfat (APS)	ROTH
Bromphenolblau	Merck
Chloramphenicol	ROTH
Complete^{MT} mini protease inhibitor, EDTA free	Roche
Coomassie Brilliant Blue R250	ROTH
Dimethylsulfoxid (DMSO)	Sigma Aldrich
Essigsäure 100%	ROTH
Ethanol 96 %	Riedel-deHaën
Ethidiumbromid	Merck
Ethyldiamintetraacetat (EDTA)	Merck
Glycerol 100%	Merck
Guanine HCl	Sigma Aldrich
Hefeextract	ROTH
Isopropyl-β-D-thiogalactopyranosid (IPTG)	ROTH
Magnesiumchlorid	Merck
Methanol	Fischer Scientific
Natriumchlorid	ROTH
Natrumhydroxid	Fluka
Pepton aus Casein	ROTH
Rotiphorese Gel 30	ROTH
Salzsäure 37%	Riedel-deHaën
Scintillation Cocktail für lipophile Proben	ROTH
Trichloressigsäure (TCA)	Fluka
Tris(hydroxymethyl)aminomethane (Tris)	ROTH
Tween 20	ROTH
β-Mercaptoethanol	Merck

10.2.2 Geräte

In Tabelle 10.2 sind die Geräte gelistet, die im Rahmen dieser Arbeit verwendet wurden.

Tabelle 10.2 *Verwendete Geräte und deren Hersteller in alphabetischer Reihenfolge*

Gerät	Hersteller
ÄKTA FPLC	Amersham Pharmacia Biosciences
Entsalzungsanlage Purelab Plus	USF Elga
Feinwaage Type 404/13	Sauter
Heizrührer IKA-COMBIMAG REG	Janke&Kunkel
PCR Mini Cycler	MJ Research
Phenylsepharosesäule XK 16	Amersham Biosciences
pH-Meter 744	Metrohm
Pipetten	Eppendorf
Q-Sepharosesäule XK 26	Amersham Biosciences
Schüttelinkubator Innova 4200	New Brunswick Scientific
Schüttelinkubator Innova 4300	New Brunswick Scientific
SDS-Gelelektrophoresekammer Mini-V8*10	Life Technologie
Sterilbank 8511	Köttermann
Szintillisationszähler	Packard
Thermomixer compfort 2 ml	Eppendorf
Ultraschall Sonifier 250	Branson
UV-Leuttisch Transilluminator	BioStep
UV-Vis-Spektrometer Smart Spec 3000	BioRad
Vakuumpumpe DNA Mini	Jouan Nordic
Vortexer VF2	Janke&Kundel
Waage Typ 572/45	Kern
Zentrifuge Avanti J-25	Berckmann Coulter
Zentrifuge Biofuge pico	Heraeus
Zentrifuge Multifuge 3	Heraeus

10.2.3 Lösungen und Puffer

Tabelle 10.3 stellt eine Übersicht über die verwendeten Lösungen und Puffer da. Zum Lösen wurde, soweit nicht anders vermerkt, Reinstwasser aus der Entsalzungsanlage Purelab Plus benutzt. Die Einstellung des pH-Wertes erfolgte mit 0,1 M Natrumhydroxidlsg. oder Salzsäure 37% am pH-Meter 744.

Tabelle 10.3 *Hergestellt Lösungen und Puffer*

Name	Bestandteile
APS-Lsg.	10% (w/v) Ammoniumpersulfat ad 10 ml
Chloramphenicol-Lsg.	0,34 g Chloramphenicol ad 10 ml, steril filtrieren
Coomasie-Blue Entfärberlsg.	10% (v/v) Essigsäure, 40% (v/v) Methanol ad 1 l
Coomasie-Blue Färbelsg.	10% Essigsäure, 49,5% Methanol, 1g Coomasie Brilliant Blau R250 ad 1 l
IPTG-Lsg.	1 M IPTG, steril filtriert
Laemmli-Puffer	0,25 M Tris, 2 M Glycerin, 1% (w/v) SDS, pH 8,3
Natrumhydroxidlsg.	0,1 M NaOH
PBS-Puffer	140 mM NaCl, 10 mM Na2HPO4, 2,8 mM KCl, 1,7 mM KH2PO4, pH 7,3
SDS Sammelgel-Puffer	1 M Tris, pH 6.8
10% SDS-Lsg.	10% (w/v) SDS ad 50 ml
SDS-Proben-Puffer	250 mM Tris, 8% (w/v) SDS, 40% (v/v) Glycerol, 0,04% (w/v) Bromphenolblau, 8% (v/v) β-Mercaptoethanol, pH 6.8
Trenngel-Puffer	1 M Tris, pH 8.8
Tris-Puffer pH 7,0	50 mM Tris-HCl, 100 mM NaCl, pH 7.0
TGT Puffer A	10 mM Tris-HCl, 1 mM EDTA, 1 mM DTT, pH 7,8
TGT Puffer B	10 mM Tris-HCl, 1 mM EDTA, 1 mM DTT, 1,0 M NaCl, pH 7,8
TGT Puffer C	10 mM Tris-HCl, 1 mM EDTA, 1 mM DTT, 1,0 M $(NH_4)_2SO_4$, pH 7,8
Hochsalzpuffer	10 mM Tris-HCl, 1 mM EDTA, 1 mM DTT, 2,0 M NaCl; 0,01% (w/v) NaN_3, pH 7,8
IK-Puffer I	8% (w/v) PEG 8000, 100 mM TRIS HCl, 1mM DTT, 10% DMSO, pH 8.5
IK-Puffer II	13% (w/v) PEG 8000, 100mM MES, 1mM DTT, 10% DMSO, pH 5.5
MS-Puffer I	5 % (w/v) PEG 8000, 100 mM TRIS HCl, 1mM DTT, 10% DMSO, pH 8.5
MS-Puffer II	8% (w/v) PEG 8000, 100mM MES, 1mM DTT, 10% DMSO, pH 5.5
Cryopuffer I	50 mM TRIS HCl, 0.5 mM DTT, 0.3 M NaCl, 2% DMSO, 4 % PEG 8000, 30 % glycerol, pH 8.5
Cryopuffer II	50 mM MES, 0.5 mM DTT, 0.3 M NaCl, 2% DMSO, 4% PEG 8000, 30% glycerol, pH 5.5
LB-Medium	1,0 % (m/v) Pepton aus Casein, 0,5 % (m/v) Hefe, 0,5 % (m/v) NaCl, autokaviert
Agar-LB-Medium	1,0 % (m/v) Pepton aus Casein, 0,5 % (m/v) Hefe, 0,5 % (m/v) NaCl, 1,5% (m/v) Agar-Agar, autoklaviert
Kanamycinlsg.	0,3 g Chloramphenicol ad 10 ml Ethanol, steril filtrieren
Lysepuffer	20 mM Tris-HCl, 10 mM EDTA, 1 mM DTT, pH 7,8, Complete™
TGT Assaypuffer	200 mM HEPES, 20 mM MgCl, 2.95 µM = 5 % CMC Tween 20, pH 7,3
TCA 5%	TCA 5% (w/v)
TCA 10%	TCA 10% (w/v)

10.2.4 Bakterienstämme, Plasmide und Primer

Verwendete Bakterienstämme und Plasmide sind in Tabelle 10.4 und Tabelle 10.5 aufgelistet. Primer die zur PCR benötigt wurden sind in Tabelle 10.6 beschreiben.

Tabelle 10.4 *Verwendete E. coli-Stämme*

Stamm	Beschreibung	Liferant
XL2-blue	*(mcrA)183(mcrB-hsdSMR-mrr)173 endA1 supE44 thi-1 recA1 gyrA96 relA1 lac*[*F'proAB laqI*^{q} ZΔM15 Tn5(Km^r)]	Stratagene
BL21(DE3) Gold	*E. coli B F– ompT hsdS(rB–mB–)dcm+ Tetr gal λ(DE3) endA Hte*	Stratagene
BL21(DE3) pLysS	F$^-$ *dcm ompT hsdS*($r_B^- m_B^-$)*galλ*(DE3) [pLys Km^r]	Stratagene
TG2	[*supE hsdΔ5 thi Δ(lac-proAB) Δ(sre-recA) 306::Tn10* (Tet^r) F' (*traD36pro AB*$^+$ *lacI*^{q} lacZΔM15)]	Stratagene

Tabelle 10.5 *Verwendete Plamide*

Plasmid	Beschreibung	Lieferent/Herstelle
pET9d-ZM4	Cm^r, Km^r; ColEI-origin, *tac*-promotor, coding for *laqI*^{q}*malE lacZα*; inserted *tgt* gene as 1.3 kb *Bam*HI/*Nco*I-fragment in pET9d	[Reuter & Ficner, 1995][73]
pET9d-ZM4-Tyr330Phe	Cm^r, Km^r; TGT-Tyr330Phe	Im Rahmen dieser Arbeit hergestellt
pET9d-ZM4-Lys52Met	Cm^r, Km^r; TGT-Lys52Met	
pET9d-ZM4-Glu339Gln	Cm^r, Km^r; TGT-Glu339Gln	
pET9d-ZM4-Arg132Glu	Cm^r, Km^r; TGT-Arg132Gly	
pET9d-ZM4-Tyr330Phe/Glu339Gln	Cm^r, Km^r; TGT-Tyr330Phe/Glu339Gln	
ptRNA2	Amp^r; *E. colitRNA*^{Tyr} as *Bst*NI-fragment under control of T7-promotor in pTZ18U	[Curnow et al., 1993][35]

10.2.5 Molekularbiologische Methoden

10.2.5.1 Überexpression und Aufreinigung von TGT und TGT Mutanten

Die Überexpression und Aufreinigung erfolgt gemäss dem Protokoll von Romier *et al.*. [87] Vom jeweiligen Bakterienstamm (Tabelle 10.4) mit dem entsprechenden Überexpressionsplasmid (Tabelle 10.5) wird eine Vorkultur in 100 ml LB-Medium (mit

0,1% (v/v) der Kanamycin- und Chloramphenicollsg.) hergestellt (12h, 37°C, 250 U/min). Für die darauffolgende Hauptkultur werden vier mal 1000 ml LB-Medium mit jeweils 25 ml der Vorkultur versetzt und inkubiert (37°C, 250 U/min). Ist eine optische Dichte von 0,6-0,8 erreicht, werden die Ansätze auf 14°C abgekühlt und die Überexpression durch die Zugaben von IPTG gestartet. Nach 24 h werden die Zellen durch Zentrifugation geerntet (Beckman Coulter, JA10, 4000 rpm, 10 min, 4°C). Das erhaltene Zellpellet wird im Lysepuffer resuspendiert. Danach werden mittels Ultraschall (Sonifier 250) die Zellwände zerstört. Nach Abzentrifugieren der Zellbestandteile (Beckman Coulter, JA 25.50 Rotor, 20000 rpm, 45 min, 4 °C) befindet sich das Protein im Überstand und kann abdekandiert werden.

Tabelle 10.6 *Verwendete PCR-Primer zur ortsspeziefischen Mutation (die eingefügte Mutation ist unterstrichen)*

Primer	Sequenz
Y330F-forward	5' GAAATGGAGCCGCGCCTTCATCCATCATTTAATTC 3'
Y330F-reverse	5' GAATTAAATGATGGATGAAGGCGCGGCTCCATTTC 3'
E339Q-forward	5' CATTTAATTCGGGCGGGTCAGATCTTGGGGGCTATG 3'
E339Q-reverse	5' CATAGCCCCCAAGATCTGACCCGCCCGAATTAAATG 3'
K52M-forward	5' GCAGCTACCGTAATGGCTTTAAAGCCGG 3'
K52M-reverse	5' CCGGCTTTAAAGCCATTACGGTAGCTGC 3'
R132G-forward	5' CTTGACGGTTCCGGCCATATGCTGTC 3'
R132G-reverse	5' GACAGCATATGGCCGGAACCGTCAAG 3'

Für die Aufreinigung des Proteins werden zwei aufeinanderfolgende Affinitätschromatographieverfahren mit Hife der ÄKTA FPLC durchgeführt. Das Zelllysat wird auf eine mit TGT-Puffer A konditionierte Q-Sepharosesäule aufgetragen. Mit einem linearen Gradienten in dem der Anteil von TGT-Puffer B von 0 auf 100% erhöht wird, wird das Protein mit einer Flussrate von 4 ml/min von der Säule gespült. Die Fraktionen die TGT enthalten werden mittels SDS-PAGE identifiziert und auf eine mit TGT-Puffer C äquilibrierte Phenylsepharosesäule aufgetragen. Um das gebunden Protein wieder von der Säule zu lösen, wird ein linearer Grandient von TGT-Puffer A mit einer Flussrate von 2 ml/min verwendet, wobei die Konzentration an TGT-Puffer A von 0 auf 100% erhöht wird. Die Fraktionen, die TGT enthalten, werden wieder mit SDS-PAGE identifiziert. Das Probenvolumen wird eingeengt bis die Proteinkonzentration ca. 3 mg/ml beträgt. Die aufkonzentrierte Proteinlösung wird gegen 5000 ml TGT-Puffer A dialysiert

(mind. 12 h) und die erhaltenen Mikrokristalle werden abzentrifugiert (JA 25.50 Rotor, 4000 rpm, 20 min, 4 °C). Zum Rücklösen der Mikrokristalle wird Hochsalzpuffer verwendet, in dem sich die Mikrokristalle auf Grund der hohen NaCl Konzentration lösen.

Bei der Herstellung und Aufreinigung der TGT Mutanten ist die Mikrokristallisation bei der Doppelmutante von TGT nicht beobachtet worden. Die Untersuchung der TGT Mutanten mittels Massenspektrometrie ergab, dass TGTTyr330Phe, TGTLys52Met und TGTArg132Gly in reiner Form vorliegen, jedoch bei TGTGlu339Gln und TGTTyr330Phe/Glu339Gln Verunreinigungen enthalten sind.

10.2.5.2 Mutationen des TGT Wildtyp

Für die Einfügung der gewünschten Mutationen in die DNA-Sequenz von TGT wird unter Zuhilfenahme des QuickChange II Site-Directed Mutagenesis Kits der Firma Quiagen eine Poymerase-Ketten-Reaktion (*PCR*) durchgeführt. Die Präparation des Wildtypplasmids erfolgt aus 15 ml Übernachtkultur des Wildtypstamms *E. coli* BL21(DE3) pLysS / pET9d-ZM4 (Tabelle 10.4) mit Kits der Firma Peqlab (*E.Z.N.A. Plasmid Miniprep Kit I* und *II*) unter Verwendung des Standardprotokolls des Herstellers (*E.Z.N.A. Plasmid Miniprep Kit I&II (Classic-Line) Instruction Manual*).

Das Prinzip basiert auf der Amplifizierung des Vektors durch eine PCR, bei der die komplementären Primer (Tabelle 10.6) die gewünschte Mutation enthalten.

PCR-Ansatz:

5 µl 10 x Reaktionspuffer
40 ng Template-DNA
125 ng Primer-forward
125 ng Primer-reverse
1 µl dNTP Mix
ddH2O auf 50 µl
1 µl DNA Polymerase

Die PCR wird nach folgendem Protokoll durchgeführt:

Startphase:	30 s 95°C	
Denaturierung:	30 s 95°C	
Hybridisierung:	1 min 45°C	
Synthese:	14 min 68°C	Zyklus 12 x
Endphase:	10 min 68°C	
	∞ 4°C	

Die Restriktionsendonuklease *DpnI* schneidet spezifisch methylierte DNA. Durch den Verdau des PCR-Ansatzes mit *DpnI* wird folglich nur die parenterale Plasmid-DNA verdaut und so die DNA isoliert, die die Mutation enthält. Anschließend wird das Plasmid in XL-2Blue Zellen transformiert (Abschnitt 10.2.5.3). Um dem Erfolg der Mutation zu überprüfen, werden alle Plasmide zur Sequenzierung an die Firma MWG geschickt. Die Sequenzierungsergebnisse sind in Anhang (11.3) aufgeführt.
Zur Überexpression der Mutanten wurde der modifizierte Plamid in BL21(DE3) Gold transformiert (Abschnitt 10.2.5.3).

10.2.5.3 Transformation von Plasmiden

Die Transformation der modifizierten Plasmide in entsprechende Bakterienzellen wird mit Hitzeschocktransformation durchgeführt. Hierzu wurden die XL-2Blue oder BL21(DE3) Gold Zellen 30 min auf Eis aufgetaut und mit 100-200 ng Plasmid DNA, welches aus dem PCR-Ansatz stammt, versetzt. Nach 10 min Inkubation auf Eis werden die Zellen einem Hitzeschock (42°C für 42 s) ausgesetzt. Nach weiteren 10 min auf Eis werden die Zellen zur Selektion auf Agarplatten mit entsprechendem Antibiotikum ausplattiert und über Nacht bei 37°C im Brutschrank inkubiert.

10.2.5.4 Herstellung und Aufreinigung von $tRNA^{Tyr}$

Die Herstellung von *E. coli* $tRNA^{Tyr}$ (ECY2) durch *in vitro* Transkription wird nach dem Protokoll von Curnow *et al*. (1993)[35] und gemäß des Herstellerprotokoll des verwendeten *T7 RiboMAX™ Express Large Scale RNA Production System* von Promega durchgeführt.
Die tRNA die in Abschnitt 8 für nanoESI-MS Experimente benutzt wird, wird ohne die Zugabe von $MgCl_2$ hergestellt. Zudem wird die tRNA mit Hilfe Calf Intestine Alkaline Phosphatase (Fermentas) gemäß des Herstellerprotokolls behandelt, um eine einheitliche Phosphorlierung am tRNA 3´-eEde zu erhalten.

10.2.5.5 Konzentrationsbestimmung von DNA, $tRNA^{Tyr}$ und Protein

Die Konzentrationsbestimmung erfolgt mit Hilfe der UV-Spektroskopie in wässriger Lösung. Als Nullabgleich wird der entsprechende Puffer verwendet in dem die DNA-, tRNA- oder die Proteinprobe gelöst vorliegt.

DNA Lösungen:

$$DNA\ Konzentration = A_{260} * 50 \frac{\mu g}{ml} * Verdünnungsfaktor$$

E. coli $tRNA^{Tyr}$ Lösungen [Curnow *et al*., 1993][35]**:**

$$1\ \mu M\ tRNA^{Tyr} \equiv 0{,}703\ A_{260}$$

Die Reinheit der Probe ist mindestens 90%, wenn der Quotient aus A_{260}/A_{280} zwischen 1,8 und 2.0 liegt. [88]

Z. mobilis TGT Lösungen:

$$1 \frac{mg}{ml} (23{,}4\ \mu M)\ Z.mobilis\ \text{TGT (WT) entspricht}\ 0{,}778\ A_{280}$$

10.2.6 Enzymkinetische Untersuchungen

Die Verwendeten Methoden basieren auf Arbeiten von Grädler *et al*. und Stengl *et al*. [1, 32]

10.2.6.1 „Trapping"-Experiment

Vor der kinetischen Charakterisierung der Inhibitoren wird der Bindemechanismus in einem „Trapping"-Experiment bestimmt. Der zweistufige Mechanismus der Basenaustauschreaktion (Abschnitt 1.4) erlaubt zwei Möglichkeiten für die Anlangerung von Inhibitoren. Zum einen kann die Bindetasche durch den Inhibitor besetzt werden und die Anlagerung von tRNA verhindern. Es ist aber auch möglich, dass die tRNA an das Protein bindet und Gunain in Position 34 von der tRNA abgespalten wird. Die freie Guaninbindetasche kann dann nicht nur durch die natürlichen Substrate besetzt werden sondern auch durch Inhibitoren die in ihrer Größe ähnlich den natürlichen Substraten sind. Für die Unterscheidung zwischen einem kompetitiven oder gemischten Inhibitorsmechanismus wird eine SDS-PAGE durchgeführt. Hierzu wurden 5 µM Z. *mobilis* TGT, 100 µM *E. coli* $tRNA^{Tyr}$ und 1 mM des entspechenden Inhibitors (gelöst in DMSO) zu 5 µl TGT-Assaypuffer gegeben und für 1 h bei 25° C inkubiert. Zur Probe werden 10 µL SDS-Proben Puffer zugegeben und eine weitere Stunde bei 25° C inkubiert. Ein Alliquot von 10 µl wird je Probe auf ein SDS-Gel gegeben. Nach der Elektrophorese wird das Gel mit Coomasie-Blue Färbelsg. angefärbt. Um die Banden sichtbar zu machen, wird das SDS-Gel mit Coomasie-Blue Entfärberlsg. entfärbt. Bei einem kompetitiven Inhibitionsmechnaismus kann eine Bande für TGT detektiert werden

und bei einem gemischt bindenden Inhibitor sind zwei Banden (TGT und TGT mit angelagerter tRNA) zu beobachten.

10.2.6.2 Kinetische Charakterisierung

Die Michaelis-Mentenparameter für TGT WT und die TGT Mutanten gegen tRNA werden bei einer Proteinkonzentration von 150 nM, 15% radioaktiv makiertem [8-^{3}H]-Guanin und unterschiedlichen tRNA Konzentrationen (0.25 -10 µM) bestimmt.

Der Versuchstaufbau und –ablauf entspricht dem des Enzymassays (Abschnitt 10.2.6.3), wobei der Anteil an Inhibitorlösung durch DMSO ersetzt wird. Hierbei wird ausgenutzt, dass TGT Guanin in Position 34 von bestimmten tRNAs ausbaut und gegen freies Guanin aus dem Reaktionsansatz ausgetauscht werden kann. Befindet sich nun im Reaktionsanatz radioaktiv makiertes Guanin (z.B. 3H-Guanin), wird die tRNA radioaktiv makiert. Die Menge an radioaktiv makierter tRNA lässt Rückschlüsse über den kinetischen Verlauf im Reaktionsansatz zu. Verwendet wird *E. coli* $tRNA^{Tyr}$ (ECY2) (Kapitel 10.2.2.4).

Eine Auftragung des Messsignals gegenüber der Reaktionszeit ermöglicht aus der Steigung der Regressionsgeraden die Anfangsgeschwindigkeit v_0 zubestimmen. Zu jeder eingesetzen Konzentration an tRNA lässt sich die zugehörige Anfangsgeschwindigkeit bestimmen. Trägt man die erhaltenen Anfangsgeschwindigkeiten gegen die jeweilige tRNA Konzentration auf, erhält man nach einer nicht linearen Kurvenanpassung an die Michaelis-Menten-Gleichung (Gleichung 10.1), ein Michaelis-Menten Diagramm.

$$v_0 = \frac{V_{max} \times [S]}{K_m + [S]} \tag{10.1}$$

Aus dem Kurvenverlauf lassen sich die maximale Reaktionsgeschwindigkeit V_{max} und die Michaelis-Konstante K_m bestimmen. K_m ist die Substratkonzentration an tRNA bei der die Reaktionsgeschwindigkeit $V_{max}/2$ beträgt (siehe 11.4).

10.2.6.3 Enzymassay

Die Bestimmung der Bindungsaffinitäten von TGT Inhibitoren wird nach dem Protokol von Stengl *et al.* durchgeführt. [32] Jedoch mussten für die hochaffinen *lin*-Benzoguanin Inhibitoren die Bedingungen angepasst werden, hierfür wird die TGT Konzentration von 150 nM auf 18nM, 9 nM oder 2 nM reduziert.

Alle getesteten Inhibitoren werden zuvor in DMSO gelöst, auf Grund ihrer mangelnden Löslichkeit im wässrigen Mileu. Die finale DMSO Konzentration im Assay beträgt 5% und beeinträchtigt die Messung nicht. Die Inhibitoren werden mit der jeweiligen Menge

an Protein für 10 min bei 37° C inkubiert. Danach wird zum Starten der Reaktion eine Mischung aus tRNA und Guanin/[8-^{3}H]-Guanin zugegeben. Alle Reaktionsansätze werden bei 37° C gehalten und nach festen Zeitintervallen werden 15 µl Aliquote entnommen. Die Zeitintervalle richten sich nach der verwendeten Proteinmenge, bei kleinen Konzentrationen an TGT werden Intervalle von bis zu 1 h gewählt, wohingegen bei hohen TGT Konzentrationen innerhalb von 1 min ein ausreichend hohes Signal erhalten wird. Die Aliquots werden sofort auf Glasfilter (GC-F, Whatman) pipetiert und die Reaktion mit 10 % TCA-Lösung. gestoppt. ^{3}H-Guanin das nicht in die tRNA eingebaut wird, wird durch Waschen der Glasfilter mit 5% TCAlsg. entfernt. Die Glasfilter werden zwei mal mit Ethanol gewaschen, um das nachfolgende Trocken der Glasfilter bei 60 °C zu beschleunigen. Zu jeder Probe werden 4 ml Scintillation Cocktail für lipophile Proben gegeben und der Anteil an radioaktiv maktierter tRNA gemessen.

Die Ergebnisse werden benutzt, um die Anfangsgeschwindigkeit der Enzymreaktion bei verschiedenen Inhibitorkonzentationen zu bestimmen. Für die Bestimmung der Inhibitionskonstanten wird die Methode nach Dixon angewendet. Hierbei ist die Anfangsgeschwindigleit v_i der Enzymreaktion bei gegebender Inhibitorkonzentration gegeben als (Gleichung 10.2):

$$v_i = \frac{V_{max} \times [S]}{K_m \times \left(1 + \frac{[I]}{K_i}\right) + [S]} \tag{10.2}$$

Die maximale Reaktionsgeschwindigkeit ist schwierig zu reproduzieren und wird daher für jede Versuchsreihe neu betimmt. Die Inhibitionskonstante lässt sich aus dem Verhältsnis von v_0/v_i bestimmen. Dazu werden Gleichung 5.1 und 5.2 kombiniert und umgeformt (Gleichung 10.3):

$$v_0 = \frac{V_{max} \times [S]}{K_m + [S]} \quad \cup \quad v_i = \frac{V_{max} \times [S]}{K_m \times \left(1 + \frac{[I]}{K_i}\right) + [S]} \Rightarrow \frac{v_o}{v_i} \times \frac{K_m + [S]}{K_m} = \frac{1}{K_i} \times [I] + \left(\frac{[S]}{K_m} + 1\right) \tag{10.3}$$

v_o, Anfangsgeschwindigkeit in Abwesenheit des Inhibitors
v_i, Anfangsgeschwindigkeit in Anwesenheit des Inhibitors
Km, Michaelis-Konstante von tRNA
[S] $tRNA^{Tyr}$ Konzentration
[I] Inhibitorkonzentration
K_i kompetitive Inhibitionskonstante

10.2.7 X-ray analysis

10.2.7.1 *Z. mobilis* TGT crystallization

Crystals appropriate for soaking ligands are obtained in a two-step procedure. First micro-crystals are grown via hanging-drop, vapour diffusion method at 273 K. Therefore, 2 µl protein solution (16.8 mg ml^{-1} TGT, 2M NaCl, 10 mM TRIS-HCL pH 7.8, 1mM EDTA, 1mM DTT) are mixed with 2 µL of IK-buffer I or II to a droplet. During a few days micro-crystals with the size of 0.05 mm^3 are observed. In a second step, a macro-seeding is performed where the crystals grew to a size of about 0.7 x 0.7 x 0.2 mm. For the macro-seeding one micro-crystal is transferred to a droplet with 2 µl of protein solution and 2 µl MS-buffer I or II.

The ligands are dissolved in DMSO and mixed with MS-buffer I or II to a final concentration of 5 mM. Into a droplet of this mixture a single crystal is introduced and soaked for about one day.

10.2.7.2 Data collection

Apo crystals or soaked crystals are transferred for about 10 seconds into a solution containing glycerol as cryo-protectant (Cryobuffer I or II) and afterwards directly flash-frozen in liquid nitrogen.

Data sets are collected in-house and at the BESSY in Berlin (details are summarized in 11.1 Crystal data). In-house data are collected at cryo conditions (100 K) with CuKα radiation (λ = 1.5418Å) using a Rigaku RU-H300R rotating-anode generator at 50 kV and 90 mA equipped with focusing mirrors and an R-AXIS IV (Xenocs mirrors) or R-AXIS IV + + (MSC, USA) image-plate system.

Additionally, data sets are collected at the BESSY-PSF Beamline 14.1 and 14.2 in Berlin at cryo conditions (100 K) (details appendix 11.1). Synchrotron radiation (at wavelength λ = 0.97803 Å) is used. A MAR CCD 165 mm detector is utilized for data collection.

The protein usually crystallizes in the monoclinic space group *C*2 containing one monomer per asymmetric unit with Matthews coefficients of 2.3–2.4. Unit cell dimensions for all crystals are listed in Table 11.1. Data processing and scaling are performed using the HKL2000 package. Data collection and processing statistics are given in apendix 11.1. [89]

10.2.7.3 Structure determination and refinement

For all crystals in *C2* space group coordinates of the TGT apo-structure (1P0D) is directly used for an initial rigid-body refinement and a cycle of conjugate gradient energy minimization, simulated annealing, and *B*-factor refinement using the CNS program package is performed. [90] For the one complex in space group *P2* a rigid body refinement using the apo-structure (1P0D) is performed using the program PHASER out of ccp4 program suite.

The high resolution of the structures allows a further refinement with the program SHELXL. [91] Here, at least 20 cycles of conjugate gradient minimization is performed with default restraints on bonding geometry and *B*-values: 5% of all data is used for R_{free} calculation. Amino acid side-chains are fitted to σA-weighted $|F_o|$ - $|F_c|$ and 2 $|F_o|$ - $|F_c|$ electron density maps using COOT. [92] In the electron density water, glycerol molecules, and the ligand are located, and subsequently included to further refinement cycles. In a final refinement, riding H-atoms are placed for the protein (not for ligand) without using additional parameters. All final validation of the model was performed with PROCHECK. [93]

11 Appendix

11.1. Crystal data

Crystal data	4	5	7	9
pdb code	**3C2Y**	**2Z7K**	**3C2Z**	**3C2N**
A. *Data collection and processing*				
Beamline	in-house	BESSY 14.1	in-house	in-house
No. crystals used	1	1	1	1
Wavelength (Å)	1.5418	0.9780	1.5418	1.5418
Space group	*C*2	*C*2	C2	*C*2
Unit cell parameters				
a (Å)	90.3	90.5	90.2	90.7
b (Å)	64.8	65.1	64.7	64.5
c (Å)	70.3	70.6	70.4	70.3
β (deg.)	96.0	96.2	96.0	95.5
B. *Diffraction data*				
Resolution range (Å)	50–1.78	30–1.28	50-1.65	25–1.58
Unique reflections	36907 (1780)*	102059 (5228)*	48527 (2416)*	54350 (2524)*
$R(I)_{sym}$ (%)‡	5.5 (37.0)*	3.8 (24.9)*	6.0 (51.0)*	4.4 (22.3)*
Completeness (%)	95.0 (92.3)*	99.6 (97.4)*	99.9 (99.5)*	98.0 (91.1)*
Redundancy	1.9 (1.9)*	2.7 (2.5)*	3.7 (3.2)*	3.0 (2.1)*
I/σ(I)	15.0 (2.3)*	21.4 (3.8)*	20.6 (2.4)*	23.0 (4.0)*
C. *Refinement*				
Program used for refinement	SHELXL	SHELXL	SHELXL	SHELXL
Resolution range (Å)	10-1.78	10-1.28	10-1.65	10-1.58
Reflections used in refinement	35094	96866	46663	52369
Final *R* values				
R_{free} (F_o; $F_o > 4\sigma$) $	21.4 (15.0)*	18.6 (14.8)*	21.7 (20.5)*	21.7 (20.6)*
R_{work} (F_o; $F_o > 4\sigma$)°	16.4 (14.0)*	16.2 (14.0)*	17.2 (16.2)*	16.8 (16.7)*
No. of atoms (non-hydrogen)				
Protein atoms	2809	2895	2760	2714
Water molecules	274	375	233	302
Ligand atoms	16	15	18	18
RMSD, angle (deg.)	2.1	2.4	2.3	2.3
RMSD, bond (Å)	0.009	0.015	0.010	0.010
Ramachandran plot||				
Most favoured regions (%)	95.5	95.1	95.0	94.6
Additionally allowed regions (%)	4.2	4.6	4.3	5.1
Generously allowed regions (%)	0.3	0.3	0.7	0.3
Mean *B*-factors (Å^2)				
Protein atoms	15.4	13.7	13.5	16.1
Water molecules	27.0	29.0	23.6	30.7
Ligand atoms	12.1	11.4	15.3	15.3

Crystal data	**19**	**20**	**17**	**18**	**23**
pdb code	**3GC5**	**3EOU**	**3GC4**	**3EOS**	**3GE7**
A. *Data collection and processing*					
Beamline	BESSY 14.1	in-house	in-house	in-house	BESSY 14.1
No. crystals used	1	1	1	1	1
Wavelength (Å)	0.91841	1.5418	1.5418	1.5418	0,91841
Space group	C2	C2	C2	C2	C2
Unit cell parameters					
a (Å)	90.3	91.4	90.3	91.2	61.3
b (Å)	65.1	64.9	65.1	64.8	65.2
c (Å)	70.8	70.2	70.8	70.1	70.5
β (deg.)	96.2	96.0	96.2	95.9	96.2
B. *Diffraction data*					
Resolution range (Å)	30-1.40	30-1.93	30-1.80	30-1.78	30-1.50
Unique reflections	79791 (3804)*	30396 (1303)*	36099 (1207)*	38665 (1752)*	69289 (2937)*
$R(I)_{sym}$ (%)‡	3.6 (30.7)*	5.3 (22.7)*	5.5 (25)*	6.0 (39.1)*	5.0 (28.4)*
Completeness (%)	99.4 (94.6)*	98.7 (85.7)*	95.6 (65.6)*	98.9 (89.9)*	96.9 (90.1)*
Redundancy	3.8 (3.5)*	3.0 (2.0)*	3.5 (1.9)*	2.6 (2.2)*	2.9 (2.4)*
I/σ(I)	33,6 (3.3)*	20. 7 (3.5)*	21.8 (2.8)*	15.3 (2.1)*	20.4 (3.2)*
C. *Refinement*					
Program used for refinement	SHELXL	SHELXL	SHELXL	SHELXL	SHELXL
Resolution range (Å)	10-1.4	10 – 1.90	10-1.8	10-1.78	10-1.5
Reflections used in refinement	76625	29597	34502	36550	60904
Final *R* values					
R_{free} (F_o; $F_o > 4\sigma$) $^{\$}$	18.94 (18.1)*	23.0 (22.1)*	19.89 (18.2)*	23.2 (21.3)*	19.5 (18.6)*
R_{work} (F_o; $F_o > 4\sigma$)°	15.98 (15.3)*	19.3 (18.3)*	16.12 (15.0)*	17.5 (16.0)*	16.2 (15.3)*
No. of atoms (non-hydrogen)					
Protein atoms	2891	2693	2747	2744	2815
Water molecules	284	214	211	244	273
Ligand atoms	20	20	27	27	26
RMSD, angle (deg.)	2.3	1.9	2.3	2.0	2.2
RMSD, bond (Å)	0.012	0.007	0.016	0.008	0.009
Ramachandran plot||					
Most favoured regions (%)	96.2	95.6	96.0	95.7	96.0
Additionally allowed regions (%)	3.5	3.7	3.7	4.0	3.7
Generously allowed regions (%)	0.3	0.7	0.3	0.3	0.3
Mean *B*-factors (Å^2)					
Protein atoms	17.0	22.9	16.0	18.9	15.0
Water molecules	27.1	31.4	25.4	28.1	24.8
Ligand atoms	12.0	30.9	14.5	16.7	22.4

Crystal data	42	43	Lys52Met
pdb code	**3GEV**	**3GFN**	**3HFY**
A. *Data collection and processing*			
Beamline	BESSY 14.1	BESSY 14.1	BESSY 14.1
No. crystals used	1	1	1
Wavelength (Å)	0.91841	0.91841	0.91841
Space group	C2	C2	C2
Unit cell parameters			
a (Å)	91.1	90.6	84.6
b (Å)	64.8	64.8	65.1
c (Å)	70.3	70.52	71.6
β (deg.)	95.9	95.9	93.7
B. *Diffraction data*			
Resolution range (Å)	30-1.53	30-1.65	50-2.0
Unique reflections	54813 (2380)*	47254 (2008)*	26320 (1301)*
$R(I)_{sym}$ (%)‡	6.3 (43.8)*	4.7 (29.9)*	9.7 (40.0)*
Completeness (%)	89.3 (77.1)*	95.9 (81.8)*	99.9 (99.0)*
Redundancy	2.6 (1.6)*	2.5 (2.2)*	4.2 (4.0)*
I/σ(I)	16.0 (1.9)*	19.0 (2.7)*	16.3 (3.9)*
C. *Refinement*			
Program used for refinement	SHELXL	SHELXL	SHELXL
Resolution range (Å)	10-1.53	10-1.65	10-2.0
Reflections used in refinement			25041
Final *R* values			
R_{free} (F_o; $F_o > 4\sigma$) $	20.9 (19.1)*	22.5 (21.2)*	27.8 (25.6)*
R_{work} (F_o; $F_o > 4\sigma$)°	17.4 (16.0)*	18.5 (17.4)*	20.4 (19.0)*
No. of atoms (non-hydrogen)			
Protein atoms	2723	2728	2620
Water molecules	207	161	99
Ligand atoms	16	16	-
RMSD, angle (deg.)	2.3	2.2	1.7
RMSD, bond (Å)	0.010	0.009	0.007
Ramachandran plot||			
Most favoured regions (%)	96.3	94.4	94.3
Additionally allowed regions (%)	3.4	5.0	5.4
Generously allowed regions (%)	0.3	0.7	0.3
Mean *B*-factors (Å^2)			
Protein atoms	13.7	18.5	25.1
Water molecules	22.3	24.0	29.2
Ligand atoms	15.6	22.2	-

*Values in parenthesis are statistics for the highest resolution shell. ‡ $R(I)_{sym} = [\Sigma_h \Sigma_i |I_i(h) - \langle I(h) \rangle| / \Sigma_h \Sigma_i I_i(h)] x100$, where $\langle I(h) \rangle$ is the mean of the $I(h)$ observation of reflection h. ° $R_{work} = \Sigma_{hkl} |F_o - F_c| / \Sigma_{hkl} |F_o|$, $ R_{free} was calculated as for R_{work} but on 5% of the data excluded from refinement. ||From Procheck.

11.2 Structure and calculated PAMPA score of *lin*-benzoguanines PAMPA sorce of the *lin*-benzohypxanthines in brackets and the corresponding K_i value

structure	**score**	Ki [μM]
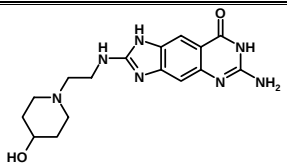	-0.08 (0.08)	0.05500
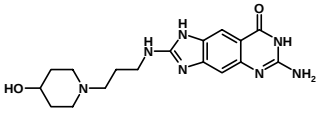	-0.06 (0.1)	0.04000
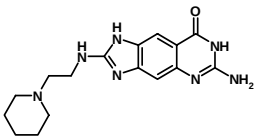	0.07 (0.23)	0.04500
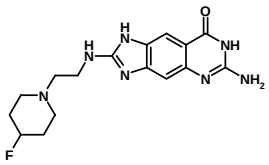	0.07 (0.22)	0.02500
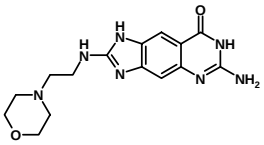	0.1 (0,26)	0.00600
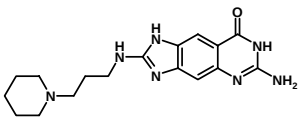	0.1	0.01500
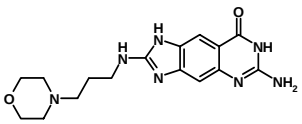	0.13 (0,29)	0.03500
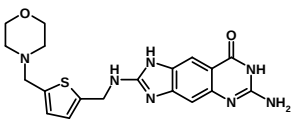	0.17 (0.33)	0.06500
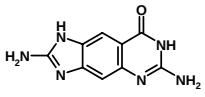	0.2 (0.35)	0.07700
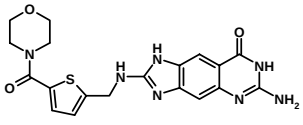	0.21 (0.37)	0.04000

structure	**Score**	Ki [μM]
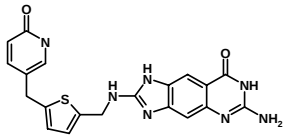	0.22 (0.38)	0.08500
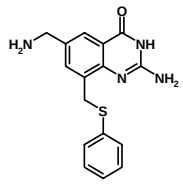	0.29	16.00000
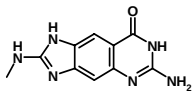	0.29	0.05300
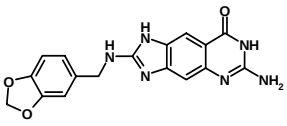	0.32 (0.48)	0.03500
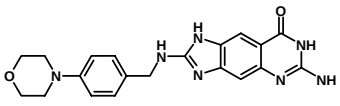	0.32 (0.48)	0.04000
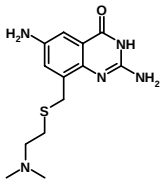	0.32	22.00000
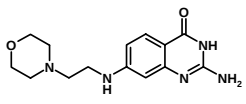	0.34	105.00000
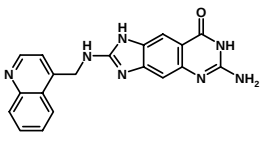	0.35 (0.51)	0.02700

structure	**Score**	Ki [μM]
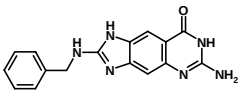	0.37 (0.52)	0.10000
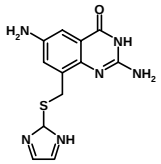	0.38	34.00000
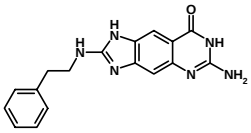	0.41 (0.56)	0.01000
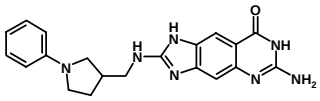	0.41 (0.57)	0.00500
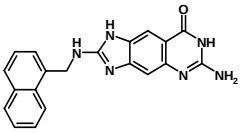	0.42 (0.43)	0.07500
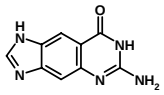	0.43	1.50000
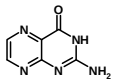	0.47	4.10000
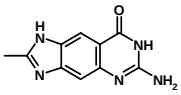	0.49	2.20000
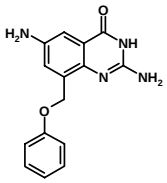	0.49	1.50000
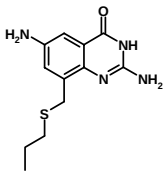	0.51	5.70000
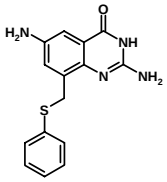	0.52	14.00000

structure	**Score**	Ki [μM]
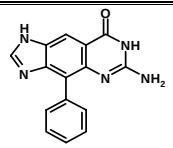	0.55	3.80000
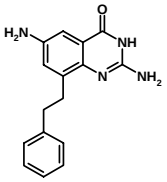	0.56	29.00000
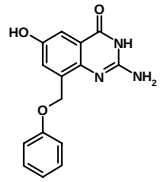	0.58	2.60000
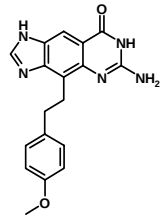	0.58	8.70000
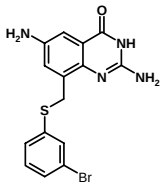	0.59	3.70000
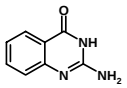	0.60	2.60000
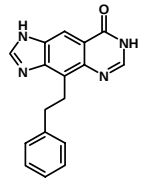	0.61	2.10000
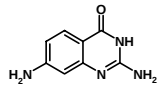	0.61	1.00000
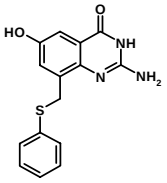	0.61	31.00000

structure	**Score**	Ki [μM]
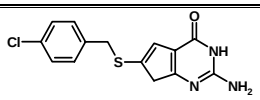	0.62	5.10000
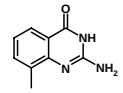	0.62	51.00000
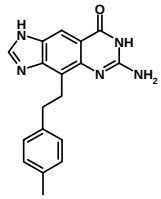	0.64	3.70000
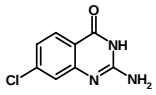	0.64	6.90000
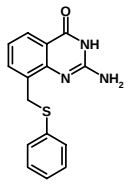	0.64	7.50000
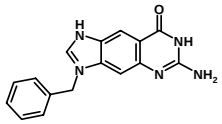	0.65	6.40000
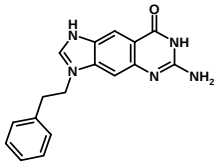	0.65	15.00000
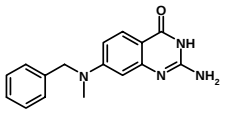	0.67	7.30000
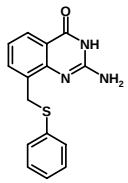	0.68	11.40000
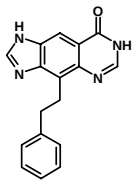	0.73	4.00000

11.3 Sequenzierungsergebnisse der TGT Mutanten

11.3.1 Tyr330Phe

```
EMBOSS_001         1                              VVEATAQETDRPRFSFSIAA-     20
                                                  .|||.|:         :|.|
EMBOSS_001         1 *DSEISDSGELSIH*GDPTVLEYLLLER*HVEAQAE---------TIVAF     41

EMBOSS_001        21 ---REGKARTGTIEMKRGVIRTPAFMPVGTAATVKALKPETVRATGADII     67
                        |.|::...|||  ...:.|||.....:..  |..|...........|
EMBOSS_001        42 LFHRAGESPHRTIE--*AGVSTPALCRARSYR--KGFKAGNSSGNWR*YI     87

EMBOSS_001        68 LGNTYHLMLRPGAERIAKLGGLHSFMGWDRPILTDSGGYQVMSLSSLTKQ    117
                     ||||||||||||||||||||||||||||||||||||||||||||||||||||
EMBOSS_001        88 LGNTYHLMLRPGAERIAKLGGLHSFMGWDRPILTDSGGYQVMSLSSLTKQ    137

EMBOSS_001       118 SEEGVTFKSHLDGSRHMLSPERSIEIQHLLGSDIVMAFDECTPYPATPSR    167
                     ||||||||||||||||||||||||||||||||||||||||||||||||||||
EMBOSS_001       138 SEEGVTFKSHLDGSRHMLSPERSIEIQHLLGSDIVMAFDECTPYPATPSR    187

EMBOSS_001       168 AASSMERSMRWAKRSRDAFDSRKEQAENAALFGIQQGSVFENLRQQSADA    217
                     ||||||||||||||||||||||||||||||||||||||||||||||||||||
EMBOSS_001       188 AASSMERSMRWAKRSRDAFDSRKEQAENAALFGIQQGSVFENLRQQSADA    237

EMBOSS_001       218 LAEIGFDGYAVGGLAVGEGQDEMFRVLDFSVPMLPDDKPHYLMGVGKPDD    267
                     ||||||||||||||||||||||||||||||||||||||||||||||||||||
EMBOSS_001       238 LAEIGFDGYAVGGLAVGEGQDEMFRVLDFSVPMLPDDKPHYLMGVGKPDD    287

EMBOSS_001       268 IVGAVERGIDMFDCVLPTRSGRNGQAFTWDGPINIRNARFSEDLKPLDSE    317
                     ||||||||||||||||||||||||||||||||||||||||||||||||||||
EMBOSS_001       288 IVGAVERGIDMFDCVLPTRSGRNGQAFTWDGPINIRNARFSEDLKPLDSE    337

EMBOSS_001       318 CHCAVCQKWSRAYIHHLIRAGEILGAMLMTEHNIAFYQQLMQKIRDSISE    367
                     ||||||||||||:||||||||||||||||||||||||||||||||||||||
EMBOSS_001       338 CHCAVCQKWSRAFIHHLIRAGEILGAMLMTEHNIAFYQQLMQKIRDSISE    387

EMBOSS_001       368 GRFSQFAQDFRARYFARNS    386
                     ||||||||||||||||||
EMBOSS_001       388 GRFSQFAQDFRARYFARNS    406
```

11.3.2 Glu339Gln

```
EMBOSS_001         1                                VVEATAQETDRPRFSFSIA     19
                                                    ...:|.:... .||||.
EMBOSS_001         1 SALERIPRISRSPRLSTHLGIHVKFVTRENISCRSTGKRRS-SRFSFH--     47

EMBOSS_001        20 AREGKARTGTIEMKRGVIRTPAFMPVGTAATVKALKPETVRATGADIILG     69
                      |.|:.....:. |.|||||||||||||||||||||||||||||||||||
EMBOSS_001        48 -RAGEKPAPALS-KAGVIRTPAFMPVGTAATVKALKPETVRATGADIILG     95
```

```
EMBOSS_001        70 NTYHLMLRPGAERIAKLGGLHSFMGWDRPILTDSGGYQVMSLSSLTKQSE    119
                     ||||||||||||||||||||||||||||||||||||||||||||||||||||
EMBOSS_001        96 NTYHLMLRPGAERIAKLGGLHSFMGWDRPILTDSGGYQVMSLSSLTKQSE    145

EMBOSS_001       120 EGVTFKSHLDGSRHMLSPERSIEIQHLLGSDIVMAFDECTPYPATPSRAA    169
                     ||||||||||||||||||||||||||||||||||||||||||||||||||||
EMBOSS_001       146 EGVTFKSHLDGSRHMLSPERSIEIQHLLGSDIVMAFDECTPYPATPSRAA    195

EMBOSS_001       170 SSMERSMRWAKRSRDAFDSRKEQAENAALFGIQQGSVFENLRQQSADALA    219
                     ||||||||||||||||||||||||||||||||||||||||||||||||||||
EMBOSS_001       196 SSMERSMRWAKRSRDAFDSRKEQAENAALFGIQQGSVFENLRQQSADALA    245

EMBOSS_001       220 EIGFDGYAVGGLAVGEGQDEMFRVLDFSVPMLPDDKPHYLMGVGKPDDIV    269
                     ||||||||||||||||||||||||||||||||||||||||||||||||||||
EMBOSS_001       246 EIGFDGYAVGGLAVGEGQDEMFRVLDFSVPMLPDDKPHYLMGVGKPDDIV    295

EMBOSS_001       270 GAVERGIDMFDCVLPTRSGRNGQAFTWDGPINIRNARFSEDLKPLDSECH    319
                     ||||||||||||||||||||||||||||||||||||||||||||||||||||
EMBOSS_001       296 GAVERGIDMFDCVLPTRSGRNGQAFTWDGPINIRNARFSEDLKPLDSECH    345

EMBOSS_001       320 CAVCQKWSRAYIHHLIRAGEILGAMLMTEHNIAFYQQLMQKIRDSISEGR    369
                     ||||||||||||||||||:||||||||||||||||||||||||||||||||
EMBOSS_001       346 CAVCQKWSRAYIHHLIRAGQILGAMLMTEHNIAFYQQLMQKIRDSISEGR    395

EMBOSS_001       370 FSQFAQDFRARYFARNS    386
                     |||||||||||||||||
EMBOSS_001       396 FSQFAQDFRARYFARNS    412
```

11.3.3 Lys52Met

```
EMBOSS_001         1 MVEATAQETDRPRFSFSIAAREGKARTGTIEMKRGVIRTPAFMPVGTAAT     50
                     ||||||||||||||||||||||||||||||||||||||||||||||||||||
EMBOSS_001         1 MVEATAQETDRPRFSFSIAAREGKARTGTIEMKRGVIRTPAFMPVGTAAT     50

EMBOSS_001        51 VKALKPETVRATGADIILGNTYHLMLRPGAERIAKLGGLHSFMGWDRPIL    100
                     |.||||||||||||||||||||||||||||||||||||||||||||||||||
EMBOSS_001        51 VMALKPETVRATGADIILGNTYHLMLRPGAERIAKLGGLHSFMGWDRPIL    100

EMBOSS_001       101 TDSGGYQVMSLSSLTKQSEEGVTFKSHLDGSRHMLSPERSIEIQHLLGSD    150
                     ||||||||||||||||||||||||||||||||||||||||||||||||||||
EMBOSS_001       101 TDSGGYQVMSLSSLTKQSEEGVTFKSHLDGSRHMLSPERSIEIQHLLGSD    150

EMBOSS_001       151 IVMAFDECTPYPATPSRAASSMERSMRWAKRSRDAFDSRKEQAENAALFG    200
                     ||||||||||||||||||||||||||||||||||||||||||||||||||||
EMBOSS_001       151 IVMAFDECTPYPATPSRAASSMERSMRWAKRSRDAFDSRKEQAENAALFG    200

EMBOSS_001       201 IQQGSVFENLRQQSADALAEIGFDGYAVGGLAVGEGQDEMFRVLDFSVPM    250
                     ||||||||||||||||||||||||||||||||||||||||||||||||||||
EMBOSS_001       201 IQQGSVFENLRQQSADALAEIGFDGYAVGGLAVGEGQDEMFRVLDFSVPM    250
```

```
EMBOSS_001      251 LPDDKPHYLMGVGKPDDIVGAVERGIDMFDCVLPTRSGRNGQAFTWDGPI    300
                    ||||||||||||||||||||||||||||||||||||||||||||||||||||
EMBOSS_001      251 LPDDKPHYLMGVGKPDDIVGAVERGIDMFDCVLPTRSGRNGQAFTWDGPI    300

EMBOSS_001      301 NIRNARFSEDLKPLDSECHCAVCQKWSRAYIHHLIRAGEILGAMLMTEHN    350
                    ||||||||||||||||||||||..:...  .:|..|.:.......:..
EMBOSS_001      301 NIRNARFSEDLKPLDSECHCAVCQNGAAPI--SII*FGRVRSGGYADDRA    348

EMBOSS_001      351 IAFYQQLMQKIRDSISEGRFSQFAQDFRARYFARNS                   386
                    ...:...|||.......|.|: ||| ..:..|..||
EMBOSS_001      349 YIAFITAMQKYGTLFRRGVFA-FAQ-ISSALFRTNS*IGCYRRGADGAAT    396

EMBOSS_001      387                         386

EMBOSS_001      397 *LLATWLTDLRFLS*GDLFP    416
```

11.3.4 Arg132Gly

```
EMBOSS_001        1                 MVEATAQETDRPRFSFSIAAREGKARTGTIEMK     33
                                    |||||||||||||||||||||||||||||||||
EMBOSS_001        1 PPRFSR*FCLTLRRRYTMVEATAQETDRPRFSFSIAAREGKARTGTIEMK     50

EMBOSS_001       34 RGVIRTPAFMPVGTAATVKALKPETVRATGADIILGNTYHLMLRPGAERI     83
                    ||||||||||||||||||||||||||||||||||||||||||||||||||||
EMBOSS_001       51 RGVIRTPAFMPVGTAATVKALKPETVRATGADIILGNTYHLMLRPGAERI    100

EMBOSS_001       84 AKLGGLHSFMGWDRPILTDSGGYQVMSLSSLTKQSEEGVTFKSHLDGSRH    133
                    ||||||||||||||||||||||||||||||||||||||||||||||||||.|
EMBOSS_001      101 AKLGGLHSFMGWDRPILTDSGGYQVMSLSSLTKQSEEGVTFKSHLDGSGH    150

EMBOSS_001      134 MLSPERSIEIQHLLGSDIVMAFDECTPYPATPSRAASSMERSMRWAKRSR    183
                    ||||||||||||||||||||||||||||||||||||||||||||||||||||
EMBOSS_001      151 MLSPERSIEIQHLLGSDIVMAFDECTPYPATPSRAASSMERSMRWAKRSR    200

EMBOSS_001      184 DAFDSRKEQAENAALFGIQQGSVFENLRQQSADALAEIGFDGYAVGGLAV    233
                    ||||||||||||||||||||||||||||||||||||||||||||||||||||
EMBOSS_001      201 DAFDSRKEQAENAALFGIQQGSVFENLRQQSADALAEIGFDGYAVGGLAV    250

EMBOSS_001      234 GEGQDEMFRVLDFSVPMLPDDKPHYLMGVGKPDDIVGAVERGIDMFDCVL    283
                    ||||||||||||||||||||||||||||||||||||||||||||||||||||
EMBOSS_001      251 GEGQDEMFRVLDFSVPMLPDDKPHYLMGVGKPDDIVGAVERGIDMFDCVL    300

EMBOSS_001      284 PTRSGRNGQAFTWDGPINIRNARFSEDLKPLDSECHCAVCQKWSRAYIHH    333
                    ||||||||||||||||||||||||||||||||||||||||||||||||||||
EMBOSS_001      301 PTRSGRNGQAFTWDGPINIRNARFSEDLKPLDSECHCAVCQKWSRAYIHH    350

EMBOSS_001      334 LIRAGEILGAMLMTEHNIAFYQQLMQKIRDSISEGRFSQFAQDFRARYFA    383
                    ||||||||||||||| |:.|.. ..||||||..|.|:...  ||||| .
EMBOSS_001      351 LIRAGEILGAMLMTEH-ISLYHS-YAKIRDSIRRGVFALLR--FRARY-R    395
```

```
EMBOSS_001       384 RNS                                 386
                     .||
EMBOSS_001       396 TNS*IAATSES*MAAARDY*LSGLPTEGCRRRTF   429
```

11.3.5 Tyr330Phe/Glu339Gln

```
EMBOSS_001       151 IVMAFDECTPYPATPSRAASSMERSMRWAKRSRDAFDSRKEQAENAALFG    200
                         |||||||||||||||||||||||||||||||||||||||||||||
EMBOSS_001         1         TPYPATPSRAASSMERSMRWAKRSRDAFDSRKEQAENAALFG     42

EMBOSS_001       201 IQQGSVFENLRQQSADALAEIGFDGYAVGGLAVGEGQDEMFRVLDFSVPM    250
                     ||||||||||||||||||||||||||||||||||||||||||||||||||||
EMBOSS_001        43 IQQGSVFENLRQQSADALAEIGFDGYAVGGLAVGEGQDEMFRVLDFSVPM     92

EMBOSS_001       251 LPDDKPHYLMGVGKPDDIVGAVERGIDMFDCVLPTRSGRNGQAFTWDGPI    300
                     ||||||||||||||||||||||||||||||||||||||||||||||||||||
EMBOSS_001        93 LPDDKPHYLMGVGKPDDIVGAVERGIDMFDCVLPTRSGRNGQAFTWDGPI    142

EMBOSS_001       301 NIRNARFSEDLKPLDSECHCAVCQKWSRAYIHHLIRAGEILGAMLMTEHN    350
                     ||||||||||||||||||||||||||||:||||||||:||||||||||||
EMBOSS_001       143 NIRNARFSEDLKPLDSECHCAVCQKWSRAFIHHLIRAGQILGAMLMTEHN    192

EMBOSS_001       351 IAFYQQLMQKIRDSISEGRFSQFAQDFRARYFARNS             386
                     |||||||||||||||||||||||||||||||||||
EMBOSS_001       193 IAFYQQLMQKIRDSISEGRFSQFAQDFRARYFARNSGSGCQSPKA    237
```

11.4 Kinetische Untersuchung von TGT Wildtyp und TGT Mutanten

Wildtyp

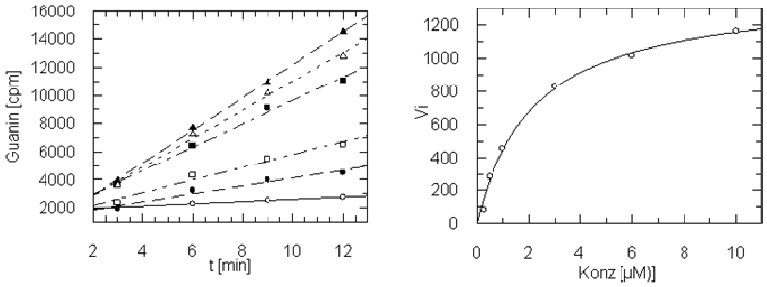

Tyr330Phe

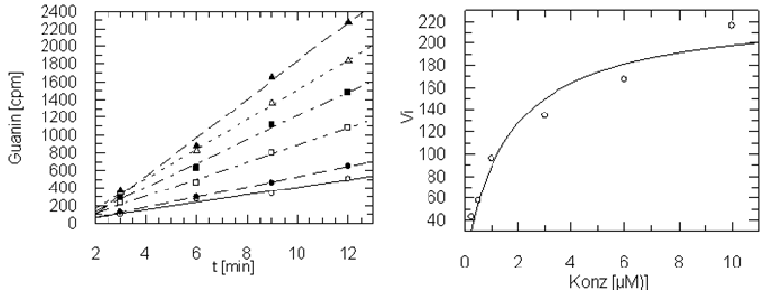

Glu339Gln

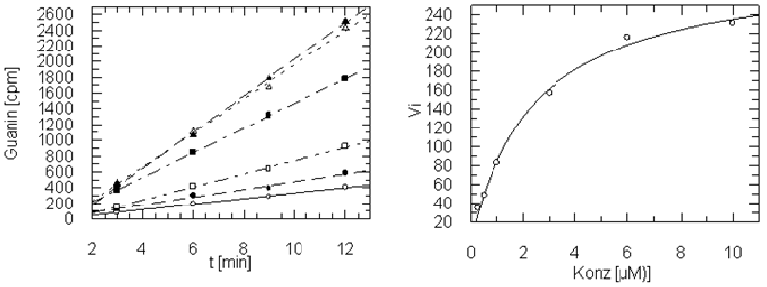

Lys52Met

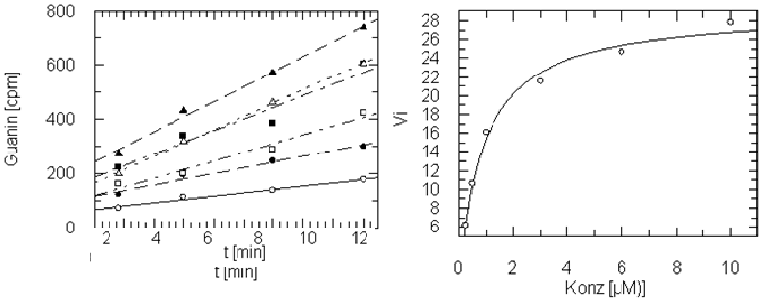

Tyr330Phe/
Glu339Gln

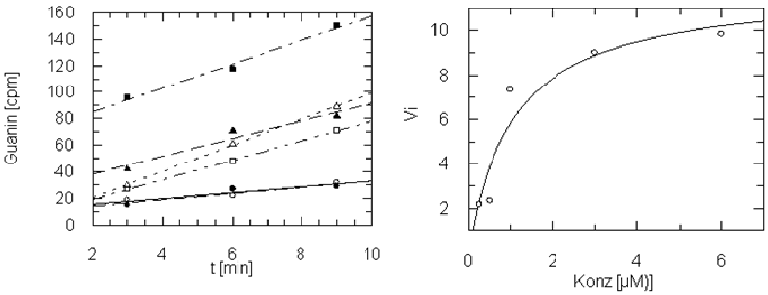

Arg132Gly

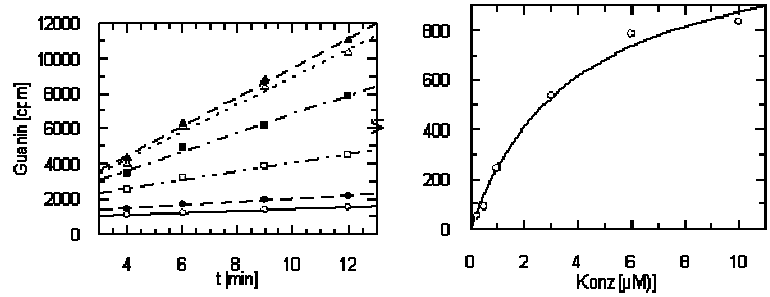

Literature

1. Grädler, U.; Gerber, H. D.; Goodenough-Lashua, D. M.; Garcia, G. A.; Ficner, R.; Reuter, K.; Stubbs, M. T.; Klebe, G. A New Target for Shigellosis: Rational Design and Crystallographic Studies of Inhibitors of tRNA-guanine Transglycosylase. *J Mol Biol* **2001,** 306, 455-467.

2. Brenk, R.; Naerum, L.; Gradler, U.; Gerber, H. D.; Garcia, G. A.; Reuter, K.; Stubbs, M. T.; Klebe, G. Virtual screening for submicromolar leads of tRNA-guanine transglycosylase based on a new unexpected binding mode detected by crystal structure analysis. *J Med Chem* **2003,** 46, 1133-43.

3. Brenk, R.; Meyer, E. A.; Reuter, K.; Stubbs, M. T.; Garcia, G. A.; Diederich, F.; Klebe, G. Crystallographic study of inhibitors of tRNA-guanine transglycosylase suggests a new structure-based pharmacophore for virtual screening. *J Mol Biol* **2004,** 338, 55-75.

4. Meyer, E.; Donati, N.; Guillot, M.; Schweizer, B.; Diederich, F.; Stengl, B.; Brenk, R.; Reuter, K.; Klebe, G. Synthesis, Biological Evaluation, and Crystallographic Studies of Extended Guanine-Based (lin-Benzoguanine) Inhibitors for tRNA-Guanine Transglycosylase (TGT). *Helv. Chim. Acta* **2006,** 89, 573-597.

5. Stengl, B.; Meyer, E.; Heine, A.; Brenk, R.; Diederich, F.; Klebe, G. Crystal Structures of tRNA-guanine Transglycosylase (TGT) in Complex with Novel and Potent Inhibitors Unravel Pronounced Induced-fit Adaptations and Suggest Dimer Formation Upon Substrate Binding. *J. Mol. Biol.* **2007,** 370, 492-511.

6. Sansonetti, P. J. Rupture, invasion and inflammatory destruction of the intestinal barrier by Shigella, making sense of prokaryote-eukaryote cross-talks. *FEMS Microbiol Rev* **2001,** 25, 3-14.

7. Kotloff, K.; Winickoff, J.; Ivanoff, B.; Clemens, J.; Swerdlow, D.; Sansonetti, P.; Adak, G.; Levine, M. Global burden of Shigella infections: implications for vaccine development and implementation of control stratagies. *Bulletin of the World Health Organisation (WHO Bull.)* 1999, pp 651-666.

8. Launay, O.; Sadorge, C.; Jolly, N.; Poirier, B.; Bechet, S.; van der Vliet, D.; Seffer, V.; Fenner, N.; Dowling, K.; Giemza, R.; Johnson, J.; Ndiaye, A.; Vray, M.; Sansonetti, P.; Morand, P.; Poyart, C.; Lewis, D.; Gougeon, M. L. Safety and immunogenicity of SC599, an oral live attenuated Shigella dysenteriae type-1 vaccine in

healthy volunteers: Results of a Phase 2, randomized, double-blind placebo-controlled trial. *Vaccine* **2009,** 27, 1184-91.

9. Sansonetti, P. J. Microbes and microbial toxins: paradigms for microbial-mucosal interactions III. Shigellosis: from symptoms to molecular pathogenesis. *Am J Physiol Gastrointest Liver Physiol* **2001,** 280, G319-23.

10. Fernandez, M. I.; Sansonetti, P. J. *Shigella* interaction with intestinal epithelial cells determines the innate immune response in shigellosis. *Int. J. Med. Microbiol.* **2003,** 293, 55-67.

11. Van Nhieu, G. T.; Bourdet-Sicard, R.; Duménil, G.; Blocker, A.; Sansonetti, P. J. Bacterial signals and cell resonses during *Shigella* entry into epithelial cells. *Cellular Microbiology* **2000,** 2, 187-193.

12. Dorman, C. J.; Porter, M. E. The *Shigella* virulence gene regulatory cascade: a paradigm of bacterial gene control mechanisms. *Molecular Microbiology* **1998,** 29, 677-684.

13. Durand, J. M.; Dagberg, B.; Uhlin, B. E.; Bjork, G. R. Transfer RNA modification, temperature and DNA superhelicity have a common target in the regulatory network of the virulence of Shigella flexneri: the expression of the virF gene. *Mol Microbiol* **2000,** 35, 924-935.

14. Durand, J. M.; Bjork, G. R.; Kuwae, A.; Yoshikawa, M.; Sasakawa, C. The modified nucleoside 2-methylthio-N6-isopentenyladenosine in tRNA of *Shigella flexneri* is required for expression of virulence genes. *J Bacteriol* **1997,** 179, 5777-5782.

15. Durand, J. M.; Okada, N.; Tobe, T.; Watarai, M.; Fukuda, I.; Suzuki, T.; Nakata, N.; Komatsu, K.; Yoshikawa, M.; Sasakawa, C. vacC, a virulence-associated chromosomal locus of *Shigella flexneri*, is homologous to tgt, a gene encoding tRNA-guanine transglycosylase (Tgt) of *Escherichia coli* K-12. *J Bacteriol* **1994,** 176, 4627-4634.

16. Reader, J. S.; Metzgar, D.; Schimmel, P.; de Crecy-Lagard, V. Identification of four genes necessary for biosynthesis of the modified nucleoside queuosine. *J Biol Chem* **2004,** 279, 6280-5.

17. Kuchino, Y.; Kasai, H.; Nihei, K.; Nishimura, S. Biosynthesis of the modified nucleoside Q in transfer RNA. *Nucleic Acids Res* **1976,** 3, 393-8.

18. Gaur, R.; Varshney, U. Genetic analysis identifies a function for the queC (ybaX) gene product at an initial step in the queuosine biosynthetic pathway in Escherichia coli. *J Bacteriol* **2005,** 187, 6893-901.

19. Van Lanen, S. G.; Reader, J. S.; Swairjo, M. A.; de Crecy-Lagard, V.; Lee, B.; Iwata-Reuyl, D. From cyclohydrolase to oxidoreductase: discovery of nitrile reductase activity in a common fold. *Proc Natl Acad Sci U S A* **2005,** 102, 4264-9.

20. Grimm, C.; Ficner, R.; Sgraja, T.; Haebel, P.; Klebe, G.; Reuter, K. Crystal structure of Bacillus subtilis S-adenosylmethionine:tRNA ribosyltransferase-isomerase. *Biochem Biophys Res Commun* **2006,** 351, 695-701.

21. Hoops, G. C.; Townsend, L. B.; Garcia, G. A. tRNA-guanine transglycosylase from Escherichia coli: structure-activity studies investigating the role of the aminomethyl substituent of the heterocyclic substrate PreQ1. *Biochemistry* **1995,** 34, 15381-7.

22. Van Lanen, S. G.; Kinzie, S. D.; Matthieu, S.; Link, T.; Culp, J.; Iwata-Reuyl, D. tRNA modification by S-adenosylmethionine:tRNA ribosyltransferase-isomerase. Assay development and characterization of the recombinant enzyme. *J Biol Chem* **2003,** 278, 10491-9.

23. Iwata-Reuyl, D. Biosynthesis of the 7-deazaguanosine hypermodified nucleosides of transfer RNA. *Bioorg Chem* **2003,** 31, 24-43.

24. Kinzie, S. D.; Thern, B.; Iwata-Reuyl, D. Mechanistic studies of the tRNA-modifying enzyme QueA: a chemical imperative for the use of AdoMet as a "ribosyl" donor. *Org Lett* **2000,** 2, 1307-10.

25. Blaise, M.; Becker, H. D.; Keith, G.; Cambillau, C.; Lapointe, J.; Giege, R.; Kern, D. A minimalist glutamyl-tRNA synthetase dedicated to aminoacylation of the tRNAAsp QUC anticodon. *Nucleic Acids Res* **2004,** 32, 2768-75.

26. Campanacci, V.; Dubois, D. Y.; Becker, H. D.; Kern, D.; Spinelli, S.; Valencia, C.; Pagot, F.; Salomoni, A.; Grisel, S.; Vincentelli, R.; Bignon, C.; Lapointe, J.; Giege, R.; Cambillau, C. The Escherichia coli YadB gene product reveals a novel aminoacyl-tRNA synthetase like activity. *J Mol Biol* **2004,** 337, 273-83.

27. Dubois, D. Y.; Blaise, M.; Becker, H. D.; Campanacci, V.; Keith, G.; Giege, R.; Cambillau, C.; Lapointe, J.; Kern, D. An aminoacyl-tRNA synthetase-like protein encoded by the Escherichia coli yadB gene glutamylates specifically tRNAAsp. *Proc Natl Acad Sci U S A* **2004,** 101, 7530-5.

28. Salazar, J. C.; Ambrogelly, A.; Crain, P. F.; McCloskey, J. A.; Soll, D. A truncated aminoacyl-tRNA synthetase modifies RNA. *Proc Natl Acad Sci U S A* **2004,** 101, 7536-41.

29. Xie, W.; Liu, X.; Huang, R. H. Chemical trapping and crystal structure of a catalytic tRNA guanine transglycosylase covalent intermediate. *Nat Struct Biol* **2003,** 10, 781-8.

30. Tidten, N.; Stengl, B.; Heine, A.; Garcia, G. A.; Klebe, G.; Reuter, K. Glutamate versus glutamine exchange swaps substrate selectivity in tRNA-guanine transglycosylase: insight into the regulation of substrate selectivity by kinetic and crystallographic studies. *J Mol Biol* **2007,** 374, 764-76.

31. Brenk, R.; Stubbs, M. T.; Heine, A.; Reuter, K.; Klebe, G. Flexible adaptations in the structure of the tRNA-modifying enzyme tRNA-guanine transglycosylase and their implications for substrate selectivity, reaction mechanism and structure-based drug design. *Chembiochem* **2003,** 4, 1066-77.

32. Stengl, B.; Reuter, K.; Klebe, G. Mechanism and substrate specificity of tRNA-guanine transglycosylases (TGTs): tRNA-modifying enzymes from the three different kingdoms of life share a common catalytic mechanism. *Chembiochem* **2005,** 6, 1926-1939.

33. Okada, N.; Nishimura, S. Isolation and characterization of a guanine insertion enzyme, a specific tRNA transglycosylase, from Escherichia coli. *J Biol Chem* **1979,** 254, 3061-3066.

34. Nakanishi, S.; Ueda, T.; Hori, H.; Yamazaki, N.; Okada, N.; Watanabe, K. A UGU sequence in the anticodon loop is a minimum requirement for recognition by Escherichia coli tRNA-guanine transglycosylase. *J Biol Chem* **1994,** 269, 32221-32225.

35. Curnow, A. W.; Garcia, G. A. tRNA-guanine transglycosylase from Escherichia coli. Minimal tRNA structure and sequence requirements for recognition. *J Biol Chem* **1995,** 270, 17264-17267.

36. Romier, C.; Reuter, K.; Suck, D.; Ficner, R. Crystal structure of tRNA-guanine transglycosylase: RNA modification by base exchange. *Embo J* **1996,** 15, 2850-2857.

37. Ashkenazi, S.; Levy, I.; Kazaronovski, V.; Samra, Z. Growing antimicrobial resistance of Shigella isolates. *J Antimicrob Chemother* **2003,** 51, 427-429.

38. CCG, C.C.G.I., MOE (Molecular Operating Environment). **2005**.

39. Clark, A. M.; Labute, P.; Santavy, M. 2D Structure Depiction. *J Chem Inf Model* **2006,** 46, 1107-1123.

40. Xie, W.; Liu, X.; Huang, R. Chemical trapping and crystal structure of a catalytic tRNA guanine transglycosylase covalent intermediate. *Nat Struct Mol Biol* **2003,** 10, 781-788.

41. Goodenough-Lashua, D.; Garcia, G. tRNA-guanine transglycosylase from E. coli: a ping-pong kinetic mechanism is consistent with nucleophilic catalysis. *Bioorg. Chem.* **2003,** 31, 331-344.

42. Hortner, S. R.; Ritschel, T.; Stengl, B.; Kramer, C.; Schweizer, W. B.; Wagner, B.; Kansy, M.; Klebe, G.; Diederich, F. Potent inhibitors of tRNA-guanine transglycosylase, an enzyme linked to the pathogenicity of the Shigella bacterium: charge-assisted hydrogen bonding. *Angew Chem Int Ed* **2007,** 46, 8266-8269.

43. Stengel, B. Structural and Functional Studies of tRNA-Guanine Transglycosylase: A putative Drug Target of Shigellosis Therapy. *Ph D Thesis, Philipps-University Marburg* **2006**.

44. Hopkins, A. L.; Groom, C. R.; Alex, A. Ligand efficiency: a useful metric for lead selection. *Drug Discov Today* **2004,** 9, 430-431.

45. Czodrowski, P.; Dramburg, I.; Sotriffer, C. A.; Klebe, G. Development, validation, and application of adapted PEOE charges to estimate pKa values of functional groups in protein-ligand complexes. *Proteins* **2006,** 65, 424-437.

46. Sheriff, S.; Hendrickson, W. A.; Smith, J. L. Structure of myohemerythrin in the azidomet state at 1.7/1.3 A resolution. *J Mol Biol* **1987,** 197, 273-296.

47. Jones, G.; Willett, P.; Glen, R. C.; Leach, A. R.; Taylor, R. Development and validation of a genetic algorithm for flexible docking. *J Mol Biol* **1997,** 267, 727-48.

48. Czodrowski, P.; Sotriffer, C. A.; Klebe, G. Atypical protonation states in the active site of HIV-1 protease: a computational study. *J Chem Inf Model* **2007,** 47, 1590-1598.

49. Czodrowski, P.; Sotriffer, C. A.; Klebe, G. Protonation changes upon ligand binding to trypsin and thrombin: structural interpretation based on pK(a) calculations and ITC experiments. *J Mol Biol* **2007,** 367, 1347-1356.

50. Gerlach, C.; Smolinski, M.; Steuber, H.; Sotriffer, C. A.; Heine, A.; Hangauer, D. G.; Klebe, G. Thermodynamic inhibition profile of a cyclopentyl and a cyclohexyl

derivative towards thrombin: the same but for different reasons. *Angew Chem Int Ed* **2007,** 46, 8511-4.

51. Barillari, C.; Taylor, J.; Viner, R.; Essex, J. W. Classification of water molecules in protein binding sites. *J Am Chem Soc* **2007,** 129, 2577-87.

52. Amadasi, A.; Spyrakis, F.; Cozzini, P.; Abraham, D. J.; Kellogg, G. E.; Mozzarelli, A. Mapping the energetics of water-protein and water-ligand interactions with the "natural" HINT forcefield: predictive tools for characterizing the roles of water in biomolecules. *J Mol Biol* **2006,** 358, 289-309.

53. Homans, S. W. Water, water everywhere--except where it matters? *Drug Discov Today* **2007,** 12, 534-9.

54. Ritschel, T.; Hoertner, S.; Heine, A.; Diederich, F.; Klebe, G. Crystal Structure Analysis and in Silico pK(a) Calculations Suggest Strong pK(a) Shifts of Ligands as Driving Force for High-Affinity Binding to TGT. *Chembiochem* **2009**.

55. Hendlich, M.; Bergner, A.; Gunther, J.; Klebe, G. Relibase: design and development of a database for comprehensive analysis of protein-ligand interactions. *J Mol Biol* **2003,** 326, 607-20.

56. Gunther, J.; Bergner, A.; Hendlich, M.; Klebe, G. Utilising structural knowledge in drug design strategies: applications using Relibase. *J Mol Biol* **2003,** 326, 621-36.

57. Gerber, P. Moloc: Molecular Modelling on Graphics Workstations. **1997**.

58. Velec, H. F.; Gohlke, H.; Klebe, G. DrugScore(CSD)-knowledge-based scoring function derived from small molecule crystal data with superior recognition rate of near-native ligand poses and better affinity prediction. *J Med Chem* **2005,** 48, 6296-303.

59. Irwin, J. J.; Shoichet, B. K. ZINC--a free database of commercially available compounds for virtual screening. *J Chem Inf Model* **2005,** 45, 177-82.

60. Kohler, P. C.; Ritschel, T.; Schweizer, W. B.; Klebe, G.; Diederich, F. High-Affinity Inhibitors of tRNA–Guanine Transglycosylase Replacing the Function of a Structural Water Cluster. *Submitted* **2009**.

61. Stengl, B. Structural and Functional Studies of tRNA-Guanine Transglycosylase: A putative Drug Target of Shigellosis Therapy. *Ph D Thesis, Philipps-University Marburg* **2006**.

62. Stewart, D. E.; Sarkar, A.; Wampler, J. E. Occurrence and role of cis peptide bonds in protein structures. *J Mol Biol* **1990,** 214, 253-60.

63. Jabs, A.; Weiss, M. S.; Hilgenfeld, R. Non-proline cis peptide bonds in proteins. *J Mol Biol* **1999,** 286, 291-304.

64. Morgenthaler, M.; Schweizer, E.; Hoffmann-Roder, A.; Benini, F.; Martin, R. E.; Jaeschke, G.; Wagner, B.; Fischer, H.; Bendels, S.; Zimmerli, D.; Schneider, J.; Diederich, F.; Kansy, M.; Muller, K. Predicting and tuning physicochemical properties in lead optimization: amine basicities. *ChemMedChem* **2007,** 2, 1100-15.

65. Carr, R. A.; Congreve, M.; Murray, C. W.; Rees, D. C. Fragment-based lead discovery: leads by design. *Drug Discov Today* **2005,** 10, 987-92.

66. Rees, D. C.; Congreve, M.; Murray, C. W.; Carr, R. Fragment-based lead discovery. *Nat Rev Drug Discov* **2004,** 3, 660-72.

67. Alex, A. A.; Flocco, M. M. Fragment-based drug discovery: what has it achieved so far? *Curr Top Med Chem* **2007,** 7, 1544-67.

68. Bosch, J.; Robien, M. A.; Mehlin, C.; Boni, E.; Riechers, A.; Buckner, F. S.; Van Voorhis, W. C.; Myler, P. J.; Worthey, E. A.; DeTitta, G.; Luft, J. R.; Lauricella, A.; Gulde, S.; Anderson, L. A.; Kalyuzhniy, O.; Neely, H. M.; Ross, J.; Earnest, T. N.; Soltis, M.; Schoenfeld, L.; Zucker, F.; Merritt, E. A.; Fan, E.; Verlinde, C. L.; Hol, W. G. Using fragment cocktail crystallography to assist inhibitor design of Trypanosoma brucei nucleoside 2-deoxyribosyltransferase. *J Med Chem* **2006,** 49, 5939-46.

69. Sanglier, S.; Atmanene, C.; Chevreux, G.; Dorsselaer, A. V. Nondenaturing mass spectrometry to study noncovalent protein/protein and protein/ligand complexes: technical aspects and application to the determination of binding stoichiometries. *Methods Mol Biol* **2008,** 484, 217-43.

70. Erlanson, D. A.; Braisted, A. C.; Raphael, D. R.; Randal, M.; Stroud, R. M.; Gordon, E. M.; Wells, J. A. Site-directed ligand discovery. *Proc Natl Acad Sci U S A* **2000,** 97, 9367-72.

71. Hurt, J. K.; Olgen, S.; Garcia, G. A. Site-specific modification of Shigella flexneri virF mRNA by tRNA-guanine transglycosylase in vitro. *Nucleic Acids Res* **2007,** 35, 4905-13.

72. Garcia, G. A.; Koch, K. A.; Chong, S. tRNA-guanine transglycosylase from Escherichia coli. Overexpression, purification and quaternary structure. *J Mol Biol* **1993,** 231, 489-97.

73. Reuter, K.; Ficner, R. Sequence analysis and overexpression of the Zymomonas mobilis tgt gene encoding tRNA-guanine transglycosylase: purification and biochemical characterization of the enzyme. *J Bacteriol* **1995,** 177, 5284-5288.

74. Ritschel, T.; Kohler, P. C.; Neudert, G.; Heine, A.; Diederich, F.; Klebe, G. Replacement of active-site water molecules to achieve nanomolar inhibition of tRNA-guanine transglycosylase. *Submitted to J Mol Biol* **2009**.

75. Gordiyenko, Y.; Robinson, C. V. The emerging role of MS in structure elucidation of protein-nucleic acid complexes. *Biochem Soc Trans* **2008,** 36, 723-31.

76. Heck, A. J.; Van Den Heuvel, R. H. Investigation of intact protein complexes by mass spectrometry. *Mass Spectrom Rev* **2004,** 23, 368-89.

77. Sanglier, S.; Leize, E.; Van Dorsselaer, A.; Zal, F. Comparative ESI-MS study of approximately 2.2 MDa native hemocyanins from deep-sea and shore crabs: from protein oligomeric state to biotope. *J Am Soc Mass Spectrom* **2003,** 14, 419-29.

78. Barraud, P.; Golinelli-Pimpaneau, B.; Atmanene, C.; Sanglier, S.; Van Dorsselaer, A.; Droogmans, L.; Dardel, F.; Tisne, C. Crystal structure of Thermus thermophilus tRNA m1A58 methyltransferase and biophysical characterization of its interaction with tRNA. *J Mol Biol* **2008,** 377, 535-50.

79. Ritschel, T. Structure based drug design & x-ray crystallography
for the development of high affine inhibitors of
tRNA-guanine transglycosylase *Ph D Thesis, Philipps-University Marburg* **2009**.

80. Gasteiger, J.; Marsili, M. Iterative partial equalization of orbital electronegativity - a rapid access to atomic charges. *Tetrahedron* **1980,** 36 3219-3228.

81. Word, J. M.; Lovell, S. C.; Richardson, J. S.; Richardson, D. C. Asparagine and glutamine: using hydrogen atom contacts in the choice of side-chain amide orientation. *J Mol Biol* **1999,** 285, 1735-1747.

82. Sadowski, J., Gasteiger, J., Klebe, G. Comparison of Automatic Three-Dimensional Model Builders Using 639 X-ray Structures. *J. Chem. Inf. Comput. Sci* **1994,** 34, 1000-8.

83. Rarey, M.; Kramer, B.; Lengauer, T.; Klebe, G. A fast flexible docking method using an incremental construction algorithm. *J Mol Biol* **1996,** 261, 470-89.

84. Tripos Inc. Sybyl. 699 South Hanley Rd., S. L., Missouri, 63144, USA 6.6 Au°age, . **2000**.

85. Case, D. A.; Cheatham, T. E., 3rd; Darden, T.; Gohlke, H.; Luo, R.; Merz, K. M., Jr.; Onufriev, A.; Simmerling, C.; Wang, B.; Woods, R. J. The Amber biomolecular simulation programs. *J Comput Chem* **2005,** 26, 1668-88.

86. Jorgensen, W. L.; Chandrasekhar, J.; Madura, J. D.; Impey, W. I.; Klein, M. L. Comparison of simple potential functions for simulatinf liquid water. *The Journal of Chemical Physiks* **1983,** 79, 926 - 935.

87. Romier, C.; Ficner, R.; Reuter, K.; Suck, D. Purification, crystallization, and preliminary x-ray diffraction studies of tRNA-guanine transglycosylase from Zymomonas mobilis. *Proteins* **1996,** 24, 516-519.

88. Sambrook, J.; Fritsch, E.; Maniatis, t. Molecular Cloning - a laboratory manual 2nd ed. *New York, Cold Springer Habour* **1989**.

89. Otwinowski, Z.; Minor, W. Processing of X-ray diffraction data collected in oscillation mode. *Methods Enzymol.* **1997,** 276, 307-326.

90. Brunger, A. T.; Adams, P. D.; Clore, G. M.; DeLano, W. L.; Gros, P.; Grosse-Kunstleve, R. W.; Jiang, J. S.; Kuszewski, J.; Nilges, M.; Pannu, N. S.; Read, R. J.; Rice, L. M.; Simonson, T.; Warren, G. L. Crystallography & NMR system: A new software suite for macromolecular structure determination. *Acta Crystllog sect. D Biol Crystallog* **1998,** 54, 905-921.

91. Sheldrick, G. M.; Schneider, T. R. SHELXL: high-resolution refinement. *Methods Enzymol.* **1997,** 277b, 319-343.

92. Emsley, P.; Cowtan, K. Coot: model-building tools for molecular graphics. *Acta Crystallog D Biol Crystallog* **2004,** 60, 2126-2132.

93. Laskowski, R. A.; MacArthur, M. W.; Moss, D. S.; Thornton, J. M. PROCHECK: a program to check the stereochemical quality of protein structures. *J Appl Crystallog* **1993,** 26, 283-291.

Publications arising from this work

Articles

Hörtner, S., Ritschel, T., Stengl, B., Kramer, C., Schweizer, W. B., Wagner, B., Kansy, M., Klebe, G., Diederich, F.
Potent inhibitors of tRNA-guanine transglycosylase, an enzyme linked to the pathogenicity of the Shigella bacterium: charge-assisted hydrogen bonding
Angew Chem 2007, 46, 8266-8269

Ritschel, T., Hörtner, S., Heine, A., Diederich, F., Klebe, G.
Crystal structure analysis and in-silico pKa calculations suggest strong pKa shifts of ligands as driving force for high affinity binding to TGT
ChemBioChem 4 (10), 716-727

Ritschel, T., Kohler, P.C., Neudert, G., Diederich, F., Klebe, G.
Importance of water cluster in the active site of TGT for computer aided drug design
Submitted to J. Mol. Biol.

Ritschel, T., Atmanene, C., Sanglier-Cianferani, S., Klebe, G.
Investigation of the protein-protein interaction (PPI) of TGT using non-denaturing ESI-MS, computer aided drug design, and protein crystallography
Submitted to J. Mol. Biol.

Kohler, P.C., Ritschel, T., Schweizer, W.B., Klebe, G., Diederich, F.
Synthesis of Nanomolar Inhibitors of tRNA–Guanine Transglycosylase Replacing the Function of a Structural Water Cluster
Accepted at Chemistry - A European Journal

Kohler, P.C., Ritschel, T., Klebe, G., Diederich, F.
An Extended Series of tRNA–Guanine Transglycosylase Inhibitors Addressing the Ribose-33 Pocket
In preparation

Pfeffer, P., Neudert, G., Englert, L., Ritschel, T., Baum, B., Klebe G.
DrugScore_FP – Profiling Protein-Ligand Interactions
In preparation

Posters

Ritschel, T., Stengl, B., Hörtner, S., François, D., Klebe, G.
Addressing a new subpocket in tRNA-guanine-transglycosylase by means of combinatorial docking
Darmstädter Molecular Modelling Workshop, der Molecular Graphics and Modelling Society, Friedrich-Alexander-University, Erlangen

Ritschel, T., Stengl, B., Hörtner, S., François, D., Klebe, G.
Unexpected Influence of Structural Water upon Inhibition of tRNA-Guanine Transglycosylase Provides Novel Concepts for Drug Design
3rd Summer School Medicinal Chemistry: "Molecular Recognition - Ligand Receptor Interactions", University Regensburg

Ritschel, T., Hörtner, S., François, D., Klebe, G.
The Importance of Water Molecules and Charge Assistance for the Inhibition of TGT
MGMS Young Modellers' Forum in Conjunction with the RSC MMG, The Brunai Gallery, London, GB

Ritschel, T., Kohler, P. C., François, D., Klebe, G.
Last Frontiers In Structure Based Drug Design: Charges, Water, and Mobility
XXth International Symposium on Medicinal Chemistry, Gesellschaft Österreichischer Chemiker, Vienna, Austria

Danksagung

Viele verschiedene Personen haben mich in den letzten Jahren unterstützt und maßgeblich zu dieser Arbeit beigetragen. Besonders bedanken möchte ich mich bei:

Prof. Dr. *Gerhard Klebe* für die interessanten und vielfältigen Aufgabenstellungen. Zusätzlich für die gewährte Freiheit bei der Bearbeitung meines Dissertationsthemas und die vielen hilfreichen Diskussionen.

Prof. Dr. *Klaus Reuter* für die gute und erfolgreiche Zusammenarbeit bei der Aufklärung des katalytisch aktiven Komplexes von TGT und tRNA.

Dr. *Andreas Heine* für die Einführung in die Methoden der Röntgenkristallographie und seine Hilfe bei der Bearbeitung zahlreicher Proteinstrukturen.

Dr. *Simone Hörtner, Philipp Kohler* und Herrn Prof. Dr. *François Diederich* von der ETH Zürich für gute Zusammenarbeit bei der Optimierung der *lin*-Benzoguanine.

Dr. *Tim Larsen*, *Marcus Freitag*, *Khattab El Gaghlab* und Prof. Dr. *Andreas Link* an der Ernst-Moritz-Arndt Universität Greifswald für die Synthese der Benzimidazole. Zudem für die freundliche Aufnahme währen meines Besuchs in Greifswald.

Cédric Atmanene und Dr. *Sarah Sanglier-Cianferani* vom Laboratoire de Spectrométrie de Masse Bio-Organique in Straßburg für den erfolgreichen Start in eine neue und äußerst vielverspechende Kooperation zur Untersuchung des TGT Dimers.

Dr. *Stefanie Bendels* und *Dr. Manfred Kansy* von der Firma F.Hoffmann-LaRoche in Basel für die Berechnung der PAMPA Werte.

Dr. *Bernhard Blumenschein* für die Einarbeitung in die experimentellen Methoden des TGT-Projekts zu Beginn meiner Arbeit.

Steffi Dörr für die ihre Unterstützung bei der Expression und Aufreinigung von TGT.

Angela Scholz und *Lydia Hartleben* durch die das Sekretariat der Arbeitsgruppe immer bestens besetzt war.

Christian Sohn für die Betreuung und Wartung der Röntgengeräte.

Sven Siebler, *Gerd Neudert*, *Andreas Spitzmüller* und alle ehemaligen Administratoren unserer Arbeitsgruppe für die gute Betreuung und Wartung unserer Rechner.

Meinen Vertiefungsstudenten *Inna Schmitt*, *Daniel Reuschel*, *Silke Budde*, *Linda Heinze*, *Julia Unigzaeva* und *Sylvie Kutter* für das Interesse und Engagement während ihrer Zeit in der Arbeitsgruppe Klebe.

Patrick Pfeffer, *Martin Sippel*, *Cornelia Koch*, *Lisa Englert*, *Andreas Spitzmüller*, *Tobias Craan*, *Gerd Neudert*, *Jürgen Behnen* und *Johannes Schulze Wischeler* für die sehr schöne Zeit in Marburg. Besonders für die vielen tollen Abfahrten in Hirschegg & Ausfahrten in Marburg.

Yvonne Brockmann, *Marcus Meier* und *Tobias Vogel* für die Begleitung durch das Studium und die Promotion und vor allem für das Korrekturlesen des Manuskripts meiner Dissertation.

Meinen Eltern für ihre Unterstützung im Studium und während der Promotion. Besonders für die vielen Gespräche, die mir neue Motivation gegeben haben, wenn ich vor mehr Fragen als Antworten stand.

Erklärung

Ich versichere, dass ich meine Dissertation

TGT a Drug Target to Study pKa Shifts, Residual Solvation & Protein - Protein Interface Formation

selbständig ohne unerlaubte Hilfe angefertigt und mich dabei keiner anderen als der von mir ausdrücklich bezeichneten Quellen bedient habe.

Die Dissertation wurde in der jetzigen oder einer ähnlichen Form noch in keiner anderen Hochschule eingereicht und hat noch keinen sonstigen Prüfungszwecken gedient.

Marburg, den 05. Juli 2009 _____

(Tina Ritschel)

Curriculum Vitae

Persönliche Daten

Familienstand: ledig

Nationalität: deutsch

Geburtsdatum: 27.11.1979

Geburtsort: Wiesbaden

Ausbildung und Studium

01/2006 – heute	Philipps-Universität Marburg **Promotion am Institut für Pharmazeutische Chemie in der Arbeitsgruppe von Prof. Dr. Gerhard Klebe**
12/2005	**Approbation zur Apothekerin**
10/2000 – 10/2005	Philipps-Universität Marburg und Universität von Kuopio, Kuopio, Finnland **Fachrichtung: Pharmazie**
06/2000	Pestalozzischule, Gymnasium, Idstein **Abschluss: Abitur**

Praktika

05/2005 – 10/2005	Prenz´l Apotheke, Berlin **Pharmaziepraktikantin:** Öffentliche Apotheke
11/2004 – 04/2005	Merck KGaA, Darmstadt **Pharmaziepraktikantin im Bereich Pharma Analytik**